Dipl.-Ing. Martin Forstinger, BSc

Modelling, Simulation, and Control of Power Train Test Beds

DOCTORAL THESIS

to achieve the university degree of

Doktor der technischen Wissenschaften

submitted to

Graz University of Technology

Supervisor

Ao. Univ.-Prof. Dipl.-Ing. Dr. techn. Anton Hofer

Institute of Automation and Control

Priv.-Doz. Dipl.-Ing. Dr. techn. Robert Bauer

Graz, August 2017

Eidesstattliche Erklärung

Ich erkläre an Eides statt, dass ich die vorliegende Arbeit selbstständig verfasst, andere als die angegebenen Quellen/Hilfsmittel nicht benutzt, und die den benutzten Quellen wörtlich und inhaltlich entnommenen Stellen als solche kenntlich gemacht habe. Das in TUGRAZonline hochgeladene Textdokument ist mit der vorliegenden Arbeit identisch.

Graz, am 16.8.2017

Datum

Unterschrift

Statutory Declaration

I declare that I have authored this thesis independently, that I have not used other than the declared sources/resources, and that I have explicitly marked all material which has been quoted either literally or by content from the used sources. The text document uploaded to TUGRAZonline is identical to the present doctoral thesis.

Graz, 16.8.2017

Date

Signature

Abstract

In this work power train test beds are discussed regarding modelling, simulation, and control. The key objective is to increase the performance of the considered test systems via new control approaches. More precisely, the tracking of the references for the relevant mechanical quantities rotational speed and torque shall be enhanced. This control task is complicated by the natural coupling of speed and torque control loops; i.e. a change in testing torque affects rotational speeds and a change in rotational speeds has an effect on the measured torques. Furthermore, due to potentially low internal damping in the mechanical structure, special focus has to be placed on the damping of resonant torque oscillations.

The availability of accurate mathematical models describing the test bed dynamics is inevitable in the controller design work-flow. Since power train test systems are mechanically diverse, a modular modelling approach is used. In a first step, the modelling task is reduced to mathematically describing the test bed components such as electric drives, mechanical shafts, or adapter gearboxes and the power train elements to be tested such as clutches, transmissions, and differential gears. The final task is then to combine these models for various system components to finally get a mathematical model describing the dynamics of the entire test bed. Numerical simulations of the test systems are complicated by the presence of friction elements that can lead to a reduction of the system's dynamic dimension. While an existing simulation strategy can be applied to handle simple systems of that type, for systems with a potential reduction of dynamic dimension by more than one, such as the lossy limited-slip differential gear, an appropriate simulation strategy is proposed in this work. Thereby, a numerically efficient simulation of the power train test beds to control is possible. This is successfully demonstrated on the basis of three different test systems.

Control performance is increased by the use of a controller designed according to the decoupling and feedback linearisation method. Then, decoupling the control loops for rotational speed and testing torque and vibration damping can be achieved in one combined controller design process. The superiority of the new controller compared to conventional test bed controllers is demonstrated by simulation studies and by experiments on commercial test beds.

Zusammenfassung

In dieser Arbeit werden Antriebsstrangprüfstände ganzheitlich betrachtet, wobei das grundsätzliche Ziel eine Verbesserung dieser Prüfstände durch regelungstechnische Maßnahmen ist. Entscheidend sind in diesem Zusammenhang Regelgüte, Regelbandbreite und Robustheit der Regelkreise für Drehzahl sowie Drehmoment. Am Antriebsstrangprüfstand wird die Regelung dadurch erschwert, dass diese beiden grundlegenden Regelgrößen gekoppelt sind und deswegen Änderungen des Prüfdrehmomentes die Drehzahlregelung stören und Änderungen der Drehzahlen das gemessene Drehmoment beeinflussen. Ein weiteres kritisches Problem stellen Resonanzerscheinungen im mechanischen Prüfstandsaufbau dar.

Zum Entwurf und Test neuer Regelungsstrategien werden mathematische Modelle, welche die Prüfstände in ausreichendem Ausmaß beschreiben, benötigt. Da es Antriebsstrangprüfstände in verschiedensten Ausprägungen gibt, wird eine modulare Modellbildung durchgeführt. Dazu werden zuerst Komponenten, die in einem typischen Prüfaufbau vorhanden sind, wie elektrische Maschinen, Verbindungswellen oder Anpassgetriebe und mögliche Prüflinge wie Differentiale und Getriebe durch Differentialgleichungen beschrieben. Diese Teilmodelle werden dann dem aktuellen Prüfaufbau entsprechend kombiniert. Die numerische Simulation der Prüfstände wird durch die Tatsache, dass einige dieser Teilmodelle Haftreibung beinhalten und sich daher die Systemordnung ändern kann, erschwert. Für einfache Probleme dieser Art existiert eine Simulationstrategie, die dieses Verhalten korrekt wiedergeben kann, für Systeme bei denen sich die Systemordnung um mehr als Eins ändern kann, wie zum Beispiel das verlustbehaftet Sperrdifferential, wird in dieser Arbeit ein Lösungsansatz vorgeschlagen. Damit ist eine effiziente Simulation der Prüfstände möglich, dies wird anhand von drei Beispielen demonstriert.

Zur Verbesserung der Regelqualität wird auf das Verfahren der Entkopplung und Linearisierung durch Zustandsrückführung zurückgegriffen. Dieses ermöglicht es, die Entkopplung der Regelkreise für Drehmoment und Drehzahl und die Dämpfung von Resonanzerscheinungen in einem gemeinsamen Reglerentwurfsprozess zu erreichen. Die Verbesserungen, die durch die Erweiterung der Regelung realisiert werden können, werden anhand umfangreicher Simulationsstudien und durch Experimente auf kommerziellen Antriebsstrangprüfständen belegt.

Acknowledgements

In this thesis the results of a research collaboration of the Institute of Automation and Control at Graz University of Technology and KS Engineers are presented. Throughout the years many people have contributed to the work described in this thesis, and I would like to express my gratitude to all of them. For a few individuals a special appreciation is appropriate:

Special thanks go to Dr. Wilfried Rossegger and to KS Engineers for funding this research collaboration and for allowing me to perform real world experiments on their test beds. I am greatly thankful to Priv.-Doz. Dr. Robert Bauer for giving me the opportunity to work on this thesis, for his permanent support, and for the close and fruitful cooperation we had. In his role as my supervisor at KS Engineers he made sure that beside the daily working on numerous R&D projects there was always time left to proceed my PhD studies.

I also want to show my gratitude to my academic supervisor at the Institute of Automation and Control Prof. Dr. Anton Hofer for constantly motivating and encouraging me and for his invaluable advice.

Furthermore, I am thankful to Prof. Dr.-Ing. Oliver Sawodny (University of Stuttgart) for his interest in my work and for his very valuable comments.

I want to thank Prof. Dr. Nicolaos Dourdoumas for his part in establishing the research collaboration with KS Engineers and for permanently inspiring and motivating me. Many thanks also to Prof. Dr. Martin Horn for providing an excellent working environment at the Institute of Automation and Control.

I am also very grateful to my colleagues at KS Engineers and at the Institute of Automation and Control for the positive working climate, for many interesting discussions on both professional and private topics, and for their help and support whenever needed.

Finally, I would like to express my gratitude to my parents for providing me with unconditional support and permanent encouragement.

Martin Forstinger

Contents

1 Introduction **1**
- 1.1 Motivation . . . 1
- 1.2 Objectives and Contributions . . . 2
- 1.3 Structure of this Work . . . 5

2 Power Train Test Beds **7**
- 2.1 State of the Art . . . 7
- 2.2 Actuators . . . 12
  - 2.2.1 Induction Machine . . . 13
  - 2.2.2 Permanent Magnet Synchronous Machine . . . 14
- 2.3 Sensors . . . 15
  - 2.3.1 Torque Measuring Flange . . . 15
  - 2.3.2 Rotary Encoder . . . 16

3 Plant Modelling **19**
- 3.1 Overview . . . 21
- 3.2 Drive System . . . 22
- 3.3 Mechanical Shaft . . . 25
- 3.4 Adapter Gearbox . . . 27
- 3.5 Clutch . . . 28
- 3.6 Differential Gear . . . 29
  - 3.6.1 Type A: Bevel Gear Differential . . . 30
  - 3.6.2 Type B: Epicyclic Differential . . . 33
  - 3.6.3 Summary . . . 35
- 3.7 Transmission . . . 37
  - 3.7.1 Automatic Transmission . . . 37
  - 3.7.2 Simplified Models . . . 47
- 3.8 Test System for Differential Gears . . . 50
- 3.9 Test System for Differential Gears with Adapter Gearboxes . . . 52
- 3.10 Test System for Transmissions . . . 53
- 3.11 Parameter Identification . . . 54
- 3.12 Torsional Vibration Analysis . . . 56

4 Simulation 61
4.1 Friction Models 62
4.2 Numerical Simulation of Variable Dynamic Dimension Systems . 64
4.2.1 One Element Affected by Coulomb or Static Friction . . . 65
4.2.2 Two Elements Affected by Coulomb or Static Friction . . . 69
4.3 Analysis of Reduced Transmission Models 84
4.4 Test System for Differential Gears 88
4.5 Test System for Differential Gears with Adapter Gearboxes . . . 91
4.6 Test System for Transmissions 93

5 Control 97
5.1 State of the Art 98
5.2 Multivariable Control 100
5.3 Model Reduction 102
5.3.1 Test System for Differential Gears 103
5.3.2 Test System for Differential Gears with Adapter Gearboxes 105
5.3.3 Test System for Transmissions 108
5.4 Input–Output Decoupling and Feedback Linearisation 110
5.4.1 Two Machine Configuration 115
5.4.2 Three Machine Configuration 121
5.4.3 Selecting the Active Damping Parameter 125
5.5 Speed Control 125
5.5.1 PI Control 126
5.5.2 P Control with Disturbance Observer 127
5.6 Torque Control 128
5.6.1 PI Control 129
5.7 Closed-loop System Analysis 130
5.8 Closed-loop Simulation Results 134
5.8.1 Control of a Test System for Differential Gears with Adapter Gearboxes 134
5.8.2 Control of a Test System for Transmissions 141

6 Experimental Results 145
6.1 Multivariable Control of a Test Bed for Differential Gears with Adapter Gearboxes 145
6.2 Multivariable Control of a Back-to-Back Configuration 148
6.3 Active Damping Control for a Test Bed for Centre Differentials . 150

7 Handling Constraints 153
7.1 Introduction 153
7.2 Reference Governor 156
7.3 Reference Governor for a Test Bed for Differential Gears 159
7.3.1 Optimisation Based Approach 164

7.3.2 Simplified Sequential Approach 169
7.3.3 Comparative Numerical Simulations with Field Weakening 176

8 Conclusions and Outlook 179

A Fundamentals of FOC 183
A.1 Fundamental Wave Model 183
A.2 Rotor Flux Oriented Reference Frame 186
A.3 Field-oriented Control 189

B Combination of Mechanical Shafts 191

C Mathematical Model for Exemplary Mechanical System 201

D Parameters for Reduced Mechanical System 207

Bibliography 209

List of Figures

2.1 Full vehicle test systems. 7
2.2 Overview of different test bed configurations for power train testing. 9
2.3 KS R2R power train test bed with electric input drive. 9
2.4 KS R2R control concept. 10
2.5 Conventional control of a test system for differential gears. 11
2.6 Results of a numerical simulation of a test system for axle differentials with the conventional control concept. 13
2.7 Induction machine. 14
2.8 Permanent magnet synchronous machine. 15
2.9 Torque measuring flange. 16
2.10 Optical rotary encoder. 17

3.1 Test system for differentials with KS R2R frequency converters and adapter gearboxes to increase testing torque [47]. 21
3.2 Test system for transmissions with conventional inverter system. 22
3.3 Field-oriented control for induction machines, torque control loop. 23
3.4 Step response of the electromagnetic air-gap torque estimate $\hat{T}_{ag}$ at different rotational speeds. 24
3.5 Rotational dynamics modelling. 25
3.6 Torsionally flexible shaft modelling. 25
3.7 Adapter gearbox modelling. 27
3.8 Friction clutch modelling. 28
3.9 Asymmetric bevel gear differential [71]. 30
3.10 Epicyclic differential [71]. 33
3.11 Differential gear model structure. 36
3.12 9G-Tronic automatic transmission. 38
3.13 Torque converter cross section. 40
3.14 Exemplary characteristic torque converter maps. 40
3.15 Torque converter modelling. 41
3.16 9G-Tronic gear set. 42
3.17 Modular modelling approach, exemplary modelling problem. . . 43
3.18 Modular modelling approach, idea. 43

3.19 Modular modelling approach, result. 44
3.20 Modular modelling approach, comparison of simulation results with the original model and results obtained by the use of the modular approach. 45
3.21 Planetary gear set model structure. 47
3.22 Simplified gearbox modelling, approach I. 48
3.23 Simplified gearbox modelling, approach II. 49
3.24 Test system for differentials with KS R2R frequency converters. . 50
3.25 Test system for differentials, model structure. 51
3.26 Test system for differentials with adapter gearboxes to increase testing torque, model structure. 53
3.27 Test system for transmissions, model structure. 54
3.28 Experimental system identification for a test bed for differential gears with chirp signal, torques measured at the electric drives. 55
3.29 Modal analysis of a test bed for differential gears with a locking differential as UUT. 58
3.30 Modal analysis of a test bed for differential gears with an open differential as UUT. 59

4.1 Overview of different static models for friction. 62
4.2 Friction torque calculation for one-dimensional problems at $x_1 = 0$ according to the force-balancing strategy. 66
4.3 Results of a numerical simulation of a scalar system with Coulomb friction using the force-balancing strategy. 68
4.4 Friction torque calculation for two-dimensional problems at $x_1 = 0$ and $x_2 = 0$ according to the force–balancing strategy, sector ①. . 73
4.5 Friction torque calculation for two-dimensional problems at $x_1 = 0$ and $x_2 = 0$ according to the force–balancing strategy, sectors ② and ③. 74
4.6 Friction torque calculation for two-dimensional problems at $x_1 = 0$ and $x_2 = 0$ according to the force–balancing strategy, sectors ④ and ⑤. 76
4.7 Friction torque calculation for two-dimensional problems at $x_1 = 0$ and $x_2 = 0$ according to the force–balancing strategy, sectors depending on system input **u** and state vector **x**. 77
4.8 Friction torque calculation for two-dimensional problems at $x_1 = 0$ and $x_2 = 0$ according to the force–balancing strategy, friction torque T_{fr1} and x_1 dynamics. 78
4.9 Friction torque calculation for two-dimensional problems at $x_1 = 0$ and $x_2 = 0$ according to the force–balancing strategy, friction torque T_{fr2} and x_2 dynamics. 79
4.10 Mechanical system for testing the proposed Variable dynamic dimension system simulation strategy for two-dimensional problems. 81

4.11 Results of a numerical simulation of a mechanical system with two friction elements using the proposed force-balancing strategy. . . 82
4.12 Rotational speed of gearbox input n_1 and output n_2 for a non-overlapping gear shift from second to first gear on a test bed, comparative numerical simulations of different transmission models. 85
4.13 Torque at gearbox input T_1 and output T_2 for a non-overlapping gear shift from second to first gear on a test bed, comparative numerical simulations of different transmission models. 86
4.14 Rotational speed of gearbox input n_1 and output n_2 for an overlapping gear shift from first to second gear on a test bed, comparative numerical simulations of different transmission models. 87
4.15 Torque at gearbox input T_1 and output T_2 for an overlapping gear shift from first to second gear on a test bed, comparative numerical simulations of different transmission models. 88
4.16 Test system for differentials with KS R2R frequency converter, measured and simulated rotational speeds of input drive *M1* and load drives *M2* and *M3*. 89
4.17 Test system for differentials with KS R2R frequency converter, measured and simulated torques at input drive *M1* and load drives *M2* and *M3*. 90
4.18 Test system for differentials with KS R2R frequency converter, measured and simulated torques at the load drives *M2* and *M3*, detail. 90
4.19 Test system for differentials with KS R2R frequency converter and adapter gearboxes, measured and simulated rotational speeds of input drive *M1* and load drives *M2* and *M3*. 92
4.20 Test system for differentials with KS R2R frequency converter and adapter gearboxes, measured and simulated torques at input drive *M1* and load drives *M2* and *M3*. 92
4.21 Test system for transmissions with conventional inverter system, measured and simulated rotational speeds of input drive *M1* and load drive *M2*. 94
4.22 Test system for transmissions with conventional inverter system, measured and simulated torques at input drive *M1* and load drive *M2*. 94

5.1 General control problem for a test system with k electric drives. . 97
5.2 Decoupling control. 102
5.3 Reduced system model for a test bed for differential gears. 104
5.4 Reduced system model for a test bed for differential gears with adapter gearboxes. 107
5.5 Reduced system model for a test bed for transmissions. 108
5.6 Input–output decoupling and feedback linearisation principle. . 110
5.7 Proposed control structure for a test bed for transmissions. . . . 120

5.8 Proposed control structure for a test bed for differential gears with adapter gearboxes and symmetric mechanical structure implying $I_{m2} = I_{m3}$, $c_{s2} = c_{s3}$, and $i_{gb2} = i_{gb3}$. 124
5.9 Poles and damping ratio of the torque transfer function depending on the controller parameter $\widetilde{d}_{s,des.}$. 126
5.10 Conventional control structure for a test bed for differential gears with adapter gearboxes with symmetric mechanical structure implying $i_{gb2} = i_{gb3}$. 134
5.11 Control of a test bed for differential gears with adapter gearboxes, references for the differential's total output torque and for the rotational speeds of $M2$ and $M3$. 135
5.12 Control of a test bed for differential gears with adapter gearboxes, simulation results with the conventional control strategy for the controlled variables T_{sum}, n_2, and n_3. 136
5.13 Multivariable control of a test bed for differential gears with adapter gearboxes, simulation results with the proposed control strategy and active damping only for the controlled variables T_{sum}, n_2, and n_3. 137
5.14 Simulation results for T_{sum} with act. damping, decoupling, and varying $\hat{I}_1$, real testing torque at the UUT and testing torque estimated by considering gearbox losses according to Equation (5.96). . . . 138
5.15 Simulation results for T_{sum} with act. damping, decoupling, and varying $\hat{I}_1$, real testing torque at the UUT and testing torque estimated by considering gearbox losses and acceleration torques according to Equation (5.98). 138
5.16 Simulation results for rotational speed n_2 with different speed controllers with and without decoupling. 139
5.17 Simulation results for a ramp response of n_2 with different speed controllers for complete decoupling and active damping only. . . 139
5.18 Simulation results for a ramp response of the differential gear's total output torque T_{sum} with decoupling, active damping, and varying damping parameter $\widetilde{d}_{s,des.}$. 140
5.19 Conventional control structure for a test bed for transmissions. . 141
5.20 Control of a test system for transmissions, simulated flange torques T_{f1} and T_{f2} for the conventional controller and the proposed multivariable control. 141
5.21 Control of a test system for transmissions, simulated rot. speeds n_1 and n_2 for the conventional controller and the proposed multivariable control. 142

6.1 Measured and simulated rotational speeds on a test bed for axle differentials with adapter gearboxes with the conventional control. 146
6.2 Measured and simulated torques on a test bed for axle differentials with adapter gearboxes with the conventional control. 146

6.3 Measured and simulated rotational speeds on a test bed for axle differentials with adapter gearboxes with input–output decoupling and active damping. 147
6.4 Measured and simulated torques on a test bed for axle differentials with adapter gearboxes with input–output decoupling and active damping. 147
6.5 Back-to-back testing configuration with KS R2R frequency converters. 148
6.6 Back-to-back testing configuration, changes of testing torque with and without active damping applied to electric drive *M1*. 149
6.7 Back-to-back testing configuration, changes of testing torque with and without load torque compensation for the load drive *M2*. . . 150
6.8 Measured rotational speeds on a test bed for centre differentials with and without active damping. 151
6.9 Measured torques on a test bed for centre differentials with and without active damping. 151

7.1 Operating range of an electric drive. 154
7.2 Multivariable control of a test bed for differential gears, torque control w.r.t. the differential's input torque. 155
7.3 Reference governor structure. 156
7.4 Reference governor implementation. 164
7.5 Multivariable control of a test bed for differential gears, simulation results obtained by the use of an optimisation based reference governor with varying prediction horizon k^*, constant α_T, and varying weighting parameter α_ω, shaped and original references. 166
7.6 Multivariable control of a test bed for differential gears, simulation results obtained by the use of an optimisation based reference governor with varying prediction horizon k^*, constant $\alpha_T = 1$, and varying weighting parameter α_ω, manipulated variables. 167
7.7 Multivariable control of a test bed for differential gears, simulation results obtained by the use of an optimisation based reference governor with prediction horizon $k^* = 0$, constant α_T, and varying weighting parameter α_ω, shaped references and controlled variables. 168
7.8 Simplified sequential reference governor approach. 170
7.9 Simplified sequential reference governor approach, detail. 172
7.10 Reference governor simplified approach, step ⑥. 172
7.11 Multivariable control of a test bed for differential gears, comparative simulation results obtained by the use of a reference governor without prediction with sequential reference shaping and an optimisation based reference governor with constant parameters $\alpha_T = 1$ and $\alpha_\omega = 100$, shaped and original references. 173

7.12 Multivariable control of a test bed for differential gears, comparative simulation results obtained by the use of a reference governor without prediction with sequential reference shaping and an optimisation based reference governor with constant parameters $\alpha_T = 1$ and $\alpha_\omega = 100$, manipulated variables. 175
7.13 Multivariable control of a test bed for differential gears, comparative simulation results obtained by the use of the simple sequential reference shaping and an optimisation based reference governor with constant parameters $\alpha_T = 1$ and $\alpha_\omega = 100$, original and shaped references with field-weakening. 176
7.14 Multivariable control of a test bed for differential gears, comparative simulation results obtained by the use of the simple sequential reference shaping and an optimisation based reference governor with constant parameters $\alpha_T = 1$ and $\alpha_\omega = 100$, manipulated variables with field-weakening. 177

A.1 Reference frames relevant for field-oriented control of induction machines. 185
A.2 Field-oriented control of induction machines, control concept. . . 189

B.1 Three-mass oscillator. 191
B.2 Three-mass oscillator with $I_3 \to 0$. 191
B.3 Two-mass oscillator. 192
B.4 Conjugate complex zero of the characteristic polynomial of the exact dynamic model including two elastic shafts and of the simplified two-mass oscillator with only one shaft for two parameter settings and varying d_{s2}. 198
B.5 Simulated rotational speed n_1 for the exact dynamic model including two elastic shafts and for the simplified two-mass oscillator with only one shaft. 199
B.6 Simulated rotational speed n_2 for the exact dynamic model including two elastic shafts and for the simplified two-mass oscillator with only one shaft. 199

List of Tables

3.1 Shifting table Daimler 9G-Tronic. 39
3.2 Mechanical system parameters for exemplary modular modelling problem. 45

4.1 Friction torque calculation for two-dimensional problems at $x_1 = 0$ and $x_2 = 0$ according to the force–balancing strategy, friction torques T_{fr1} and T_{fr2} depending on the sectors specified in Figure 4.7. . . 78
4.2 CPU-time of a 70 s numerical simulation of a test bed for differential gears. 91
4.3 CPU-time of a 100 s numerical simulation of a test bed with adapter gearboxes for differential gears. 93
4.4 CPU-time of a 70 s numerical simulation of a test bed for automatic transmissions. 95

7.1 Operating ranges of the electric drives *M1*, *M2*, and *M3* on a test bed for differential gears. 165

B.1 System parameters for the comparative analysis of the three-mass oscillator with $I_3 \to 0$ and the simplified two-mass oscillator. . . 198

C.1 Mechanical system parameters for an exemplary test system for differential gears. 205

D.1 Parameters for the reduced mechanical system of a test bed for differential gears with adapter gearboxes. 207

List of Abbreviations

2WD	Two-wheel drive
4WD	Four-wheel drive
ABS	Anti-lock braking system
ASR	Acceleration skid control
AT	Automatic transmission
AW	Anti-windup
BIBO	Bounded input – bounded output
CVT	Continuously variable transmission
DCT	Dual-clutch transmission
DTC	Direct torque control
ECU	Electronic control unit
ESP	Electronic stability program
FOC	Field-oriented control
ICE	Internal combustion engine
IGBT	Insulated gate bipolar transistor
IM	Induction machine
LTI	Linear time-invariant
MIMO	Multiple-input multiple-output
MPC	Model predictive control
PI	Proportional-integral
PID	Proportional-integral-derivative
PMSM	Permanent magnet synchronous machine
R2R	Road to Rig
RLS	Road load simulation
SISO	Single-input single-output
UUT	Unit under test
VDDS	Variable dynamic dimension system

Glossary

Symbol	**Definition**	**Unit**
φ	Angular position	rad
ω	Angular velocity	rad/s
n	Rotational speed	rpm
T	Torque	N m
I	Moment of inertia	$\mathrm{kg\,m^2}$
T_{ag}	Air-gap torque	N m
$\hat{T}_{ag}$	Estimated air-gap torque	N m
$T_{ag,ref.}$	Air-gap torque reference	N m
T_f	Shaft torque measurement	N m
I_m	Rotor inertia electric drive	$\mathrm{kg\,m^2}$
$T_{ag,max}$	Maximum air-gap torque electric drive	N m
$T_{ag,min}$	Minimum air-gap torque electric drive	N m
ω_{max}	Maximum angular velocity electric drive	rad/s
ω_{min}	Minimum angular velocity electric drive	rad/s
ω_r	Rated angular velocity electric drive	rad/s
$T_{ref.}$	Torque reference	N m
$n_{2,ref.}$	Rotational speed reference, drive $M2$	rpm
$n_{3,ref.}$	Rotational speed reference, drive $M3$	rpm
T_s	Shaft torque	N m
c_s	Shaft stiffness parameter	N m/rad
d_s	Shaft damping coefficient	N m s/rad
θ_{bl}	Backlash gap	rad
T_c	Clutch torque	N m
T_{ci}	Input torque clutch	N m
T_{co}	Output torque clutch	N m
ω_{ci}	Input angular velocity clutch	rad/s
ω_{co}	Output angular velocity clutch	rad/s

Symbol	Definition	Unit
i_d	Transmission ratio differential	–
T_{dl}	Loss torque differential	N m
T_{dsl}	Slip-limiting torque differential	N m
T_{di}	Torque differential input	N m
T_{do1}	Torque differential output 1	N m
T_{do2}	Torque differential output 2	N m
T_{sum}	Total output torque differential	N m
ω_{di}	Angular velocity differential input	rad/s
ω_{do1}	Angular velocity differential output 1	rad/s
ω_{do2}	Angular velocity differential output 2	rad/s
i_{gb}	Transmission ratio gearbox	–
T_{gbi}	Input torque gearbox	N m
T_{gbo}	Output torque gearbox	N m
ω_{gbi}	Angular velocity gearbox input	rad/s
ω_{gbo}	Angular velocity gearbox ouput	rad/s
ζ	Damping ratio of second order differential equation	–
ω_0	Natural angular frequency of second order differential equation	rad/s
T_{fr}	Friction torque	N m
$T_{fr,c}$	Coulomb friction torque	N m
$T_{fr,v}$	Viscous friction torque	N m
$T_{fr,s}$	Static friction torque	N m
N	System order	–
m	Number of system inputs, number of system outputs	–
$\mathbf{A}$	Dynamic matrix	
$\mathbf{B}$	Input matrix	
$\mathbf{C}$	Output matrix for state variables	
$\mathbf{D}$	Output matrix for system inputs	
$\mathbf{x}$	State vector	
$\mathbf{u}$	Input vector	
$\mathbf{y}$	Output vector	
$\mathbf{T}_{fr}$	Vector containing friction torques	
$\mathbf{K}$	Friction torque matrix	
$\mathbf{k}$	Friction torque vector	
$\mathbf{w}$	Input vector for decoupled system	
$\mathbf{v}$	Input vector for decoupled system with specified dynamics	

Symbol	Definition	Unit
$\mathbf{r}$	Reference vector	
$\widetilde{\mathbf{r}}$	Shaped reference vector	
$\widetilde{\mathbf{y}}$	Vector of constrained system outputs	
$\boldsymbol{\delta}$	Vector relative degree	
δ	Total relative degree	–
δ_i	Relative degree of system output y_i	–
$\overline{\mathbf{D}}$	Decoupling matrix	
T_d	Sampling interval	s
R_ω	Controller for angular velocity	
R_T	Controller for torque	
$\widetilde{d}_{s,des.}$	Active damping controller gain	N m s/rad
$T_{damp.}$	Torque for damping torsional vibrations	N m
$T_{accel.}$	Decoupling torque for accelerating the input drive	N m
$\widetilde{\mathbf{O}}_\infty$	Reference governor safe set	
k^*	Reference governor prediction horizon	–
α_T	Reference governor weighting parameter for torque	–
α_ω	Reference governor weighting parameter for angular velocity	–

Chapter 1

Introduction

1.1 Motivation

In recent years, the importance of test rigs has significantly risen in various industries. Having the possibility to perform tests under well-defined, reproducible conditions has become a necessity in *product development* as well as in *quality management processes*. For this reason, it is not surprising that also in the automotive industry test beds have become an essential tool. This holds for the vehicle development process [1] as well as for quality assurance by end-of-line testing [2]. Vehicle developers are facing great challenges such as reducing emissions, automated driving, or the electrification of the power train. To succeed in finding solutions for those problems is highly dependent on the availability of adequate test systems. But as the demands regarding vehicle development and the complexity of new power train systems are increasing, the test beds have to enhance too. While early testing solutions were primarily used for stationary testing, *highly dynamic* test beds are demanded nowadays to be able to provide realistic testing also in transient situations [3, 4]. Especially the electrification of the power train is a great challenge in automotive testing. Inserting electric motors in the power train often significantly increases the amount of testing required as these new power train configurations are more complex. Furthermore, typically rotational speeds and torque dynamics are higher causing new difficulties for test bed design and control. Another challenge is the increasing number of driver assistance systems related to automated driving. Therefore, with the progress in vehicle development and power train design also the test beds have to evolve. To be able to perform the desired realistic testing, the test systems have to be capable of emulating highly dynamic loads that are close to real world driving situations [5]. Many of the challenges in doing so can be addressed by modern control engineering techniques.

The advantages of using sophisticated test systems are numerous: as already mentioned, tests are reproducible, testing conditions can easily be altered, tests can be performed in a safe environment, and various components can be tested individually. This last point makes them important for the so-called *front-loading* strategy in the development process. Thereby, the strategy of moving ('loading') large quantities of development work in the early stages ('front') of the product development process is denoted, see e.g. [6]. This allows the number of prototype test vehicles to be reduced and development time to be shortened since a parallel development of the car's components is possible. If adequate test systems are available, these automotive components can be tested individually while the vehicle's remaining power train is emulated by software and electric drives so that the testing conditions are close to the loads arising in typical driving manoeuvres. If in this way problems can be identified and resolved early, potentially lots of money and development time can be saved.

1.2 Objectives and Contributions

Among the wide variety of test systems used in the automotive industry, this thesis focuses on so-called *power train test beds*. These test beds are used to test the vehicle's full power train or only some power train components. In the automotive context the term *power train* commonly describes those vehicle components that generate the mechanical power and deliver it to the road surface. This traditionally includes the engine, clutch, transmission, drive shaft, differential gear, side shafts, and wheels [7]. In modern hybrid vehicles also the batteries, inverters, and electric drives have to be considered. Commonly, testing only the internal combustion engine (ICE) is done on so-called engine test beds and is thus excluded here [8]. In general, except for some basic considerations in the next chapter, power train testing configurations including an ICE will not be further discussed; consequently, the subject of this work is actually testing the *driveline*, which typically includes all parts between the engine and the wheels [7].

The aim of this work is to increase the performance of the considered test systems and to extend their range of application via new approaches regarding control. More precisely, the tracking of references for the relevant mechanical quantities rotational speed[1] and torque shall be enhanced. As the availability of these test beds for controller testing is often limited and applying a new control strategy directly on the plant is risky, simulation is an essential tool. Therefore, a special focus is placed on deriving mathematical models covering the entire test system that can be used for numerical simulation. An important requirement for these models is that they can be parametrised with reasonable effort, but nonetheless capture all the details important for assessing new controllers. One particular goal is that a modelling framework is developed that can be applied to different types of power train test systems (see e.g. Figure 2.2). As their mechanical structure strongly depends on the power train configuration to be tested, finding a mathematical model that can cover every relevant testing situation is probably impossible. To be able to handle this mechanical diversity, a *modular* modelling approach is applied. At first, a library consisting of compact mathematical models for the components typically required for testing such as electric drive systems, mechanical shafts, and adapter gearboxes is presented. This library also contains models for the power train components to be tested such as clutches, differential gears, or transmissions. All these models are developed in particular for test bed simulation; therefore, they are partially different than publicly available models for other purposes. By the use of this model library, a mathematical model for the entire test system can be easily put together by combining these individual models. This modelling approach significantly reduces the modelling effort as many of the individual sub-models can be reused when another test system has to be modelled.

---

[1] Although according to the International System of Units the angular movement of a body is specified by its angular velocity ω given in rad/s, among practitioners rotational speed n given in revolutions per minute (rpm) is widely used instead.

When the test bed behaviour shall be analysed, usually numerical simulations are performed. These are complicated by the physical nature of many power train components. Their working principle is often based on using Coulomb and static friction to first synchronise and finally lock together rotating bodies. One typical example is the clutch. A system showing this behaviour is called a *variable dynamic dimension system (VDDS)* because the system order is reduced when some bodies are forced to the same angular velocity. To handle this situation correctly and computationally efficient, a special simulation strategy is required. One approach traditionally used to simulate VDDSs is often referred to as *force-balancing*; this idea was proposed by Karnopp in 1985 [9]. The basic principle is that when two bodies are locked together, friction is calculated to exactly maintain this sticking situation. When more than two bodies that can lock together are involved, this basic concept must be extended. Strategies that can handle these problems as well can be found in literature, see e.g. [10]. However, with these approaches friction is calculated physically incorrect in some situations. For this reason, this work presents a friction simulation approach for systems with a maximum order reduction of two that can solve the friction calculation problem correctly. This algorithm can then be used to simulate a lossy limited-slip differential or a simplified dual-clutch transmission (DCT) model. Additionally, it is outlined how the friction calculation scheme can be extended for systems with even more friction elements.

Based on these mathematical models and the efficient friction simulation strategy, numerical simulations of test beds can be performed to identify the control related problems. It is shown that, although the phrase *power train test bed* covers a wide range of different testing solutions, the aspects relevant for control are very similar. The basic challenge is in general to control the electric drives typically used to test the unit under test (UUT). Control has to make sure that the reference signals for testing rotational speed and testing torque are adequately tracked. As test beds are *multivariable dynamic systems*, these mechanical quantities are always coupled. This makes an independent control of rotational speed and torque difficult, see e.g. [11, 12]. With the conventional control strategy based on individually designed tracking controllers for rotational speed and torque, this coupling often negatively affects control performance, in particular if the test-run contains fast changes of testing torque or testing rotational speed. Furthermore, due to potentially low internal damping in the mechanical structure, special focus has to be placed on the damping of *resonant torque oscillations*. These two problems shall be resolved by the use of improved control strategies. Important requirements regarding control are that controllers can be executed in real-time, that they are robust with respect to a modification of the mechanical test set-up, and that they can be parametrised by practitioners who are no experts in control engineering.

To overcome both mentioned problems, a *multivariable control* approach is applied. This control concept is based on input–output decoupling and feedback linearisation. Before the controller can be determined, a suitable plant model must be identified. Therefore, a way to reduce the rather detailed models used for simulation is shown. These physically motivated simplifications are used to develop significantly simpler models for differential gear test systems and for transmission test beds. The decoupling controllers are then determined based on these mathematical models. To enable test bed operators to continue to use their preferred controllers, the control problem is solved in two steps. In the first stage, decoupling the control loops and vibration damping is ensured. It is shown that both of these goals can be achieved within one combined controller design process. The resulting decoupling and damping network is only based on system states that are measured; therefore, no state observe is required. This ensures that the number of tuning parameters is kept small. These decoupling controllers for two and three machine testing configurations are one main contribution of this work. In a second stage, feedback controllers for rotational speed and torque are added. Since the control loops are decoupled and torsional vibrations are already sufficiently damped, designing the feedback controllers is easier compared to the conventional control approach. Simulation studies and experimental results indicate that control performance can be significantly improved with the proposed multivariable control concept.

One drawback of the multivariable control strategy is that handling *actuator constraints* such as limited electromagnetic torque becomes more complicated. For this reason, a reference shaping pre-filter according to the reference governor approach is added. Reference profiles that are too demanding are then corrected and constraint violations can be avoided. Since solving the optimisation problem within the reference governor algorithm is problematic regarding real-time execution, a reduced pre-filter is presented as well. This structure does not rely on any prediction into the future and is consequently computationally significantly simpler. Furthermore, instead of solving a global optimisation problem, a sequential reference calculation scheme is used. Nevertheless, for the discussed test system the results are very close to the optimisation based approach.

1.3 Structure of this Work

This document is organised as follows: In Chapter 2 an overview of available power train test systems is given. Different testing strategies are presented and various common testing configurations with varying scope of testing are shown. Furthermore, the control concept often used in industrial practice is briefly explained and problems related to this type of control are visualised by a numerical simulation. The chapter is closed by a short description of sensors and actuators normally available on these test beds. In Chapter 3 various modelling aspects are discussed. Following a modular modelling approach, at first mathematical models describing the dynamics of individual test bed components are presented. This model library covers typical test bed components such as electric drives, mechanical shafts, and adapter gearboxes as well as the power train elements to be tested such as differential gears or transmissions. Finally, these sub-models are combined to model three exemplary real-world testing configurations: two test systems for differential gears and a test bed for automatic transmissions (ATs). At the beginning of Chapter 4 simulation issues caused by friction models involving Coulomb and static friction are discussed. As these friction models can accurately describe many phenomena occurring in the power train, they are widely-used for power train modelling. Therefore, suitable simulation strategies for these special dynamic systems are presented. Then the results of simulation studies based on the developed friction calculation approach are presented. These simulations start with an analysis of various transmission models with different complexity, and are concluded by a verification of the simulation models for the test systems discussed in Chapter 3 via comparison with experimental data. The control of power train test beds is discussed in Chapter 5. At the beginning of this chapter the detailed mathematical models used for simulation are reduced to cover only the most essential test bed dynamics. By the use of these dynamic systems, controllers based on input–output decoupling and feedback linearisation are determined for two and three machine testing configurations. Furthermore, feedback controllers for rotational speed and torque are discussed and tested in numerical simulations. In Chapter 6 some measurement data are given, which show the performance of the proposed modifications regarding control for selected commercial power train test systems. Finally, the admissible operating range of a test bed for differential gears is discussed in Chapter 7. To avoid that the operational limits of the electric drives are exceeded, a pre-filter following the reference governor approach is proposed. This chapter is concluded by the presentation of a reduced reference governor structure that is executable in real-time.

Chapter 2

Power Train Test Beds

2.1 State of the Art

There are various test systems available to test the power train or driveline of a vehicle [13]. Traditionally, roller chassis dynamometers (see e.g. Figure 2.1a) were applied to test the entire vehicle; those are still used for quantifying exhaust emissions and fuel consumption according to standardised driving cycles [14]. Additionally, as on these test systems the tyres are really rotating, an assessment of noise emissions is possible. However, due to the heavy rotating rollers, the dynamics achievable with these test beds is rather limited.

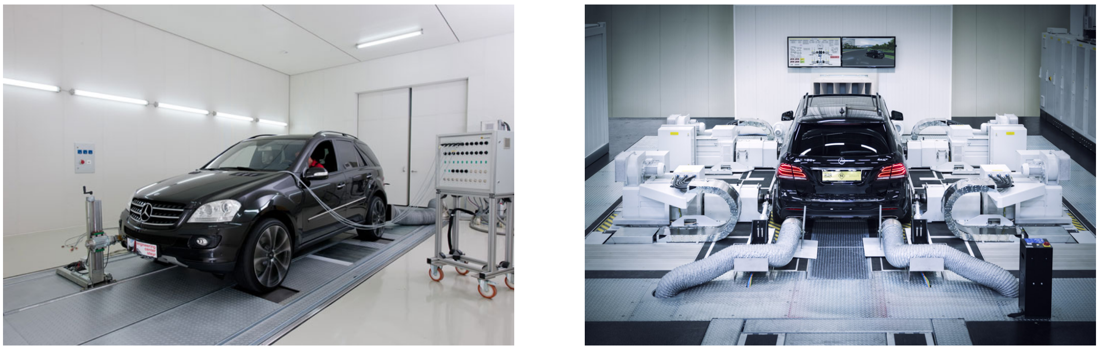

(a) Roller chassis dynamometer, © KS Engineers.

(b) KS R2R full vehicle Road to Rig test bed, © KS Engineers.

Figure 2.1: Full vehicle test systems.

Therefore, a new generation of test systems was developed (see e.g. Figure 2.1b); instead of using rollers the electric drives are attached directly to the driveline [5, 15, 16]. To do so, either special test wheels are used or the electric motors are directly connected to the side shafts. This testing concept brings two main advantages compared to a roller chassis dynamometer: lower inertias introduce the possibility to increase the dynamics to be able to perform more realistic tests and additionally, this type of testing solution offers the chance to test not the entire vehicle but just some components and to emulate the remaining parts by software. These advantages are coming with the different mechanical set-up; to be able to fully utilise them, sophisticated control strategies are required [5, 16].

Increased dynamic capabilities are especially important to provide realistic testing for all road conditions and driving manoeuvres. The test systems have to cover the range from dry to icy road, have to handle interventions from driver assistance systems such as anti-lock braking system (ABS), acceleration skid control (ASR), or electronic stability program (ESP) and also have to be able to manage misuse tests such as sidestepping the clutch or turning with hand brake on. These dynamic requirements are a challenge in the design of controllers for the electric machines used to emulate the road loads. Therefore, in addition to powerful hardware, sophisticated controllers for rotational speed and torque are desperately needed. The more realistic the tests performed on the power train test beds are, the more they can be used in the vehicle development process, for instance for electronic control unit (ECU) application on the test bed, see e.g. [3, 4, 17–19].

The second important advantage, scalability of the scope of test, is mostly challenging for the overall test bed control system as 'missing' vehicle components might have to be emulated by software. Thus, appropriate models for these emulated components are needed. This component based testing is getting more important in the vehicle design process since development and testing of various components can be performed parallel. Possible applications would be testing the power train while the vehicle chassis is not yet available or testing a transmission while the remaining power train components are still in development. In Figure 2.2 various settings for power train test systems are shown exemplarily. Figure 2.2a and Figure 2.2b present testing scenarios for the complete driveline, while in Figure 2.2c and Figure 2.2d just single components are tested. In Figure 2.2a the testing of the power train of a four-wheel drive (4WD) vehicle is shown; one can see that electric load machines are attached to all four side shafts to emulate the road loads. The input drive could be the ICE or an additional electric drive. In Figure 2.2b a similar situation is presented; since the UUT is now a driveline for a two-wheel drive (2WD) vehicle, just two electric load machines are required. In Figure 2.2c a testing scenario for a transmission is presented; here typically electric drives are used as input and load machine. Finally, in Figure 2.2d a test system for a differential is shown where electric drives are again used as input and load machines. Figure 2.2 is presenting just a selection of the most popular testing scenarios; in general, any driveline component, thus also a single clutch or shaft, or any meaningful combination of those elements can be tested. Not shown, but sometimes also applied are additional up- or downspeed gearboxes to be able to deliver the desired testing conditions regarding rotational speed and torque with given electric drives.

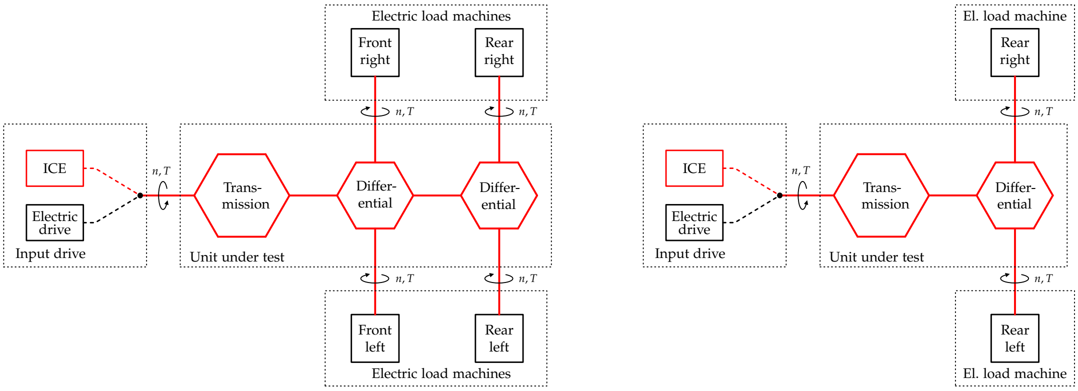
Electric load machines
Front right
Rear right
n, T
n, T
ICE
Electric drive
Input drive
n, T
Trans-mission
Differ-ential
Differ-ential
Unit under test
n, T
n, T
Front left
Rear left
Electric load machines
El. load machine
Rear right
n, T
ICE
Electric drive
Input drive
n, T
Trans-mission
Differ-ential
Unit under test
n, T
Rear left
El. load machine

(a) 4WD driveline testing.

(b) 2WD driveline testing.

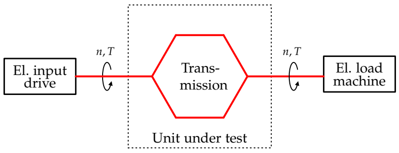
El. input drive
n, T
Trans-mission
n, T
El. load machine
Unit under test

(c) Transmission testing.

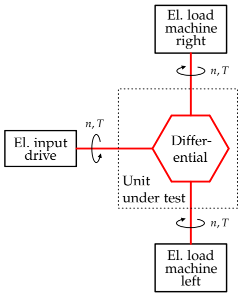
El. load machine right
n, T
El. input drive
n, T
Differ-ential
Unit under test
n, T
El. load machine left

(d) Differential testing.

Figure 2.2: Overview of different test bed configurations for power train testing.

Since including the ICE in the tests has many drawbacks such as the necessary supply with fuel, cooling water, and charge air and the effort to handle exhaust gases and heat, the ICE is often replaced by an electric drive [20]. For this reason, testing scenarios including an ICE will not be discussed any further in this work. Exemplarily, a test set-up where the ICE is replaced by an electric drive and consequently just the driveline is tested is shown in Figure 2.3.

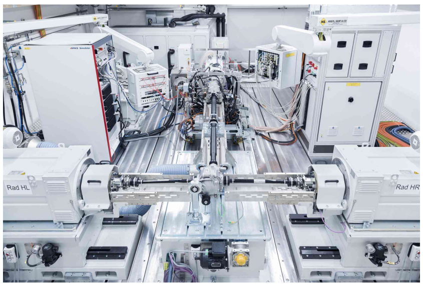

Figure 2.3: KS R2R power train test bed with electric input drive, © KS Engineers.

Although according to Figure 2.2 there are many different variants of power train test systems, the control related aspects are similar. Basically, the electric drives are always operated either in speed or torque control mode where torque control could be with respect to the measured shaft torque or with respect to the machine's electromagnetic torque. Complexity regarding control is strongly related to the amount of simulation demanded; the more models must be included, the more the complexity rises. If the driveline shall be tested in a most realistic test set-up according to Figure 2.4, at least models for the ICE, wheels and tyres, and the vehicle dynamics are required. If just the transmission shall be tested using this Road to Rig (R2R) strategy, the complexity may be increased even further as then additional models for the differentials and various mechanical shafts are needed. On the other hand, a power train test bed may also be manually operated where references for torque and rotational speed are given directly. These references could either be defined by standardised testing procedures or by measurements carried out on the test track. This wide variety of different testing strategies and test bed operation modes requires to restrict the scope of this work to some particular problems. For this reason, in this thesis the focus is placed on improving speed and torque control. This task may seem to be simpler and thus less significant than the model based testing strategies previously explained, but eventually all these different testing modes are based on reliable underlying speed and torque control. Therefore, improving these basic control modes might have a positive impact on other more advanced testing strategies as well.

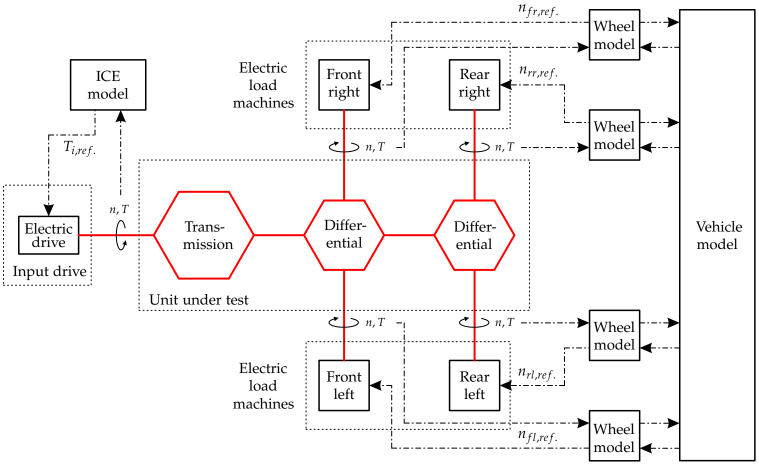
ICE model
$T_{i,ref.}$
Electric drive
Input drive
n,T
Electric load machines
Front right
Rear right
$n_{fr,ref.}$
$n_{rr,ref.}$
Wheel model
Wheel model
n,T
n,T
Trans-mission
Differ-ential
Differ-ential
Unit under test
Vehicle model
n,T
n,T
Wheel model
Electric load machines
Front left
Rear left
$n_{rl,ref.}$
$n_{fl,ref.}$
Wheel model

Figure 2.4: KS R2R model based control concept, © KS Engineers.

Although power train test beds are a very common tool in the automotive industry, there is not much research work available dealing with the speed and torque control on these test beds. [11] and [12] are some of the few publications on designing and controlling power train test systems. In both works multivariable control strategies were proposed to reduce the coupling of the controlled variables, which is negatively affecting the control loops. But the authors discussed rather special problem settings. The control strategy often applied in practice is to use proportional-integral-derivative (PID) controllers to control each electric drive individually. Typically, first the speed control loops are closed, then the torque controllers can be designed to reach acceptable closed-loop dynamics [21]. With this strategy the control performance might be satisfying in steady-state, but rotational speed and torque are still coupled in dynamic operation.

The state of the art regarding test bed control shall be explained on the basis of the test set-up for differential gears as presented in Figure 2.2d and in Figure 2.5 in more detail. On a test bed for axle differential gears often a torque reference and two references for rotational speeds are given. The torque reference $T_{ref.}$ may be specified for the differential gear's input or for the total output torque. The references for rotational speeds are mostly given for the differential gear's outputs, either directly as total speeds for both individual outputs, or as the mean rotational speed in combination with the desired difference in rotational speeds. As these signals can always easily be converted to total rotational speeds, henceforth it will be assumed that these total references $n_{2,ref.}$ and $n_{3,ref.}$ are given. Each electric drive is equipped with an encoder to measure the rotational speeds n_1, n_2, and n_3. Frequently also a torque sensor is available to measure the shaft torques T_{f1}, T_{f2}, and T_{f3} directly at the electric motor. These measurement systems are further discussed in Section 2.3. The actuators from a control engineering point of view are the electric drives where typically the desired electromagnetic air-gap torques $T_{ag1,ref.}$, $T_{ag2,ref.}$, and $T_{ag3,ref.}$ are used as control inputs. In Section 2.2 the electric machines usually employed for automotive testing are briefly described.

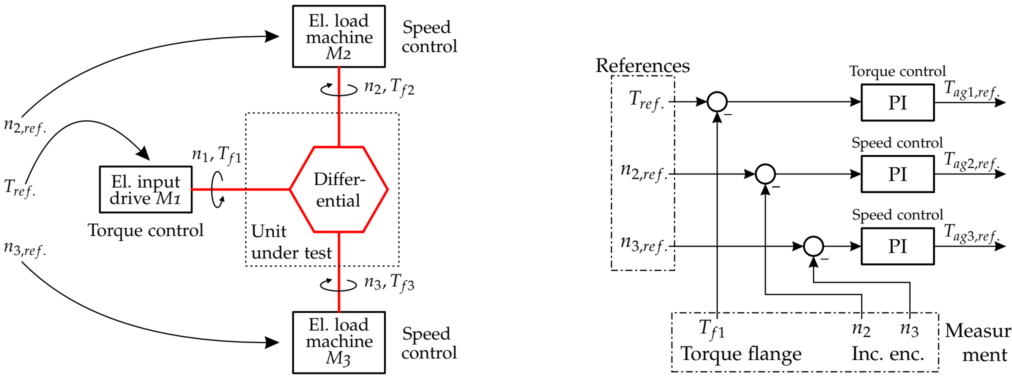
El. load machine M2
Speed control
n_2, T_{f2}
$n_{2,ref.}$
n_1, T_{f1}
$T_{ref.}$
El. input drive M1
Torque control
Differential
Unit under test
$n_{3,ref.}$
n_3, T_{f3}
El. load machine M3
Speed control
References
Torque control
$T_{ref.}$
PI
$T_{ag1,ref.}$
Speed control
$n_{2,ref.}$
PI
$T_{ag2,ref.}$
Speed control
$n_{3,ref.}$
PI
$T_{ag3,ref.}$
T_{f1}
Torque flange
n_2 n_3
Inc. enc.
Measurement

(a) Differential testing, control concept. **(b)** Block diagram control structure.

Figure 2.5: Conventional control of a test system for differential gears.

As previously mentioned, a classic electric drive system can be operated in either speed or torque control mode; since there are two speed references and one torque reference, running two drives in speed control mode and the third one in torque control mode is a reasonable choice. Figure 2.5a presents the setting that is widely-used: the input drive is torque controlled to track the given torque reference while the remaining drives are speed controlled to track the given rotational speed set-points. As the rotational speeds of a differential's input and outputs are algebraically joint, an alternative setting such as operating *M2* in torque control mode and *M1* in speed control mode is also possible, but rarely used. Often, practitioners use proportional-integral (PI) feedback controllers since parameter tuning is relatively simple and vanishing steady-state tracking error can be achieved. Figure 2.5b shows the corresponding controller block diagram; this control approach is obviously based on single-input single-output (SISO) models: the control loops are designed separated from each other and every air-gap torque is just related to one control loop. This implies that each controller cannot consider the control actions executed by the other controllers. Because of the mechanical test bed set-up the controlled variables rotational speed and torque are coupled; thus, the control loops are coupled as well. With the SISO controller setting often satisfying speed control performance can be achieved while controlling the testing torque is typically rather difficult. This can be seen in Figure 2.6 where simulation results of the testing situation shown in Figure 2.5a are presented. It can be seen that the speed control performance is rather good; even the fast change of testing torque at $t = 4\,\mathrm{s}$ causes only some minor speed tracking error. In the testing torque though the coupling of the control loops is more obvious; while the rotational speed is changed the testing torque is not kept at its reference value.

Additionally, within this conventional approach the torsional flexibility of the mechanical system and thus resonance phenomena are not considered in the controller design. As the control actions are based on their associated individual tracking errors only, reasonable vibration damping is hard to achieve. This is also demonstrated in Figure 2.6; whenever the shaft torques vary, either because of a change of testing torque or because of a change in rotational speed, torsional vibrations are excited, which negatively affect the torque control performance.

2.2 Actuators

From a control engineering point of view the electric drives are the actuators on these test beds, the input drives delivering the testing torque as well as the dynamometers representing the loads. In the majority of cases, these are either *induction machines (IMs)* with squirrel cage rotor or *permanent magnet synchronous machines (PMSMs)*. Both types have their individual advantages and disadvantages and the appropriate drives have to be selected according to the testing objectives. For the use in automotive testing applications precise torque and speed control is essential; therefore, an inverter system typically based on insulated gate bipolar transistors (IGBTs) is required. Generally, full four-quadrant operation is desired, i.e. torque can be absorbed and delivered for clockwise and anticlockwise rotation and

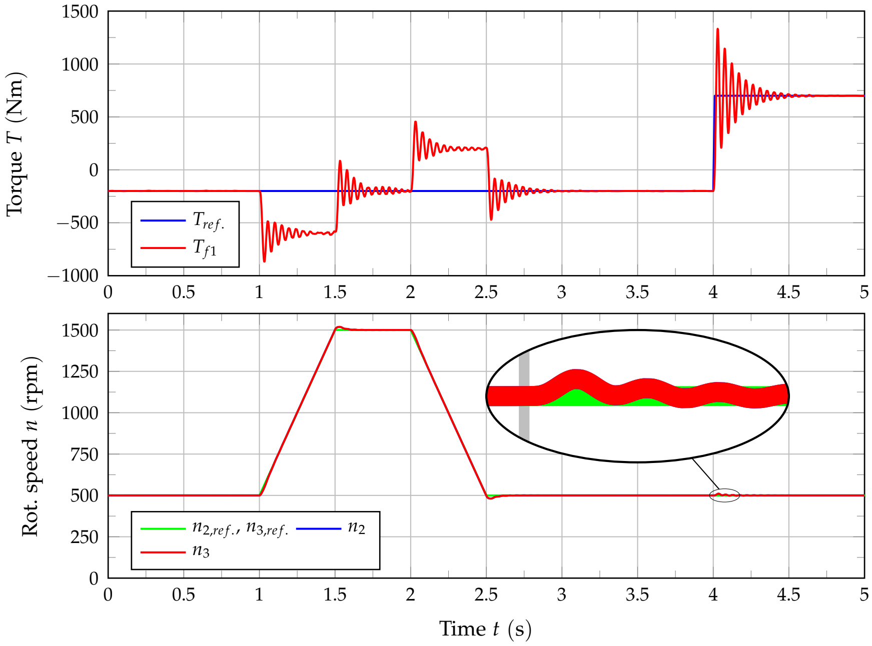

Figure 2.6: Results of a numerical simulation of a test system for axle differentials with the conventional control concept.

consequently the energy flow can be from the grid to the drive system and vice versa. With field-oriented control (FOC) and direct torque control (DTC) there are two well-established control strategies for three-phase motors available making sure that the electric machine's supply voltage is chosen such that the desired electromagnetic torque is produced. Both motor types provide their rated torque, possibly even more if the inverter offers overload capacity, for varying rotational speed beginning at standstill. But due to limited DC-voltage in the inverter, the disposable torque has to be reduced above some rotational speed (field weakening).

Passive dynamometers such as eddy current brakes, water brakes, or friction dynamometers are normally not used for power train testing and are therefore not considered any further [13]. Other actuators that might be used on a power train test bed such as actuators for throttle, brakes, and gear shifting or conditioning systems are not considered either since they are not relevant for speed and torque control.

2.2.1 Induction Machine

IMs, especially those with squirrel cage rotor, are widely used in industry nowadays. Also for automotive testing applications asynchronous machines play an important role. Figure 2.7a shows a simplified cross section of a typical IM. In the stator three separate coils form the three-phase stator windings. The rotor is separated from the stator by the air-gap. For squirrel cage motors the rotor slots are just filled with conductive bars that are short circuited at front and rear forming a cage [22, 23]. In Figure 2.7b a exemplary IM used for power train testing is shown. The IM's advantages compared to PMSMs are numerous: The motor itself is cheaper as no permanent magnets are needed and as there are more suppliers on the market. Additionally, for a given torque specification typically a smaller inverter is sufficient. These two facts make the overall drive system consisting of motor and inverter significantly cheaper. Furthermore, they are more robust because there are no permanent magnets involved that could be demagnetised due to over current or over temperature. There are also advantages regarding safety and misuse as e.g. there is no induced voltage at the motor terminals when the machine is rotating while the inverter is switched off and a switch off in the field weakening region is uncritical [13].

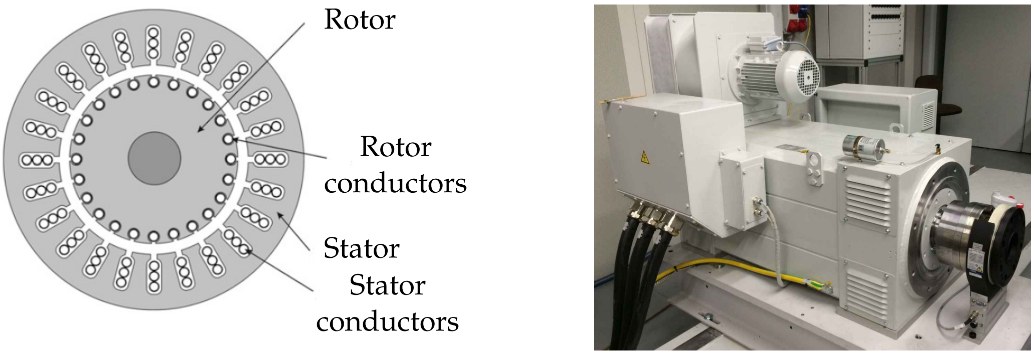

(a) Induction machine, cross section [22]. **(b)** Induction machine, Vascat.

Figure 2.7: Induction machine.

2.2.2 Permanent Magnet Synchronous Machine

For automotive testing solutions PMSMs are the alternative to IMs. As shown in Figure 2.8a, their stator design is similar to the IM's stator, the rotor however is different. Here permanent magnets are part of the rotor to generate the magnetic rotor flux [22, 23]. In Figure 2.8b a exemplary PMSM used for automotive testing is presented. The different rotor design is responsible for the PMSM's biggest advantage: a significantly smaller rotor inertia. A smaller rotor inertia allows to perform more dynamic testing as faster changes of rotational speed are possible. But instead of modifying the rotor design, the machine's effective moment of inertia can be reduced by sophisticated machine controllers too [2, 15]. This technological advance makes it possible to use IMs for applications, where initially PMSMs were needed. Furthermore, PMSMs can be designed to be more compact, which makes it

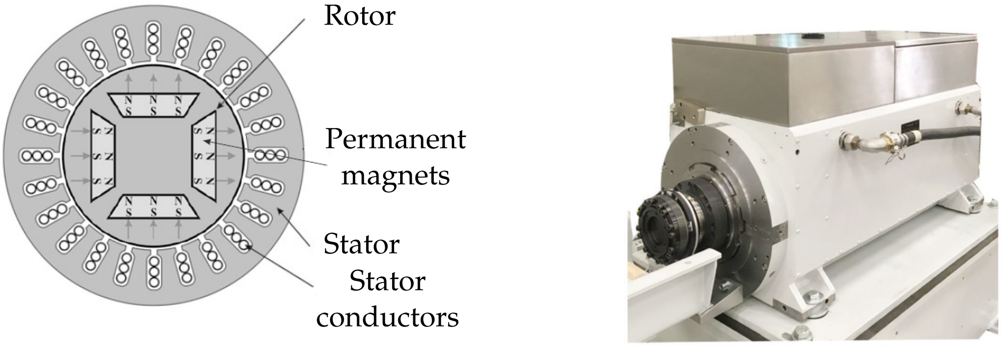

(a) Permanent magnet synchronous machine, cross section [22].

(b) Permanent magnet synchronous machine, Krebs & Aulich.

Figure 2.8: Permanent magnet synchronous machine.

easier to place them on the test bed. Finally, their air-gap torque accuracy is higher since the electromagnetic torque depends on inductances, while the IM's torque is highly dependent on the rotor resistance, which will change with temperature.

2.3 Sensors

In automotive testing the measurement of various physical quantities is required. The two probably most important quantities are rotational speed and torque as these define the mechanical loads. The accuracy with which both torque and rotational speed are measured is fundamental to all the other derived measurements made in the test cell. On a power train test bed these measurements are typically directly related to the electric drives. Each electric motor is equipped with a torque flange to measure the shaft torque and with an incremental encoder to measure its rotational speed. Other methods for measuring these quantities will not be discussed further, see e.g. [8].

2.3.1 Torque Measuring Flange

The torque delivered or absorbed by the ICE and/or the electric drives is the most important physical quantity on an automotive test bed. Therefore, high-precision torque measurement systems are required. Those have to be capable of metering the torque for stationary conditions as well as in highly dynamic situations. On modern power train test systems torque measurement flanges represent the state of the art [8, 13]. These allow to perform in-line measurement, i.e. the torque measuring device is part of the drive shaft, see Figure 2.9b. For this reason, the shaft torque is measured directly and no corrections under transient conditions are necessary. A torque transducer as shown in Figure 2.9a consists of a rotor, which is bolted directly to the flange of the electric motor, and an antenna (stator). In the rotor the torsion caused by torque is measured by strain gauges; this information is then transmitted to the stator where the torque is determined by using digital signal processing.

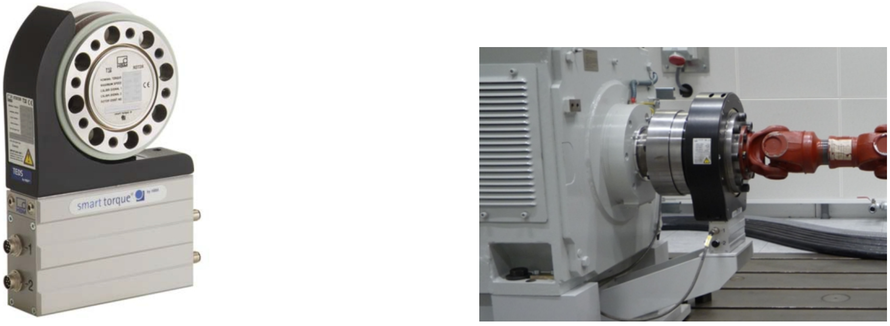

(a) Torque measuring flange HBM T12 [24]. **(b)** Torque sensor with covering attached to electric drive.

Figure 2.9: Torque measuring flange.

Knowing the shaft torques is obviously important for shaft torque control, but precise torque metering is also required for many model based testing strategies as e.g. road load simulation (RLS) or R2R testing [5]. As some of these applications are sensitive regarding delays in the torque control loop, it is important that the torque measuring device is connected to the control system via a fast interface. Additionally, filtering in the torque flange should be reduced to a minimum.

2.3.2 Rotary Encoder

Rotational speed is typically measured by rotary encoders using either optical scanning or an inductive scanning principle. Both methods are contact-free and thus free of wear. The optical scanning principle using graduations applied to a glass carrier and photosensitive detectors, which is widely-used in automotive testing, is depicted in Figure 2.10a. Since optical encoders are very sensitive to dust, they have to be capsuled, see e.g. Figure 2.10b. Two basic measurement methods are available: absolute measuring and incremental measuring. The absolute encoder provides the rotor position immediately upon switch on; as each distinct shaft angle has its unique digital code, no reference mark is required to determine the absolute position. An incremental encoder has no absolute code but a periodic grating structure; therefore, it provides cyclical output signals (pulses) only when the encoder shaft is rotated. These pulses can either be used for relative positioning,

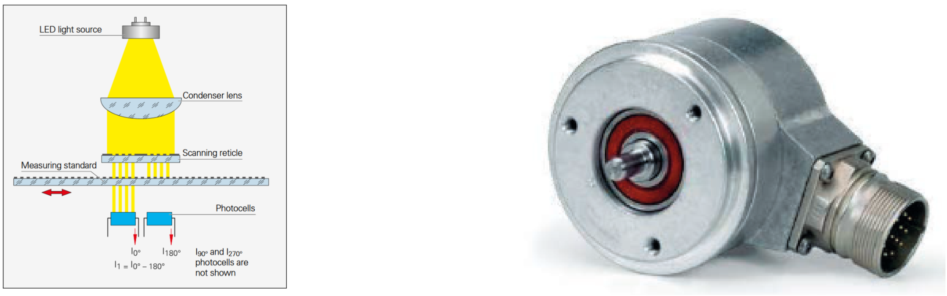
LED light source
Condenser lens
Scanning reticle
Measuring standard
Photocells
$I_{0°}$
$I_{180°}$
$I_1 = I_{0° - 180°}$
$I_{90°}$ and $I_{270°}$ photocells are not shown

(a) Photoelectric scanning according to the imaging scanning principle [25].

(b) Capsuled rotary encoder, Heidenhain [25].

Figure 2.10: Optical rotary encoder.

then the pulses just have to be counted or for gathering rotational speed information by evaluating the frequency of the signal. To be able to determine the direction of rotation too, often two output channels normally labelled 'A' and 'B' with a phase shift of 90° are available. Depending on the direction of rotation one signal is lagging the other in phase. To increase the encoder's resolution, instead of square waves two sine waves (sine and cosine) can be generated, these can then be highly interpolated. This is particularly beneficial at low rotational speeds. As in the incremental encoder actually the relative position is measured, calculating the rotational speed resembles a differentiation with respect to time. Thus, measurement noise is amplified and frequently an additional low-pass filter is applied before this signal can be used for control.

Chapter 3

Plant Modelling

The availability of mathematical models of dynamic systems is inevitable in the controller design work-flow for two fundamental reasons: Firstly, based on mathematical models an analysis of the plant to be controlled is possible. Information about the plant's dynamic behaviour as well as steady-state observations can serve as a basis for controller design. Secondly, having appropriate plant models allows the utilisation of numerical simulation. This is essential in the field of test bed control since controller testing can be done in a safe environment without any risk to the test bed hardware. Furthermore, simulation allows to perform misuse experiments or experiments exceeding some operational limits that could potentially damage the test bed. Additionally, power train test beds are in general quite expensive equipment and therefore cannot be permanently occupied for controller development. For these reasons, intensely testing control concepts in simulation until finally a working controller is available is common. Then ideally just some verifying experiments on the test bed are necessary.

However, a mathematical model can never describe every detail of a plant's behaviour. Usually, a trade-off between model accuracy and limiting factors such as model complexity, modelling effort, numerical efficiency, and parametrisation effort is inevitable. Very often different purposes require models with different complexity. For controller design mostly models covering the essential plant behaviour are sufficient. Otherwise, the mathematical effort required in the controller design procedure could be excessive. However, for simulation purposes very detailed models covering many more aspects are desired to make the simulation results close to reality.

Modelling and simulation of power train test beds is not excessively studied in literature. For this reason, there is no established modelling procedure available. However, in the field of engine testing many works dealing with modelling aspects were published, see e.g. [26–32] and the references therein. Typically, mechanical systems with distributed parameters are reduced to lumped systems consisting of concentrated elements such as moments of inertias and inertia-free torsionally flexible shafts. In most of these works the torsional dynamics of the test systems were modelled as a two-mass oscillator with linear shaft characteristics. Sporadically, three-mass oscillators providing an additional eigenfrequency were used as well. Another similar class of problems are servo-drive systems, which are also well studied in literature, see e.g. [33–37]. These systems frequently contain torsionally flexible couplings and are often modelled as two or three-mass oscillators too. For these problems regularly a single modelling process giving a certain system model is sufficient. A modification of the mechanical set-up such as a change of engine to be tested, dynamometer, or shaft usually only requires to adapt some system parameters.

Typical power train test systems however are mechanically much more complex and diverse, see e.g. Figure 2.2; therefore, another modelling approach must be used. In [38] a *modular modelling strategy* was applied to model an automatic transmission (AT); every single system component was modelled individually, then these sub-models were combined to get a mathematical model for the overall system. This idea shall be adapted and applied for power train test bed modelling. Using this modular approach has the advantage that a modification of the test set-up does not require a completely new modelling process, but just an exchange or a rearrangement of the basic sub-models. Consequently, before models for specific power train test systems are presented, compact mathematical models based on differentials equations for the individual components shall be derived.

If the modelling task is reduced to mathematically describing the test bed components such as electric drives, mechanical shafts, or adapter gearboxes and the power train elements to be tested such as clutches, transmissions, and differential gears, much more literature is available. Especially vehicle power trains are studied excessively due to their importance for vehicle development. Modelling and simulation strategies for the entire power train are discussed in many publications, see e.g. [38–41]. But also reduced models for single power train components such as clutches, transmissions, and differentials are available, see [10, 42–45]. These models were all initially developed for a certain purpose; since the requirements for test bed simulation are different, modifications will be necessary before they can be used to build up a 'model library'. The final task is then to combine the models for various system components to ultimately get a mathematical model describing the dynamics of the entire test system. As these mathematical models shall be used for simulation and controller design only, no constraints regarding real-time execution have to be considered. Among the variety of different modelling strategies, grey box models are widely used [46]. These are based on differential equations derived from the fundamental laws of nature, with parameters that often have to be identified by the use of experimental data. Black box models derived purely from measurement data are typically not desired as with every change of the test bed set-up an entirely new modelling process is required.

3.1 Overview

In Figure 3.1 and Figure 3.2 two representative test systems for testing differential gears respectively transmissions are presented. These show the system components that have to be considered in the modelling process. The majority of these components are mechanical, the drive systems including the inverters are electrical and the controllers are digital systems. In general, two different problem set-ups regarding modelling and control are conceivable: In Figure 3.1 a test bed equipped with KS R2R frequency converters is shown. This inverter was developed for highly dynamic drive applications. Here the real-time control system is responsible for controlling the inverter output voltages as well as for superimposed control tasks. The outputs of this control system are directly the switching commands for the semiconductor stage; these signals are determined by using FOC. This system architecture offers the possibility to modify the machine controllers if necessary. Additionally, time delays caused by external inverter interfaces and bus communication are eliminated because inverter control and superimposed speed or torque control loops are executed on one processor system. From a modelling point of view exactly knowing the inverter control structure including all relevant system and controller parameters is beneficial as it allows to perform more detailed simulations.

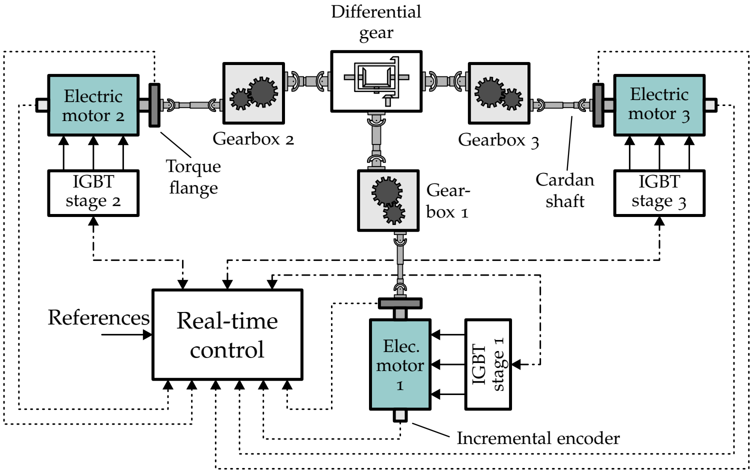

Figure 3.1: Test system for differentials with KS R2R frequency converters and adapter gearboxes to increase testing torque [47].

The alternative approach is shown in Figure 3.2, here conventional inverter systems are used. These are typically operated via a fieldbus interface. This interface allows to select either speed control or torque control operation mode, and to set references for the controlled variable as well as to receive feedback information such as rotational speed. However, this bus communication frequently introduces some time lag. Every further superimposed controller has to be implemented on an additional real-time system. These inverters are problematic for modelling and simulation since the control algorithms are not publicly available.

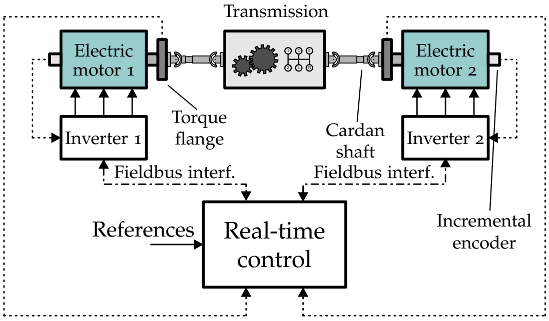

Figure 3.2: Test system for transmissions with conventional inverter system.

The mechanical system typically consists of the power train configuration to be tested and some test bed components required for testing. These are the rotor inertias of the electric machines, flanges, shafts, possibly up- or downspeed gearboxes, and in-line torque measurement devices. In the following sections, mathematical models for all these test bed components and some power train elements that could potentially be tested are derived.

Since these mathematical models shall be used for numerical simulation, simulation relevant aspects have to be considered in the modelling process. Some power train components that must be modelled and simulated are a so-called variable dynamic dimension system (VDDS) because the dynamic dimension of the system can change over time[42]. Handling this system behaviour correctly in numerical simulation is tricky; in Chapter 4 this problem will be further analysed and an adequate simulation strategy will be presented. But this simulation strategy relies on a suitable structure of the mathematical model; therefore, in the modelling process a special focus has to be placed on the potential change of the system's dynamic dimension.

3.2 Drive System

Modelling the electric drives has to cover the entire drive system consisting of the *electric motor* and the *inverter*. Consequently, the motor control strategy applied is a relevant factor. Considering the inverter's control strategy is particularly important if the demands regarding dynamics are high or when the drive system is operated close to its limits. For less challenging applications often simpler models are sufficient. For control the response of the air-gap torque T_{ag} to the demanded torque reference $T_{ag,ref.}$ is most relevant. The KS R2R frequency converter uses field-oriented control (FOC) to control the electric machine. The basic ideas regarding FOC are summarised in Appendix A. FOC was proposed by Hasse [48] and Blaschke [49] respectively to operate three-phase machines with high dynamic performance, see also [23, 50]. The torque control loop within FOC is shown in Figure 3.3 for the control of an IM. Assuming that the rotor flux Ψ_{Rd} is kept constant by additional control loops, see also Appendix A, the task of torque control is actually based on controlling the current i_{Sq} since the electromagnetic torque is given by

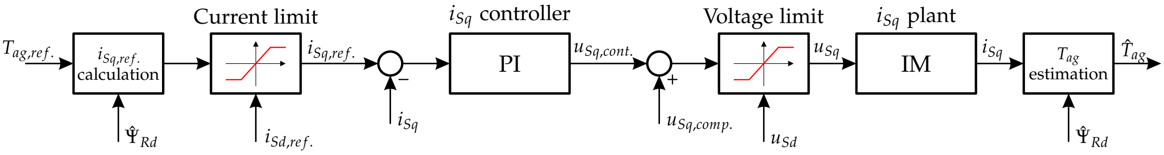

Figure 3.3: FOC for IMs, torque control loop.

$$T_{ag} = \frac{3}{2} p \frac{L_m}{L_R} \Psi_{Rd} i_{Sq}, \tag{3.1}$$

where p, L_R, and L_m are machine parameters. Only for handling limitations regarding voltage and current, the flux control path has to be considered as well; for more details see Appendix A. The air-gap torque T_{ag} is not a direct measurement but estimated within the inverter control software according to

$$\hat{T}_{ag} = \frac{3}{2} p \frac{L_m}{L_R} \hat{\Psi}_{Rd} i_{Sq}, \tag{3.2}$$

based on the estimated rotor flux $\hat{\Psi}_{Rd}$ and the measured stator current.[1] Since the rotor flux is usually changed rather slowly, the dynamics of the torque control loop are essentially given by the dynamics of the current control loop for i_{Sq}.

To identify this relationship, the electric machine can be disconnected from the remaining test set-up and accelerated to a certain rotational speed. Then, step response experiments of the air-gap torque $\hat{T}_{ag}$ are performed. In Figure 3.4 step responses for two different rotational speeds are presented. Both curves show some delay; this dead time originates from the digital implementation of FOC including the actuation of the semiconductor stage and measurement of phase currents. The torque dynamics obviously depend on the rotational speed; this is due to the limited inverter output voltage. At low rotational speed the induced voltage is low, thus more inverter capacity is left for changing the stator current component i_{Sq}. At higher rotational speed less voltage reserve is left to change the stator current. This can be seen in Figure 3.4: at 1500 rpm the voltage limit is permanently reached during the change in air-gap torque; therefore, the torque slope is nearly constant. For this reason, simplified models e.g. containing dead-time and first-order low-pass behaviour as used in [26] are not always capable of adequately describing the air-gap torque dynamics.

---

[1] As shown in [51] and [52], the rotor time constant must be known to estimate the electromagnetic air-gap torque correctly. Since the rotor resistance varies with changing rotor temperature, also the rotor time constant changes. Therefore, the rotor resistance is typically adapted during operation to provide correct torque estimates.

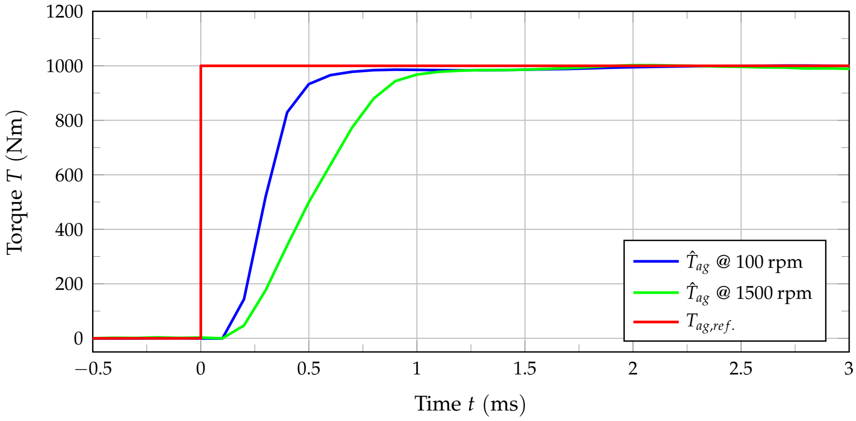

Figure 3.4: Step response of the electromagnetic air-gap torque estimate $\hat{T}_{ag}$ at different rotational speeds.

Consequently, within the simulation studies presented in this work the drive system is modelled in more detail whenever KS R2R frequency converters are used. For the IM the fundamental wave model given by System (A.16) with current-dependent mutual inductance and with the electromagnetic torque T_{ag} as system output is used. FOC is modelled as it is realised on the digital signal processor system, see Figure A.2. To reduce simulation time, the switching within the KS R2R frequency converter's semiconductor stage is neglected. Instead, the inverter is modelled as a continuous system; however, the current dependent non-linearity and dead time introduced by the switching timing of the semiconductors are considered nevertheless, see also [53].

The mechanical subsystem is essentially the rotary dynamics of the machine's rotor with moment of inertia I_m rotating at angular velocity ω. In Figure 3.5a the system structure with the relevant quantities is shown; the rotor can obviously be accelerated by its own air-gap torque T_{ag} and by the shaft torque T_s coming from the rest of the mechanical system. The mathematical model can be derived from Newton's differential equation of motion:

$$I_m \frac{\mathrm{d}\omega}{\mathrm{d}t} = T_{ag} - T_s \tag{3.3}$$

In fact, the fundamental wave model used for modelling the IM cannot cover every detail regarding the machine's air-gap torque T_{ag}; additionally, the air-gap

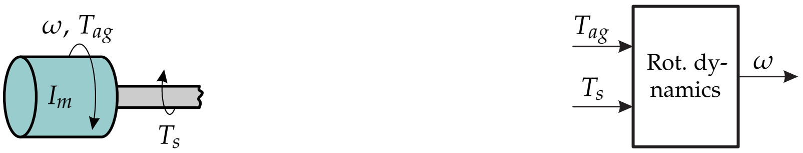

(a) Electric drive, rotor dynamics. **(b)** Rotational dynamics model structure.

Figure 3.5: Rotational dynamics modelling.

torque T_{ag} may periodically deviate from its mean value due to imperfections in the inverter system and in the motor windings, see e.g. [54]. For simulation purposes these torque harmonics are considered as well.

3.3 Mechanical Shaft

Shafts are part of the mechanical system and connect various components by transmitting torque. Depending on the material used and the dimensions of the shafts, these interconnections can be assumed to be *torsionally stiff* or *flexible*, see also [38]. When mechanically complex test beds are modelled, often just some shafts are assumed to be flexible while the remaining connections are treated as rigid for simplicity. For rigid connections the relevant rotating bodies can be modelled as one combined moment of inertia. If two bodies are coupled via an elastic connection, both have to be treated separately, i.e. modelled by their individual moment of inertia. Additionally, the connecting element has to be modelled. Frequently, the mechanical shaft is modelled as inertia-free; its moment of inertia is then added to the two components the shaft is connecting. In Figure 3.6 a typical modelling approach for a cardan shaft is exemplarily presented. The two ends of the shaft are rotating at rotational speeds ω_1 and ω_2 with angular positions φ_1 and φ_2 respectively. The shaft itself is represented by a Kelvin-Voigt model with the torsional stiffness parameter c_s given in N m/rad and the damping coefficient d_s given in N m s/rad [55].

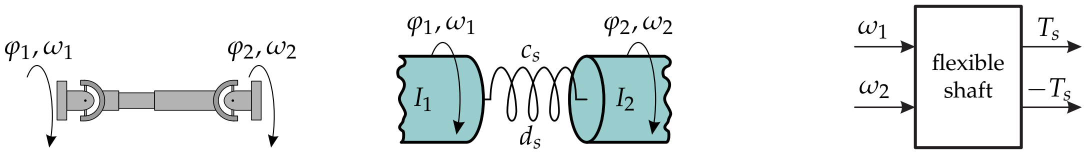

(a) Cardan shaft. **(b)** Simplified shaft model. **(c)** Shaft model structure.

Figure 3.6: Torsionally flexible shaft modelling.

The shaft torque T_s can then be calculated according to

$$\begin{aligned} T_s &= d_s\left(\omega_1-\omega_2\right)+c_s\left(\varphi_1-\varphi_2\right) \\ T_s &= d_s\left(\omega_1-\omega_2\right)+c_s\int\left(\omega_1-\omega_2\right)\mathrm{d}t, \end{aligned} \tag{3.4}$$

where the shaft parameters c_s and d_s can even be arbitrary functions of angular positions or velocities. In automotive test systems usually linear shafts are preferred; therefore, constant shaft parameters are often assumed, see also [26, 56]. If additionally *backlash* must be considered, Equation (3.4) is not sufficient and approaches presented in [57–60] can be used instead. In [57] different models for systems with gear play are presented, but those models converge when the shaft's internal damping tends to zero. As on power train test beds usually only shafts with low internal damping are used, more complex models are needless and the classical 'dead-zone model'

$$T_s = \begin{cases} d_s\left(\omega_1-\omega_2\right)+c_s\left(\varphi_1-\varphi_2-\frac{\theta_{bl}}{2}\right) & \text{if } \varphi_1-\varphi_2\geq\frac{\theta_{bl}}{2} \\ 0 & \text{if } \left|\varphi_1-\varphi_2\right|<\frac{\theta_{bl}}{2} \\ d_s\left(\omega_1-\omega_2\right)+c_s\left(\varphi_1-\varphi_2+\frac{\theta_{bl}}{2}\right) & \text{if } \varphi_1-\varphi_2\leq-\frac{\theta_{bl}}{2} \end{cases}, \tag{3.5}$$

where θ_{bl} is the backlash gap, will be used in the following simulations. If this angle is set to zero, Equation (3.5) converges to Equation (3.4). When cardan shafts are used, angle-dependent transmission errors can potentially occur if the cardan joints are not aligned straightly, see e.g. [61]. With double cardan shafts as shown in Figure 3.6a and typically used on test beds at least velocity errors can be avoided; however, oscillating torques may still be present when the shaft rotates [62]. Therefore, vanishing bending angles and for this reason straightly aligned cardan joints are desired. If this is the case, any angle-dependent torque transmission error can be neglected.

Often, it is unnecessary to model every mechanical shaft by its individual parameters and some shafts can be combined and modelled as one equivalent shaft. As shown in Appendix B, a serial connection of k torsionally flexible shafts with individual parameters c_{si} and d_{si} for $i = 1, 2, \dots, k$ can be approximated by one shaft with parameters $\widetilde{c}_s$ and $\widetilde{d}_s$ determined according to

$$\widetilde{c}_s = \frac{1}{\frac{1}{c_{s1}}+\frac{1}{c_{s2}}+\cdots+\frac{1}{c_{sk}}} \tag{3.6}$$

respectively

$$\widetilde{d}_s = \frac{\widetilde{c}_s^2}{c_{s1}^2}d_{s1}+\frac{\widetilde{c}_s^2}{c_{s2}^2}d_{s2}+\cdots+\frac{\widetilde{c}_s^2}{c_{sk}^2}d_{sk}. \tag{3.7}$$

3.4 Adapter Gearbox

Power train test systems are typically used to test a wide variety of UUTs demanding different levels of testing torque and testing rotational speed. Since the operating ranges of the electric machines are fixed, additional adapter gearboxes are often used to be able to provide the required testing conditions. These can either be upspeed gearboxes to increase the rotational speed range or downspeed gearboxes to increase the feasible testing torque. This latter situation is presented in Figure 3.1. In Figure 3.7a a simplified gearbox model with the quantities relevant for modelling is shown. The gearbox input is associated with angular velocity ω_{gbi} and torque T_{gbi} while ω_{gbo} and T_{gbo} belong to the gearbox output. I_1 and I_2 are the moments of inertia of input gear respectively output gear. The transmission ratio i_{gb} is given by

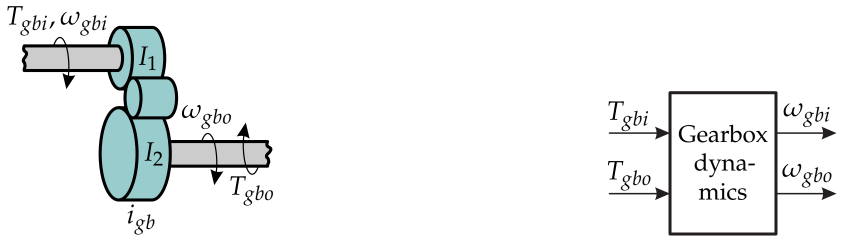

(a) Simplified gearbox model. **(b)** Gearbox model structure.

Figure 3.7: Adapter gearbox modelling.

$$i_{gb} = \frac{\omega_{gbi}}{\omega_{gbo}}. \tag{3.8}$$

The system dynamics can then be determined either corresponding to the gearbox input

$$\frac{\mathrm{d}\omega_{gbi}}{\mathrm{d}t} = i_{gb}\frac{\mathrm{d}\omega_{gbo}}{\mathrm{d}t} = \frac{T_{gbi} - \frac{T_{gbo}}{i_{gb}}}{\underbrace{I_1 + \frac{I_2}{i_{gb}^2}}_{=:I_{gbi}}} \tag{3.9}$$

or corresponding to the gearbox output

$$\frac{\mathrm{d}\omega_{gbo}}{\mathrm{d}t} = \frac{1}{i_{gb}}\frac{\mathrm{d}\omega_{gbi}}{\mathrm{d}t} = \frac{T_{gbi}i_{gb} - T_{gbo}}{\underbrace{I_1 i_{gb}^2 + I_2}_{=:I_{gbo}}}. \tag{3.10}$$

I_{gbi} is the moment of inertia of the gearbox related to the gearbox input while I_{gbo} is related to the gearbox output. The dynamic gearbox model shown in Figure 3.7b can be based on either Equation (3.9) or Equation (3.10). This dynamic model was derived under the assumption of ideal gears. For simulation sometimes effects caused by non-ideal gears must be considered too, see e.g. [63, 64]. This transmission error is often composed of gear play and orders. Orders are in general periodic torque disturbances at rotating frequency or its multiples caused by inhomogeneities of rotating elements. Within gearboxes frequently orders related to the number of gear teeth arise. As their frequency varies with rotational speed, they can excite eigenfrequencies of the multi-mass mechanical system. For this reason, they are operationally critical and thus included in the simulation models.

3.5 Clutch

Friction elements such as the clutch are used to engage and disengage the transmission of mechanical power in the vehicle's driveline, see also [7, 62, 65]. In a car with classic manual transmission the clutch is located between the engine and the gearbox input and is required for vehicle start and gear shifts. In addition to this obvious purpose, friction elements are used within various types of transmissions. In manual transmissions as well as in most automatic transmissions gear shifts are achieved by unlocking some gears and locking some other gears. This process can also be interpreted as engaging and disengaging a clutch. Therefore, an appropriate dynamic clutch model is essential for power train simulations. In Figure 3.8a a simplified illustration showing the relevant quantities for modelling is presented. T_{ci} and T_{co} are input and output torque while I_{ci} and I_{co} are the moments of inertia of the two clutch elements that can be locked. ω_{ci} and ω_{co} are the angular velocities of the clutch disks. The clutch torque T_c is responsible for engaging and disengaging the clutch: if T_c is zero, both clutch disks move without any connection; if T_c is high enough, the two clutch elements are forced to the same rotational speed. The system dynamics can be obtained by applying the law of conservation of angular momentum to both rotating bodies:

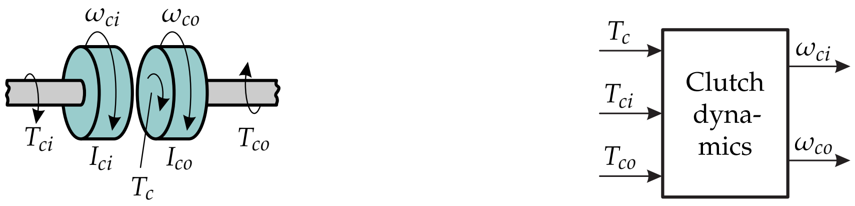

(a) Simplified clutch model. **(b)** Clutch model structure.

Figure 3.8: Friction clutch modelling.

$$I_{ci}\frac{\mathrm{d}\omega_{ci}}{\mathrm{d}t} = T_{ci} - T_c \tag{3.11a}$$

$$I_{co}\frac{\mathrm{d}\omega_{co}}{\mathrm{d}t} = T_c - T_{co} \tag{3.11b}$$

The clutch torque T_c is typically a function of the difference in angular velocities of the two clutch disks, e.g. according to the Stribeck friction model as suggested for wet clutches in [45] and [66]

$$T_c = \mu_c \left[T_{c,c} + \left(T_{c,s} - T_{c,c}\right) \mathrm{e}^{-\frac{|\omega_{ci}-\omega_{co}|}{\omega_{c,s}}} + k_{c,v}\left|\omega_{ci} - \omega_{co}\right| \right] \mathrm{sgn}\left(\omega_{ci} - \omega_{co}\right), \tag{3.12}$$

where $T_{c,s}$ is the maximum torque that can be transmitted by the locked clutch, $T_{c,c}$ is the Coulomb friction torque, $k_{c,v}$ is the viscous friction coefficient, and $\omega_{c,s}$ is the sliding speed coefficient [67]. $\mu_c \in [0, 1]$ is the clutch actuation signal. However, according to [65], for a dry clutch often the simpler model

$$T_c = \mu_c T_{c,c} \mathrm{sgn}\left(\omega_{ci} - \omega_{co}\right) \tag{3.13}$$

is sufficient. A simulation strategy for the dynamic clutch model capable of handling both engaged and disengaged clutch correctly is given in Section 4.2.1.

3.6 Differential Gear

A differential is a particular type of gear set that is widely used in automotive applications. Due to the differential, the two driven wheels of a 2WD vehicle can rotate at different speeds as they follow different ways around a corner. These *axle differentials* usually split the torque symmetrically to both driven wheels. In addition to the axle differentials, a conventional 4WD vehicle also requires a *centre differential* for distributing the engine torque to the front and rear axle. Often, more than fifty percent of the available torque is required at the rear axle; for this reason, these differentials may offer asymmetric torque splitting.

In a conventional open differential the torque distribution is constant, even if the angular velocities of the two output shafts differ. The drawback of this functionality is that if just little torque can be transmitted by one wheel, e.g. due to an icy patch or dynamic cornering, the torque at the other wheel is reduced too. To overcome this problem, *limited-slip* differentials are used. These limited-slip differentials can either be simply mechanical (passive) or electronically controlled (active). Both types are usually based on clutches or other friction elements to alter the torque distribution if the angular velocities of the output axles differ. This friction reduces the torque at the faster wheel and increases the torque at the slower wheel. For additional information on differentials see e.g. [7, 62, 68, 69].

As differentials play an important role in vehicle dynamics, accurate mathematical models are desired. In literature often kinematic models covering only the stationary system behaviour are used, see e.g. [68] and [70]. If transient phenomena are important as well, dynamic models are necessary. In [66] various dynamic mathematical models for differentials are discussed by the use of bond graphs. However, losses were completely neglected and the models are limited to symmetric stationary torque splitting. Therefore, dynamic models for two types of lossy limited-slip differentials with asymmetric torque splitting are derived in the following sections. These results were already published in [71].

3.6.1 Type A: Bevel Gear Differential

Differential gears are often built as a bevel gear set, especially if a torque distribution of 1:1 to both output axles is desired. But by using an asymmetric mechanical structure as shown in Figure 3.9, also other torque distributions are possible. The input shaft with attached bevel gear I_0 rotates at angular velocity ω_{di} and transmits the input torque T_{di} from engine and gearbox to the differential cage; since the radius of the ring gear r_c is usually greater than the radius of the drive gear r_0, the angular velocity is reduced while the torque is increased. The differential cage I_c and with it the differential bevel pinion I_3 are rotating about the A–B axis at angular velocity ω_c, dragging the two other bevel gears and the output shafts I_1 and I_2 with them. These output gears are affected by the differential's output torques T_{do1} and T_{do2}. When the vehicle moves straight, the two output axles rotate at the same speed and the differential bevel pinion I_3 does not rotate about its own axis. If the angular velocities ω_{do1} and ω_{do2} differ, the differential bevel pinion I_3 rotates about its own axis ($|\omega_{3b}| > 0$) while there is no change in torque distribution for the open differential. Limited-slip functionality can be added by introducing the friction torque T_{dsl} to slow down the rotation of the bevel gear I_3. Mechanically there are many different ways of providing this slip-limiting friction torque, see

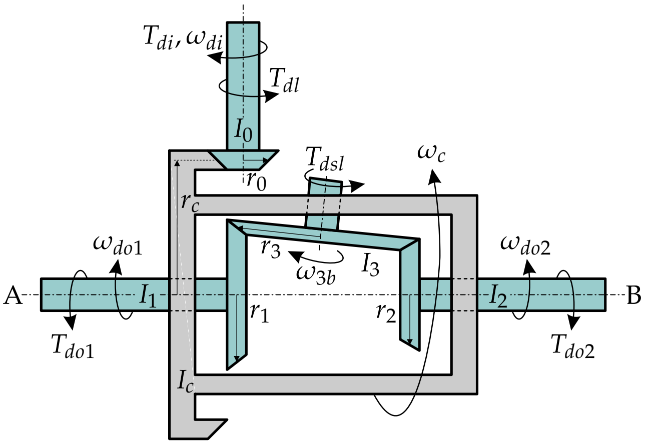

Figure 3.9: Asymmetric bevel gear differential [71].

e.g. [68], but these mechanical considerations are just secondary for modelling. The second friction torque T_{dl} accounts for all losses in the differential gear. Commercial differential gears may include more differential bevel pinions, but for simplicity modelling is done for a system with only one of these as shown in Figure 3.9.

To keep the mathematical model clear and simple, ideal gears with infinite torsional stiffness and negligible backlash are assumed. Then the algebraic constraints

$$r_0\omega_{di} = r_c\omega_c \tag{3.14a}$$
$$r_1\omega_{do1} = r_1\omega_c + r_3\omega_{3b} \tag{3.14b}$$
$$r_2\omega_{do2} = r_2\omega_c - r_3\omega_{3b} \tag{3.14c}$$

have to be fulfilled. r_1 and r_2 are the radii of the output gears while r_3 is the radius of the differential bevel pinion I_3. The dynamics of the differential gear shown in Figure 3.9 can be described by the following set of differential equations

$$I_0\frac{\mathrm{d}\omega_{di}}{\mathrm{d}t} = T_{di} - T_{dl} - r_0F_0 \tag{3.15a}$$
$$I_1\frac{\mathrm{d}\omega_{do1}}{\mathrm{d}t} = r_1F_1 - T_{do1} \tag{3.15b}$$
$$I_2\frac{\mathrm{d}\omega_{do2}}{\mathrm{d}t} = r_2F_2 - T_{do2} \tag{3.15c}$$
$$I_3\frac{\mathrm{d}\omega_{3b}}{\mathrm{d}t} = r_3F_2 - r_3F_1 - T_{dsl} \tag{3.15d}$$
$$\widetilde{I}_c\frac{\mathrm{d}\omega_c}{\mathrm{d}t} = r_cF_0 - r_1F_1 - r_2F_2, \tag{3.15e}$$

where $\widetilde{I}_c$ is the overall moment of inertia for rotation about the A–B axis including differential cage and bevel pinion I_3. The force F_0 acts between ring gear and drive gear, F_1 between differential bevel pinion and the left bevel gear, and F_2 between differential bevel pinion and the right bevel gear. By the use of the Algebraic constraints (3.14), the number of state variables can be reduced and the forces F_0, F_1, and F_2 can be determined. This results in the following differential equations for the input shaft's angular velocity

$$\begin{aligned} D_c\frac{\mathrm{d}\omega_{di}}{\mathrm{d}t} &= i_d^2\left(T_{di} - T_{dl}\right)\left(I_1\frac{r_3^2}{r_1^2} + I_2\frac{r_3^2}{r_2^2} + I_3\right) - i_dT_{dsl}\left(I_2\frac{r_3}{r_2} - I_1\frac{r_3}{r_1}\right) \\ &\quad - i_dT_{do1}\left(I_2\frac{r_3^2}{r_2^2} + I_2\frac{r_3^2}{r_1r_2} + I_3\right) - i_dT_{do2}\left(I_1\frac{r_3^2}{r_1^2} + I_1\frac{r_3^2}{r_1r_2} + I_3\right) \end{aligned} \tag{3.16}$$

and for the angular velocity of the differential bevel pinion I_3

$$\begin{aligned} D_c\frac{\mathrm{d}\omega_{3b}}{\mathrm{d}t} &= i_d\left(T_{di} - T_{dl}\right)\left(I_2\frac{r_3}{r_2} - I_1\frac{r_3}{r_1}\right) - T_{dsl}\left(I_d + I_1 + I_2\right) \\ &\quad - T_{do1}\left(I_d\frac{r_3}{r_1} + I_2\frac{r_3}{r_1} + I_2\frac{r_3}{r_2}\right) + T_{do2}\left(I_d\frac{r_3}{r_2} + I_1\frac{r_3}{r_1} + I_1\frac{r_3}{r_2}\right) \end{aligned} \tag{3.17}$$

with

$$D_c = I_d \left(\frac{I_1 r_3^2}{r_1^2} + \frac{I_2 r_3^2}{r_2^2} + I_3 \right) + I_1 I_2 \left(\frac{r_3}{r_1} + \frac{r_3}{r_2} \right)^2 + I_1 I_3 + I_2 I_3, \tag{3.18}$$

where $i_d := {}^{r_c}/_{r_0}$ is the torque transmission ratio from drive shaft to differential cage and $I_d := \widetilde{I}_c + i_d^2 I_0$ is representing the overall moment of inertia of input shaft and differential cage.

The relevant angular velocities of the output axles can be calculated from the two state variables by using the Algebraic constraints (3.14):

$$\omega_{do1} = \frac{\omega_{di}}{i_d} + \frac{r_3}{r_1}\omega_{3b} \tag{3.19a}$$

$$\omega_{do2} = \frac{\omega_{di}}{i_d} - \frac{r_3}{r_2}\omega_{3b} \tag{3.19b}$$

Of special interest is the stationary torque distribution depending on the dimensions of the bevel gears. By setting the system dynamics to zero (steady state), the torques at the output shafts can be computed if input torque T_{di}, slip-limiting torque T_{dsl}, and loss torque T_{dl} are known

$$T_{do1} = \underbrace{\frac{r_1}{r_1 + r_2}}_{=:\gamma_1} i_d \left(T_{di} - T_{dl} \right) - \gamma_0 T_{dsl} \tag{3.20a}$$

$$T_{do2} = \underbrace{\frac{r_2}{r_1 + r_2}}_{=:\gamma_2} i_d \left(T_{di} - T_{dl} \right) + \gamma_0 T_{dsl} \tag{3.20b}$$

where

$$\gamma_0 := \frac{r_1 r_2}{r_3 \left(r_1 + r_2 \right)}. \tag{3.21}$$

If the friction torques T_{dsl} and T_{dl} are zero too, the ratio of output torques is equal to the ratio of bevel gear radii $\left({}^{T_{do1}}/_{T_{do2}} = {}^{r_1}/_{r_2} \right)$. By using the two constants γ_1 and γ_2 defined in Equation (3.20), the angular velocity of the differential input can be determined if the angular velocities of the two output shafts are given

$$\omega_{di} = i_d \left(\gamma_1 \omega_{do1} + \gamma_2 \omega_{do2} \right). \tag{3.22}$$

Due to the asymmetric torque splitting, the differential cage's angular velocity is not equal to the average angular velocity of the two output shafts. This is an important difference to the symmetric differential.

3.6.2 Type B: Epicyclic Differential

Another common type of differentials are epicyclic differentials based on a planetary gear set as shown in Figure 3.10, see also [43, 62, 68]. Here the drive shaft is connected to the planet carrier I_c and the two output shafts are connected to ring gear I_r and sun gear I_s. Due to different radii of sun gear r_s and ring gear r_r, the input torque T_{di} is asymmetrically transmitted to the two output axles. These output axles are affected by the differential's output torques T_{do1} and T_{do2}. If the angular velocities ω_{do1} and ω_{do2} of ring respectively sun gear match the angular velocity of the planet carrier ω_{di}, the angular velocity ω_{3p} of the planet gears I_p with radius r_p is zero. Otherwise, the planets rotate and the planetary gear set behaves like a common open differential keeping the output torque ratio constant at the nominal value independently of the angular velocities of the output axles. Limited-slip functionality can be included by adding friction between sun and ring gear to slow down the increase of differential angular velocities. An alternative approach for modelling is to assume that the slip-limiting friction torque T_{dsl} slows down the rotation of the planet gears. Then a friction torque of T_{dsl}/n_p affects each of the n_p individual planets. An additional friction torque T_{dl} is used to account for all the losses in the differential gear.

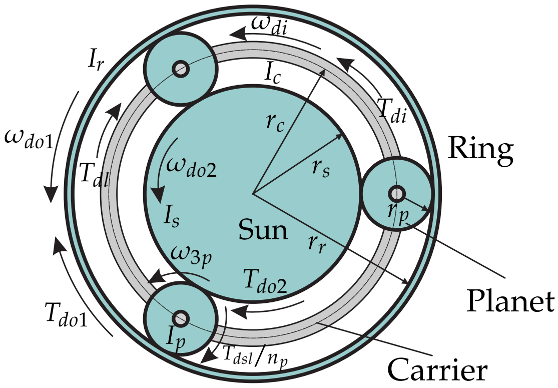

Figure 3.10: Epicyclic differential [71].

As before ideal gears are assumed and the following algebraic constraints can be formulated:

$$r_r \omega_{do1} = r_r \omega_{di} + r_p \omega_{3p} \tag{3.23a}$$

$$r_s \omega_{do2} = r_s \omega_{di} - r_p \omega_{3p} \tag{3.23b}$$

The dynamics of the mechanical system shown in Figure 3.10 can be described by the following set of differential equations:

$$\widetilde{I}_c \frac{\mathrm{d}\omega_{di}}{\mathrm{d}t} = T_{di} - T_{dl} - n_p r_r F_r - n_p r_s F_s \tag{3.24a}$$

$$I_1 \frac{\mathrm{d}\omega_{do1}}{\mathrm{d}t} = n_p r_r F_r - T_{do1} \tag{3.24b}$$

$$I_2 \frac{\mathrm{d}\omega_{do2}}{\mathrm{d}t} = n_p r_s F_s - T_{do2} \tag{3.24c}$$

$$I_p \frac{\mathrm{d}\omega_{3p}}{\mathrm{d}t} = r_p F_s - r_p F_r - \frac{T_{dsl}}{n_p} \tag{3.24d}$$

$\widetilde{I}_c$ stands for the overall moment of inertia of planet carrier and attached planet gears while n_p is the number of planet gears. The differential equation for the planet gears (3.24d) must be considered only once because due to the mechanical structure, all the planets are forced to rotate at the same angular velocity ω_{3p}. The force F_s acts at the intersection of sun gear and planet gears and F_r between planet gears and ring gear. By utilising the Algebraic constraints (3.23), the forces F_s and F_r can be determined and the number of state variables can be reduced. These steps lead to the following pair of differential equations for the planet carrier's angular velocity

$$\begin{aligned} D_c \frac{\mathrm{d}\omega_{di}}{\mathrm{d}t} = {} & (T_{di} - T_{dl}) \left(I_r \frac{r_p^2}{r_r^2} + I_s \frac{r_p^2}{r_s^2} + \widetilde{I}_p \right) - T_{dsl} \left(I_r \frac{r_p}{r_r} + I_s \frac{r_p}{r_s} \right) \\ & - T_{do1} \left(I_s \frac{r_p^2}{r_s^2} + I_s \frac{r_p^2}{r_r r_s} + \widetilde{I}_p \right) - T_{do2} \left(I_r \frac{r_p^2}{r_r^2} + I_r \frac{r_p^2}{r_r r_s} + \widetilde{I}_p \right) \end{aligned} \tag{3.25}$$

and for the angular velocity of the planet gears

$$\begin{aligned} D_c \frac{\mathrm{d}\omega_{3p}}{\mathrm{d}t} = {} & (T_{di} - T_{dl}) \left(I_s \frac{r_p}{r_s} - I_r \frac{r_p}{r_r} \right) - T_{dsl} \left(\widetilde{I}_c + I_r + I_s \right) \\ & - T_{do1} \left(\widetilde{I}_c \frac{r_p}{r_r} + I_s \frac{r_p}{r_s} + I_s \frac{r_p}{r_r} \right) + T_{do2} \left(\widetilde{I}_c \frac{r_p}{r_s} + I_r \frac{r_p}{r_r} + I_r \frac{r_p}{r_s} \right) \end{aligned} \tag{3.26}$$

with

$$D_c = \widetilde{I}_c \left(I_r \frac{r_p^2}{r_r^2} + I_s \frac{r_p^2}{r_s^2} + \widetilde{I}_p \right) + I_r I_s \left(\frac{r_p}{r_r} + \frac{r_p}{r_s} \right)^2 + I_r \widetilde{I}_p + I_s \widetilde{I}_p, \tag{3.27}$$

where $\widetilde{I}_p := n_p I_p$ is the overall moment of inertia of the n_p rotating planet gears I_p.

The relevant angular velocities of the two output axles can be calculated based on the Algebraic constraints (3.23) from the two state variables:

$$\omega_{do1} = \omega_{di} + \frac{r_p}{r_r} \omega_{3p} \tag{3.28a}$$

$$\omega_{do2} = \omega_{di} - \frac{r_p}{r_s} \omega_{3p} \tag{3.28b}$$

As for the bevel gear differential, the stationary torques at the output shafts can be determined by setting the system dynamics to zero

$$T_{do1} = \underbrace{\frac{r_r}{r_s + r_r}}_{=:\gamma_1} (T_{di} - T_{dl}) - \gamma_0 T_{dsl} \tag{3.29a}$$

$$T_{do2} = \underbrace{\frac{r_s}{r_s + r_r}}_{=:\gamma_2} (T_{di} - T_{dl}) + \gamma_0 T_{dsl} \tag{3.29b}$$

where

$$\gamma_0 := \frac{r_r r_s}{r_p (r_r + r_s)}. \tag{3.30}$$

If the friction torques T_{dsl} and T_{dl} are zero too, the ratio of output torques is equal to the ratio of ring and sun gear radii ($T_{do1}/T_{do2} = r_r/r_s$). This formula shows that a differential of that type cannot have symmetric torque splitting ($\gamma_1 = \gamma_2$) since the diameter of the ring gear must always be greater than the sun gear's diameter. With γ_1 and γ_2 as defined in Equation (3.29) the angular velocity of planet carrier and input shaft can be determined if the angular velocities of the output shafts are given

$$\omega_{di} = \gamma_1 \omega_{do1} + \gamma_2 \omega_{do2}. \tag{3.31}$$

3.6.3 Summary

Both types of differential gears can be described by two differential equations: Equation (3.16) and Equation (3.17) for the bevel gear type and Equation (3.25) and Equation (3.26) for the planetary gear type. Each set of differential equations can also be formulated using a common vector-matrix-notation

$$\frac{\mathrm{d}}{\mathrm{d}t} \begin{bmatrix} \omega_{di} \\ \omega_3 \end{bmatrix} = \begin{pmatrix} b_{11} & b_{12} & b_{13} \\ b_{21} & b_{22} & b_{23} \end{pmatrix} \begin{bmatrix} T_{di} \\ T_{do1} \\ T_{do2} \end{bmatrix} - \begin{pmatrix} k_{11} & k_{12} \\ k_{21} & k_{22} \end{pmatrix} \begin{bmatrix} T_{dl} \\ T_{dsl} \end{bmatrix}, \tag{3.32}$$

where ω_3 stands for the angular velocity of the differential bevel pinion ω_{3b} for the bevel gear differential or for the angular velocity of the planets ω_{3p} for the epicyclic differential. The angular velocities of the output axles can then be determined according to

$$\begin{bmatrix} \omega_{do1} \\ \omega_{do2} \end{bmatrix} = \begin{pmatrix} c_{11} & c_{12} \\ c_{21} & c_{22} \end{pmatrix} \begin{bmatrix} \omega_{di} \\ \omega_3 \end{bmatrix}. \tag{3.33}$$

The resulting model structure is shown in Figure 3.11: based on the system inputs T_{di}, T_{do1}, and T_{do2} the system outputs ω_{di}, ω_{do1}, and ω_{do2} are determined.

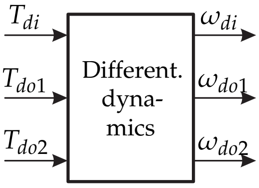

Figure 3.11: Differential gear model structure.

Until now the friction torques T_{dl} and T_{dsl} have just been introduced to consider losses and limited-slip functionality in general, but nearly no information has been given how these torques have to be chosen. The friction torque T_{dl} was introduced to account for losses in the differential gear; thus assuming that it depends on the angular velocity of the input shaft ω_{di} is obvious. Available experimental data showed that in addition to ω_{di} the input torque T_{di} should be considered too:

$$T_{dl}(\omega_{di}) = (T_{dl0} + k_{dlT} |T_{di}|) \operatorname{sgn}(\omega_{di}) + k_{dl\omega}\omega_{di} \tag{3.34}$$

The coefficients T_{dl0}, k_{dlT}, and $k_{dl\omega}$ can be identified from experimental data. The friction torque T_{dsl} provides for limited-slip functionality and should therefore depend on the angular velocity ω_{3b} of the differential bevel pinion for the bevel gear set and on the angular velocity ω_{3p} of the planets for epicyclic differential. Since both of these angular velocities were labelled ω_3, a general dependence on this state variable can be formulated. The maximum locking friction may consist of a constant torque T_{dsl0} depending just on the sign of ω_3, another portion depending on the input torque T_{di} and the sign of ω_3, and a third linear part depending on the angular velocity ω_3 only (see also [68])

$$T_{dsl}(\omega_3) = (T_{dsl0} + k_{dslT} |T_{di}|) \operatorname{sgn}(\omega_3) + k_{dsl\omega}\omega_3. \tag{3.35}$$

These friction coefficients are determined by the differential's mechanical structure and especially the ratio of load dependent and load independent friction torque is important for the limited-slip differential's influence on vehicle dynamics. The torque offset's dependency on input torque and angular velocity ω_3 does not have to be necessarily linear, but often this assumption leads to satisfying results. If Equation (3.35) is not sufficient, a non-linear dependency on ω_3 may be included by adding the term $k_{dslT\omega} |T_{di}| f_\omega(\omega_3)$ to Equation (3.35).

Using the state variables chosen in Section 3.6.1 and Section 3.6.2 has proven to be beneficial as then the friction torque T_{dl} just depends on ω_{di} while the friction torque T_{dsl} depends on ω_3 only. This is comfortable for simulation, as will be seen in Section 4.2.2 where a simulation strategy for the dynamic differential model, capable of handling both friction torques and potential reductions of dynamic dimension correctly, is given.

3.7 Transmission

In almost all vehicles driven by an ICE a gearbox is part of the power train, only electric vehicles may get along without a transmission. The problems related to the working principle of the ICE such as no torque production at zero speed, a narrow speed range for maximum power, and the efficiency very much depending on its operating point make the gearbox and eventually a clutch necessary. Its key role is to transmit the mechanical power from the engine to the driven wheels in every possible situation as e.g. at low as well as at high speed, in reverse, or when starting from rest [7, 69, 72]. In consequence, the transmission's main task is to change the ratio of engine and wheel speed to operate the engine at the rotational speeds it is supposed to. Often the engine crankshaft rotates faster than the differential's input shaft; therefore, in many driving situations rotational speed is reduced by the gearbox while the torque is increased. Additionally, disconnecting the engine from the rest of the driveline when the car is at standstill with engine running must be possible; this may be realised within the gearbox or by an additional clutch.

Over the years many different transmission types have been presented; while early ones were mainly manually actuated, nowadays more and more automated gearboxes are used. In the field of automotive testing the automated transmission is probably more relevant than the manual one as it is more complex and therefore more testing is required. From a test bed modelling point of view the gearbox is the most complex part of the driveline. The wide variety of different types and concepts makes this task even more challenging. For this reason, simplified transmission models that can easily be adapted depending on the gearbox that shall be modelled are highly appreciated. To be able to assess possible drawbacks of these modelling simplifications, a more detailed model will be derived for one exemplary transmission (automatic transmission) that can then be compared in simulations to the simplified models. For more details on gearboxes see e.g. [43, 62, 68, 69, 73–75].

3.7.1 Automatic Transmission

An automated transmission frees the driver from shifting the gears manually; instead, the gear shifts are actuated automatically. Common types of automated transmissions are the classic automatic transmission (AT), the dual-clutch transmission (DCT), and the continuously variable transmission (CVT); the latter two shall not be considered any further in this work. The term *automatic transmission* is usually used to refer to a combination of a torque converter with a subsequent gear set based on epicyclic gears [7, 69]. The torque converter is a hydrokinetic device that is used to transfer the torque generated by the engine to the gear sets and consequently replaces the friction clutch. A subsequent combination of planetary gear sets, clutches, and brakes is forming the gear train responsible for providing the different gear ratios. The clutches and brakes required to change the gear ratio are actuated by a hydraulic system and controlled by an ECU. This structure allows to to perform gear shifts without power interruption (*powershifts*) [72].

Over time manufacturers presented different automatic transmissions based on various combinations of gear sets and friction elements resulting in a different number of gears, see e.g. [76–79]. As an example, a nine-speed automatic transmission recently presented by Daimler is shown in Figure 3.12 and will be further discussed. In addition to the torque converter, this transmission is based on four planetary gear sets. Three clutches (D, E, F) and three brakes (A, B, C) are used to change the gear ratio. As can be seen from Table 3.1, in every gear but neutral (N) three friction elements are engaged while the remaining clutches respectively brakes are disengaged. When the gear is changed, an engaged friction element must be disengaged while another previously disengaged element is engaged. This means that in addition to gear shifts to neighbouring gears, as e.g. from first to second gear, also direct multiple gear shifts, as e.g. from third to first gear, are possible. To provide gear shifts without power interruption, so-called overlapping gear shifts are performed. Here the new friction element starts to engage before the old one is completely disengaged resulting in slipping in both friction elements for a short time interval.

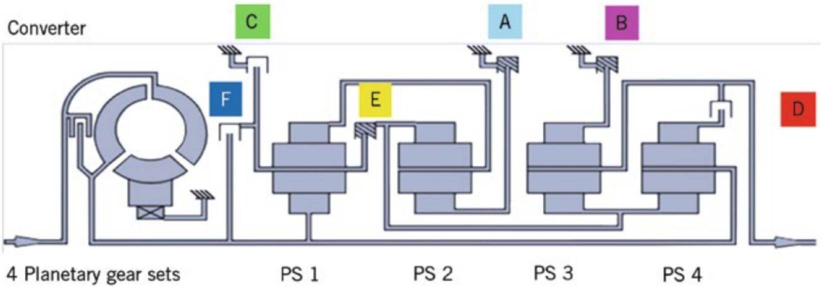

Figure 3.12: 9G-Tronic automatic transmission [76].

Furthermore, in Table 3.1 the total gear ratios are summarised; these can be calculated based on the individual gear ratios of the single epicyclic gear sets

$$g_i := \frac{r_{ri}}{r_{si}} \quad \text{for} \quad i \in \{1, 2, 3, 4\}, \tag{3.36}$$

where r_{ri} is the ring gear radius and r_{si} is the sun gear radius of the planetary gear set i.

The typical modelling approach for ATs is to derive mathematical models for torque converter and gear train individually and then combine these two sub-models, see e.g. [38, 41, 43, 70].

Table 3.1: Shifting table Daimler 9G-Tronic.

Gear	Brake			Clutch			Gear ratio	
	A	B	C	D	E	F		
R	X	X	X				$\frac{-g_1 g_2(1+g_3)}{1+g_2}$	-4.932
N	X	X						0.000
1	X	X			X		$\frac{(1+g_1+g_2)(1+g_3)}{1+g_2}$	5.503
2		X			X	X	$1+g_3$	3.333
3	X	X				X	$\frac{(1+g_3)g_2}{1+g_2}$	2.315
4	X	X		X			$\frac{1+g_3+g_4}{1+g_4}$	1.661
5	X			X		X	$\frac{g_2 g_4}{g_2 g_4-1}$	1.211
6				X	X	X	1	1.000
7	X			X	X		$\frac{g_4}{1+g_4-\frac{1+g_2}{1+g_1+g_2}}$	0.865
8			X	X	X		$\frac{g_4}{1+g_4}$	0.717
9	X		X	X			$\frac{g_1 g_2 g_4}{1+g_2+g_1 g_2+g_1 g_2 g_4}$	0.601

Torque Converter Model

The torque converter is a fluid coupling that is used to transfer mechanical power from the engine to the input of the subsequent gear set. It typically consists of three principal elements: the pump's *impeller* which is driven by the engine, the *turbine* which drives the gear set, and the *stator* that is placed between impeller and turbine, see Figure 3.13. The key characteristic of a torque converter is that it allows the ICE to run faster than the subsequent gear set. This implies that the turbine runs slower than the impeller and leads to a multiplication of the engine torque. This is possible because of the stator and is particularly beneficial when starting from rest. Another important advantage is the damping of engine torque pulsations. The detailed operational principle can be found in [69] and [74]. Because of losses associated with the working principle of the torque converter (slip is necessary for torque transmission), an additional *lock-up clutch* is used to temporarily link impeller and turbine mechanically. This allows to avoid the torque converter slip and thus power losses.

In literature many models for torque converters were proposed, see e.g. [38, 41, 43, 70, 80]. For simplicity, often static models based on stationary maps are used to model the torque converter's behaviour. These maps are functions of the ratio of

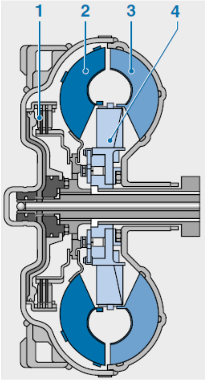

1 Lock-up clutch
2 Turbine
3 Impeller
4 Stator

Figure 3.13: Torque converter cross section [74].

turbine speed ω_t and pump speed ω_p

$$\nu := \frac{\omega_t}{\omega_p}. \tag{3.37}$$

The torque converter's most important characteristic is the ratio of turbine torque T_t and pump torque T_p

$$\mu\left(\nu\right) := \frac{T_t}{T_p}, \tag{3.38}$$

which is, as can be seen in Figure 3.14, dependent on the speed ratio ν. The pump torque absorbed by the impeller is typically modelled as

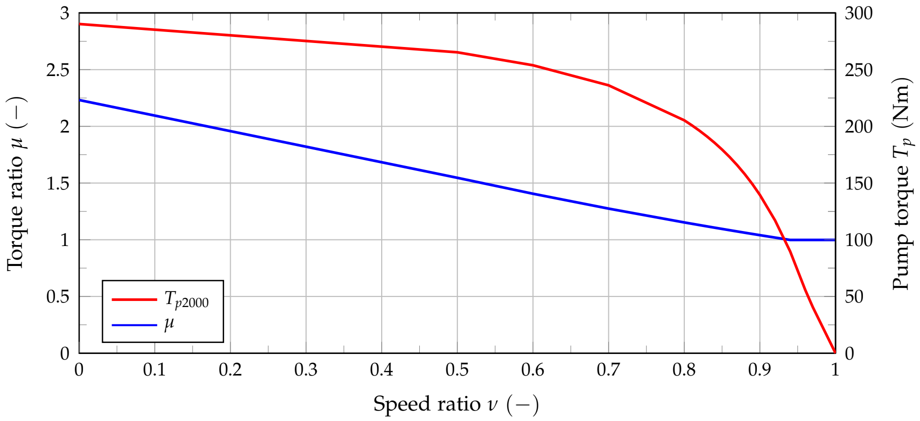

Figure 3.14: Exemplary characteristic torque converter maps.

$$T_p = \left(\frac{\omega_p}{\omega_{pc}}\right)^2 T_{pc}\left(\nu\right), \tag{3.39}$$

where ω_{pc} is a constant reference angular velocity and T_{pc} is the pump torque at this rotational speed, see also [41]. Figure 3.14 shows this pump curve for a reference speed of 2000 rpm; the pump torque obviously depends on the speed ratio ν too. To finalise the model for the torque converter, the lock-up clutch has to be considered as well. For that purpose the model of a friction clutch already given in Section 3.5 can be used, and only the pump and turbine torque have to be added; this is shown in Figure 3.15. For this system the differential equations for pump speed ω_p

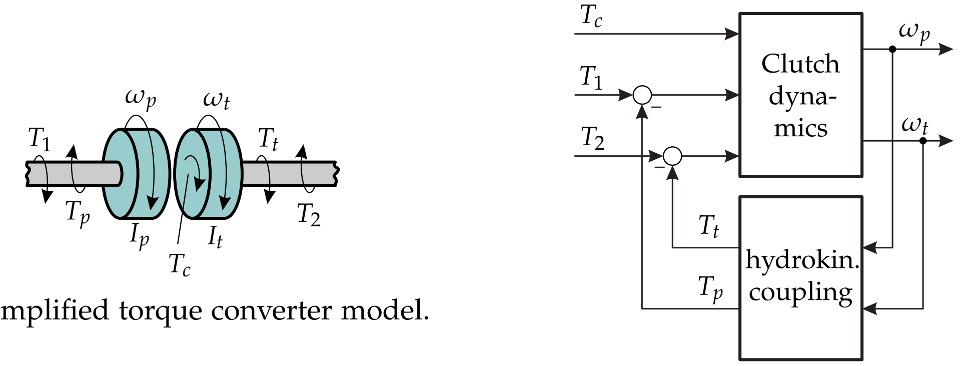

(a) Simplified torque converter model.

(b) Torque converter model structure.

Figure 3.15: Torque converter modelling.

$$I_p \frac{\mathrm{d}\omega_p}{\mathrm{d}t} = T_1 - T_c - T_p \tag{3.40}$$

and turbine speed ω_t

$$I_t \frac{\mathrm{d}\omega_t}{\mathrm{d}t} = T_c + T_t - T_2 \tag{3.41}$$

can then easily be determined. I_t and I_p are the moments of inertia of turbine respectively impeller. T_c is the friction torque generated by the lock-up clutch. T_1 is the input torque typically coming from the ICE and T_2 is the torque converter's output torque. Pump torque T_p and turbine torque T_t can be determined according to Equation (3.39) and Equation (3.38) respectively. The simulation problem can then easily be reduced to the clutch simulation problem with modified input and output torque.

Gear Set Model

In Figure 3.16 the gear set of the 9G-tronic automatic transmission is shown in more detail. It essentially consists of planetary gear sets, clutches, brakes, and connections linking these elements. 'R', 'C', and 'S' denote ring gear, planet carrier, and sun gear of the epicyclic gear set. Due to the complexity of the gearbox, it is time-consuming to determine a mathematical model describing the dynamics of the entire system. If the moments of inertia of the epicyclic gears are considered and the mechanical

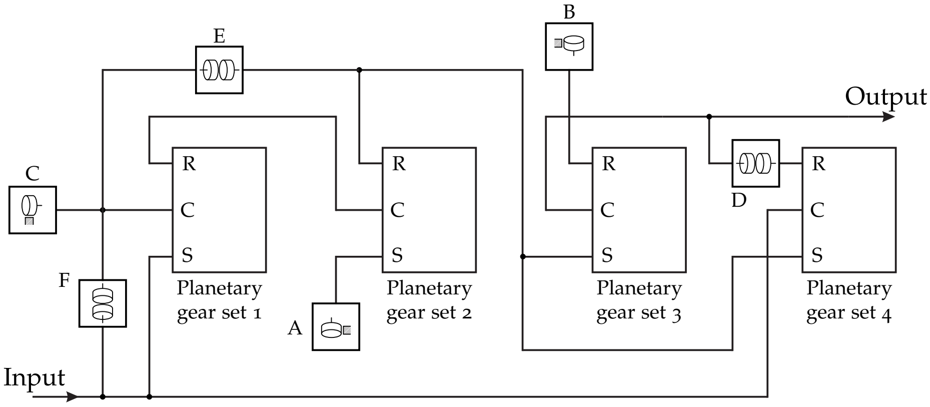

Figure 3.16: 9G-Tronic gear set.

connections within the gear set are assumed to be torsionally rigid, a mathematical model of the form

$$\frac{d\mathbf{x}}{dt} = \mathbf{A}\mathbf{x} + \mathbf{B}\mathbf{u} - \mathbf{K}\mathbf{T}_{fr} \qquad (3.42)$$

has to be determined. The state vector $\mathbf{x}$ contains the relevant angular velocities, $\mathbf{A}$ is the dynamic matrix, the input vector $\mathbf{u}$ contains the gear set's input torque and output torque, $\mathbf{B}$ is the input matrix, $\mathbf{T}_{fr}$ is a vector containing the torques of the six friction elements (clutches and brakes), and $\mathbf{K}$ is a matrix determining how these friction torques are taking effect. This approach is used in [40], but for a significantly simpler gearbox layout and by the use of some simplifications. In addition to the modelling issues, this approach is also problematic for simulation as the transmission model given by Equation (3.42) is a VDDS and a special simulation strategy would be required.

However, if the internal connections within the gear set are assumed to be at least slightly torsionally flexible, several less complex sub-models can be used instead of one global mathematical model. These sub-models are the planetary gear sets, clutches, and brakes. These are modelled as dynamic systems with torques as input variables and angular velocities as system outputs. The required connections can then be realised via shaft models; these have angular velocities as system inputs and torques as outputs, see Section 3.3. One further advantage of this strategy is that if another gearbox layout has to be modelled, not an entire new modelling process is necessary since just some components have to be modified or exchanged.

Modular Transmission Modelling Approach

This alternative approach based on modelling the individual transmission components independently and then linking them together was previously used in e.g. [81] and [38]. This concept shall be briefly explained on the basis of the mechanical system shown in Figure 3.17. This system consists of a clutch and two further

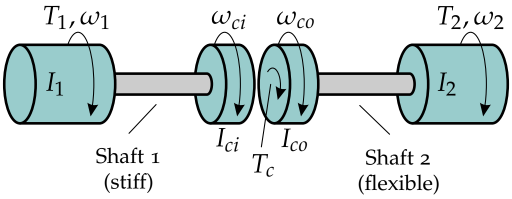
T_1, ω_1
ω_{ci}
ω_{co}
T_2, ω_2
I_1
I_2
I_{ci}
I_{co}
T_c
Shaft 1
(stiff)
Shaft 2
(flexible)

Figure 3.17: Modular modelling approach, exemplary modelling problem.

rotating bodies with inertias I_1 and I_2. These three components are linked via two mechanical shafts. While shaft 1 connecting clutch and body I_1 is assumed to be torsionally stiff, shaft 2 connecting clutch and body I_2 is flexible with stiffness parameter c_{s2} and internal damping d_{s2}. Consequently, the set of differential equations

$$\begin{aligned}(I_1 + I_{ci})\frac{\mathrm{d}\omega_1}{\mathrm{d}t} = (I_1 + I_{ci})\frac{\mathrm{d}\omega_{ci}}{\mathrm{d}t} &= T_1 - T_c \\ I_{co}\frac{\mathrm{d}\omega_{co}}{\mathrm{d}t} &= T_c - T_{s2} \\ I_2\frac{\mathrm{d}\omega_2}{\mathrm{d}t} &= T_2 + T_{s2} \\ \frac{\mathrm{d}\varphi_2}{\mathrm{d}t} &= \omega_2 \\ \frac{\mathrm{d}\varphi_{co}}{\mathrm{d}t} &= \omega_{co}\end{aligned} \tag{3.43}$$

with shaft torque

$$T_{s2} = d_{s2}\left(\omega_{co} - \omega_2\right) + c_{s2}\left(\varphi_{co} - \varphi_2\right) \tag{3.44}$$

describes the system dynamics. Because of the torsionally stiff shaft, the two bodies with inertias I_1 and I_{ci} must have the same angular velocity; ω_1 and ω_{ci} are therefore identical.

If shaft 1 is also assumed to be torsionally flexible with parameters c_{s1} and d_{s1}, the system shown in Figure 3.18 results. Then the differential equations

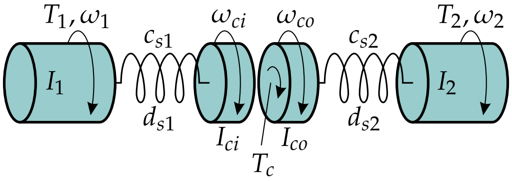
T_1, ω_1
c_{s1}
ω_{ci}
ω_{co}
c_{s2}
T_2, ω_2
I_1
I_2
d_{s1}
I_{ci}
I_{co}
d_{s2}
T_c

Figure 3.18: Modular modelling approach, idea.

$$
\begin{aligned}
I_1 \frac{\mathrm{d}\omega_1}{\mathrm{d}t} &= T_1 - T_{s1} \\
I_{ci} \frac{\mathrm{d}\omega_{ci}}{\mathrm{d}t} &= \underbrace{T_{s1}}_{T_{ci}} - T_c \\
I_{co} \frac{\mathrm{d}\omega_{co}}{\mathrm{d}t} &= T_c - \underbrace{T_{s2}}_{T_{co}} \\
I_2 \frac{\mathrm{d}\omega_2}{\mathrm{d}t} &= T_2 + T_{s2} \\
\frac{\mathrm{d}\varphi_{ci}}{\mathrm{d}t} = \omega_{ci}, \quad \frac{\mathrm{d}\varphi_{co}}{\mathrm{d}t} &= \omega_{co} \\
\frac{\mathrm{d}\varphi_k}{\mathrm{d}t} &= \omega_k \text{ for } k \in \{1, 2\}
\end{aligned}
\tag{3.45}
$$

with shaft torques

$$T_{s1} = d_{s1} (\omega_1 - \omega_{ci}) + c_{s1} (\varphi_1 - \varphi_{ci}) \tag{3.46a}$$

$$T_{s2} = d_{s2} (\omega_{co} - \omega_2) + c_{s2} (\varphi_{co} - \varphi_2) \tag{3.46b}$$

describe the system dynamics. Since the number of differential equations and consequently the system order is increased, this approach seems to be more complex. However, as presented in Figure 3.19, now the mechanical system can be composed of sub-models that were already identified before. The clutch model was determined in Section 3.5; input and output torque for the clutch model are outputs signals of the shaft models that were discussed in Section 3.3 and labelled T_{ci} and T_{co} in System (3.45). The two rotating bodies can be described as was the rotor inertia in Section 3.2; the interactions with the rest of the mechanical system are again given by the shaft torques T_{s1} and T_{s2} defined in Equation (3.46). The shaft torques can easily be determined based on the angular velocity of the rotating bodies.

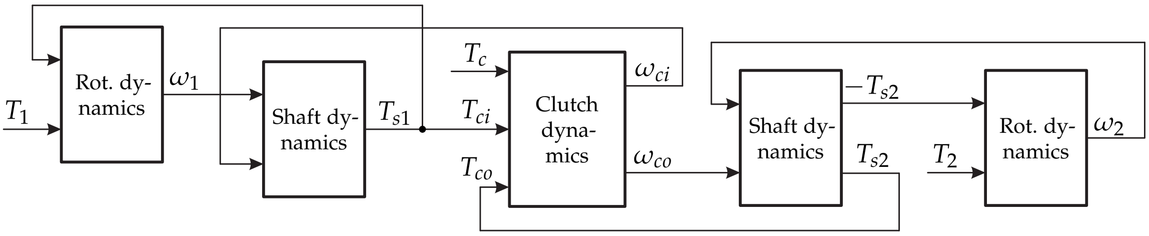

Figure 3.19: Modular modelling approach, result.

These two different modelling approaches resulting in the dynamic systems described by Equations (3.43) respectively Equations (3.45) were implemented within the Matlab®/Simulink® software environment. Then a numerical simulation using a variable step size solver ('ode45') with the system parameters given in Table 3.2 was performed.

Table 3.2: Mechanical system parameters for exemplary modular modelling problem.

Parameter	Value	Unit
I_1	1.0	kg m^2
I_2	2.0	kg m^2
I_{ci}, I_{co}	0.1	kg m^2
c_{s1}	500	kN m/rad
c_{s2}	5	kN m/rad
d_{s1}	10	N m s/rad
d_{s2}	3	N m s/rad

The results of this simulation are presented in Figure 3.20. The system inputs T_1 and T_2 were set to 100 N m from $t = 0.2$ s to $t = 0.75$ s; otherwise these torques were zero. Since the clutch was disengaged at the beginning of the simulation, the two inertias are accelerated to different rotational speeds. At $t = 0.5$ s the clutch was engaged by increasing the torque T_c to 200 N m. Thereby the two clutch disks are synchronised. In the upper plot of Figure 3.20 the rotational speed of body I_1 calculated according to Equations (3.43) is given in blue while the rotational speed of body I_2 is given in black. The results for the modular modelling approach are given in red and green respectively. In the second plot the difference in rotational speeds due to the different mathematical models is shown. As c_{s1} was

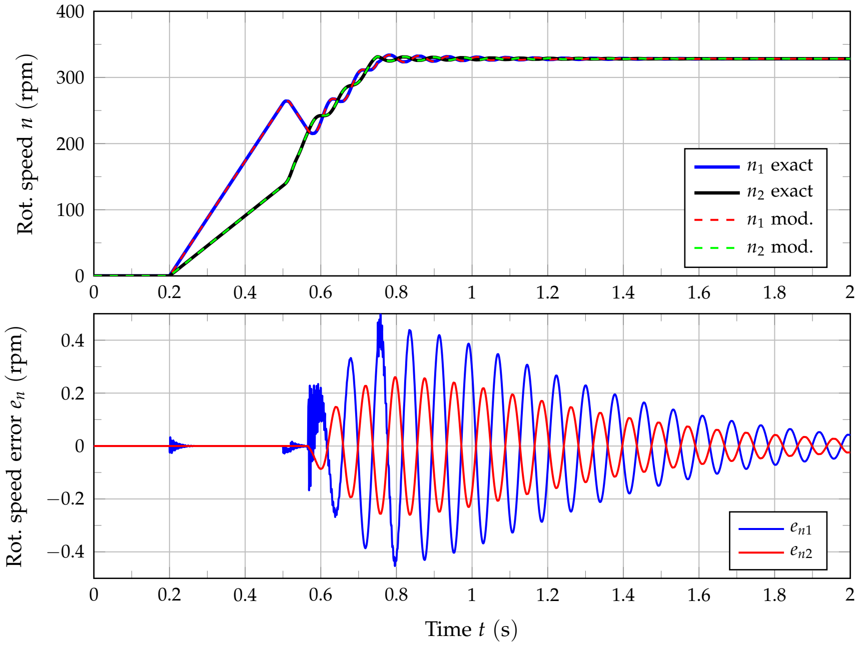

Figure 3.20: Modular modelling approach, comparison of simulation results with the original model and results obtained by the use of the modular approach.

chosen big enough, both simulations yield similar results. The additional flexible coupling increases the dynamic dimension of the system and leads to a second eigenfrequency; this can be seen in the error signal of the rotational speed n_1, but as it is sufficiently damped, this oscillation decays fast. The lower plot shows that the first eigenmode is slightly different too, but this discrepancy is negligible compared to other modelling and parameter uncertainties typically complicating numerical simulations of transmission systems.

This modular modelling and simulation approach clearly has drawbacks such as an increase in dynamic dimension, potentially the need for a small simulation step size because of high torsional stiffness parameters, and the required choice of additional shaft parameters, see also [81] and [38]. However, variable step size solvers and powerful processor systems overcome the numerical simulation problems and the choice of shaft parameters is often uncritical. The benefit is a significant reduction of modelling effort; therefore, this approach shall be used to model the internals of the gear stage within the AT. A model for a friction clutch was presented in Section 3.5; this model can also be used to model a brake. Torsionally flexible mechanical connections and suitable models were discussed in Section 3.3. The model for the planetary gear set can be based on the results from Section 3.6.2 where the epicyclic differential gear was discussed.

Planetary Gear Set

In Section 3.6.2 a mathematical model for a differential based on the planetary gear set was derived. This set of equations can also be used to model the planetary gear set within the AT; just the slip-limiting torque T_{dsl} has to be set to zero. If for simplicity additionally losses are neglected ($T_{dl} = 0$), the differential equations for the angular velocity of the planet carrier

$$\frac{\mathrm{d}\omega_{cp}}{\mathrm{d}t} = \frac{\left(T_{cp} + T_{rp} + T_{sp}\right)\widetilde{I}_p + \left(T_{cp} + T_{rp}\right)\frac{I_s r_p^2}{r_s^2} + \left(T_{cp} + T_{sp}\right)\frac{I_r r_p^2}{r_r^2} + T_{rp}\frac{I_s r_p^2}{r_r r_s} + T_{sp}\frac{I_r r_p^2}{r_r r_s}}{D_c} \tag{3.47}$$

and for the angular velocity of the planet gears

$$\frac{\mathrm{d}\omega_{pp}}{\mathrm{d}t} = \frac{T_{cp}\left(I_s\frac{r_p}{r_s} - I_r\frac{r_p}{r_r}\right) + T_{rp}\left(\widetilde{I}_c\frac{r_p}{r_r} + I_s\frac{r_p}{r_s} + I_s\frac{r_p}{r_r}\right) - T_{sp}\left(\widetilde{I}_c\frac{r_p}{r_s} + I_r\frac{r_p}{r_s} + I_r\frac{r_p}{r_r}\right)}{D_c} \tag{3.48}$$

with

$$D_c = \widetilde{I}_c\left(I_r\frac{r_p^2}{r_r^2} + I_s\frac{r_p^2}{r_s^2} + \widetilde{I}_p\right) + I_r I_s\left(\frac{r_p}{r_r} + \frac{r_p}{r_s}\right)^2 + I_r\widetilde{I}_p + I_s\widetilde{I}_p \tag{3.49}$$

can be used to model the dynamics of the planetary gear set. The angular velocities of sun gear ω_{sp} and ring gear ω_{rp} are

$$\omega_{rp} = \omega_{cp} + \frac{r_p}{r_r}\omega_{pp} \tag{3.50a}$$

$$\omega_{sp} = \omega_{cp} - \frac{r_p}{r_s}\omega_{pp}. \tag{3.50b}$$

This set of equations describes the dynamics of the planetary gear set; the resulting model structure is presented in Figure 3.21. T_{cp} and ω_{cp} are torque and angular velocity related to the planet carrier, T_{rp} and ω_{rp} belong to the ring gear while T_{sp} and ω_{sp} are related to the sun gear. In contrast to Section 3.6.2 where positive torques applied to sun and ring gear were acting in a way that those gears were slowed down, here positive torques T_{sp} and T_{rp} act accelerative.

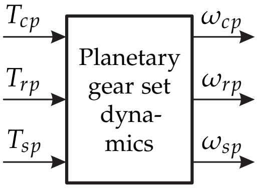

Figure 3.21: Planetary gear set model structure.

Finally, a model for the automatic transmission's gear set as shown in Figure 3.16 can be obtained by combining models for planetary gear sets, clutches, brakes, and flexible shafts. The results of numerical simulations based on this model are presented in Section 4.3. Together with the model for the torque converter a mathematical model for the AT can be formed.

3.7.2 Simplified Models

As the mathematical model for the automatic transmission's gear set depicted in Figure 3.16 is rather complex and requires many system parameters to be known or identified, often simplified models are demanded as well. These cannot cover all the details, but provide an easy to use and simple alternative. In addition to the AT, these models should also be suitable for numerical simulations of other transmission types. Therefore, the torque converter uniquely used in ATs shall not be considered. When the complete automatic transmission system is to be simulated, the torque converter model only has to be added to the simplified transmission models presented below as for a manual transmission an additional friction clutch might be added.

In Figure 3.22a a very simple gearbox model, which essentially consists of a clutch and a gear ratio, is presented. The gear stage and the clutch disks are assumed to be inertia-free; the transmission's moment of inertia is represented by the input inertia I_{gbi} and output inertia I_{gbo}. i_{gb} is the transmission ratio of the gear stage while T_c is the clutch torque. T_{gbi} and T_{gbo} are input and output torque, ω_{gbi} and ω_{gbo} are the angular velocities of gearbox input and output. Since there are no flexible couplings within the mechanical system, a second order dynamic system is sufficient to model the dynamics:

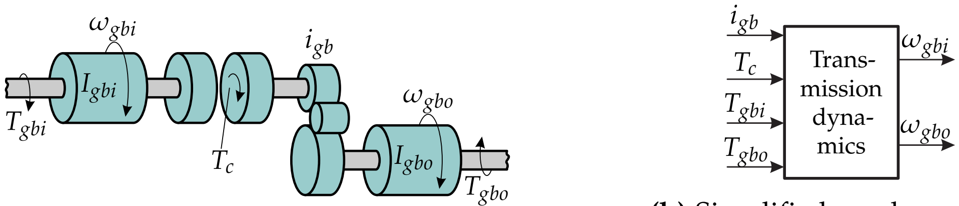

(a) Simplified gearbox model, approach I.

(b) Simplified gearbox model structure, approach I.

Figure 3.22: Simplified gearbox modelling, approach I.

$$I_{gbi}\frac{\mathrm{d}\omega_{gbi}}{\mathrm{d}t} = T_{gbi} - T_c \tag{3.51a}$$

$$I_{gbo}\frac{\mathrm{d}\omega_{gbo}}{\mathrm{d}t} = i_{gb}T_c - T_{gbo} \tag{3.51b}$$

As in Section 3.5, the clutch torque T_c is a function of the relative angular velocity of the clutch disks

$$T_c = T_c\left(\omega_{gbi} - i_{gb}\omega_{gbo}\right). \tag{3.52}$$

The resulting model structure is shown in Figure 3.22b; besides the input and output torque also the clutch torque T_c and the transmission ratio i_{gb} are system inputs. A gear shift can be realised by disengaging the clutch, changing the transmission ratio from its initial value to the transmission ratio related to the next gear, and finally engaging the clutch again.

The shifting table for the AT presented in Section 3.7.1 however shows that a typical gear shift involves two friction elements. These two elements are essential for gear shifts without power interruption. Since the above model is based on just one friction clutch, its use is limited to modelling manual transmissions where gear shifts are non-overlapping. Therefore, in Figure 3.23a a second simplified gearbox model with two friction clutches and two gear stages capable of handling overlapping gear shifts is presented [82]. This system resembles a DCT, but can also be used to model the gear set within the AT. The transmission gears and the clutch disks are assumed to be inertia-free for modelling; the moment of inertia of the transmission is represented by the input inertia I_{gbi} and by the output inertia

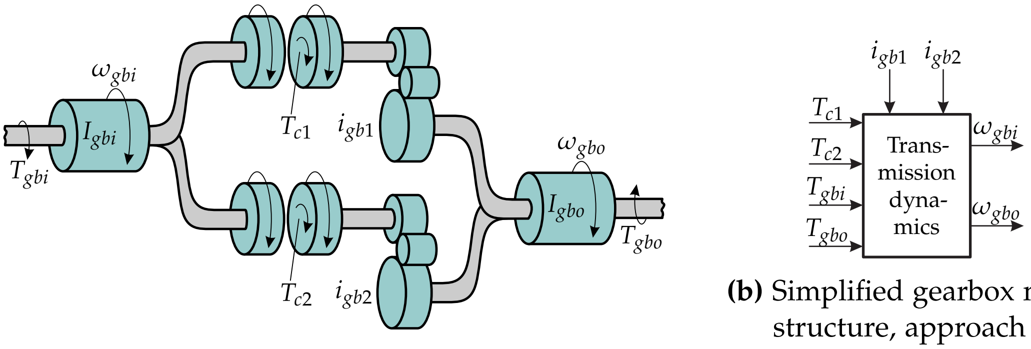

(a) Simplified gearbox model, approach II.

(b) Simplified gearbox model structure, approach II.

Figure 3.23: Simplified gearbox modelling, approach II.

I_{gbo}. T_{gbi} and T_{gbo} are input respectively output torque while ω_{gbi} and ω_{gbo} are the angular velocities of gearbox input and output. Since there are no flexible couplings within the mechanical system, as before, two state variables are sufficient to model the dynamics:

$$I_{gbi}\frac{\mathrm{d}\omega_{gbi}}{\mathrm{d}t} = T_{gbi} - T_{c1} - T_{c2} \tag{3.53a}$$

$$I_{gbo}\frac{\mathrm{d}\omega_{gbo}}{\mathrm{d}t} = i_{gb1}T_{c1} + i_{gb2}T_{c2} - T_{gbo} \tag{3.53b}$$

As in Section 3.5, the clutch torques T_{c1} and T_{c2} are functions of the relative velocities of the clutch disks

$$T_{c1} = T_{c1}\left(\omega_{gbi} - i_{gb1}\omega_{gbo}\right) \tag{3.54a}$$

$$T_{c2} = T_{c2}\left(\omega_{gbi} - i_{gb2}\omega_{gbo}\right). \tag{3.54b}$$

i_{gb1} and i_{gb2} are the two transmission ratios involved in the gear shift: one is the current gear ratio while the other is the gear ratio after the gear shift. The resulting model structure is shown in Figure 3.23b. As in Figure 3.22b, input and output torque are system inputs; additionally, the two clutch torques can be specified. The transmission ratios i_{gb1} and i_{gb2} can be classified as system inputs as well, but these must be fixed before the gear shift.

These models with different complexity shall be assessed by the use of numerical simulations, these results are presented in Chapter 4. The simulation strategies required for correctly handling engaged and disengaged clutches are presented before the simulation results in Section 4.2.1 and Section 4.2.2.

3.8 Case Study I: Test System for Differential Gears

The modular modelling strategy based on combining various subsystems that were discussed earlier in this chapter is demonstrated on the basis of three different test bed configurations. The first example is a test system for differentials equipped with three IMs as presented in Figure 3.24. This test bed can be used to test a wide variety of differential gears, which can be axle or centre differentials, passive or electronically controlled, and possibly slip-limiting. Typically, three electric drives are needed to perform the required tests: machine *M1* provides the testing torque to emulate the vehicle's combustion engine and transmission while machines *M2* and *M3* are used to generate the mechanical loads. The electric drives and the UUT are coupled via double cardan shafts. Each of the three IMs is equipped with a torque flange to measure the shaft torque and with an incremental encoder to measure the machine's rotational speed. A real-time control system is used to perform speed and torque control as well as to control the electric drives via FOC.

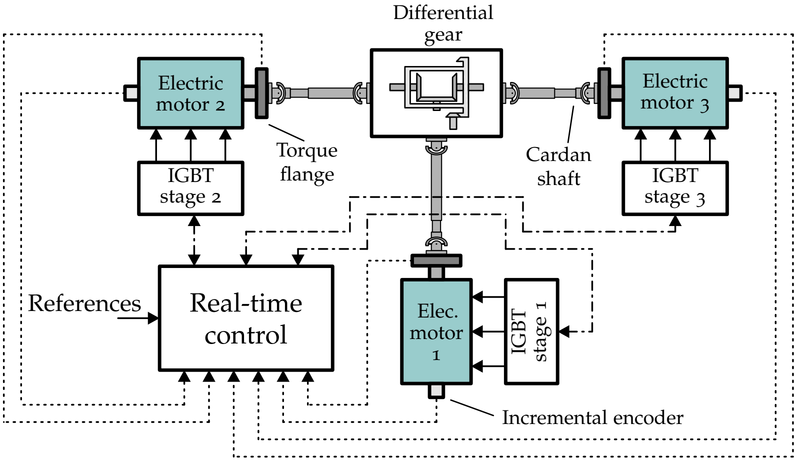

Figure 3.24: Test system for differentials with KS R2R frequency converters.

In Figure 3.25 the structure of the model used for numerical simulations of the test bed discussed in this section is shown in a graphical representation. The modular system structure is obvious. In addition to the model for the limited-slip differential, the mechanical system consists of several blocks for describing rotational dynamics interconnected by shaft models. As mentioned earlier, the mechanical shafts are assumed to be inertia-free; therefore, their moments of inertia have to be added to the other inertias in the system. The cardan shaft models are characterised by their torsional elasticities c_{s1}, c_{s2}, c_{s3} and their internal dampings d_{s1}, d_{s2}, d_{s3}. According to Section 3.3, also a backlash gap can be specified for each shaft if necessary. The cardan shafts' backlash gaps θ_{bl1}, θ_{bl2}, and θ_{bl3} include also the gear play in the UUT. The IMs are represented in the mechanical system by their rotor inertias I_{m1},

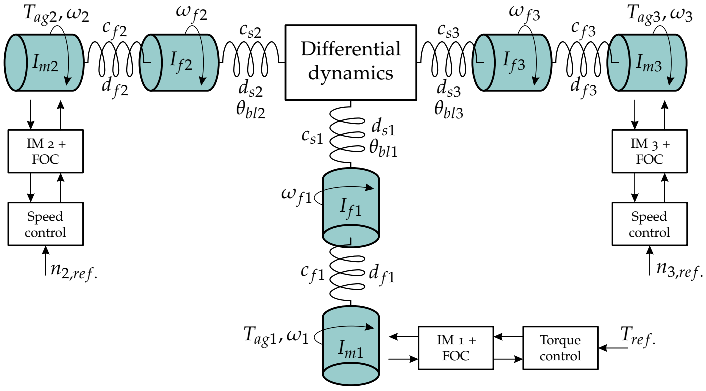

Figure 3.25: Test system for differentials, model structure.

I_{m2}, and I_{m3}. A combination of an elastic coupling with elasticity c_{f1} and damping d_{f1} and an inertia I_{f1} is used to model the torsional dynamics of the torque sensor attached to machine *M1*. The torsional flexibility within the torque measuring flange is directly related to its measuring principle based on the twist of a torsion element as described in Section 2.3.1. These torque flange modelling components also have to be included for the drives *M2* and *M3* with their individual parameters I_{f2}, c_{f2}, d_{f2} and I_{f3}, c_{f3}, d_{f3} respectively. These parameters are not necessarily identical as different torque transducers and various further adapter flanges might be used. Due to these additional torsional dynamics, three extra eigenfrequencies are introduced within the mechanical system.

The UUT could be any type of differential; to be able to finally compare measurement data and simulation results, a specific differential gear must be chosen for modelling and simulation. Because of the modular modelling approach, a change of the UUT would only require to modify the differential's system model. Since the UUT considered here is a symmetric limited-slip bevel gear axle differential, Equation (3.16) and Equation (3.17) can be used to model its dynamics. Due to the symmetric structure, the number of system parameters can be reduced as $I_1 = I_2$ and $r_1 = r_2$ hold. As shown in Appendix C, then the more compact Differential equations (C.13) and (C.14) can be used to model the differential's dynamics and only the two moments of inertia I_{di} and I_{3b} need to be known. These can be identified by the use of experiments on the test bed. Even the ratio $^{r_3}/_{r_1}$ is not required to be known since it is only a scaling parameter for the slip limiting torque T_{dsl}. The differential under test considered here showed a dependency of the locking friction torque T_{dsl} on the angular position of the differential bevel pinion; as a consequence, Equation (3.35) was altered by adding a dependency on the integral of the differential bevel pinion's angular velocity ω_3. Furthermore, the locking friction torque's dependency on ω_3 was not exactly linear; for this reason, the non-linear component f_ω, mentioned in Section 3.6.3 for modelling T_{dsl}, was a linear function of angular velocity for small ω_3 and constant otherwise (saturation function). The differential gear considered here is a passive system; therefore, its behaviour cannot be changed during the test-runs.

Since the test bed shown Figure 3.24 is equipped with the KS R2R frequency converter, the electrical subsystems can be modelled in great detail. The IMs are modelled using the fundamental wave model given by System (A.16) where the system outputs are the air-gap torques T_{ag1}, T_{ag2}, and T_{ag3} and the phase currents needed for control. FOC is represented by the discrete time control scheme presented in Figure A.2. The control system is completed by superordinate discrete time PI controllers for rotational speed and torque as shown in Figure 2.5b.

In Appendix C the differential equations describing the dynamics of the mechanical system shown in Figure 3.25 are summarised. The complete mathematical system model including the IMs and FOC cannot be specified as parts of the inverter control functionality are confidential.

3.9 Case Study II: Test System for Differential Gears with Adapter Gearboxes

The second modelling and simulation example is the test system that was presented in Figure 3.1 in Section 3.1. This test bed closely resembles the testing solution for differentials presented in Figure 3.24 that was previously discussed; the essential difference are three downspeed gearboxes. These are used to increase the torque by reducing the rotational speed to reach the required testing conditions (total load torque up to 60 kN m). The adapter gearbox was already modelled before in Section 3.4; consequently, these new additional gearbox models only have to be included in the model structure presented before in Figure 3.25. This leads to the final model as shown in Figure 3.26.

The new gearboxes are characterised by their transmission ratios i_{gb1}, i_{gb2}, and i_{gb3} and by their moments of inertia I_{gb1}, I_{gb2}, and I_{gb3}. As seen in Section 3.4, the moments of inertia of the gearboxes can be specified for the high- or the low-speed side; here the parameters for the high-speed side are given. Double cardan shafts are used to couple the gearboxes to the rest of the mechanical system; these can be modelled using elastic shaft models with their individual parameters for elasticity and internal damping.[2] Since again KS R2R frequency converters are used, the remaining model structure does not have to be changed, only system parameters must be adjusted. This holds for the UUT as well; although here a rear axle truck

---

[2] Since all backlash phenomena are assumed to be covered by the backlash gaps specified for the cardan shafts connecting gear boxes and differential, no backlash gap needs to be given for the remaining shafts.

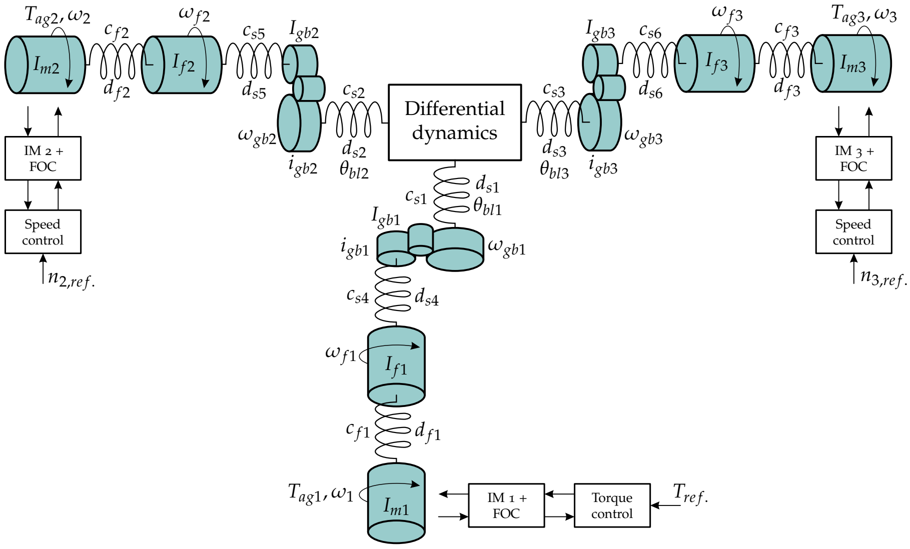
T_{ag2}, ω_2
c_{f2}
ω_{f2}
c_{s5}
I_{gb2}
I_{m2}
I_{f2}
d_{f2}
d_{s5}
c_{s2}
ω_{gb2}
i_{gb2}
d_{s2}
θ_{bl2}
IM 2 + FOC
Speed control
$n_{2,ref.}$
Differential dynamics
c_{s3}
d_{s3}
θ_{bl3}
I_{gb3}
c_{s6}
d_{s6}
ω_{gb3}
i_{gb3}
ω_{f3}
c_{f3}
d_{f3}
I_{f3}
T_{ag3}, ω_3
I_{m3}
IM 3 + FOC
Speed control
$n_{3,ref.}$
c_{s1}
d_{s1}
θ_{bl1}
I_{gb1}
i_{gb1}
ω_{gb1}
c_{s4}
d_{s4}
ω_{f1}
I_{f1}
c_{f1}
d_{f1}
T_{ag1}, ω_1
I_{m1}
IM 1 + FOC
Torque control
$T_{ref.}$

Figure 3.26: Test system for differentials with adapter gearboxes to increase testing torque, model structure.

differential designed for much higher torques is tested, the same model as before can be used.

3.10 Case Study III: Test System for Transmissions

The final modelling example is a test system for transmissions as presented in Figure 3.2 in Section 3.1. Here just two electric machines are needed to perform the testing. The input drive *M1* provides the testing torque while the output drive *M2* is again used to generate the mechanical loads that would come from the road in a real world driving experiment. The UUT could be any type of transmission, automatic as well as manually actuated. In this modelling and simulation example, a testing scenario for an AT is assumed. A graphical representation of the resulting system model used for simulation is presented in Figure 3.27. The model structure is similar to the two examples previously presented. Both IMs are represented in the mechanical system by their individual rotor inertias I_{m1} and I_{m2}. The torque measuring flanges are again modelled as a combination of the moment of inertias I_{f1} and I_{f2} and their internal elastic couplings with parameters c_{f1}, d_{f1} and c_{f2}, d_{f2} respectively. The mechanical connections to the UUT are modelled as torsionally flexible shafts with parameters c_{s1}, d_{s1}, θ_{bl1} and c_{s2}, d_{s2}, θ_{bl2}. Since instead of the KS R2R inverter a conventional inverter system is used in this application, a detailed modelling of inverter and IM as before is not possible. The inverter's internal control algorithms are unknown; therefore, a simplified model containing dead-time and first-order low-pass dynamics as discussed in Section 3.2 is used. As common for

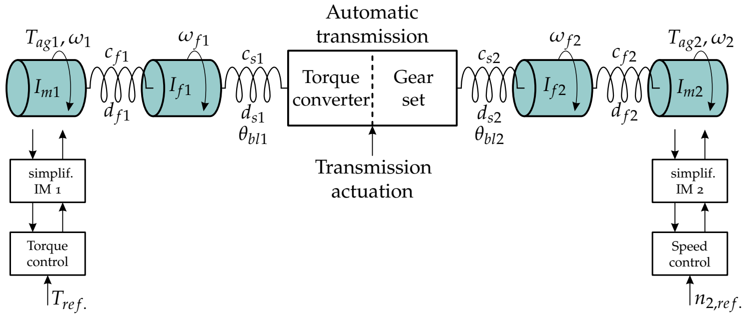
T_{ag1}, ω_1
c_{f1}
ω_{f1}
c_{s1}
Automatic transmission
c_{s2}
ω_{f2}
c_{f2}
T_{ag2}, ω_2
I_{m1}
I_{f1}
Torque converter
Gear set
I_{f2}
I_{m2}
d_{f1}
d_{s1}
θ_{bl1}
d_{s2}
θ_{bl2}
d_{f2}
simplif. IM 1
Transmission actuation
simplif. IM 2
Torque control
Speed control
$T_{ref.}$
$n_{2,ref.}$

Figure 3.27: Test system for transmissions, model structure.

these testing situations, the input drive is operated in torque control mode while the load drive is speed controlled.

In contrast to the differential gear, the AT changes its behaviour over time as e.g. gear shifts occur. On the test bed the transmission actuation required to perform a gear shift is carried out by a superimposed test bed control system. For simulation the simplified gearbox model presented in Figure 3.23 in combination with the torque converter model from Section 3.7.1 is used; these are capable of describing the transmission system for stationary gear and for gear shifts. The actuation signal for the torque converter model is the lock-up clutch torque while the gearbox model requires the two clutch torques and transmission ratios to be known.

3.11 Parameter Identification

The simulation models presented previously are rather complex, this directly results in a high number of system parameters. These parameters have to be identified before simulation. The parameters required to simulate the IMs are typically identified during the test bed commissioning process. The parameters used within FOC are user-defined and therefore known as well. The mechanical system parameters such as inertias, torsional shaft stiffness, and internal damping can be gathered from various sources: The inertias of the electric machines are frequently known from the motor data sheets or from the test bed commissioning process. The torque measuring flanges' parameters are usually given in the data sheet. Parameters for shafts and adapter flanges can often be determined based on their geometric dimensions and given material properties.

After using all this information typically some uncertainty remains. To finally tune the parameters of the mechanical system, it is usually inevitable to analyse measurement data from the test bed. As the mechanical system mostly shows low internal damping, torsional vibrations due to resonance phenomena are a permanent problem on these test systems. Therefore, correctly simulating these torsional vibrations is essential. To be able to match the torsional vibration modes within the simulation model to the critical frequencies of the test bed, suitable experiments have to be performed. Two different types of experiments and identification procedures have proven to be practical. One possible approach is to apply a *chirp signal* to one or more actuators and to analyse the torques measured by the torque sensors; this strategy was also used in [26], but for a significantly simpler system. This experiment was performed on a test bed for differentials as shown in Figure 3.24. The reference for the air-gap torque of the input drive *M1* was chosen as

$$T_{ag1,ref.}(t) = 500\,\mathrm{N\,m} + 100\,\mathrm{N\,m}\sin\left(2\pi\int_0^t f_{exc}(\tau)\mathrm{d}\tau\right) \tag{3.55}$$

with f_{exc} increasing linearly over time from 0 Hz to 1000 Hz in 100 s. The 500 N m torque offset is practical to avoid parasitic phenomena caused by gear play. In Figure 3.28 a characteristic system response is shown. The sign of the measured torques T_{f2} and T_{f3} was changed for clarity. This plot is dominated by a low frequency resonance peak visible in the torque measured at the input and the output drives. Additional higher resonances occur partially in all measurement signals or only at the input or only at the output drives. This frequency response can be used to finally tune the system parameters by comparing measurement data and simulation results. Additionally, the number of relevant resonance peaks determines the number of flexible shaft couplings required in the mechanical system model. Another popular method for the identification of relevant resonant frequencies, and for analysing rotating mechanical systems in general is the use of *Campbell diagrams*, see e.g. [83–85]. Instead of using chirp signals this method is often based on rotational speed ramps.

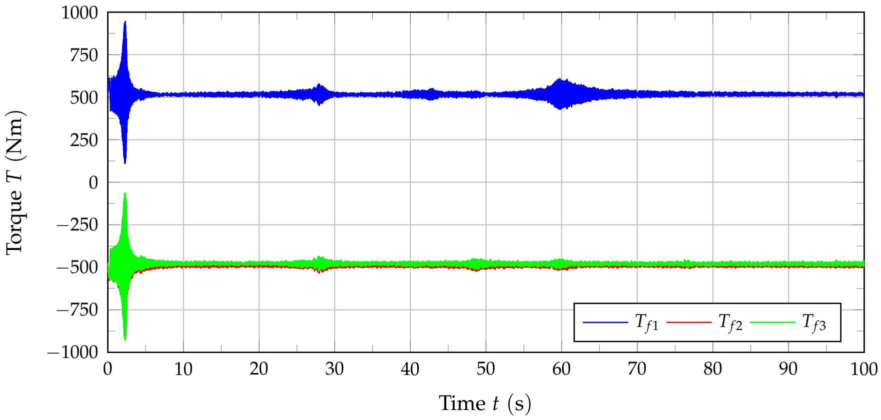

Figure 3.28: Experimental system identification for a test bed for differential gears with chirp signal, torques measured at the electric drives.

3.12 Torsional Vibration Analysis

Since torsional vibrations are critical on power train test systems, a *modal analysis* for the test bed for differential gears shown in Figure 3.24 is performed. The non-linear differential equations describing the mechanics of the test bed are given in Appendix C. It is shown that by the use of some simplifications, linear time-invariant (LTI) system models can be derived. This results in a model describing the test bed with a locking differential as UUT and another model for a test bed with an open differential without any slip-limiting functionality as UUT. These linear system models can be used to calculate the modal analysis. By computing the *eigenvalues* of the dynamic matrix the eigenfrequencies of the system are determined; the *eigenvectors* give information about the vibrational behaviour at those eigenfrequencies [55, 86]. Since the system is modelled by a set of first-order differential equations with angular velocities and angular positions as state variables, each eigenvector contains the information of the modal form twice: The eigenvector components for angular velocity are equal to the eigenvector components for angular position times the corresponding eigenvalue. The results of a numerically calculated modal analysis for the test bed with a locking differential are depicted in Figure 3.29.[3] The rotating bodies are labelled with their individual moment of inertia according to Figure 3.25. As stated in Appendix C, the differential gear is characterised by its overall moment of inertia I_{di} relating to the input shaft. In each sub-plot a single eigenmode is discussed by depicting the elements of the relevant eigenvector qualitatively. In Figure 3.29a the rigid body mode is shown; here all the inertias rotate in phase. Due to the transmission ratio of the differential gear, the eigenvector elements related to the differential's outputs are smaller. In Figure 3.29b the first non-zero eigenmode is shown; here the two output drives clearly oscillate against each other. This can be identified by the opposite sign of the eigenvector entries relevant for load drive $M2$ respectively load drive $M3$. The eigenmode at 21.9 Hz depicted in Figure 3.29c is often problematic, here the input drive oscillates against the two load drives. The next eigenmode shown in Figure 3.29d is characterised by the fact that the UUT oscillates against the three electric drives. The eigenmodes related to the torque measuring flanges are presented in Figure 3.29e, Figure 3.29f, and Figure 3.29g. These oscillation modes strongly affect the torque measurement signals.

The results of a numerically calculated modal analysis for the test bed with an open differential are depicted in Figure 3.30. These plots show some similarities with the results discussed above; however, some aspects are different. Since here the differential's output axles can have different angular velocities, an extra degree of freedom is introduced. For a convenient visualisation this extra system state is not shown directly. Instead, the behaviour of the two output axles labelled I_{do1} and I_{do2} is analysed. Rigid body modes are presented in Figure 3.30a; contrary to above no unique modal form exists for this problem setting. Because of the open differential's behaviour, the angular velocities of the two output axles can be arbitrary as long as their average speed matches the angular velocity of the differential's input scaled by the inverse of transmission ratio i_d. In Figure 3.30b the eigenmode where the input drive oscillates against the load drives is shown. The eigenmode presented in Figure 3.30d is characterised by the fact that the UUT oscillates against the electric drives. These two figures are very similar to Figure 3.29c and Figure 3.29d. This implies that these two oscillation modes are hardly affected by the type of differential gear that is tested. The eigenmodes related to the torque sensors are presented in Figure 3.30e, Figure 3.30f, and Figure 3.30g; these are again similar to the torque flange related oscillation modes from Figure 3.29. Only the eigenfrequencies are slightly different. In Figure 3.30c an eigenmode that is new compared to Figure 3.29 is shown. This new oscillation mode is characterised by strong torsional vibrations of the two outputs of the differential gear against each other, which is due to the behaviour of the open differential gear. This mode cannot occur with the locking differential discussed above. As shown in Figure 3.29b, with an locking differential the load drives would rather oscillate against each other.

---

[3] For the modal analysis a characteristic parameter set for this type of test bed was used, see Table C.1. As internal shaft damping coefficients are typically low, negligible damping was assumed for the modal analysis. Then eigenmodes are called 'real' and the bodies move in a way that they all reach their maximum or minimum positions at the same point in time [86]. This allows a simple two-dimensional visualisation.

The torsional vibration modes shown in Figure 3.29 and Figure 3.30 are characteristic for the power train test beds discussed in this work. Also other realistic parameter settings lead to similar results. The fact that most oscillation modes are nearly independent on the type of differential gear that is tested allows to design universal controllers for varying UUTs. Even different testing topologies typically show these phenomena with electric drives oscillating against each other or the UUT oscillating against some electric drives.

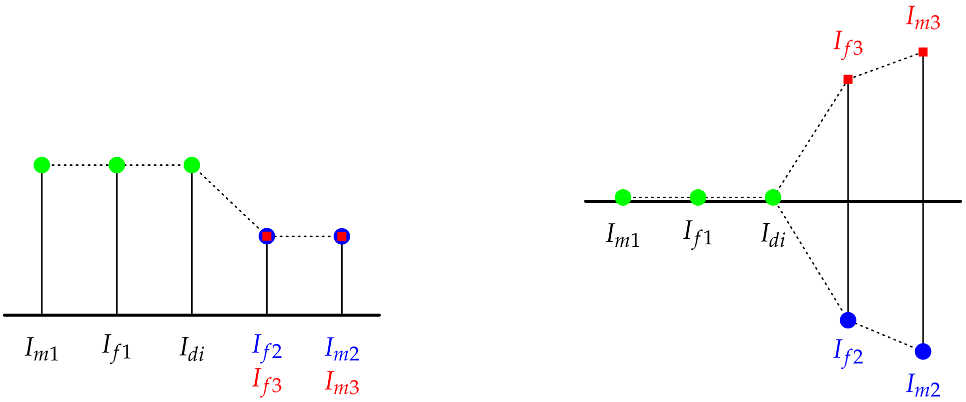
I_{m1}
I_{f1}
I_{di}
I_{f2}
I_{f3}
I_{m2}
I_{m3}
I_{f3}
I_{m3}
I_{m1}
I_{f1}
I_{di}
I_{f2}
I_{m2}

(a) Rigid body mode.

(b) Eigenmode $f_1 = 10.5\,\text{Hz}$.

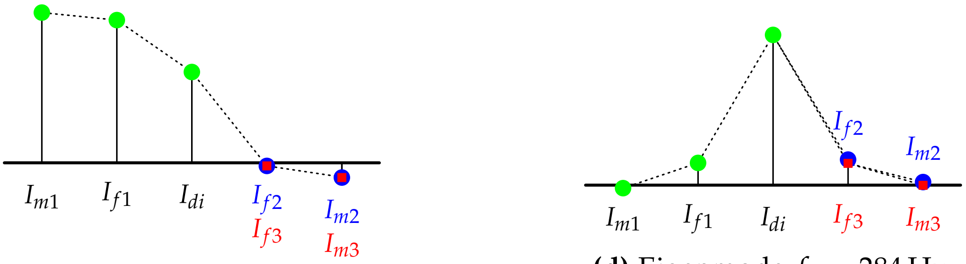
I_{m1}
I_{f1}
I_{di}
I_{f2}
I_{f3}
I_{m2}
I_{m3}
I_{f2}
I_{m2}
I_{m1}
I_{f1}
I_{di}
I_{f3}
I_{m3}

(c) Eigenmode $f_2 = 21.9\,\text{Hz}$.

(d) Eigenmode $f_3 = 284\,\text{Hz}$.

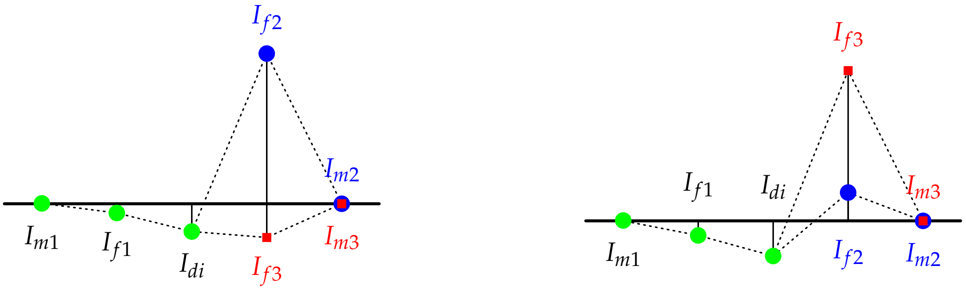
I_{f2}
I_{m2}
I_{m1}
I_{f1}
I_{di}
I_{f3}
I_{m3}
I_{f3}
I_{f1}
I_{di}
I_{m3}
I_{m1}
I_{f2}
I_{m2}

(e) Eigenmode $f_4 = 473\,\text{Hz}$.

(f) Eigenmode $f_5 = 499\,\text{Hz}$.

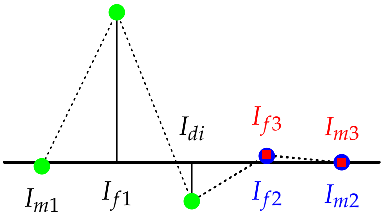
I_{di}
I_{f3}
I_{m3}
I_{m1}
I_{f1}
I_{f2}
I_{m2}

(g) Eigenmode $f_6 = 605\,\text{Hz}$.

Figure 3.29: Modal analysis of a test bed for differential gears with a locking differential as UUT.

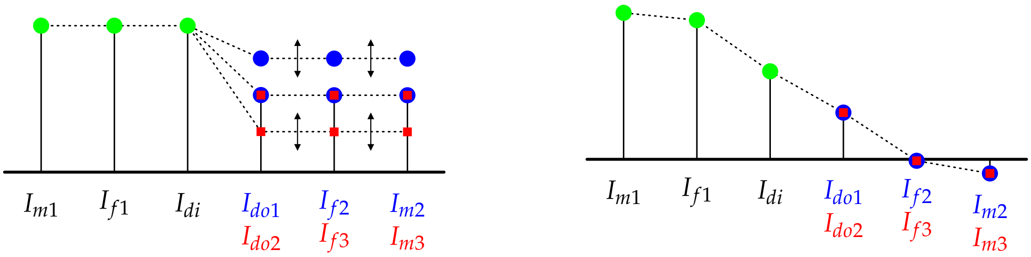
I_{m1}
I_{f1}
I_{di}
I_{do1}
I_{do2}
I_{f2}
I_{f3}
I_{m2}
I_{m3}

(a) Rigid body modes.

(b) Eigenmode $f_1 = 21.9\,\text{Hz}$.

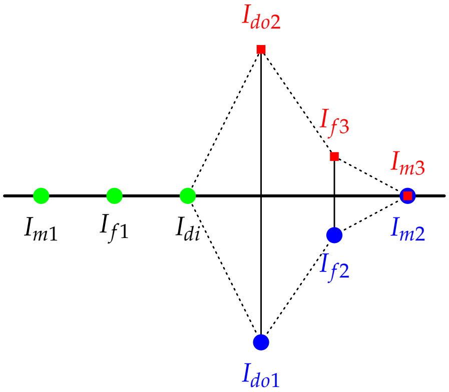
I_{do2}
I_{f3}
I_{m3}
I_{m1}
I_{f1}
I_{di}
I_{m2}
I_{f2}
I_{do1}

(c) Eigenmode $f_2 = 230\,\text{Hz}$.

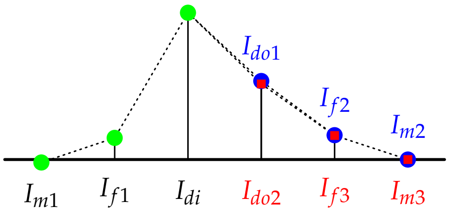
I_{do1}
I_{f2}
I_{m2}
I_{m1}
I_{f1}
I_{di}
I_{do2}
I_{f3}
I_{m3}

(d) Eigenmode $f_3 = 284\,\text{Hz}$.

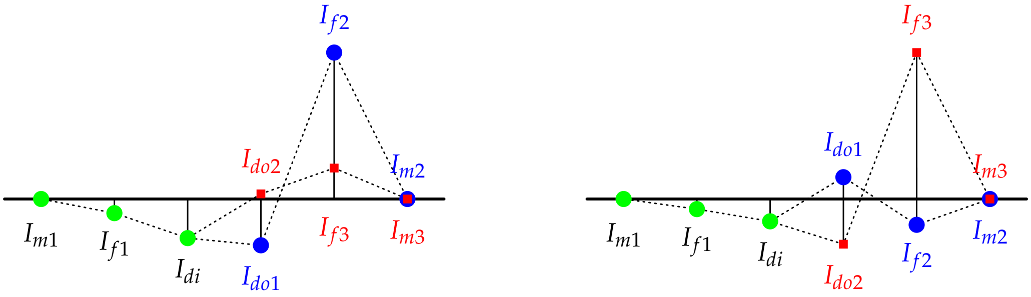
I_{f2}
I_{do2}
I_{m2}
I_{m1}
I_{f1}
I_{di}
I_{do1}
I_{f3}
I_{m3}
I_{f3}
I_{do1}
I_{m3}
I_{m1}
I_{f1}
I_{di}
I_{do2}
I_{f2}
I_{m2}

(e) Eigenmode $f_4 = 483\,\text{Hz}$.

(f) Eigenmode $f_5 = 508\,\text{Hz}$.

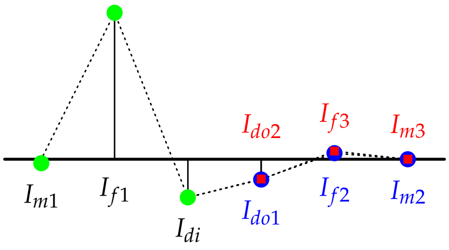
I_{do2}
I_{f3}
I_{m3}
I_{m1}
I_{f1}
I_{di}
I_{do1}
I_{f2}
I_{m2}

(g) Eigenmode $f_6 = 605\,\text{Hz}$.

Figure 3.30: Modal analysis of a test bed for differential gears with an open differential as UUT.

Chapter 4

Simulation

The numerical simulations of power train test systems that are needed during the controller design process are based on the mathematical models presented in Chapter 3. These simulations are done using the Matlab®/Simulink® software environment. Consequently, the differential equations describing the test bed components that were derived in Chapter 3 must be implemented. However, since some of the discussed mechanical systems contain friction elements, a direct implementation is not advisable. Due to static and Coulomb friction torques, the dynamic dimension of these systems can change over time. In literature a system with this property is called a *variable dynamic dimension system (VDDS)* [42]. A typical example is the clutch; if the clutch torque is zero, the two clutch disks rotate independently from each other. As two moments of inertia rotate at their individual angular velocities, the system order is obviously two. If the clutch torque is increased, the difference in angular velocities will decrease, but because the angular velocities are still different, the system order remains two. When the clutch is finally completely engaged, the two clutch disks are forced to the same angular velocity; therefore, the system order is now reduced to one. For simulation this means that the angular velocities of the two clutch disks have to be kept identical for the engaged clutch. An alternative interpretation is that the differential angular velocity of the clutch disks must be vanishing. This has to be guaranteed by an appropriate simulation strategy, which will be discussed in this chapter. Since zeroing a state variable is easier to achieve than to force two system states to identical values, this strategy is pursued henceforth. As a consequence, the actually free choice of system states should be in a way so that the potentially vanishing differential velocities are chosen as state variables. This phenomenon of reduced system order is directly related to the friction model used. Some rather popular friction models are discussed in the following section.

4.1 Friction Models

There are many friction models available in literature, see e.g. [67, 87–89], each with certain advantages and disadvantages. Which one of these models is used usually depends on the purpose of the friction modelling. A very important criterion is that observed friction phenomena can be accurately described with as little computational resources as possible. Since friction is based on complex physical mechanisms, most friction models have to be simplifications to make simulation and especially identification of friction parameters practically doable.

The available friction models can be divided into *static* and *dynamic* models depending on the presence of frictional memory to include dynamics between angular velocity and friction torque. This work will focus on static models for friction because of their simplicity. Figure 4.1 shows some fundamental static models for friction based on *Coulomb friction* $T_{fr,c}$, *viscous friction* $T_{fr,v}$, and *static friction* $T_{fr,s}$. This figure also includes the *Stribeck model* to describe the Stribeck effect. Coulomb friction tends to bring the relative speed of two surfaces to zero, static friction then keeps them at zero relative speed. Due to these properties, those phenomena are widely used in automotive mechanical systems to synchronise rotating bodies.

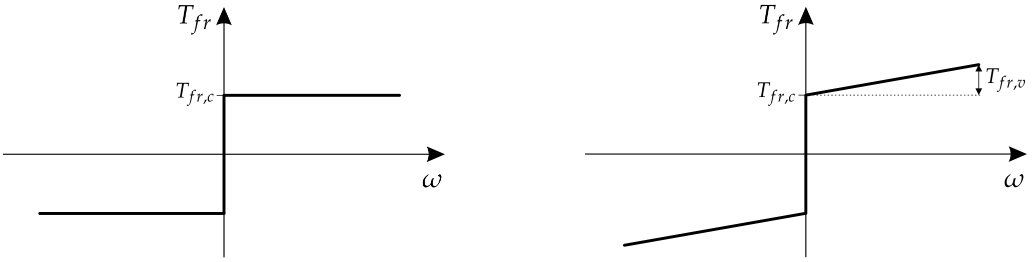

(a) Coulomb friction model. **(b)** Coulomb and viscous friction model.

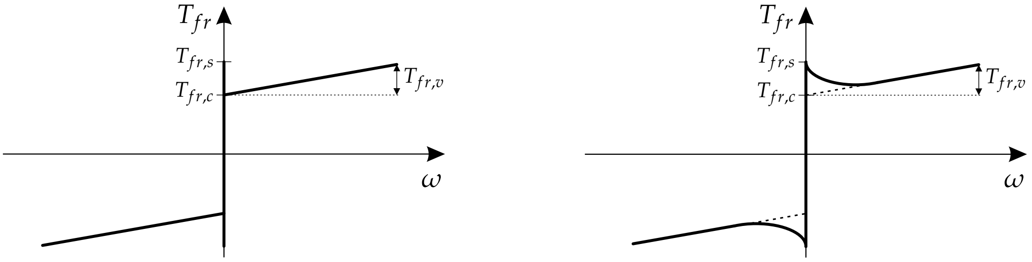

(c) Coulomb, viscous, and static friction model. **(d)** Coulomb and viscous friction with Stribeck effect.

Figure 4.1: Overview of different static models for friction.

In every model shown in Figure 4.1 the friction torque T_{fr} is a static function of the angular velocity ω between the two relevant contact surfaces. The friction models shown in Figure 4.1 are called *discontinuous* friction models because they include a discontinuity at $\omega = 0$. At zero velocity the friction torque cannot be described as a function of velocity only; instead, the resulting friction torque must be equal to the sum of external torques, with an upper and lower bound given by the static friction torque $T_{fr,s}$.

In Section 3.5 the clutch torque was modelled as

$$T_c = \mu_c \left[T_{c,c} + \left(T_{c,s} - T_{c,c} \right) \mathrm{e}^{-\frac{|\omega_{ci} - \omega_{co}|}{\omega_{c,s}}} + k_{c,v} \left| \omega_{ci} - \omega_{co} \right| \right] \operatorname{sgn}\left(\omega_{ci} - \omega_{co} \right); \qquad (4.1)$$

this is a static model for friction including the Stribeck effect as shown in Figure 4.1d. This calculation formula for the effective clutch torque T_c is obviously only valid for $\omega_{ci} \neq \omega_{co}$ while

$$T_c = \begin{cases} T_{ext.} & \text{if } |T_{ext.}| \leq T_{c,s} \\ T_{c,s} \operatorname{sgn}\left(T_{ext.} \right) & \text{otherwise} \end{cases}, \qquad (4.2)$$

where $T_{ext.}$ is the sum of external torques, holds for $\omega_{ci} = \omega_{co}$.

The friction torques defined in Section 3.6.3 to model loss torque T_{dl} and slip-limiting torque T_{dsl} for the differential gear are also in accordance with the static models for friction given in Figure 4.1. Both of them are composed of Coulomb friction $T_{fr,c}$ and viscous friction $T_{fr,v}$

$$T_{dl}(\omega_{di}) = \underbrace{\left(T_{dl0} + k_{dlT} \left| T_{di} \right| \right)}_{T_{fr,c}} \operatorname{sgn}\left(\omega_{di} \right) + \underbrace{k_{dl\omega} \omega_{di}}_{T_{fr,v}} \qquad (4.3)$$

$$T_{dsl}(\omega_3) = \underbrace{\left(T_{dsl0} + k_{dslT} \left| T_{di} \right| \right)}_{T_{fr,c}} \operatorname{sgn}\left(\omega_3 \right) + \underbrace{k_{dsl\omega} \omega_3}_{T_{fr,v}}. \qquad (4.4)$$

As for the clutch torque, here the sticking situation would have to be considered separately too; consequently, these formulas are only simplified representations and the alternative definition for the vanishing signum function is implicitly assumed. Equations (4.3) and (4.4) illustrate that the state variables chosen in the modelling process in Section 3.6.1 and Section 3.6.2 are convenient because each friction torque depends on just one state variable instead of a linear combination of both states. Because of the dependence on the differential's input torque T_{di}, the graphs presented in Figure 4.1 are not sufficient to show every friction dependency, but just the dependency on the angular velocities is critical for simulation aspects.

4.2 Numerical Simulation of Variable Dynamic Dimension Systems

The discontinuity at zero velocity shown in Figure 4.1 may lead to serious numerical problems in simulation. If friction is modelled by using a switching function as the signum function, there cannot be real sticking because once a state variable is near zero there is switching between positive and negative maximum static friction torque [87]. This leads to chattering which requires small simulation time steps. As a consequence, the simulation of systems including static and Coulomb friction requires some additional considerations; since only the discontinuity at zero velocity causes these simulation issues, viscous friction is typically not problematic.

To overcome these difficulties, the friction models can be altered by replacing the discontinuity at zero velocity by a continuous function with finite slope, see e.g. [88]. Choosing this slope too steep however may lead to stiff systems of differential equations requiring again a small integration step size, which might slow down the simulation dramatically. Additionally, there will never be real sticking because there is non-zero velocity even if the external torques are permanently less than the maximum static friction torque $T_{fr,s}$, especially if the slope of the curve approximating the discontinuity is not steep enough. An alternative approach for dealing with a VDDS is the concept of hybrid systems [90] where all possible sub-models with different system order are determined and a switching logic is used to commute between these sub-models. This strategy can be used for systems with rather small complexity such as the clutch [91] where only two system models for disengaged respectively engaged clutch are required. When the system becomes more complex and contains more friction elements, the number of sub-models required rises potentially exponentially and the correct handling of the transitions from one sub-model to another gets extensive [44, 75, 92, 93].

To resolve these simulation problems, in 1985 Karnopp proposed a *force-balance* model for one-dimensional problems using a small velocity window [9]. Outside this velocity window the moving body is assumed to be slipping and the friction torque or force can be an arbitrary function of velocity. Inside the velocity window the body is sticking and the friction force is determined to compensate the external forces; this keeps the body's velocity at a small constant value somewhere inside the velocity window. If the external forces are greater than the maximum static friction force, the sticking phase is left and the slipping state arises. In [94] Tariku and Rogers proposed a slightly modified concept using sign changes of sliding velocity instead of the small velocity window as criterion for the detection of sticking. The basic idea of force-balancing was initially presented for one-dimensional problems. This is briefly recapitulated in the next section before an extension to two-dimensional problems is presented.

4.2.1 One Element Affected by Coulomb or Static Friction

In this section problems of the form

$$\frac{\mathrm{d}\mathbf{x}}{\mathrm{d}t} = \mathbf{A}\mathbf{x} + \mathbf{B}\mathbf{u} - \mathbf{k}T_{fr1}(x_1) \tag{4.5}$$

are analysed with special focus on friction simulation. The N-dimensional vector $\mathbf{x} = [x_1, x_2, \dots, x_N]^{\mathrm{T}}$ is the state vector, $\mathbf{A} \in \mathbb{R}^{N \times N}$ is the dynamic matrix, the m system inputs are given by the input vector $\mathbf{u}$ while $\mathbf{B} \in \mathbb{R}^{N \times m}$ is the input matrix. The friction torque $T_{fr1} = T_{fr1}(x_1)$ is a function of the system state x_1 only, the vector $\mathbf{k} = [k_{11}, k_{21}, \dots, k_{N1}]^{\mathrm{T}}$ determines the friction torque's influence on the system dynamics. The simulation problem is completed by the definition of the friction torque T_{fr1} depending on x_1

$$T_{fr1}(x_1) = \begin{cases} t_{fr1}(x_1) & \text{if } x_1 \neq 0 \\ T_{fr1,s} & \text{if } x_1 = 0 \end{cases} \tag{4.6}$$

with

$$\begin{aligned} t_{fr1}(x_1) &> 0 \text{ if } x_1 > 0 \\ t_{fr1}(x_1) &< 0 \text{ if } x_1 < 0. \end{aligned} \tag{4.7}$$

$t_{fr1}(x_1)$ represents the friction torque for sliding while $T_{fr1,s}$ stands for the maximum static friction torque. If a dynamic system is not given in the form of System (4.5), as e.g. T_{fr1} also depends on other system states, a regular state transformation may be applied. At this point only physically meaningful systems where friction is dissipative are considered. A necessary criterion is that $k_{11} > 0$ has to hold.

When integrating Equation (4.5) numerically to calculate the state vector $\mathbf{x}$, the resulting friction torque has to be determined at every simulation time step. Because force-balancing is used, it is necessary to distinguish whether the system state x_1 is sticking or sliding; therefore, a distinction of cases is required.

Case 1

If $x_1 \neq 0$, no difficulty arises because no sticking occurs and the resulting friction torque is

$$T_{fr1} = t_{fr1}(x_1). \tag{4.8}$$

The dynamics of System (4.5) is then given by

$$\frac{\mathrm{d}\mathbf{x}}{\mathrm{d}t} = \mathbf{A}\mathbf{x} + \mathbf{B}\mathbf{u} - \mathbf{k}t_{fr1}(x_1). \tag{4.9}$$

Case 2

If $x_1 = 0$, as proposed by Karnopp, the friction torque required to keep this state at zero (${}^{\mathrm{d}x_1}/_{\mathrm{d}t} = 0$) can be determined according to

$$\widetilde{T}_{fr1} = \frac{1}{k_{11}} \left(\mathbf{a}_1^{\mathrm{T}} \mathbf{x} + \mathbf{b}_1^{\mathrm{T}} \mathbf{u} \right), \tag{4.10}$$

where $\mathbf{b}_1^{\mathrm{T}}$ is the first row of $\mathbf{B}$ and $\mathbf{a}_1^{\mathrm{T}}$ is the first row of $\mathbf{A}$. Using this virtual torque $\widetilde{T}_{fr1}$ the resulting friction torque is

$$T_{fr1} = \begin{cases} \widetilde{T}_{fr1} & \text{if } |\widetilde{T}_{fr1}| \leq T_{fr1,s} \\ T_{fr1,s}\mathrm{sgn}(\widetilde{T}_{fr1}) & \text{otherwise} \end{cases}. \tag{4.11}$$

Consequently, the dynamics of System (4.5) is given by

$$\frac{\mathrm{d}\mathbf{x}}{\mathrm{d}t} = \begin{cases} \begin{bmatrix} 0 \\ \begin{pmatrix} \mathbf{a}_2^{\mathrm{T}} \\ \vdots \\ \mathbf{a}_N^{\mathrm{T}} \end{pmatrix} \mathbf{x} + \begin{pmatrix} \mathbf{b}_2^{\mathrm{T}} \\ \vdots \\ \mathbf{b}_N^{\mathrm{T}} \end{pmatrix} \mathbf{u} - \begin{bmatrix} k_{21} \\ \vdots \\ k_{N1} \end{bmatrix} \widetilde{T}_{fr1} \end{bmatrix} & \text{if } |\widetilde{T}_{fr1}| \leq T_{fr1,s} \\ \mathbf{A}\mathbf{x} + \mathbf{B}\mathbf{u} - \mathbf{k}T_{fr1,s}\mathrm{sgn}(\widetilde{T}_{fr1}) & \text{otherwise} \end{cases}, \tag{4.12}$$

where $\mathbf{a}_i^{\mathrm{T}}$ and $\mathbf{b}_i^{\mathrm{T}}$ are the i^{th} row of $\mathbf{A}$ and $\mathbf{B}$ respectively. Depending on the available static friction the system state will either stay at $x_1 = 0$ or start slipping (${}^{\mathrm{d}x_1}/_{\mathrm{d}t} \neq 0$). These findings are presented in Figure 4.2, where the friction torque T_{fr1} is plotted as a function of $\mathbf{a}_1^{\mathrm{T}}\mathbf{x} + \mathbf{b}_1^{\mathrm{T}}\mathbf{u}$. It is obvious that three different cases can occur. In situation ① the external torques are compensated by the friction torque. In area ② the maximum positive static friction torque must be applied, while in section ③ the

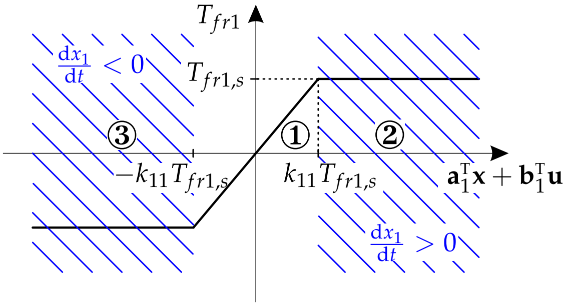

Figure 4.2: Friction torque calculation for one-dimensional problems at $x_1 = 0$ according to the force-balancing strategy.

maximum negative static friction torque is required. Additionally, regions where a transition from sticking to slipping state occurs are marked in blue in Figure 4.2.

This simulation strategy can also be applied to systems of the more general form

$$\frac{\mathrm{d}\mathbf{x}}{\mathrm{d}t} = \mathbf{A}\mathbf{x} + \mathbf{B}\mathbf{u} - \underbrace{\begin{pmatrix} k_{11} & \dots & k_{1p} \\ k_{21} & \dots & k_{2p} \\ \vdots & \ddots & \vdots \\ k_{N1} & \dots & k_{Np} \end{pmatrix}}_{=:\mathbf{K}} \underbrace{\begin{bmatrix} T_{fr1} \\ T_{fr2} \\ \vdots \\ T_{frp} \end{bmatrix}}_{=:\mathbf{T}_{fr}}, \tag{4.13}$$

where N is the system order and $p \leq N$ is the number of friction torques. Each friction torque $T_{fri} = T_{fri}\left(x_i\right)$ is a function of the system state x_i only for $i \in \{1, \dots, p\}$. The diagonal elements k_{11} to k_{pp} of $\mathbf{K}$ must be positive to ensure that friction is dissipative. To avoid couplings among the friction terms that would complicate friction calculation, the elements in the first p rows of $\mathbf{K}$ apart from the diagonal elements k_{11} to k_{pp} must be zero. If these conditions are fulfilled, this friction simulation problem can be divided into sub-problems similar to System (4.5).

Simulation Example

This simulation strategy has been implemented in Simulink® using zero crossing detection and a variable step size solver to detect sticking reliably [95]. Additionally, the state variable affected by friction is set to zero and kept at this value actively while sticking. This prevents variations in velocity due to errors from numerical friction calculation. The simulation strategy shall be tested on the basis of the scalar dynamic system

$$\frac{\mathrm{d}x}{\mathrm{d}t} = u - T_{fr}(x), \tag{4.14}$$

where the friction torque T_{fr} is given by Coulomb friction $T_{fr,c}$ according to Figure 4.1a only. This system is obviously in the form of System (4.5). The simulation results are presented in Figure 4.3. The system input u and the initial condition of the state variable x were selected so that some transitions from slipping to sticking and vice versa occur. It can be seen that sticking is detected reliably at $t \approx 1.3\,\mathrm{s}$ and $t \approx 3.5\,\mathrm{s}$. During the sticking phases the system input u is compensated by the friction torque T_{fr} so that the system variable x remains at zero. This comes without any chattering resulting in a very small simulation step size. When at $t \approx 2.0\,\mathrm{s}$ the system input u exceeds the maximum static friction, the system changes from sticking to slipping.

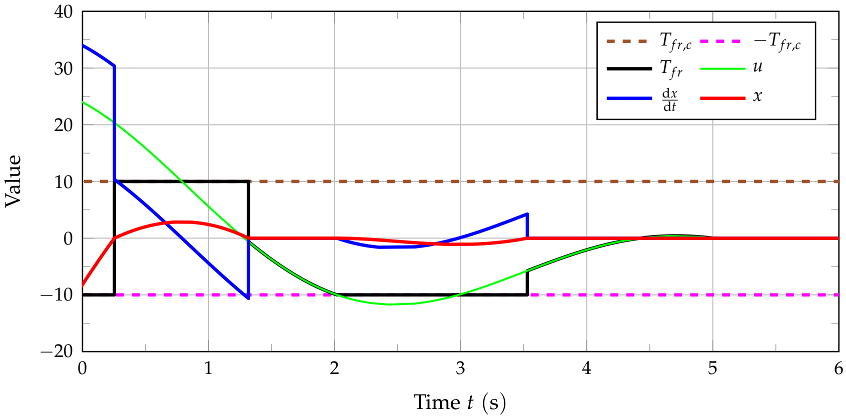

Figure 4.3: Results of a numerical simulation of a scalar system with Coulomb friction using the force-balancing strategy.

Power Train Example: Clutch

In Section 3.5 a mathematical model for a friction clutch was presented. This system is a typical example for a VDDS. If the clutch is disengaged, the two clutch disks rotate at angular velocities ω_{ci} and ω_{co}; consequently, the mathematical model is a second order system. However, if the clutch is engaged, these two elements are forced to the same angular velocity and thus the dynamic dimension is reduced from two to one. To bring the mathematical model from Section 3.5 into a form equivalent to System (4.5), the state transformation[1]

$$\begin{bmatrix} \omega_0 \\ \Delta\omega_c \end{bmatrix} = \begin{pmatrix} 1 & -\frac{I_{co}}{I_{ci}+I_{co}} \\ 1 & -1 \end{pmatrix} \begin{bmatrix} \omega_{ci} \\ \omega_{co} \end{bmatrix} \tag{4.15}$$

can be applied. This results in

$$\frac{d\omega_0}{dt} = \frac{T_{ci}}{I_{ci}+I_{co}} - \frac{T_{co}}{I_{ci}+I_{co}} \tag{4.16a}$$

$$\frac{d\Delta\omega_c}{dt} = \frac{T_{ci}}{I_{ci}} + \frac{T_{co}}{I_{co}} - \left(\frac{1}{I_{ci}} + \frac{1}{I_{co}}\right) T_c. \tag{4.16b}$$

The clutch torque T_c is then a function of the relative angular velocity of the two clutch disks $\Delta\omega_c$

$$T_c = T_c\left(\omega_{ci} - \omega_{co}\right) = T_c\left(\Delta\omega_c\right). \tag{4.17}$$

Another example for this type of simulation problem is the torque converter with lock-up clutch as presented in Section 3.7.1.

---

[1] This state transformation is only one possibility, other choices of system states are admissible as well.

4.2.2 Two Elements Affected by Coulomb or Static Friction

If two elements that are affected by Coulomb or static friction are part of the simulation problem, a system of differential equations of the form

$$\frac{\mathrm{d}\mathbf{x}}{\mathrm{d}t} = \mathbf{A}\mathbf{x} + \mathbf{B}\mathbf{u} - \underbrace{\begin{pmatrix} k_{11} & k_{12} \\ k_{21} & k_{22} \\ \vdots & \vdots \\ k_{N1} & k_{N2} \end{pmatrix}}_{=:\mathbf{K}} \underbrace{\begin{bmatrix} T_{fr1} \\ T_{fr2} \end{bmatrix}}_{=:\mathbf{T}_{fr}} \tag{4.18}$$

results. The N-dimensional vector $\mathbf{x} = [x_1, x_2, \ldots, x_N]^{\mathrm{T}}$ is the state vector, $\mathbf{A} \in \mathbb{R}^{N\times N}$ is the dynamic matrix, the m system inputs are given by the input vector $\mathbf{u}$, while $\mathbf{B} \in \mathbb{R}^{N\times m}$ is the input matrix. The friction torque $T_{fr1} = T_{fr1}\left(x_1\right)$ is a function of the system state x_1 while $T_{fr2} = T_{fr2}\left(x_2\right)$ is a function of the system state x_2 only. The simulation problem is completed by the definition of the friction torques T_{fr1} and T_{fr2}

$$T_{fri}(x_i) = \begin{cases} t_{fri}(x_i) & \text{if } x_i \neq 0 \\ T_{fri,s} & \text{if } x_i = 0 \end{cases} \tag{4.19}$$

with

$$\begin{aligned} t_{fri}(x_i) &> 0 \text{ if } x_i > 0 \\ t_{fri}(x_i) &< 0 \text{ if } x_i < 0 \end{aligned} \tag{4.20}$$

for $i \in \{1, 2\}$. $t_{fri}(x_i)$ represents the friction torque for sliding while $T_{fri,s}$ stands for the maximum static friction torque for sticking. The matrix $\mathbf{K} \in \mathbb{R}^{N\times 2}$ determines the friction torques' influence on the system dynamics. In the following, only systems where friction is dissipative are considered. If $H(\mathbf{x}) = \frac{1}{2}\mathbf{x}^{\mathrm{T}}\mathbf{x}$ is the energy function of the autonomous system, its time derivative is

$$\frac{\mathrm{d}H(\mathbf{x})}{\mathrm{d}t} = p = \mathbf{x}^{\mathrm{T}}\left(\mathbf{A}\mathbf{x} - \mathbf{K}\mathbf{T}_{fr}\right) = \mathbf{x}^{\mathrm{T}}\mathbf{A}\mathbf{x}\underbrace{-\mathbf{x}^{\mathrm{T}}\mathbf{K}\mathbf{T}_{fr}}_{=:p_{fr}}. \tag{4.21}$$

As at this point only the influence of friction is investigated, the term $\mathbf{x}^{\mathrm{T}}\mathbf{A}\mathbf{x}$ is excluded and

$$p_{fr} = \underbrace{-\begin{bmatrix} x_1 & x_2 \end{bmatrix} \mathbf{K}_{22}\mathbf{T}_{fr}(x_1, x_2)}_{=:p_{fr,12}} - \begin{bmatrix} x_3 & \cdots & x_N \end{bmatrix} \mathbf{K}_r\mathbf{T}_{fr}(x_1, x_2) \tag{4.22}$$

with matrices

$$\mathbf{K}_{22} := \begin{pmatrix} k_{11} & k_{12} \\ k_{21} & k_{22} \end{pmatrix}, \quad \mathbf{K}_r := \begin{pmatrix} k_{31} & k_{32} \\ \vdots & \vdots \\ k_{N1} & k_{N2} \end{pmatrix} \tag{4.23}$$

remains. By using

$$\mathbf{T}_{fr} = \begin{pmatrix} \widetilde{t}_{fr1}(x_1) & 0 \\ 0 & \widetilde{t}_{fr2}(x_2) \end{pmatrix} \begin{bmatrix} x_1 \\ x_2 \end{bmatrix} \tag{4.24}$$

with functions $\widetilde{t}_{fr1}(x_1) > 0$ and $\widetilde{t}_{fr2}(x_2) > 0$, the term $p_{fr,12}$ in Equation (4.22) can be further analysed:

$$p_{fr,12} = -\begin{bmatrix} x_1 & x_2 \end{bmatrix} \mathbf{K}_{22} \begin{pmatrix} \widetilde{t}_{fr1}(x_1) & 0 \\ 0 & \widetilde{t}_{fr2}(x_2) \end{pmatrix} \begin{bmatrix} x_1 \\ x_2 \end{bmatrix} \tag{4.25}$$

As $\widetilde{t}_{fr1}(x_1) > 0$ and $\widetilde{t}_{fr2}(x_2) > 0$ hold, this quadratic form is negative for non-zero x_1 and x_2 if the matrix $\mathbf{K}_{22}$ is positive definite. Therefore, a positive definite friction matrix $\mathbf{K}_{22}$ is a necessary criterion for friction to be dissipative. This i.a. implies that $k_{11} > 0$ and $k_{22} > 0$ must hold.

When Equation (4.18) is integrated numerically to calculate the state vector $\mathbf{x}$, the resulting friction torques have to be determined at every simulation time step. To do so, the basic idea of force-balancing can also be applied to this dynamic system. But since there is not just one moving body affected by friction, an extension is required. Applying force-balancing is particularly difficult because in addition to the external torques given by the system input $\mathbf{u}$, T_{fr1} has to be considered as well when calculating T_{fr2} and vice versa. In simulation this could result in an algebraic loop. A solution for this problem was proposed in [71]; in the following, these results are presented in a slightly modified form. As in the simpler problem setting discussed before, it is necessary to distinguish whether a system state is sticking or sliding. Since there are now two state variables affected by friction, four cases in total are possible [10, 71].

Case 1

If $x_1 \neq 0$ and $x_2 \neq 0$, no difficulty arises because none of the state variables is zero and the resulting friction torques are

$$T_{fri} = t_{fri}(x_i) \tag{4.26}$$

for $i \in \{1,2\}$. The dynamics of System (4.18) is given by

$$\frac{\mathrm{d}\mathbf{x}}{\mathrm{d}t} = \mathbf{A}\mathbf{x} + \mathbf{B}\mathbf{u} - \mathbf{K} \begin{bmatrix} t_{fr1}(x_1) \\ t_{fr2}(x_2) \end{bmatrix}. \tag{4.27}$$

Case 2

If $x_1 = 0$ and $x_2 \neq 0$, the friction torque T_{fr2} is given by

$$T_{fr2} = t_{fr2}(x_2). \tag{4.28}$$

The state variable x_1 is zero and as proposed by Karnopp, the friction torque required to keep this state at zero ($\mathrm{d}x_1/\mathrm{d}t = 0$) can be determined as

$$\widetilde{T}_{fr1} = \frac{1}{k_{11}} \left[\mathbf{a}_1^{\mathrm{T}} \mathbf{x} + \mathbf{b}_1^{\mathrm{T}} \mathbf{u} - k_{12} t_{fr2} \left(x_2 \right) \right], \tag{4.29}$$

where $\mathbf{a}_1^{\mathrm{T}}$ is the first row of $\mathbf{A}$ and $\mathbf{b}_1^{\mathrm{T}}$ is the first row of $\mathbf{B}$. By the use of this virtual torque $\widetilde{T}_{fr1}$, the resulting friction torque is

$$T_{fr1} = \begin{cases} \widetilde{T}_{fr1} & \text{if } |\widetilde{T}_{fr1}| \leq T_{fr1,s} \\ T_{fr1,s} \mathrm{sgn}(\widetilde{T}_{fr1}) & \text{otherwise} \end{cases}. \tag{4.30}$$

Consequently, the dynamics of System (4.18) is given by

$$\frac{\mathrm{d}\mathbf{x}}{\mathrm{d}t} = \begin{cases} \begin{bmatrix} 0 \\ \begin{pmatrix} \mathbf{a}_2^{\mathrm{T}} \\ \vdots \\ \mathbf{a}_N^{\mathrm{T}} \end{pmatrix} \mathbf{x} + \begin{pmatrix} \mathbf{b}_2^{\mathrm{T}} \\ \vdots \\ \mathbf{b}_N^{\mathrm{T}} \end{pmatrix} \mathbf{u} - \begin{pmatrix} k_{21} & k_{22} \\ \vdots & \vdots \\ k_{N1} & k_{N2} \end{pmatrix} \begin{bmatrix} \widetilde{T}_{fr1} \\ t_{fr2}(x_2) \end{bmatrix} \end{bmatrix} & \text{if } |\widetilde{T}_{fr1}| \leq T_{fr1,s} \\ \mathbf{A}\mathbf{x} + \mathbf{B}\mathbf{u} - \mathbf{K} \begin{bmatrix} T_{fr1,s} \mathrm{sgn}(\widetilde{T}_{fr1}) \\ t_{fr2}(x_2) \end{bmatrix} & \text{otherwise} \end{cases}, \tag{4.31}$$

where $\mathbf{a}_i^{\mathrm{T}}$ and $\mathbf{b}_i^{\mathrm{T}}$ are the i^{th} row of $\mathbf{A}$ and $\mathbf{B}$ respectively. Depending on the maximum static friction the critical state variable will either stay at $x_1 = 0$ or start slipping ($\mathrm{d}x_1/\mathrm{d}t \neq 0$).

Case 3

The case $x_1 \neq 0$ and $x_2 = 0$ is equivalent to 'Case 2' if the system states x_1 and x_2 are interchanged.

Case 4

If $x_1 = 0$ and $x_2 = 0$, the virtual friction torques required to keep these two state variables at zero can be determined by setting $\mathrm{d}x_1/\mathrm{d}t$ and $\mathrm{d}x_2/\mathrm{d}t$ to zero what leads to

$$\begin{bmatrix} \widetilde{T}_{fr1} \\ \widetilde{T}_{fr2} \end{bmatrix} = \mathbf{K}_{22}^{-1} \left[\begin{pmatrix} \mathbf{a}_1^\mathrm{T} \\ \mathbf{a}_2^\mathrm{T} \end{pmatrix} \mathbf{x} + \begin{pmatrix} \mathbf{b}_1^\mathrm{T} \\ \mathbf{b}_2^\mathrm{T} \end{pmatrix} \mathbf{u} \right] . \tag{4.32}$$

If $|\widetilde{T}_{fri}| \leq T_{fri,s}$ for $i \in \{1,2\}$, a valid solution for the friction torques is found and the system dynamics are

$$\frac{\mathrm{d}\mathbf{x}}{\mathrm{d}t} = \begin{bmatrix} 0 \\ 0 \\ \begin{pmatrix} \mathbf{a}_3^\mathrm{T} \\ \vdots \\ \mathbf{a}_N^\mathrm{T} \end{pmatrix} \mathbf{x} + \begin{pmatrix} \mathbf{b}_3^\mathrm{T} \\ \vdots \\ \mathbf{b}_N^\mathrm{T} \end{pmatrix} \mathbf{u} - \begin{pmatrix} k_{31} & k_{32} \\ \vdots & \vdots \\ k_{N1} & k_{N2} \end{pmatrix} \begin{bmatrix} \widetilde{T}_{fr1} \\ \widetilde{T}_{fr2} \end{bmatrix} \end{bmatrix} . \tag{4.33}$$

The state variables x_1 and x_2 will then obviously remain at zero ($\mathrm{d}x_i/\mathrm{d}t = 0$ for $i \in \{1,2\}$).

Since there is limited static friction, if either the absolute value of $\widetilde{T}_{fr1}$ is greater than $T_{fr1,s}$ or the absolute value of $\widetilde{T}_{fr2}$ is greater than $T_{fr2,s}$, further calculations are necessary to determine a correct solution. Just limiting the calculated friction torques to their maximum values as suggested in [10] is not sufficient because both relevant system states are dependent on both friction torques and limiting e.g. T_{fr1} influences the state variable x_2 as well. An idea to find a solution nevertheless is presented below.

The conditions

$$|\widetilde{T}_{fr1}| \leq T_{fr1,s} \tag{4.34a}$$

$$|\widetilde{T}_{fr2}| \leq T_{fr2,s} \tag{4.34b}$$

can be visualised in a two-dimensional plane if x- and y-axis are chosen as

$$x = \mathbf{a}_1^\mathrm{T}\mathbf{x} + \mathbf{b}_1^\mathrm{T}\mathbf{u} \tag{4.35a}$$

$$y = \mathbf{a}_2^\mathrm{T}\mathbf{x} + \mathbf{b}_2^\mathrm{T}\mathbf{u}. \tag{4.35b}$$

Condition (4.34a) can be interpreted in this x-y plane as the area between the two parallel straight lines

$$y = \frac{k_{22}}{k_{12}} x \pm \frac{(k_{11}k_{22} - k_{12}k_{21})\, T_{fr1,s}}{k_{12}}. \tag{4.36}$$

Also Condition (4.34b) can be translated into a region between the two parallel straight lines

$$y = \frac{k_{21}}{k_{11}} x \pm \frac{(k_{11}k_{22} - k_{12}k_{21})\, T_{fr2,s}}{k_{11}}. \tag{4.37}$$

The intersection of these lines forms a parallelogram where Condition (4.34) holds, see sector ① in Figure 4.4. On the border of this parallelogram at least one of the two important friction torques is at its positive or negative maximum value. The same holds for the area outside of this central sector. This outer region will be further investigated in the following.

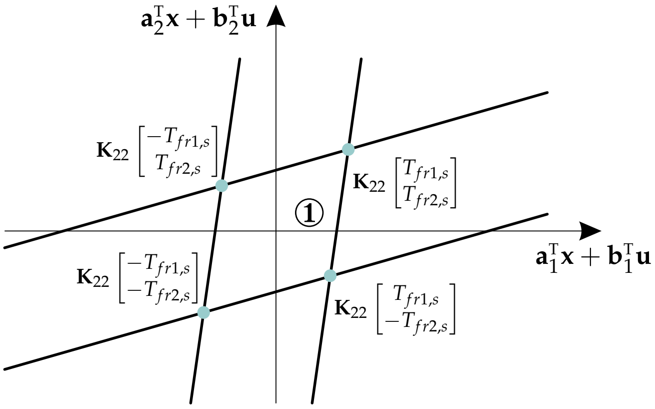
$\mathbf{a}_2^{\mathrm{T}}\mathbf{x} + \mathbf{b}_2^{\mathrm{T}}\mathbf{u}$
$\mathbf{a}_1^{\mathrm{T}}\mathbf{x} + \mathbf{b}_1^{\mathrm{T}}\mathbf{u}$
$\mathbf{K}_{22}\begin{bmatrix}-T_{fr1,s}\\ T_{fr2,s}\end{bmatrix}$
$\mathbf{K}_{22}\begin{bmatrix}T_{fr1,s}\\ T_{fr2,s}\end{bmatrix}$
①
$\mathbf{K}_{22}\begin{bmatrix}-T_{fr1,s}\\ -T_{fr2,s}\end{bmatrix}$
$\mathbf{K}_{22}\begin{bmatrix}T_{fr1,s}\\ -T_{fr2,s}\end{bmatrix}$

Figure 4.4: Friction torque calculation for two-dimensional problems at $x_1 = 0$ and $x_2 = 0$ according to the force–balancing strategy, sector ①.

If T_{fr2} is assumed to be at its positive maximum value

$$T_{fr2} = T_{fr2,s}, \tag{4.38}$$

the dynamics of the state variable x_2 must fulfil

$$\frac{\mathrm{d}x_2}{\mathrm{d}t} \geq 0 \tag{4.39}$$

because otherwise the friction torque would have to be different. By using Equation (4.38), the friction torque T_{fr1} required to maintain $\mathrm{d}x_1/\mathrm{d}t = 0$ can be determined as

$$T_{fr1} = \frac{1}{k_{11}} \left(\mathbf{a}_1^{\mathrm{T}}\mathbf{x} + \mathbf{b}_1^{\mathrm{T}}\mathbf{u} - k_{12} T_{fr2,s} \right). \tag{4.40}$$

Since T_{fr1} is limited by the maximum respectively minimum static friction torque, Equation (4.40) only gives the final result if

$$|T_{fr1}| \leq T_{fr1,s} \tag{4.41}$$

holds. Condition (4.41) is equivalent to situations given by certain **x** and **u** that are between the two vertical lines

$$x = \pm k_{11} T_{fr1,s} + k_{12} T_{fr2,s} \tag{4.42}$$

in the afore introduced x-y plane. Condition (4.39) can be further analysed by evaluating the system dynamics for the friction torques given by Equation (4.38) and Equation (4.40). This criterion can then be interpreted as the area in the x-y plane lying above the straight line

$$y = \frac{k_{21}}{k_{11}} x + \frac{(k_{11}k_{22} - k_{12}k_{21})\, T_{fr2,s}}{k_{11}}. \tag{4.43}$$

The intersection of these two regions forms a special area in the x-y plane labelled sector ②, see Figure 4.5. If the given $\mathbf{x}$ and $\mathbf{u}$ are within this sector, the friction torques needed to calculate the system dynamics are given by Equation (4.38) and Equation (4.40).

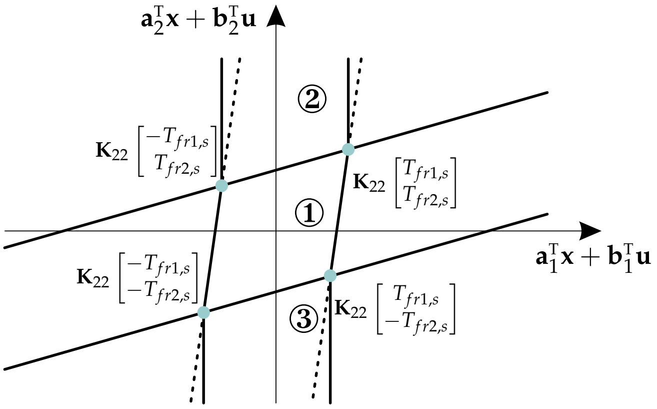
$\mathbf{a}_2^{\mathrm{T}}\mathbf{x} + \mathbf{b}_2^{\mathrm{T}}\mathbf{u}$
②
$\mathbf{K}_{22}\begin{bmatrix}-T_{fr1,s}\\ T_{fr2,s}\end{bmatrix}$
$\mathbf{K}_{22}\begin{bmatrix}T_{fr1,s}\\ T_{fr2,s}\end{bmatrix}$
①
$\mathbf{a}_1^{\mathrm{T}}\mathbf{x} + \mathbf{b}_1^{\mathrm{T}}\mathbf{u}$
$\mathbf{K}_{22}\begin{bmatrix}-T_{fr1,s}\\ -T_{fr2,s}\end{bmatrix}$
③
$\mathbf{K}_{22}\begin{bmatrix}T_{fr1,s}\\ -T_{fr2,s}\end{bmatrix}$

Figure 4.5: Friction torque calculation for two-dimensional problems at $x_1 = 0$ and $x_2 = 0$ according to the force–balancing strategy, sectors ② and ③.

If however T_{fr2} is assumed to be at its negative maximum value

$$T_{fr2} = -T_{fr2,s}, \tag{4.44}$$

the dynamics of the state variable x_2 must fulfil

$$\frac{\mathrm{d}x_2}{\mathrm{d}t} \leq 0. \tag{4.45}$$

Similar to before, the friction torque T_{fr1} required to maintain $\mathrm{d}x_1/\mathrm{d}t = 0$ can be determined as

$$T_{fr1} = \frac{1}{k_{11}} \left(\mathbf{a}_1^{\mathrm{T}}\mathbf{x} + \mathbf{b}_1^{\mathrm{T}}\mathbf{u} + k_{12}T_{fr2,s} \right) \tag{4.46}$$

by using Equation (4.44). If we again assume

$$|T_{fr1}| \leq T_{fr1,s}, \tag{4.47}$$

the friction calculation problem is solved. Condition (4.47) defines an area between the two vertical lines

$$x = \pm k_{11} T_{fr1,s} - k_{12} T_{fr2,s} \tag{4.48}$$

in the discussed x-y plane. By Condition (4.45) the area below the straight line

$$y = \frac{k_{21}}{k_{11}} x - \frac{\left(k_{11} k_{22} - k_{12} k_{21}\right) T_{fr2,s}}{k_{11}} \tag{4.49}$$

is specified. The combination of these criteria forms sector ③, see also Figure 4.5.

To continue with partitioning the x-y plane into well-defined sectors, now the other relevant friction torque T_{fr1} is assumed to be at its positive maximum value

$$T_{fr1} = T_{fr1,s} \tag{4.50}$$

and the dynamics of the state variable x_1 must fulfil

$$\frac{\mathrm{d}x_1}{\mathrm{d}t} \geq 0. \tag{4.51}$$

Similar to before the friction torque T_{fr2} required to maintain $\mathrm{d}x_2/\mathrm{d}t = 0$ can be determined as

$$T_{fr2} = \frac{1}{k_{22}} \left(\mathbf{a}_2^{\mathrm{T}} \mathbf{x} + \mathbf{b}_2^{\mathrm{T}} \mathbf{u} - k_{21} T_{fr1,s} \right). \tag{4.52}$$

If this friction torque fulfils

$$|T_{fr2}| \leq T_{fr2,s}, \tag{4.53}$$

the friction calculation problem is solved. This condition can be interpreted as the area in the x-y plane located between the two horizontal lines

$$y = \pm k_{22} T_{fr2,s} + k_{21} T_{fr1,s}. \tag{4.54}$$

Condition (4.51) is equivalent to situations given by certain $\mathbf{x}$ and $\mathbf{u}$ that are to the right of the straight line

$$y = \frac{k_{22}}{k_{12}} x + \frac{\left(k_{11} k_{22} - k_{12} k_{21}\right) T_{fr1,s}}{k_{12}}. \tag{4.55}$$

The intersection of these two regions once more defines a sector in the x-y plane (sector ④), see Figure 4.6.

To finalise the first part of these considerations, T_{fr1} is assumed to be at its negative maximum value

$$T_{fr1} = -T_{fr1,s} \tag{4.56}$$

so that the dynamics of the state variable x_1 must fulfil

$$\frac{\mathrm{d}x_1}{\mathrm{d}t} \leq 0. \tag{4.57}$$

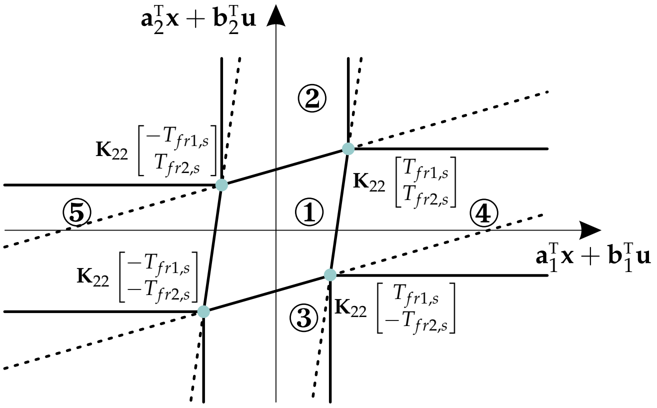
$\mathbf{a}_2^T\mathbf{x} + \mathbf{b}_2^T\mathbf{u}$
②
$\mathbf{K}_{22}\begin{bmatrix}-T_{fr1,s}\\T_{fr2,s}\end{bmatrix}$
$\mathbf{K}_{22}\begin{bmatrix}T_{fr1,s}\\T_{fr2,s}\end{bmatrix}$
⑤
①
④
$\mathbf{a}_1^T\mathbf{x} + \mathbf{b}_1^T\mathbf{u}$
$\mathbf{K}_{22}\begin{bmatrix}-T_{fr1,s}\\-T_{fr2,s}\end{bmatrix}$
③
$\mathbf{K}_{22}\begin{bmatrix}T_{fr1,s}\\-T_{fr2,s}\end{bmatrix}$

Figure 4.6: Friction torque calculation for two-dimensional problems at $x_1 = 0$ and $x_2 = 0$ according to the force–balancing strategy, sectors ④ and ⑤.

Then the friction torque T_{fr2} required to maintain $\mathrm{d}x_2/\mathrm{d}t = 0$ can be determined as

$$T_{fr2} = \frac{1}{k_{22}}\left(\mathbf{a}_2^T\mathbf{x} + \mathbf{b}_2^T\mathbf{u} + k_{21}T_{fr1,s}\right). \tag{4.58}$$

If we once more assume

$$|T_{fr2}| \leq T_{fr2,s}, \tag{4.59}$$

the friction calculation problem is solved. This condition specifies an area in the x-y plane that is between the two horizontal lines

$$y = \pm k_{22}T_{fr2,s} - k_{21}T_{fr1,s}. \tag{4.60}$$

Condition (4.57) defines the region to the left of the straight line

$$y = \frac{k_{22}}{k_{12}}x - \frac{(k_{11}k_{22} - k_{12}k_{21})\,T_{fr1,s}}{k_{12}}. \tag{4.61}$$

These two conditions identify sector ⑤, see also Figure 4.6.

At this point five of the nine possible situations regarding the system input **u** and the state vector **x** are dealt with. All these situations are characterised by the fact that at least one of the system states relevant for friction calculation will remain in sticking state. The bold lines in Figure 4.6 mark settings where at least one of the two friction torques is at its minimum or maximum value.

To finally complete this friction calculation scheme, T_{fr2} is once more assumed to be at its positive maximum value

$$T_{fr2} = T_{fr2,s}, \tag{4.62}$$

which implies that the dynamics of the state variable x_2 must fulfil

$$\frac{\mathrm{d}x_2}{\mathrm{d}t} \geq 0. \tag{4.63}$$

Now T_{fr1} is assumed to be at its positive maximum value too

$$T_{fr1} = T_{fr1,s} \tag{4.64}$$

and as a consequence, also the dynamics of the state variable x_1 must satisfy

$$\frac{\mathrm{d}x_1}{\mathrm{d}t} \geq 0. \tag{4.65}$$

Condition (4.65) defines the region to the right of the vertical line

$$x = k_{11}T_{fr1,s} + k_{12}T_{fr2,s} \tag{4.66}$$

while Condition (4.63) restricts to situations located above the horizontal line

$$y = k_{22}T_{fr2,s} + k_{21}T_{fr1,s}. \tag{4.67}$$

The intersection of these two regions forms sector ⑥, see Figure 4.7. Similar criteria for the system input **u** and the state vector **x** can be determined for the sectors ⑦–⑨ following the calculation procedure shown above. This leads to the results presented in Figure 4.7 and Table 4.1. Depending on the system input **u** and the state vector **x** a certain sector in Figure 4.7 is determined and according to Table 4.1 the desired friction torques can be calculated.

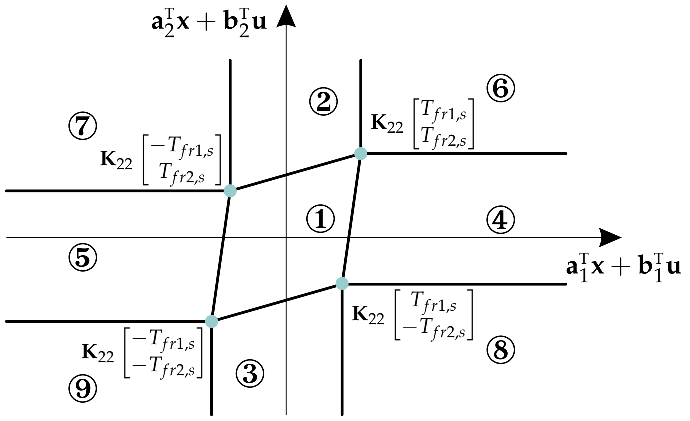
$\mathbf{a}_2^T\mathbf{x} + \mathbf{b}_2^T\mathbf{u}$
②
⑥
⑦
$\mathbf{K}_{22}\begin{bmatrix}T_{fr1,s}\\T_{fr2,s}\end{bmatrix}$
$\mathbf{K}_{22}\begin{bmatrix}-T_{fr1,s}\\T_{fr2,s}\end{bmatrix}$
①
④
⑤
$\mathbf{a}_1^T\mathbf{x} + \mathbf{b}_1^T\mathbf{u}$
$\mathbf{K}_{22}\begin{bmatrix}T_{fr1,s}\\-T_{fr2,s}\end{bmatrix}$
$\mathbf{K}_{22}\begin{bmatrix}-T_{fr1,s}\\-T_{fr2,s}\end{bmatrix}$
⑧
③
⑨

Figure 4.7: Friction torque calculation for two-dimensional problems at $x_1 = 0$ and $x_2 = 0$ according to the force–balancing strategy, sectors depending on system input **u** and state vector **x**.

In Figure 4.8 and Figure 4.9 some characteristics of the simulation approach discussed in this work are compared to the conventional approach as used in [10]. Since these two methods differ in the way 'Case 4' is handled, results for $x_1 = 0$ and $x_2 = 0$ are presented. In Figure 4.8 the friction torque T_{fr1} and the system state x_1 are analysed while in Figure 4.9 results related to the friction torque T_{fr2} and the

Table 4.1: Friction torque calculation for two-dimensional problems at $x_1 = 0$ and $x_2 = 0$ according to the force–balancing strategy, friction torques T_{fr1} and T_{fr2} depending on the sectors specified in Figure 4.7.

Sector	T_{fr1}	T_{fr2}
1	$\frac{k_{22}\mathbf{a}_1^{\mathrm{T}}\mathbf{x}+k_{22}\mathbf{b}_1^{\mathrm{T}}\mathbf{u}-k_{12}\mathbf{a}_2^{\mathrm{T}}\mathbf{x}-k_{12}\mathbf{b}_2^{\mathrm{T}}\mathbf{u}}{k_{11}k_{22}-k_{21}k_{12}}$	$\frac{k_{11}\mathbf{a}_2^{\mathrm{T}}\mathbf{x}+k_{11}\mathbf{b}_2^{\mathrm{T}}\mathbf{u}-k_{21}\mathbf{a}_1^{\mathrm{T}}\mathbf{x}-k_{21}\mathbf{b}_1^{\mathrm{T}}\mathbf{u}}{k_{11}k_{22}-k_{21}k_{12}}$
2	$\frac{1}{k_{11}}\left(\mathbf{a}_1^{\mathrm{T}}\mathbf{x}+\mathbf{b}_1^{\mathrm{T}}\mathbf{u}-k_{12}T_{fr2,s}\right)$	$T_{fr2,s}$
3	$\frac{1}{k_{11}}\left(\mathbf{a}_1^{\mathrm{T}}\mathbf{x}+\mathbf{b}_1^{\mathrm{T}}\mathbf{u}+k_{12}T_{fr2,s}\right)$	$-T_{fr2,s}$
4	$T_{fr1,s}$	$\frac{1}{k_{22}}\left(\mathbf{a}_2^{\mathrm{T}}\mathbf{x}+\mathbf{b}_2^{\mathrm{T}}\mathbf{u}-k_{21}T_{fr1,s}\right)$
5	$-T_{fr1,s}$	$\frac{1}{k_{22}}\left(\mathbf{a}_2^{\mathrm{T}}\mathbf{x}+\mathbf{b}_2^{\mathrm{T}}\mathbf{u}+k_{21}T_{fr1,s}\right)$
6	$T_{fr1,s}$	$T_{fr2,s}$
7	$-T_{fr1,s}$	$T_{fr2,s}$
8	$T_{fr1,s}$	$-T_{fr2,s}$
9	$-T_{fr1,s}$	$-T_{fr2,s}$

state variable x_2 are revealed. In both figures the friction torque is shown in hatched red when it is equal to the maximum static friction torque and shown in hatched blue when it is at its negative maximum value. If the friction torque is between these extremal values, it is colour coded as a mixture of red and blue according to its value. Both figures show that the two friction calculation approaches yield different results for some situations. In particular the region where the individual friction torque is neither at its maximum nor at its minimum value is different.

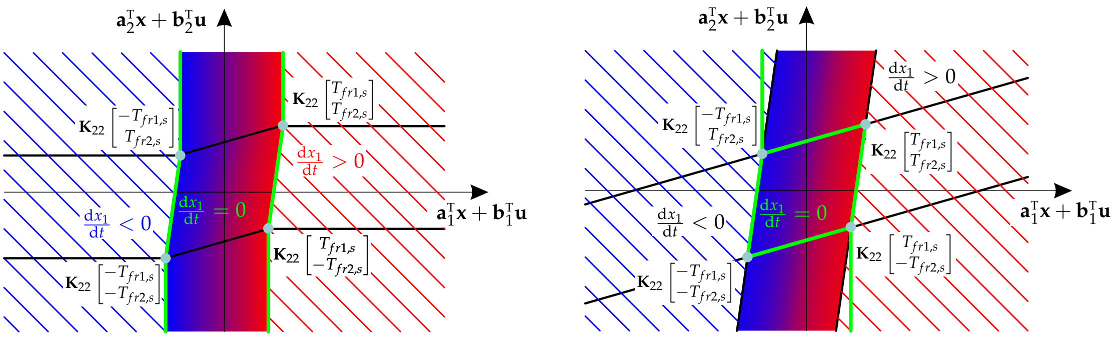
$\mathbf{a}_2^{\mathrm{T}}\mathbf{x}+\mathbf{b}_2^{\mathrm{T}}\mathbf{u}$
$\mathbf{K}_{22}\begin{bmatrix}T_{fr1,s}\\T_{fr2,s}\end{bmatrix}$
$\mathbf{K}_{22}\begin{bmatrix}-T_{fr1,s}\\T_{fr2,s}\end{bmatrix}$
$\frac{\mathrm{d}x_1}{\mathrm{d}t}>0$
$\frac{\mathrm{d}x_1}{\mathrm{d}t}=0$
$\frac{\mathrm{d}x_1}{\mathrm{d}t}<0$
$\mathbf{a}_1^{\mathrm{T}}\mathbf{x}+\mathbf{b}_1^{\mathrm{T}}\mathbf{u}$
$\mathbf{K}_{22}\begin{bmatrix}T_{fr1,s}\\-T_{fr2,s}\end{bmatrix}$
$\mathbf{K}_{22}\begin{bmatrix}-T_{fr1,s}\\-T_{fr2,s}\end{bmatrix}$

(a) T_{fr1} calculation, proposed approach. **(b)** T_{fr1} calculation, conventional approach.

Figure 4.8: Friction torque calculation for two-dimensional problems at $x_1 = 0$ and $x_2 = 0$ according to the force–balancing strategy, friction torque T_{fr1} and x_1 dynamics.

Additionally, the dynamics of the two state variables x_1 and x_2 is analysed. With the

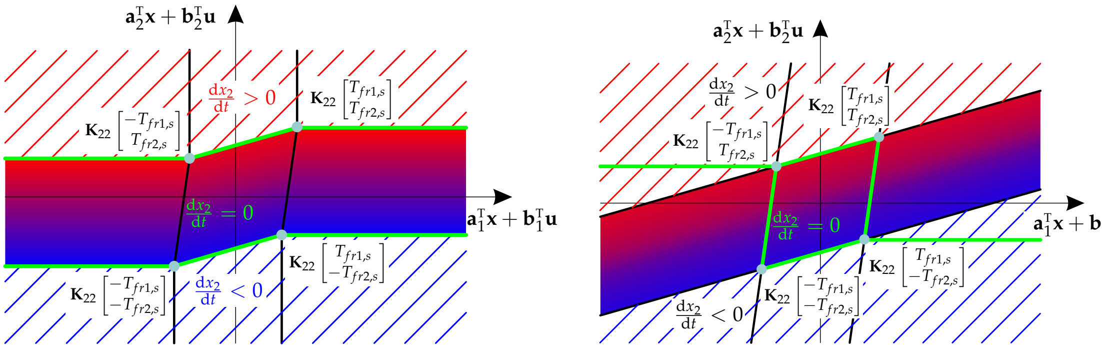
$\mathbf{a}_2^\mathrm{T}\mathbf{x} + \mathbf{b}_2^\mathrm{T}\mathbf{u}$
$\frac{\mathrm{d}x_2}{\mathrm{d}t} > 0$
$\mathbf{K}_{22}\begin{bmatrix}T_{fr1,s}\\T_{fr2,s}\end{bmatrix}$
$\mathbf{K}_{22}\begin{bmatrix}-T_{fr1,s}\\T_{fr2,s}\end{bmatrix}$
$\frac{\mathrm{d}x_2}{\mathrm{d}t} = 0$
$\mathbf{a}_1^\mathrm{T}\mathbf{x} + \mathbf{b}_1^\mathrm{T}\mathbf{u}$
$\mathbf{K}_{22}\begin{bmatrix}T_{fr1,s}\\-T_{fr2,s}\end{bmatrix}$
$\mathbf{K}_{22}\begin{bmatrix}-T_{fr1,s}\\-T_{fr2,s}\end{bmatrix}$
$\frac{\mathrm{d}x_2}{\mathrm{d}t} < 0$

(a) T_{fr2} calculation, proposed approach. **(b)** T_{fr2} calculation, conventional approach.

Figure 4.9: Friction torque calculation for two-dimensional problems at $x_1 = 0$ and $x_2 = 0$ according to the force–balancing strategy, friction torque T_{fr2} and x_2 dynamics.

approach presented in this work a transition from sticking state to slipping state can only occur when the corresponding friction torque is at its proper extremal value; these regions are marked hatched in Figure 4.8a and Figure 4.9a. For instance, when $T_{fr1} = T_{fr1,s}$, the system dynamics must fulfil $\mathrm{d}x_1/\mathrm{d}t \geq 0$, while when $T_{fr1} = -T_{fr1,s}$ holds, $\mathrm{d}x_1/\mathrm{d}t \leq 0$ follows. If the absolute value of the friction torque is less than the maximum static friction ($|T_{fr}| < T_{fr,s}$), the corresponding state variable has to remain at zero ($\mathrm{d}x/\mathrm{d}t = 0$). The border of this open region is marked in green in Figure 4.8a and Figure 4.9a. This border identifies the only situations where $|T_{fr}| = T_{fr,s}$ holds and $\mathrm{d}x/\mathrm{d}t$ is nevertheless zero.

As can be seen in Figure 4.8b and Figure 4.9b, with the conventional approach based on only limiting the results of Equation (4.32) the situation is different. Here the dynamics of the state variables are not directly related to the corresponding friction torques. While with the proposed approach the areas where the system states x_1 respectively x_2 remain at zero are two different open regions, here for both system states only one compact region exists where the sticking state is maintained. This is the central sector where Equation (4.32) already gives the correct friction torques. The border of this area is again marked in green. In other situations the dynamics of the system states relating to the total torque $\mathbf{a}_1^\mathrm{T}\mathbf{x} + \mathbf{b}_1^\mathrm{T}\mathbf{u}$ or $\mathbf{a}_2^\mathrm{T}\mathbf{x} + \mathbf{b}_2^\mathrm{T}\mathbf{u}$ is different than expected. These situations are marked by green lines in Figure 4.8b and Figure 4.9b. For instance, when $\mathbf{a}_1^\mathrm{T}\mathbf{x} + \mathbf{b}_1^\mathrm{T}\mathbf{u}$ is infinitesimally increased, the system dynamics may change from $\mathrm{d}x_1/\mathrm{d}t < 0$ to $\mathrm{d}x_1/\mathrm{d}t > 0$ without a region in between with $\mathrm{d}x_1/\mathrm{d}t = 0$ caused by friction. One further problem with the conventional approach is that there are some situations where transitions from sticking to slipping are physically wrong as e.g. $\mathrm{d}x_1/\mathrm{d}t > 0$ although $T_{fr1} < 0$. These problems can be overcome with the simulation approach presented in this work.

This simulation strategy can be applied to dynamic systems containing more friction elements than System (4.18) as well if splitting up the problem into subsystems meeting the requirements stated at the beginning of this section is possible. For instance, the dynamic system

$$\frac{\mathrm{d}\mathbf{x}}{\mathrm{d}t} = \mathbf{Ax} + \mathbf{Bu} - \underbrace{\begin{pmatrix} k_{11} & k_{12} & 0 & 0 \\ k_{21} & k_{22} & 0 & 0 \\ 0 & 0 & k_{33} & k_{34} \\ 0 & 0 & k_{43} & k_{44} \\ k_{51} & k_{52} & k_{53} & k_{54} \\ \vdots & \vdots & \vdots & \vdots \\ k_{N1} & k_{N2} & k_{N3} & k_{N4} \end{pmatrix}}_{=:\mathbf{K}} \underbrace{\begin{bmatrix} T_{fr1} \\ T_{fr2} \\ T_{fr3} \\ T_{fr4} \end{bmatrix}}_{=:\mathbf{T}_{fr}} \tag{4.68}$$

with $T_{fri} = T_{fri}(x_i)$ for $i \in \{1, 2, 3, 4\}$ can be divided into a friction simulation problem for the pair of state variables x_1 and x_2 and a separate problem for the combination of system states x_3 and x_4. These can be handled using the proposed simulation strategy if the two sub-problems fulfil the requirements regarding their individual friction matrices as stated before.

Furthermore, if this separation into sub-problems is impossible, the approach presented for systems with two friction elements can be extended. If for instance a model where three friction torques $T_{fr1}(x_1)$, $T_{fr2}(x_2)$, and $T_{fr3}(x_3)$ are affecting the system states x_1, x_2, and x_3 is to be simulated, the distinction of cases must be extended from four to nine situations. But in eight of the cases at most two system states are zero; these can be traced back to the problems already discussed. Only for the situation with three state variables in sticking state a new friction calculation procedure is required. But this problem can be solved according to the idea used in this section to handle 'Case 4'. The only difficulty is the significantly increased number of $3^3 = 27$ sectors to be individually analysed.

Simulation Example

This simulation strategy has also been implemented in Simulink® and shall be tested on the basis of the mechanical system presented in Figure 4.10. This system consists of two clutches where one disk of Clutch 1 is torsionally stiffly connected to a disk of Clutch 2. T_1 and T_2 are external torques representing the system inputs. The dynamics of this system is given by

$$I_{ci1}\frac{\mathrm{d}\omega_1}{\mathrm{d}t} = T_1 - T_{c1}(\omega_1 - \omega_2) \tag{4.69a}$$

$$(I_{c1o} + I_{2ci})\frac{\mathrm{d}\omega_2}{\mathrm{d}t} = T_{c1}(\omega_1 - \omega_2) - T_{c2}(\omega_2 - \omega_3) \tag{4.69b}$$

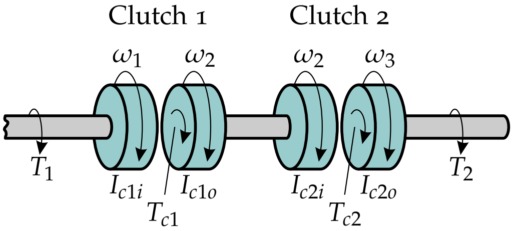

Figure 4.10: Mechanical system for testing the proposed VDDS simulation strategy for two-dimensional problems.

$$I_{c2o}\frac{\mathrm{d}\omega_3}{\mathrm{d}t} = T_2 + T_{c2}\left(\omega_2 - \omega_3\right). \tag{4.69c}$$

The friction torques T_{c1} and T_{c2} are functions of the clutch disks' differential angular velocities and chosen as Coulomb friction only. To create a dynamic system that is in the form of System (4.18), the regular state transform[2]

$$\begin{bmatrix} x_1 \\ x_2 \\ x_3 \end{bmatrix} = \underbrace{\begin{pmatrix} 1 & -1 & 0 \\ 0 & 1 & -1 \\ 1 & 0 & 0 \end{pmatrix}}_{=:\mathbf{T}} \begin{bmatrix} \omega_1 \\ \omega_2 \\ \omega_3 \end{bmatrix} \tag{4.70}$$

can be applied, then

$$\frac{\mathrm{d}x_1}{\mathrm{d}t} = \frac{1}{I_{c1i}}T_1 - \left(\frac{1}{I_{c1i}} + \frac{1}{I_{c1o} + I_{2ci}}\right) T_{c1}\left(x_1\right) + \frac{1}{I_{c1o} + I_{2ci}} T_{c2}\left(x_2\right) \tag{4.71a}$$

$$\frac{\mathrm{d}x_2}{\mathrm{d}t} = -\frac{1}{I_{c2o}}T_2 + \frac{1}{I_{c1o} + I_{c2i}} T_{c1}\left(x_1\right) - \left(\frac{1}{I_{c1i} + I_{c2o}} + \frac{1}{I_{c2o}}\right) T_{c2}\left(x_2\right) \tag{4.71b}$$

$$\frac{\mathrm{d}x_3}{\mathrm{d}t} = \frac{1}{I_{c1i}}T_1 - \frac{1}{I_{c1i}} T_{c1}\left(x_1\right) \tag{4.71c}$$

results. A numerical simulation with $I_{c1i} = I_{c1o} = 1\,\mathrm{kg\,m^2}$ and $I_{c2i} = I_{c2o} = 1\,\mathrm{kg\,m^2}$ was performed for this dynamic system using the simulation strategy proposed before; the results are presented in Figure 4.11. In the upper plot the angular velocities ω_1, ω_2, ω_3 and the state variables x_1, x_2, x_3 used for simulation are shown. The system states x_1 and x_2 are of special interest as the clutch torques directly depend on these variables. Therefore, they are critical regarding transitions form sticking to slipping and vice versa. At $t \approx 0.25\,\mathrm{s}$ Clutch 2 is completely engaged; then ω_2 and ω_3 are identical and x_2 is zero. Beginning at $t \approx 0.6\,\mathrm{s}$ also x_1 is zero; consequently, now all three bodies rotate at the same angular velocity. Figure 4.11 clearly shows that these events are handled correctly without any chattering. In the

---

[2] This state transform is not unique; the only requirement is that the relative velocities of the two clutches are state variables in the transformed system. The remaining third system state however can be chosen freely as long as the transformation matrix **T** is regular.

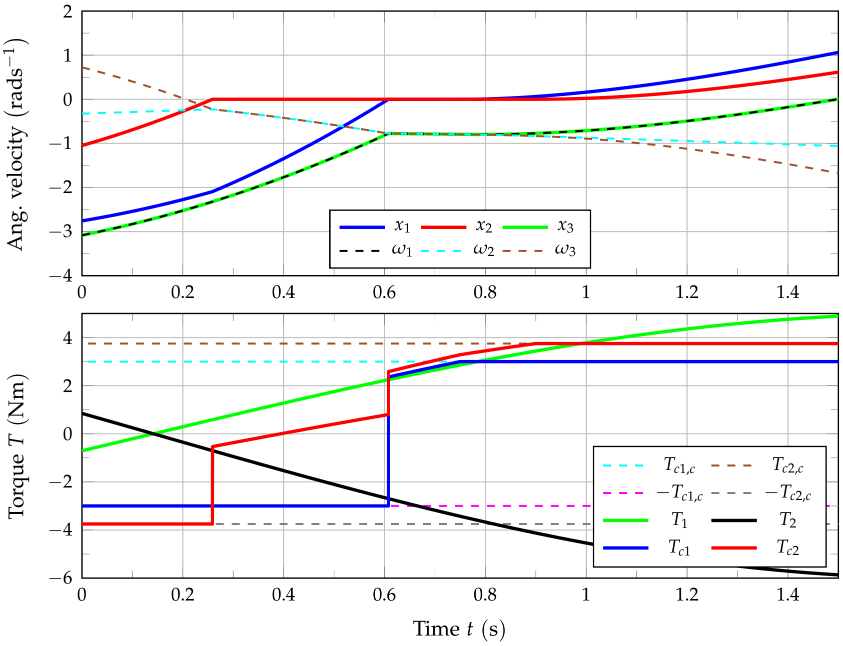

Figure 4.11: Results of a numerical simulation of a mechanical system with two friction elements using the proposed force-balancing strategy.

lower plot the input torques T_1 and T_2, the maximum clutch torques given by the Coulomb friction torques $T_{c1,c}$ and $T_{c2,c}$, and the resulting effective clutch torques T_{c1} and T_{c2}, calculated according to the force-balancing strategy, are presented. This plot clearly shows that during the sticking phases the clutch torques are chosen exactly in a way that external torques are compensated. For this reason, the system states remain at zero. At $t \approx 0.75\,\mathrm{s}$ the external torques can no longer be compensated and the angular velocities of the two disks of Clutch 1 begin to differ; finally, at $t \approx 0.9\,\mathrm{s}$ the state variable x_2 starts to increase too. Consequently, the three angular velocities are different again. This simulation example shows that with the presented simulation strategy the changes of dynamic dimension caused by transitions from sticking to slipping and vice versa are no longer problematic.

Power Train Example I: Limited-slip Differential Gear

The limited-slip differential as discussed in Section 3.6 is a typical VDDS. If e.g. in the bevel gear differential the friction torque T_{dsl} is great enough, the differential bevel pinion is locked and the two output axles are forced to identical angular velocities. As by this angular velocity also the rotational dynamics of the input shaft is defined, just one state variable is required to describe the system dynamics; this means a reduction of dynamic dimension from two to one. If furthermore the losses are high, this angular velocity might be forced to zero as well meaning a further reduction of dynamic dimension. This situation might not occur too often in practice, but at least at every start-up all angular velocities are zero. In contrast to the clutch, where only one friction torque had to be handled and therefore the reduction of dynamic dimension was limited to one, now two friction torques are present that can reduce the dynamic dimension by two. Since the mathematical model for the limited-slip differential

$$\underbrace{\frac{\mathrm{d}}{\mathrm{d}t}\begin{bmatrix}\omega_{di}\\ \omega_3\end{bmatrix}}_{\mathbf{x}} = \underbrace{\begin{pmatrix}b_{11} & b_{12} & b_{13}\\ b_{21} & b_{22} & b_{23}\end{pmatrix}}_{\mathbf{B}}\underbrace{\begin{bmatrix}T_{di}\\ T_{do1}\\ T_{do2}\end{bmatrix}}_{\mathbf{u}} - \underbrace{\begin{pmatrix}k_{11} & k_{12}\\ k_{21} & k_{22}\end{pmatrix}}_{\mathbf{K}}\underbrace{\begin{bmatrix}T_{dl}\\ T_{dsl}\end{bmatrix}}_{\mathbf{T}_{fr}} \tag{4.72}$$

with

$$T_{dl} = T_{dl}(\omega_{di}) \tag{4.73a}$$

$$T_{dsl} = T_{dsl}(\omega_3) \tag{4.73b}$$

is already given in the form of System (4.18), the simulation strategy proposed before can be used directly. If the angular velocities of the output axles had been used as state variables in the mathematical model, a state transformation would have had to be applied before the numerical simulation can be done.

Power Train Example II: Simplified Transmission Model

The simplified transmission model with DCT-structure presented in Section 3.7.2 is a VDDS as well. This model is based on two clutches, each can be engaged and disengaged. For simulation this means that there are two differential angular velocities affected by friction; these can be in either sticking or slipping state. Since the transmission ratios of the two gear sets are different during normal operation, the differential angular velocities of the clutches are different as well. Consequently, only one friction element can be in sticking mode at a time. However, when all angular velocities are zero as e.g. when starting from standstill, both clutches will have zero differential angular velocities. To be able to handle this special situation and also normal operation without the need to switch between different system models, the simulation strategy presented before shall be used. To bring the mathematical model into the form of System (4.18) the state transformation

$$\begin{bmatrix}\Delta\omega_{c1}\\ \Delta\omega_{c2}\end{bmatrix} = \begin{pmatrix}1 & -i_{gb1}\\ 1 & -i_{gb2}\end{pmatrix}\begin{bmatrix}\omega_{gbi}\\ \omega_{gbo}\end{bmatrix} \tag{4.74}$$

is applied. Then the differential equations

$$\frac{\mathrm{d}\Delta\omega_{c1}}{\mathrm{d}t} = \frac{T_{gbi}}{I_{gbi}} + \frac{i_{gb1}T_{gbo}}{I_{gbo}} - T_{c1}\left(\frac{1}{I_{gbi}} + \frac{i_{gb1}^2}{I_{gbo}}\right) - T_{c2}\left(\frac{1}{I_{gbi}} + \frac{i_{gb1}i_{gb2}}{I_{gbo}}\right) \tag{4.75a}$$

$$\frac{\mathrm{d}\Delta\omega_{c2}}{\mathrm{d}t} = \frac{T_{gbi}}{I_{gbi}} + \frac{i_{gb2}T_{gbo}}{I_{gbo}} - T_{c1}\left(\frac{1}{I_{gbi}} + \frac{i_{gb1}i_{gb2}}{I_{gbo}}\right) - T_{c2}\left(\frac{1}{I_{gbi}} + \frac{i_{gb2}^2}{I_{gbo}}\right) \tag{4.75b}$$

with

$$T_{c1} = T_{c1}(\Delta\omega_{c1}) \tag{4.76a}$$

$$T_{c2} = T_{c2}(\Delta\omega_{c2}) \tag{4.76b}$$

can be obtained. Transformation (4.74) is regular if $i_{gb1} \neq i_{gb2}$; as various gears will have different gear ratios, this condition is fulfilled and the transformation can be applied.

Since simulation strategies for the dynamic models for the power train elements discussed in Chapter 3 are available by now, numerical simulations for various problem settings are performed in the following sections.

4.3 Analysis of Reduced Transmission Models

To be able to assess usability and limitations of simplified transmission modelling approaches, numerical simulations including some gear shifts were performed. In a first step, the gear shifts were simulated by the use of the different simplified gearbox models presented in Section 3.7.2. Then the results are compared to simulation experiments based on the detailed model of the automatic transmission as presented in Section 3.7.1. The purpose of these experiments was not to optimise the timing of the gear shifts for maximum drivability or performance, but to investigate the properties and characteristics of different gearbox models. Since the focus is on analysing different models for the gear stage, no torque converter was considered. The gear shifts were simulated in a test bed environment similar to the test system shown in Figure 3.2: an electric drive at the gearbox input replaces the engine and provides the torque while another drive at the gearbox output generates the load. This drive is operated in speed control mode with constant reference as the angular velocity of the gearbox output is typically directly related to the vehicle's speed, which does not change much during a gear shift. The reference signal for the input drive is the desired electromagnetic air-gap torque. With automatic transmissions the gear shifts are often executed as powershifts without power interruption, but depending on the driving situation shifts with power interruption are possible as well [38].[3] These latter processes are also called *non-overlapping* gear shifts as one friction element is completely disengaged before another is engaged and are similar to gear shifts in manual transmissions. As an example, a gear shift from second to first gear is discussed for both presented simplified transmission models.

---

[3] This holds in particular for testing situations where the transmission actuation is controlled by the test bed automation system.

In Figure 4.12 the rotational speeds of gearbox input n_1 and gearbox output n_2 are presented for the non-overlapping gear shift from second to first gear; in Figure 4.13 input and output torque are shown. Results obtained by the use of the simulation model including the complete gear stage based on four planetary gear sets are presented in blue and labelled 'detailed model'. Simulation data based on the simple gearbox model including only one clutch and gear stage are shown in green and labelled 'reduced model I'. Results related to the modelling approach based on two clutches and gear stages similar to the DCT are presented in red and labelled 'reduced model II'. In the detailed model one clutch is completely opened before another clutch is engaged during this type of gear shift. This procedure can also be applied to the DCT related modelling approach. The simpler model contains only one clutch; here at first, this single clutch has to be disengaged, then the transmission ratio is changed, and finally the clutch is engaged again. While the transmission of mechanical power is interrupted the gearbox input is accelerated by the torque generated by the input drive as it would be by the ICE in a driving experiment. According to the rotational speeds in Figure 4.12, both simplified gearbox models can capture the essential dynamics. Only some deviations, particularly visible during the phase of disengaged clutches, remain. In fact, both reduced approaches lead to identical results; this is intuitive because their only difference is the number of 'parallel' gear stages consisting of clutch

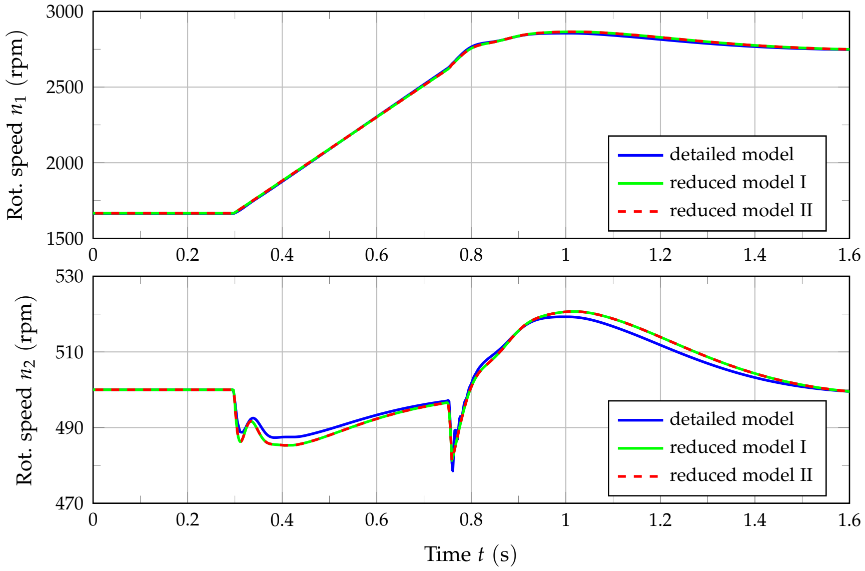

Figure 4.12: Rotational speed of gearbox input n_1 and output n_2 for a non-overlapping gear shift from second to first gear on a test bed, comparative numerical simulations of different transmission models.

and transmission ratio. Since these elements were modelled inertia-free, the DCT approach with one clutch torque set to zero is equivalent to the gearbox model containing only one gear stage. Also the torque curves presented in Figure 4.13 show only minor deviations. As both reduced models are significantly less complex than the detailed model, these slightly different results are to be expected and acceptable for test bed simulations. Important is in particular that the phenomena related to engaging and disengaging the clutches are modelled well.

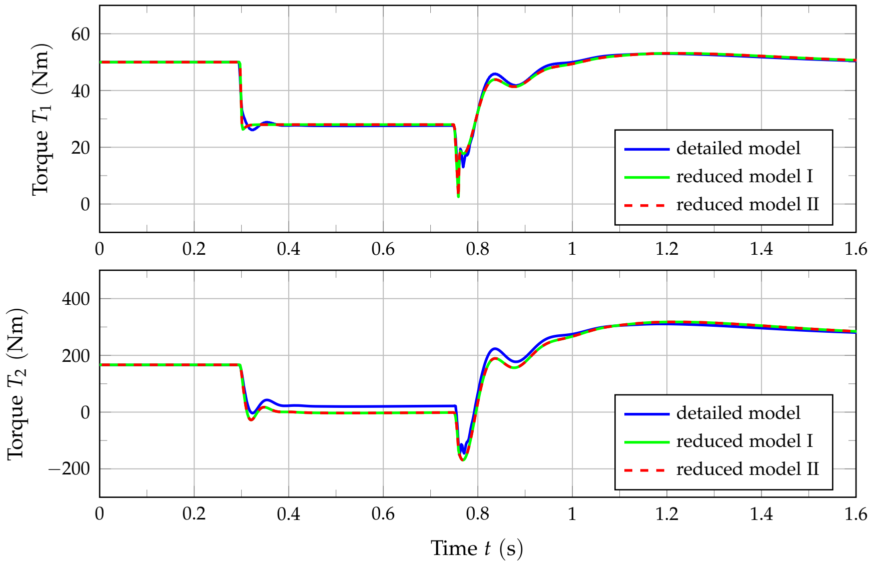

Figure 4.13: Torque at gearbox input T_1 and output T_2 for a non-overlapping gear shift from second to first gear on a test bed, comparative numerical simulations of different transmission models.

Powershifts are characterised by the fact that two friction elements are engaged (*overlapping*) for a short time interval. This behaviour is analysed by means of a gear shift from first to second gear with positive gearbox input torque. In the vehicle this would mean that the engine speed must decrease in spite of the positive engine torque. The overlapping gear shift is only simulated for the DCT approach because two clutches are required.

In Figure 4.14 and Figure 4.15 results of numerical simulations for the overlapping gear shift from first to second gear are presented. Here the two friction elements involved in the gear shift are actuated in parallel; while one element is disengaged the other is engaged resulting in a gear shift without power interruption. This allows to reduce the rotational speed of the engine, or the input drive in a testing situation, during the gear shift although the torque generated by the input drive is still positive. The rotational speeds of gearbox input and output shown in Figure 4.14 and the torques given in Figure 4.15 indicate that the reduced gearbox model is capable of describing the dynamic behaviour of the AT sufficiently. The

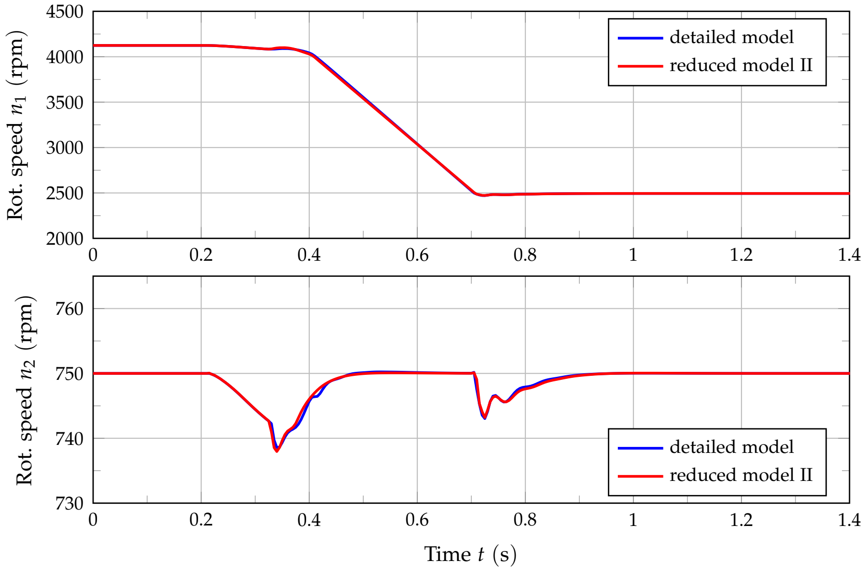

Figure 4.14: Rotational speed of gearbox input n_1 and output n_2 for an overlapping gear shift from first to second gear on a test bed, comparative numerical simulations of different transmission models.

torque curves shown in Figure 4.15 slightly differ, but this discrepancy is minor compared to other modelling and parameter uncertainties typically complicating numerical simulations of transmission systems. Therefore, this reduced model is used henceforth for numerical simulations including transmissions. Its main advantage is that it is computationally simpler than the detailed model resulting in a significantly reduced simulation time. Additionally, less system parameters must be known.

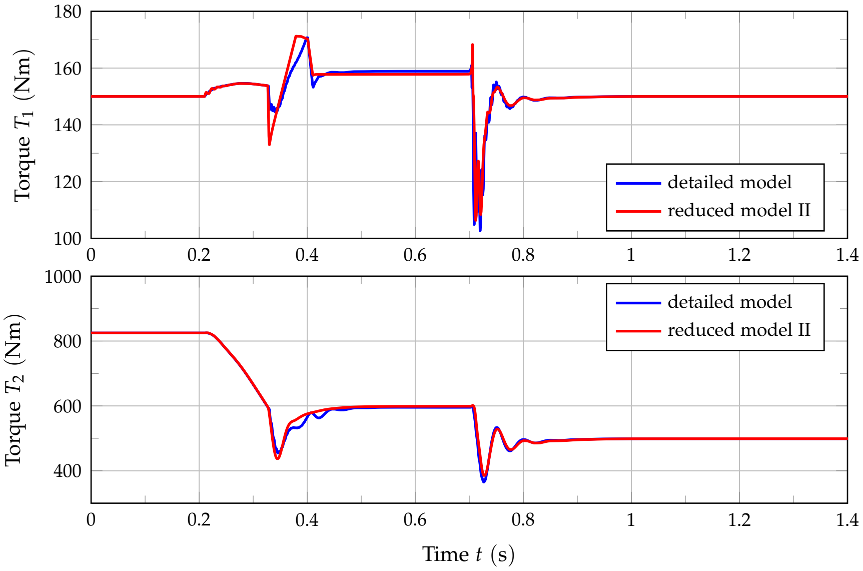

Figure 4.15: Torque at gearbox input T_1 and output T_2 for an overlapping gear shift from first to second gear on a test bed, comparative numerical simulations of different transmission models.

4.4 Case Study I: Test System for Differential Gears

Since at this point a simulation strategy for the limited-slip differential system model is available, numerical simulations of the test system for differentials as presented in Figure 3.24 can be performed. The model depicted in Figure 3.25 and additionally partially given in Appendix C was implemented in Simulink®; then this simulation model was used to simulate a typical testing experiment. The references for testing torque and testing rotational speeds were directly taken from the experimental test-run carried out on the test bed. A closed-loop simulation was chosen because then the system inputs are these references for rotational speed and torque, which are known exactly. An open-loop simulation with electromagnetic torques as system inputs would require these torques to be known. But measurement data from the test bed could be corrupted by errors in the air-gap torque estimation [52], see also Section 3.2. Additionally, the closed-loop simulation covers the entire test system and is therefore most relevant. The simulation results are then compared to measurement data from a commercial test bed equipped with three 700 kW IMs. The UUT was a symmetric limited-slip bevel gear axle differential. These experimental results were recorded at 10 kHz. A representative section of this comparison is given in Figure 4.16 and Figure 4.17.

Figure 4.16 shows the rotational speed of the input drive *M1* and of the load drives *M2* and *M3*. The rotational speed of the input drive is scaled by the inverse of the differential's transmission ratio i_d, thus this signal approximately represents the rotational speed of the differential cage. As the differential's structure is symmetric, the rotational speed of the differential cage is given by the mean value of the rotational speeds of the differential's outputs. But due to the shaft elasticities, the rotational speeds measured at the electric drives can slightly differ from those at the differential gear for transient situations. Figure 4.16 shows a good match of measurement data and simulation results. This is to be expected because two of the electric drives are operated in speed control mode and the rotational speed of the remaining drive is defined by the differential's transmission ratio. The experiment presented here was performed to test the differential's slip-limiting functionality; for this reason, the rotational speed references for the load drives were partially chosen differently.

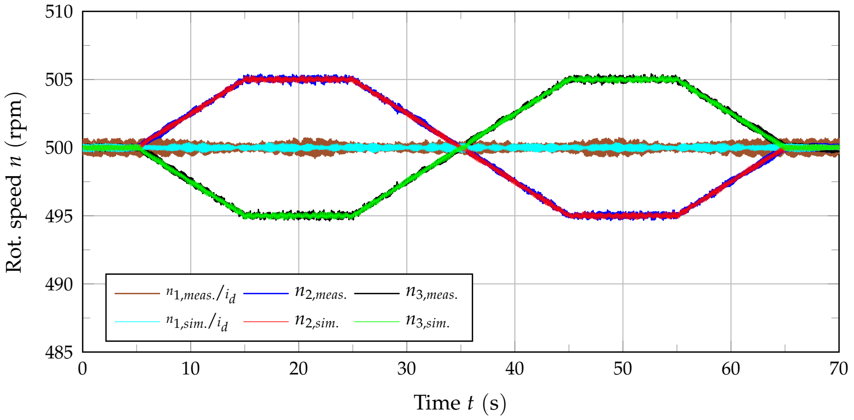

Figure 4.16: Test system for differentials with KS R2R frequency converter, measured and simulated rotational speeds of input drive *M1* and load drives *M2* and *M3*.

In Figure 4.17 the torques measured by the measuring flanges at the electric machines are presented; additionally, their simulation equivalents are shown. For clarity the torque T_{f1} measured at the input drive is scaled by the factor 0.5 and the transmission ratio i_d to simplify the comparison to the output torques T_{f2} and T_{f3}. As this scaled input torque is higher than the average output torque, losses definitely have to be considered. The slip-limiting functionality becomes obvious when the rotational speeds of the two outputs of the differential begin to differ. Then the torque at the slower output shaft rises while the torque at the faster shaft is reduced. Note as well that there is still stationary asymmetric torque splitting at the end of the experiment although the rotational speeds of the two output axles are identical again. This phenomenon is illustrated by Equation (3.20) for $T_{dsl} \neq 0$ and related to the friction torque's discontinuity at zero relative angular velocity.

In Figure 4.18 measured and simulated output torques are compared again with special focus on the sign change of the differential bevel pinion's angular velocity. Obviously, also for this situation the output torque splitting is modelled quite

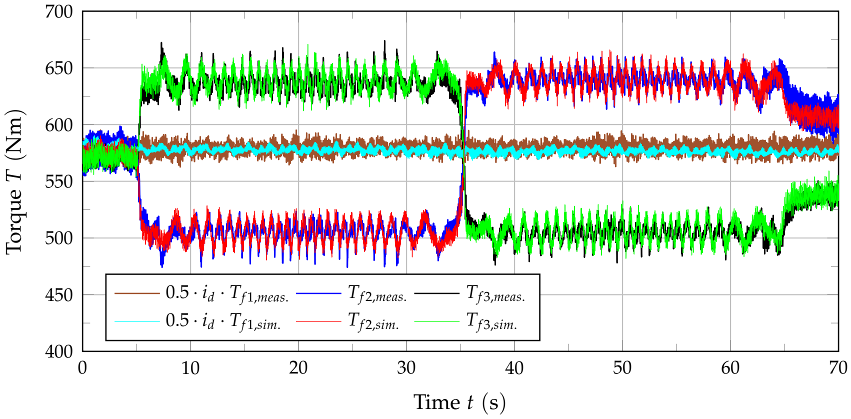

Figure 4.17: Test system for differentials with KS R2R frequency converter, measured and simulated torques at input drive *M1* and load drives *M2* and *M3*.

well. The high frequency signal components are torsional vibrations due to resonance phenomena in the multi-mass mechanical system as well as various torque harmonics coming from the electric drives and the UUT. In particular the torque variations related to the rotation of the differential bevel pinion is obvious. This effect can easily be identified in Figure 4.17 by the varying frequency of these torque components when the difference in rotational speed of the differential's outputs is changed. Overall the simulation results presented in this section show a rather good match with the measurement data.

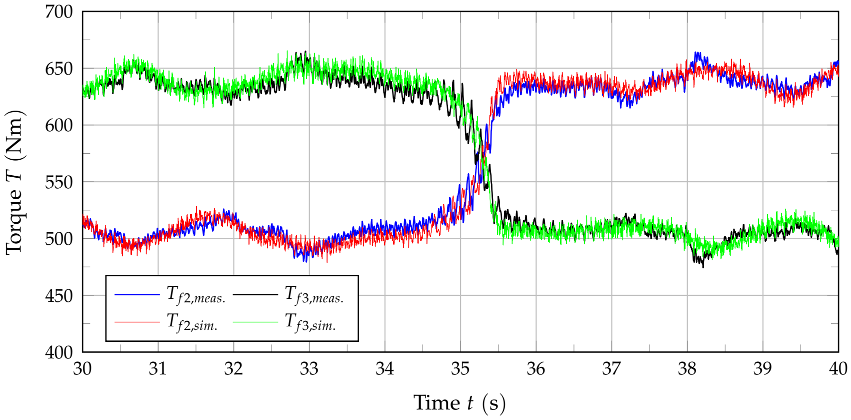

Figure 4.18: Test system for differentials with KS R2R frequency converter, measured and simulated torques at the load drives *M2* and *M3*, detail.

Simulations were performed on a laptop computer equipped with an i5-3230M CPU and 8 GB RAM using the variable step-size solver 'ode45'. The simulation model contains elements modelled in discrete time such as the control algorithms as well as components modelled in continuous time. These latter form a dynamic system that describes the electric machines and the entire mechanical system. Achieving efficient numerical simulations is challenging because this system includes a rather high number of state variables with slow and fast dynamics ('stiff system') and non-linearities such as gear play and friction. This can lead to small integration step sizes for some situations, which slow down the simulation. Furthermore, because of the discrete time components, the integration step size cannot exceed 100 µs which is the inverse of the 10 kHz sampling rate used for control. In spite of these challenges, the simulation model including the proposed friction calculation strategy is computationally rather efficient. In Table 4.2 the CPU-time of the simulation is shown for the different 'Simulation modes' available in Simulink®. In particular with the 'Rapid Accelerator' setting the simulation is fast. The simulation of the 70 s section of the experiment discussed in this section is completed within only 66 s with this setting.

Table 4.2: CPU-time of a 70 s numerical simulation of a test bed for differential gears.

Simulation Mode	CPU-time
Normal	1051 s
Accelerator	260 s
Rapid Accelerator	66 s

4.5 Case Study II: Test System for Differential Gears with Adapter Gearboxes

Also for the test system presented in Figure 3.1 numerical simulations were performed. The simulation model was based on the graphical representation of the dynamic system given in Figure 3.26. Since except for the adapter gearboxes the testing configuration is similar to the one discussed in the previous section, the simulation model could be derived from the model used before. As due to the downspeed gearboxes now significantly higher torques are expected, system parameters of the differential and some mechanical shafts obviously had to be modified. To verify the mathematical model, a typical testing experiment was carried out on the commercial test bed and in simulation.

In Figure 4.19 the rotational speeds of the three IMs are given while in Figure 4.20 the torques at the measuring flanges are presented. Compared to the results shown in Figure 4.17 and Figure 4.18, the sign of the torque measured at the load drives is changed for clarity. In both figures the physical quantities measured at the electric drives are shown. Because of the downspeed gearboxes with transmission ratios of $i_{gb1} = 8.1$ for the input drive and $i_{gb2} = 10.4$ for the differential's output, the torque at the UUT is significantly higher. Both figures prove that the simulation

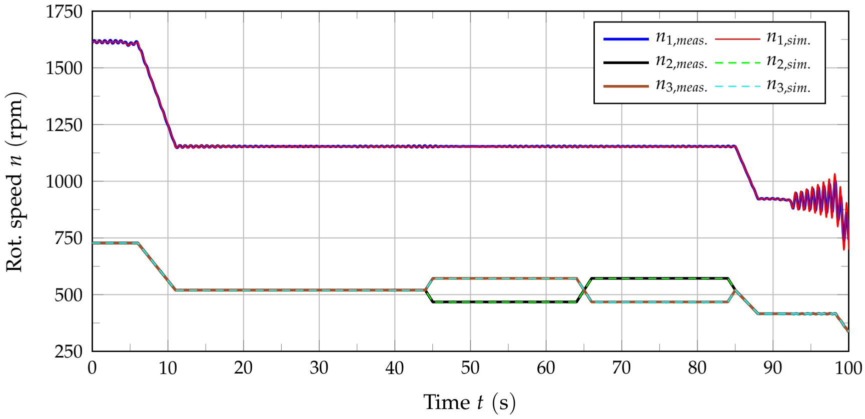

Figure 4.19: Test system for differentials with KS R2R frequency converter and adapter gearboxes, measured and simulated rotational speeds of input drive *M1* and load drives *M2* and *M3*.

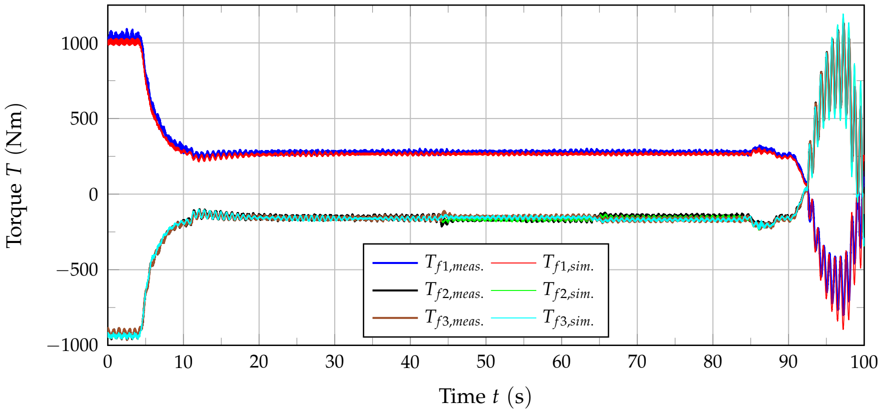

Figure 4.20: Test system for differentials with KS R2R frequency converter and adapter gearboxes, measured and simulated torques at input drive *M1* and load drives *M2* and *M3*.

model is capable of describing the test bed characteristics adequately. Transient as well as stationary phenomena are in accordance with the experimental results. Clearly, the torsional vibration behaviour is an important simulation aspect. This includes accurately modelling the dynamics of the mechanical system, resulting in the correct resonant frequencies and damping properties, as well as providing proper excitement for these resonances. In the experiment that is presented in this section an eigenmode at approximately 1.3 Hz is most problematic; this is obvious throughout the entire experiment. This eigenmode is characterised by the fact that the input drive oscillates against the output drives, see also Figure 3.30b in Section 3.12 where the results of a modal analysis for a similar testing configuration are shown. This is most obvious at $t \approx 90\,\mathrm{s}$ when the sign of the testing torque is changing. Due to gear play in the mechanical system, this means a strong excitation for resonant oscillations; in combination with low internal damping of the cardan shafts large torque oscillations arise. Changes in testing torque and testing rotational speed can cause resonant oscillations too; this can be seen at $t \approx 11\,\mathrm{s}$. Figure 4.20 shows that the differential's output torques are hardly affected by a difference in rotational speeds of the output shafts; consequently, the differential's limited-slip functionality is weak.

As proven by Table 4.3, numerical simulation is again rather efficient, especially in 'Rapid Accelerator' mode.

Table 4.3: CPU-time of a 100 s numerical simulation of a test bed with adapter gearboxes for differential gears.

Simulation Mode	CPU-time
Normal	1768 s
Accelerator	469 s
Rapid Accelerator	92 s

4.6 Case Study III: Test System for Transmissions

In contrast to the two test systems for differentials considered before, here a test bed for transmissions is discussed. The test bed configuration is given in Figure 3.2; the model structure is depicted in Figure 3.27. The UUT is an automatic transmission. To verify the mathematical model, a typical testing experiment was carried out on a commercial test bed and in simulation. For simulation the references for testing torque and testing rotational speed were directly taken from the test-run on the test bed.

The rotational speeds of input and output drive are presented in Figure 4.21 and torques at the measuring flanges are shown in Figure 4.22. n_1 and T_{f1} belong to the input drive while n_2 and T_{f2} are associated to the load drive. In both figures a section of a longer test-run is displayed. During the test-run the AT is tested by the use of speed and torque ramps in every gear. These testing phases are interrupted by gear shifts: at $t \approx 14\,\mathrm{s}$ a downshift from second to first gear occurs while at $t \approx 64\,\mathrm{s}$ an upshift from first to second gear is performed. During the gear shifts the rotational speed of the load drive is kept constant by the inverter's speed controller. As in the simulation case studies presented before, the system model used for simulation is capable of describing most relevant test bed phenomena sufficiently. However, since the UUT is more complex than the previously discussed passive

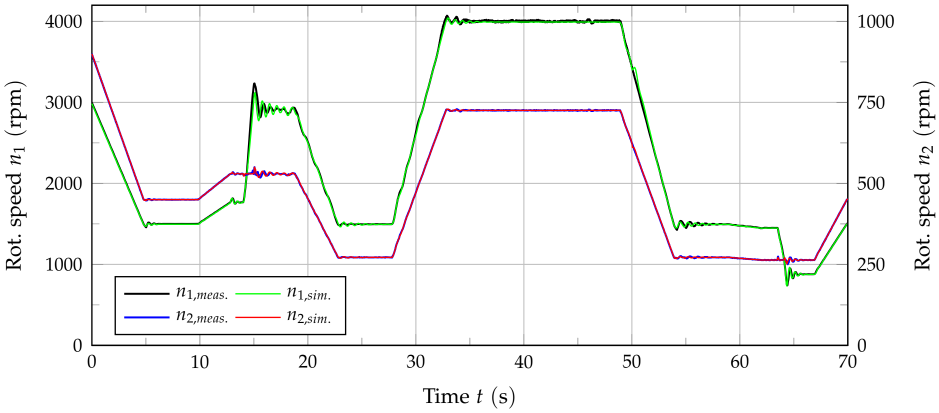

Figure 4.21: Test system for transmissions with conventional inverter system, measured and simulated rotational speeds of input drive *M1* and load drive *M2*.

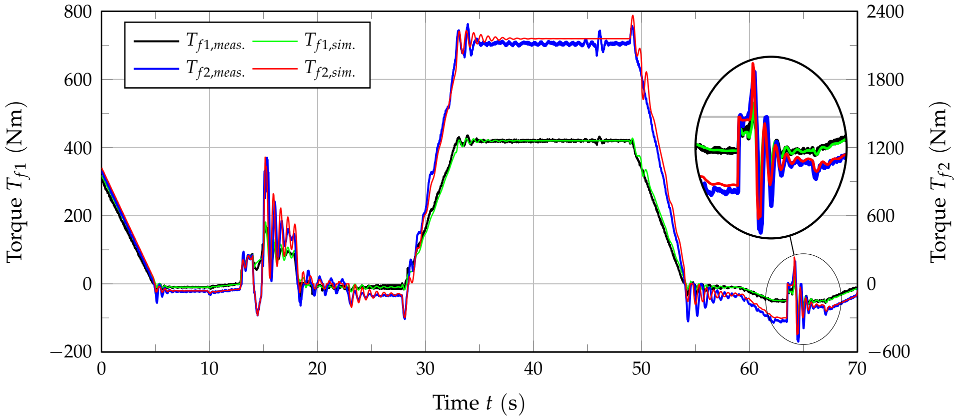

Figure 4.22: Test system for transmissions with conventional inverter system, measured and simulated torques at input drive *M1* and load drive *M2*.

differential gears, the parametrisation effort in particular for the gear shifts and for the torque converter is significantly increased. For these reasons, some discrepancy of experimental data and simulation results remain.

The testing conditions for the transmission that are presented in Figure 4.21 and Figure 4.22 are not equivalent to typical load situations in driving experiments since the electric input drive and the load drive affect the testing situation. For instance, the strong torque oscillations coming with the gear shifts would be problematic for driving comfort. The purpose of modelling and simulation however was to be able to describe the test system; therefore, loads for the UUT divergent from driving experiments are not relevant at this point.

The CPU-time required for the 70 s section of the test-run discussed here is given in Table 4.4.

Table 4.4: CPU-time of a 70 s numerical simulation of a test bed for automatic transmissions.

Simulation Mode	CPU-time
Normal	328 s
Accelerator	99 s
Rapid Accelerator	10 s

Chapter 5

Control

In this chapter tracking controllers for rotational speed and torque are designed based on the mathematical models presented in Chapter 3. These controllers are tested by the use of numerical simulations relying on the simulation strategies discussed in Chapter 4. The individual control problem strongly depends on the testing configuration to control involving various numbers of electric machines and testing objectives. In spite of these test bed specific challenges, this chapter starts with some more general considerations. A schematic representation of the control problem in general is given in Figure 5.1. For each of the k electric drives rotational speed n and flange torque T_f are measured; these quantities can be used in the control algorithms. In this representation the manipulated variables are the references for the electromagnetic air-gap torques $T_{ag,ref.}$. For test beds equipped with the KS R2R inverter system also FOC for controlling the electric machines is part of the control algorithm. For clarity, these machine controllers are not shown in Figure 5.1; generally, for the following considerations it is assumed that controllers for the electric drives are already available and the focus will be placed on speed and torque control. References for the controlled variables are determined by a higher-level system. Since these could be computed at runtime, it

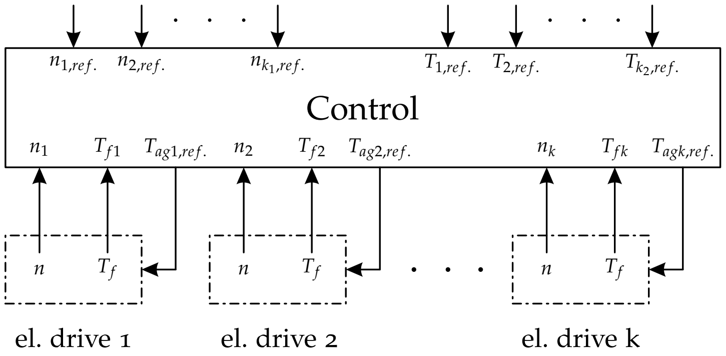

Figure 5.1: General control problem for a test system with k electric drives.

must be assumed that future references are unknown. Depending on the testing situation, the number of rotational speed and torque references varies. In general, k_1 references for rotational speed and k_2 torque references are given. At this level of control typically $k_1 + k_2 = k$ holds; thus, the number of references equals the number of electric drives.

As testing configurations are rather diverse, it is cumbersome to design controllers for this general problem setting. Instead, controllers for some selected testing scenarios are developed; the basic ideas and results can then be applied to other testing problems as well.

The requirements regarding control are plentiful: Obviously, good reference tracking is a key objective. This implicitly includes that torsional vibrations are sufficiently dampened because otherwise tracking the torque references is difficult. As shown in Figure 2.6, decoupling the controlled variables rotational speed and torque is a necessity for satisfying reference tracking; as a consequence, multiple-input multiple-output (MIMO) controllers are demanded. The second key objective is that a final production controller is delivered. Therefore, it should be universally applicable, this implies that the control structure designed for a given testing configuration should not depend on the UUT. The number of system parameters required for control should be limited and controller parameter tuning needs to be intuitive and simple. To motivate the operators of the test beds to use the new controllers, these should be similar to the current production controller based on PI controllers as shown in Figure 2.5b. For this reason, instead of introducing a completely new control concept, an improvement of the controller used at present is preferable. Another important factor is computational effort; the control algorithms must not exceed the computational capacity of the real-time system used for control. Furthermore, besides the measurement equipment mentioned before no extra measurement systems can be added.

Measurement data is gathered at a sampling rate of 10 kHz, thus also controllers should be computed at this rate. Using this high sampling rate means that discretisation effects can be neglected and that controller design can be based on a continuous time system description.

5.1 State of the Art

Although power train test beds are a very common tool in the automotive industry, there is not much research work available dealing with speed and torque control on these test beds. [11] and [12] are some of the few publications on designing and controlling power train test systems. Both however discuss rather special testing situations. But, there are similar challenges in the control of engine test beds. Here the two controlled variables are engine speed and engine torque while the actuators are the ICE and the dynamometer. One control strategy often applied in practice is to use PID controllers to control ICE and dynamometer individually. Frequently, first the speed control loop is closed, then the torque controller can be designed to reach acceptable closed-loop dynamics [21]. As briefly mentioned in Chapter 2, this also represents the conventional control concept for power train test beds. With this strategy the control performance might be satisfying in steady-state, but rotational speed and torque are still coupled in dynamic operation. Therefore, most recent approaches for controlling engine test beds are based on multivariable control to be able to reduce the interactions of speed and torque control loop.

In [96] two separate PI controllers were used to control rotational speed and testing torque, but each control action passes through a decoupling network and physically acts on both ICE and dynamometer to decouple rotational speed and torque. However, the authors neglected the torsional flexibility of the shaft connecting ICE and dynamometer and thereby resonance phenomena. In [21] a decoupling controller based on balancing the bandwidths of the two control loops with a special focus on robustness was presented, but the flexible shaft was not considered either. In [31] the test bed was modelled as a two-mass oscillator including the torsional flexibility. Optimisation based control was then used to simultaneously control engine speed and torque. In [97] again a multivariable approach was presented; this test bed control strategy is based on model reference adaptive control. Additionally, in [26, 98] another optimisation based control concept following the model predictive control (MPC) approach was proposed. Further alternative control strategies for engine test beds were presented in [28, 30, 99]. In [100] instead of controlling an ICE test bed, control for a test bed for electric drives is discussed; again a decoupling approach without considering any torsional flexibility is used.

Some of these ideas can be applied to control a driveline test bed, but there are some important differences: Instead of the highly non-linear ICE with possibly uncertain dynamic behaviour, an electric drive with well-known torque dynamics, which is usually easier to control, is used. This typically results in less dead time and a significantly faster torque control loop. Additionally, the complexity of the mechanical system increases when the simple connecting shaft used on the engine test bed is replaced by a complex power train component such as a transmission.

As already mentioned, the second important requirement in addition to decoupling rotational speed and torque is the damping of resonant torque oscillations in the multi-mass mechanical system. This is rather critical since these systems are often poorly damped. These torsional vibrations can be excited by a change in load torque, by gear play, or by torque harmonics from the electric drives [54] and from the mechanical test set-up including the UUT [63]. Any hardware solution such as adding passive damping elements or modifying the shaft stiffness parameters is undesirable in general. Such an approach would cause additional cost, could limit the achievable dynamics, and moreover, redesigns of the shafts might be required with every change of the UUT. Passive damping elements are furthermore typically not free of wear. As a consequence, active damping strategies are preferred. These solutions provide vibration damping by applying an additional torque generated by the electric drives. In [32] an approach utilising the measured shaft torque and Kalman filtering was presented for vibration damping on engine test beds. Also in [56] engine test beds are discussed; here feed forward disturbance rejection is used to reduce torsional vibrations.

In addition to engine test beds, these oscillation problems are often discussed in the context of elastic drive systems. Here there is no ICE, but their oscillatory nature is similar and the goal is also to perform speed and sometimes torque control. There are many publications available dealing with the control of two- or multi-mass systems with focus on oscillation damping. Various approaches based on additional state feedback [36, 101–109], adaptive control [110, 111], MPC [37, 109, 112–115], or flatness based control [116] were presented. However, most of these applications require speed control and vibration damping to be accomplished using just one electric drive. This restriction always leads to a compromise because an improved speed control performance frequently comes with worse oscillation damping properties [36]. However, when a power train test bed has to be controlled, at least two electric drives are available; this can be utilised to improve oscillation damping without negatively affecting the speed control performance.

Another popular method for vibration damping is the use of Notch filters to attenuate the loop gain at certain frequencies and thus reduce torsional vibrations [117]. These filters must be tuned to the problematic oscillation frequency and are therefore useless when the critical frequency changes because of a modification of the test set-up. This problem can be overcome by the use of adaptive filters [118, 119]. However, this approach can be problematic in industrial practice where potentially multiple resonant frequencies occur.

5.2 Multivariable Control

Many industrial control problems belong to the class of multivariable control. As mentioned earlier, on engine test beds rotational speed and testing torque must be controlled. Since the actuators are ICE and dynamometer, which are mechanically connected, these control loops are definitely coupled [21]. On test beds for electric drives, the situation is similar [100]; here instead of an ICE an electric machine is tested. As shown in this work, power train test beds require multivariable control of rotational speed and torque as well; compared to test beds for electric drives the control problem could be extended as more than two actuators might be available. Other applications generally requiring decoupled control are steel processing lines [120, 121], paper machines [122, 123], printing machines [124], and web transportation systems [125]. Here, tension and speed usually have to be controlled independently, but the basic ideas can also be adopted to control rotational speed and torque on a drive train test bed. These applications are in particular interesting as resonance phenomena are critical too [126].

Because of its practical relevance and due to the fact that many classical control design procedures for SISO systems are no longer applicable, multivariable control has been intensely studied. Many control strategies were proposed over the years; these can be classified into *centralised control* and *decentralised control* [127]. Centralised control is based on one central controller that has information about all the available sensor data and references and produces signals for all the available actuators. Since this controller has all the information available, this is, at least in theory, the most powerful control strategy. However, in practice there are problems such as controller tuning is not intuitive because all control loops are closed simultaneously, typically an accurate plant model is necessary, computational complexity may be excessive for practical usage, and a small failure can cause instability of the overall system. Examples for centralised control are state feedback control and output feedback control including observers [128]. Also many optimisation-based control concepts belong to the class of centralised controllers, either related to optimal state feedback or in the context of MPC.

The key idea of decentralised control is to decompose the MIMO plant to control into several SISO plants. Consequently, the controller design process is based on two stages: first the subsystems to control must be identified and possibly decoupled, then independently designed feedback control for these subsystems is added. By following this approach, controllers are usually less complex as they only have to control one subsystem instead of the entire MIMO plant. Additionally, controller implementation and plant start-up are easier because the SISO control loops can be closed one after the other. Furthermore, when satisfying decoupling is achieved, the controllers for the subsystems can be designed using conventional SISO control techniques. The simplest approach belonging to this class is *multi-loop control* where manipulated and controlled variables are paired in a way that loop interactions are minimised before these SISO control loops are closed. In practice, the controllers for these sub-problems are often designed *sequentially*; this is particularly common if the bandwidth of the control loops are quite different [129]. However, control performance is typically not satisfying if these subsystems are strongly coupled. Then *decoupling control* as shown in Figure 5.2 is an appropriate alternative. The basic idea of decoupling is to transform the system's transfer function matrix into a diagonal one so that each system output y_i is controlled by the new control input v_i, but independent of the other control inputs v_j for $j \neq i$ with i and $j \in \{1, 2, \ldots, m\}$. If this decoupling is available, the MIMO control problem is equivalent to a set of m independent SISO control problems. As shown in Figure 5.2b, the decoupling can be realised via *feedforward control* using a pre-compensator, which is in general

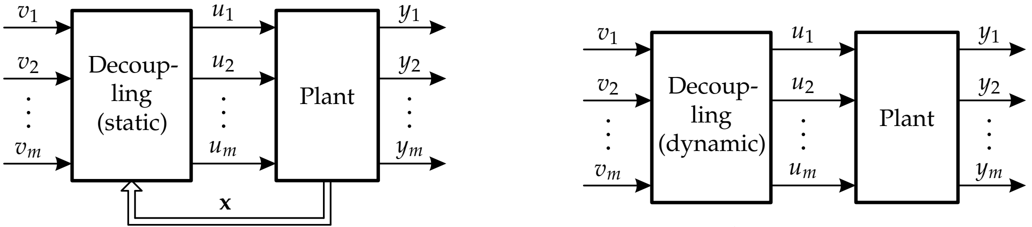

(a) Feedback decoupling.

(b) Feedforward decoupling.

Figure 5.2: Decoupling control.

a dynamic system if dynamic decoupling is desired or a set of constant gains if only steady-state decoupling is required [129]. The alternative is to use *static state feedback*; this approach is presented in Figure 5.2a and requires at least some system states to be available. If chosen appropriately, the decoupling can significantly improve the overall system performance. Problematic is that advantages related to the decentralised control approach such as the usability of standard industrial controllers are potentially lost; the resulting controller implementation is in general centralised. However, when the decoupling structure is known, the feedback controllers for the resulting SISO plants can be designed independently, which is typically still easier than following the classic centralised approach based on only one overall controller.

The requirements regarding control stated at the beginning of this chapter exclude considering some of the control strategies mentioned above. To allow test bed operators to continue using PI controllers, but nevertheless reduce the coupling of rotational speed and torque, a decoupling strategy shall be used. Since feedforward decoupling using a pre-compensator cannot damp torsional vibrations, a decoupling strategy based on state feedback is applied.

5.3 Model Reduction

As shown in Chapter 3, the test systems discussed in this work can be modelled accurately as a higher order, potentially non-linear system based on a multi-mass oscillator. The resulting models for the three test systems that were analysed are depicted in a graphical representation in Figure 3.25, Figure 3.26, and Figure 3.27; additionally, the differential equations describing the mechanical system of a test bed for differential gears are given in Appendix C. However, because of their complexity, these mathematical models are not suitable for model based controller design. Furthermore, their high number of system parameters that must be identified is problematic. For these reasons, reduced system models are determined by the use of some simplifying assumptions. Most of the ideas required for model reduction were already presented in [47] and are repeated in the following sections.

5.3.1 Case Study I: Test System for Differential Gears

In Section 3.8 a test system for differential gears was modelled for simulation purposes. In the following, this very detailed model is reduced by physically motivated simplifications. The differential gear was modelled as a second order dynamic system. But as the differential gear's structure is often symmetric and its moments of inertia are negligible compared to the electric drives, the complexity of the mathematical model presented in Section 3.8 can be reduced and instead of a dynamic model a purely kinematic model can be used. Furthermore, modern commercial differential gears are developed for high efficiency; therefore, losses are neglected and the differential gear can be modelled using the following set of algebraic equations:

$$\omega_{di} = i_d \frac{\omega_{do1} + \omega_{do2}}{2} \tag{5.1a}$$

$$T_{do1} = \frac{i_d}{2} T_{di} - \frac{T_{dsl}}{2} \tag{5.1b}$$

$$T_{do2} = \frac{i_d}{2} T_{di} + \frac{T_{dsl}}{2} \tag{5.1c}$$

Then the only relevant properties of the UUT are the torque transmission ratio i_d and the friction torque T_{dsl} responsible for limited-slip functionality. Additionally, the mathematical description of the test bed's mechanical structure can be reduced: The torsional flexibility within the in-line torque sensors is significantly less than the torsional flexibility of the cardan shafts connecting electric drives and UUT. Additionally, the moments of inertia I_{f1}, I_{f2}, and I_{f3} representing the torque measurement flanges are negligible compared to the heavy rotors of the electric drives. Therefore, these elements for modelling the torque transducers are no longer considered. Since the damping coefficients of the cardan shafts are rather low, damping is neglected and the shafts are modelled as pure torsion springs.[1] Furthermore, gear play in the cardan shafts, in the gearboxes, and in the differential gear is neglected.

Finally, the models describing the electric drives must be reduced. Since a technologically advanced inverter system is used, both dead time and first-order dynamics typically affecting the torque control loop can be neglected. This allows the air-gap torques T_{ag} to be replaced by their reference values $T_{ag,ref.}$. The system model resulting from these simplifying assumptions is shown in Figure 5.3.

---

[1] If the mechanical test set-up provides more internal damping so that damping cannot be neglected, model reduction is complicated as the determination of an overall system damping is not trivial. As shown in Appendix B, the combination of multiple shafts with internal damping to a single equivalent shaft can only be done exactly for certain parameter settings.

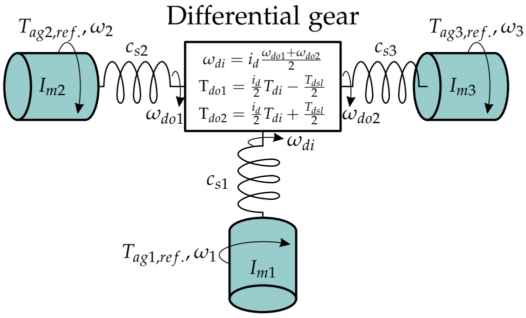

Figure 5.3: Reduced system model for a test bed for differential gears.

In most applications the test set-up is symmetric; the parameters of the cardan shafts at the two outputs of the differential gear are then identical ($c_{s2} = c_{s3}$). With this additional assumption an equivalent torsional stiffness parameter

$$\widetilde{c}_s := \frac{2c_{s1}c_{s2}}{i_d^2 c_{s1} + 2c_{s2}} = \frac{2c_{s1}c_{s3}}{i_d^2 c_{s1} + 2c_{s3}} \tag{5.2}$$

can be defined and the system shown in Figure 5.3 can be described by the following set of six differential equations derived from the conservation of angular momentum:

$$\frac{\mathrm{d}\omega_1}{\mathrm{d}t} = -\frac{\widetilde{c}_s\varphi_1}{I_{m1}} + \frac{i_d\widetilde{c}_s\varphi_2}{2I_{m1}} + \frac{i_d\widetilde{c}_s\varphi_3}{2I_{m1}} + \frac{T_{ag1,ref.}}{I_{m1}} \tag{5.3a}$$

$$\frac{\mathrm{d}\omega_2}{\mathrm{d}t} = \frac{i_d\widetilde{c}_s\varphi_1}{2I_{m2}} - \frac{i_d^2\widetilde{c}_s\varphi_2}{4I_{m2}} - \frac{i_d^2\widetilde{c}_s\varphi_3}{4I_{m2}} - \frac{T_{dsl}}{2I_{m2}} + \frac{T_{ag2,ref.}}{I_{m2}} \tag{5.3b}$$

$$\frac{\mathrm{d}\omega_3}{\mathrm{d}t} = \frac{i_d\widetilde{c}_s\varphi_1}{2I_{m3}} - \frac{i_d^2\widetilde{c}_s\varphi_2}{4I_{m3}} - \frac{i_d^2\widetilde{c}_s\varphi_3}{4I_{m3}} + \frac{T_{dsl}}{2I_{m3}} + \frac{T_{ag3,ref.}}{I_{m3}} \tag{5.3c}$$

$$\frac{\mathrm{d}\varphi_k}{\mathrm{d}t} = \omega_k \text{ for } k \in \{1,2,3\} \tag{5.3d}$$

The measurable plant outputs are the rotational speeds of the electric drives ω_1, ω_2, and ω_3 and the torques measured by the torque sensors at the electric drives. According to the system structure presented in Figure 5.3, these are the torques transmitted by the three torsionally flexible shafts:

$$T_{f1} = \widetilde{c}_s\varphi_1 - \frac{i_d\widetilde{c}_s}{2}\varphi_2 - \frac{i_d\widetilde{c}_s}{2}\varphi_3 \tag{5.4a}$$

$$T_{f2} = \frac{i_d}{2}\left(\widetilde{c}_s\varphi_1 - \frac{i_d\widetilde{c}_s}{2}\varphi_2 - \frac{i_d\widetilde{c}_s}{2}\varphi_3\right) - \frac{T_{dsl}}{2} \tag{5.4b}$$

$$T_{f3} = \frac{i_d}{2}\left(\widetilde{c}_s\varphi_1 - \frac{i_d\widetilde{c}_s}{2}\varphi_2 - \frac{i_d\widetilde{c}_s}{2}\varphi_3\right) + \frac{T_{dsl}}{2} \tag{5.4c}$$

The angular rotor positions φ_1, φ_2, and φ_3 are not relevant for control. According to Equation (5.4), only a special linear combination of φ_1, φ_2, and φ_3 is of interest. Therefore, the mathematical system model can be reduced by introducing the new state variable

$$\Delta\varphi := \varphi_1 - i_d\frac{\varphi_2 + \varphi_3}{2}. \tag{5.5}$$

Then instead of the six Differential equations (5.3), a set of four differential equations is sufficient to model the dynamics of the mechanical system shown in Figure 5.3

$$\frac{\mathrm{d}\omega_1}{\mathrm{d}t} = -\frac{\widetilde{c}_s\Delta\varphi}{I_{m1}} + \frac{T_{ag1,ref.}}{I_{m1}} \tag{5.6a}$$

$$\frac{\mathrm{d}\omega_2}{\mathrm{d}t} = \frac{i_d\widetilde{c}_s\Delta\varphi}{2I_{m2}} - \frac{T_{dsl}}{2I_{m2}} + \frac{T_{ag2,ref.}}{I_{m2}} \tag{5.6b}$$

$$\frac{\mathrm{d}\omega_3}{\mathrm{d}t} = \frac{i_d\widetilde{c}_s\Delta\varphi}{2I_{m3}} + \frac{T_{dsl}}{2I_{m3}} + \frac{T_{ag3,ref.}}{I_{m3}} \tag{5.6c}$$

$$\frac{\mathrm{d}\Delta\varphi}{\mathrm{d}t} = \omega_1 - \frac{i_d\omega_2}{2} - \frac{i_d\omega_3}{2} \tag{5.6d}$$

and instead of Equation (5.4) the torques at the measuring flanges can be specified as

$$T_{f1} = \widetilde{c}_s\Delta\varphi \tag{5.7a}$$

$$T_{f2} = \frac{i_d}{2}\widetilde{c}_s\Delta\varphi - \frac{T_{dsl}}{2} \tag{5.7b}$$

$$T_{f3} = \frac{i_d}{2}\widetilde{c}_s\Delta\varphi + \frac{T_{dsl}}{2}. \tag{5.7c}$$

This forth order dynamic system can cover the fundamental test bed dynamics including the most relevant resonance phenomena and the coupling of rotational speed and torque and is therefore used for controller design.

5.3.2 Case Study II: Test System for Differential Gears with Adapter Gearboxes

Due to additional adapter gearboxes, the test system modelled in Section 3.9 is mechanically more complex than the test bed discussed in the previous section. Nevertheless, model reduction can be performed based on the same ideas as used before. Additionally, simplifications regarding the adapter gearboxes are applicable.

Because of the three downspeed gearboxes, the mechanical system is divided into a low-speed part (differential gear) and a high-speed part (electric drives). By scaling torques, angular velocities, and cardan shaft parameters related to the low-speed part based on the transmission ratios of the gearboxes at the differential's input i_{gb1} and outputs $i_{gb2} = i_{gb3}$, these two levels of rotational speed can be combined and the mathematical model can be developed for the high-speed side. While rotational speeds and torques are transformed by multiplication with respectively division by the gearboxes' transmission ratios, the shaft parameters are scaled according to

$$c'_{s1} = \frac{c_{s1}}{i_{gb1}^2}, \quad c'_{s2} = \frac{c_{s2}}{i_{gb2}^2}, \quad c'_{s3} = \frac{c_{s3}}{i_{gb3}^2} = \frac{c_{s3}}{i_{gb2}^2}. \tag{5.8}$$

The apostrophe is used to distinguish between transformed and original values. Then also the differential gear's system parameters i_d and T_{dsl} have to be scaled according to

$$T'_{dsl} = \frac{1}{i_{gb2}} T_{dsl} \tag{5.9a}$$

$$i'_d = i_d \frac{i_{gb1}}{i_{gb2}} \tag{5.9b}$$

before the differential gear's reduced System description (5.1) can be formulated on the high-speed side. Additionally, for the test system considered here it is admissible to assume that the cardan shafts connecting electric drives and gearboxes are significantly less flexible than the shafts connecting gearboxes and differential gear; this is especially to be expected because the levels of rotational speeds were different originally and shaft parameters were transformed using Equation (5.8). Therefore, the coupling of electric drives and gearboxes can be treated as torsionally stiff and their moments of inertia can be combined. The resulting system model is shown in Figure 5.4. I_1 is the sum of the moment of inertia of the electric drive *M1* I_{m1} and the moment of inertia of gearbox 1 I_{gb1}, while I_2 represents one output of the differential gear and is also composed of the moment of inertia of the electric machine I_{m2} and the moment of inertia of the output gearbox I_{gb2}. The moments of inertia at the second output of the differential gear are specified accordingly.

In spite of the adapter gearboxes, the system model is similar to the mechanical system presented before in Figure 5.3. Consequently, the mathematical model is only slightly different. When again a symmetric test set-up ($c'_{s2} = c'_{s3}$) is assumed, the equivalent torsional stiffness is

$$\widetilde{c}_s := \frac{2c'_{s1}c'_{s2}}{{i'_d}^2 c'_{s1} + 2c'_{s2}} = \frac{2c'_{s1}c'_{s3}}{{i'_d}^2 c'_{s1} + 2c'_{s3}}. \tag{5.10}$$

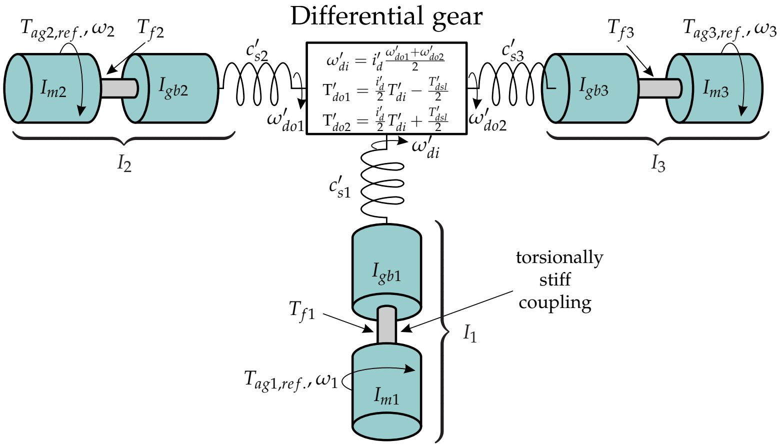
Differential gear
$T_{ag2,ref.}, \omega_2$
T_{f2}
I_{m2}
I_{gb2}
c'_{s2}
ω'_{do1}
$\omega'_{di} = i'_d \frac{\omega'_{do1}+\omega'_{do2}}{2}$
$T'_{do1} = \frac{i'_d}{2} T'_{di} - \frac{T'_{dsl}}{2}$
$T'_{do2} = \frac{i'_d}{2} T'_{di} + \frac{T'_{dsl}}{2}$
c'_{s3}
ω'_{do2}
T_{f3}
$T_{ag3,ref.}, \omega_3$
I_{gb3}
I_{m3}
I_2
I_3
ω'_{di}
c'_{s1}
I_{gb1}
torsionally stiff coupling
T_{f1}
I_1
$T_{ag1,ref.}, \omega_1$
I_{m1}

Figure 5.4: Reduced system model for a test bed for differential gears with adapter gearboxes.

As for the setting without adapter gearboxes, the angular positions φ_1, φ_2, and φ_3 are not relevant for control, thus the new state variable

$$\Delta\varphi := \varphi_1 - i'_d \frac{\varphi_2 + \varphi_3}{2} \tag{5.11}$$

is introduced. Then the mechanical system shown in Figure 5.4 can be described by the following set of differential equations derived from the conservation of angular momentum:

$$\frac{\mathrm{d}\omega_1}{\mathrm{d}t} = -\frac{\widetilde{c}_s \Delta\varphi}{I_1} + \frac{T_{ag1,ref.}}{I_1} \tag{5.12a}$$

$$\frac{\mathrm{d}\omega_2}{\mathrm{d}t} = \frac{i'_d \widetilde{c}_s \Delta\varphi}{2I_2} - \frac{T'_{dsl}}{2I_2} + \frac{T_{ag2,ref.}}{I_2} \tag{5.12b}$$

$$\frac{\mathrm{d}\omega_3}{\mathrm{d}t} = \frac{i'_d \widetilde{c}_s \Delta\varphi}{2I_3} + \frac{T'_{dsl}}{2I_3} + \frac{T_{ag3,ref.}}{I_3} \tag{5.12c}$$

$$\frac{\mathrm{d}\Delta\varphi}{\mathrm{d}t} = \omega_1 - \frac{i'_d \omega_2}{2} - \frac{i'_d \omega_3}{2} \tag{5.12d}$$

Besides the angular velocities of the electric drives ω_1, ω_2, and ω_3 the torques measured by the torque measuring flanges are relevant for control:

$$T_{f1} = \frac{I_{m1}}{I_1} \widetilde{c}_s \Delta\varphi + \frac{I_{gb1}}{I_1} T_{ag1,ref.} \tag{5.13a}$$

$$T_{f2} = \frac{I_{m2}}{I_2} \frac{i'_d}{2} \widetilde{c}_s \Delta\varphi - \frac{I_{m2}}{I_2} \frac{T'_{dsl}}{2} - \frac{I_{gb2}}{I_2} T_{ag2,ref.} \tag{5.13b}$$

$$T_{f3} = \frac{I_{m3}}{I_3} \frac{i'_d}{2} \widetilde{c}_s \Delta\varphi + \frac{I_{m3}}{I_3} \frac{T'_{dsl}}{2} - \frac{I_{gb3}}{I_3} T_{ag3,ref.} \tag{5.13c}$$

While the system dynamics are equivalent to the test system without adapter gearboxes, these system outputs are obviously affected by the moments of inertia of the adapter gearboxes and therefore different than in Equation (5.7). However, when the moments of inertia of the gearboxes tend to zero, above calculation formula for the flange torques converges to Equation (5.7). Consequently, controller design is only required for this extended testing situation with adapter gearboxes; controllers for the simpler testing configuration can then be derived from the controller for this extended test system.

5.3.3 Case Study III: Test System for Transmissions

Finally, a reduced model for a test bed for transmissions as discussed in Section 3.10 is derived. For controller design the transmission models discussed in Section 3.7.2 can be further reduced: The torque converter is not considered as in modern automatic transmissions the lock-up clutch is controlled to limit torque converter slip for increased efficiency [74]. Since in a testing situation the moment of inertia of the transmission is often significantly smaller than the moments of inertia of the electric drives, the UUT is assumed to be inertia-free. Furthermore, for modelling a constant gear is assumed; consequently, the friction elements required to interrupt the power transmission are not considered. Therefore, the transmission is modelled as

$$\omega_{gbi} = i_{gb}\omega_{gbo} \tag{5.14a}$$

$$T_{gbo} = i_{gb}T_{gbi}. \tag{5.14b}$$

Neglecting the moment of inertia of the UUT means that a two-mass oscillator results instead of a three-mass oscillator. Since damping the first eigenmode is the priority and as the second eigenmode is typically at a rather high frequency and difficult to damp anyway, this simplification is admissible. If furthermore the torsional flexibility of the torque measuring flanges is neglected, the system model presented in Figure 5.5 results.

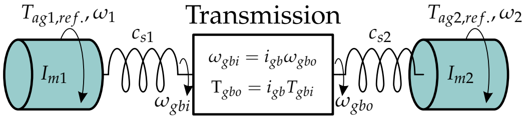

Figure 5.5: Reduced system model for a test bed for transmissions.

To model this mechanical system, the equivalent torsional stiffness parameter

$$\widetilde{c}_s := \frac{c_{s1}c_{s2}}{i_{gb}^2 c_{s1} + c_{s2}} \tag{5.15}$$

is defined; then the rotational dynamics can be specified as

$$\frac{\mathrm{d}\omega_1}{\mathrm{d}t} = -\frac{\widetilde{c}_s \Delta\varphi}{I_{m1}} + \frac{T_{ag1,ref.}}{I_{m1}} \tag{5.16a}$$

$$\frac{\mathrm{d}\omega_2}{\mathrm{d}t} = \frac{i_{gb}\widetilde{c}_s \Delta\varphi}{I_{m2}} + \frac{T_{ag2,ref.}}{I_{m2}} \tag{5.16b}$$

$$\frac{\mathrm{d}\Delta\varphi}{\mathrm{d}t} = \omega_1 - i_{gb}\omega_2, \tag{5.16c}$$

where

$$\Delta\varphi := \varphi_1 - i_{gb}\varphi_2. \tag{5.17}$$

Since the UUT was assumed to be inertia-free, the torque transmitted along the output shaft equals the torque at the input shaft scaled by the transmission ratio i_{gb}

$$T_{f1} = \widetilde{c}_s \Delta\varphi \tag{5.18a}$$

$$T_{f2} = i_{gb}\widetilde{c}_s \Delta\varphi. \tag{5.18b}$$

If the controlled variables are the torque at the transmission input and the angular velocity of the load drive, the system outputs are

$$y_1 = T_{f1} \tag{5.19a}$$

$$y_2 = \omega_2. \tag{5.19b}$$

As the Differential equations (5.16) and the Output equations (5.19) are forming a LTI system, transfer functions from the system inputs $T_{ag1,ref.}$ and $T_{ag2,ref.}$ to the system outputs T_{f1}

$$T_{f1}(s) = \underbrace{\frac{\widetilde{c}_s}{I_{m1}\left(s^2 + \frac{\widetilde{c}_s}{I_{m1}} + \frac{\widetilde{c}_s i_{gb}^2}{I_{m2}}\right)}}_{=:G_{11}(s)} T_{ag1,ref.}(s) - \underbrace{\frac{\widetilde{c}_s i_{gb}}{I_{m2}\left(s^2 + \frac{\widetilde{c}_s}{I_{m1}} + \frac{\widetilde{c}_s i_{gb}^2}{I_{m2}}\right)}}_{=:G_{12}(s)} T_{ag2,ref.}(s) \tag{5.20}$$

and ω_2

$$\omega_2(s) = \underbrace{\frac{\widetilde{c}_s i_{gb}}{I_{m1}I_{m2}s\left(s^2 + \frac{\widetilde{c}_s}{I_{m1}} + \frac{\widetilde{c}_s i_{gb}^2}{I_{m2}}\right)}}_{=:G_{21}(s)} T_{ag1,ref.}(s) + \underbrace{\frac{s^2 + \frac{\widetilde{c}_s}{I_{m1}}}{I_{m2}s\left(s^2 + \frac{\widetilde{c}_s}{I_{m1}} + \frac{\widetilde{c}_s i_{gb}^2}{I_{m2}}\right)}}_{=:G_{22}(s)} T_{ag2,ref.}(s) \tag{5.21}$$

can be used to analyse the control problem. The challenges for control are obvious: Since the number of system inputs and outputs is greater than one, this plant is a typical MIMO system. Both controlled variables are affected by both system inputs, which means that those control loops are coupled. Additionally, due to the torsional flexibility in the mechanical system and zero shaft damping, the denominator polynomials of the transfer functions defined in Equation (5.20) and Equation (5.21) show conjugate complex zeros located at

$$s_{1,2} = \pm j \sqrt{\widetilde{c}_s \left(\frac{1}{I_{m1}} + \frac{i_{gb}^2}{I_{m2}} \right)} \tag{5.22}$$

potentially resulting in resonant oscillations. These findings are not only relevant for this testing situation, but also valid for the three machine testing configurations discussed before. Above challenges regarding control are addressed in the following sections.

5.4 Input–Output Decoupling and Feedback Linearisation

To achieve decoupling and vibration damping, a feedback *input–output decoupling* and *linearisation* strategy is applied [130–134]. Figure 5.6a shows the control structure related to this concept for a typical MIMO plant. Most of the following considerations are only straightforward extensions of the feedback linearisation design procedure for SISO plants [130, 133]. The plant with m-dimensional input vector $\mathbf{u} = [u_1, u_2, \ldots, u_m]^\mathrm{T}$ and m-dimensional output vector $\mathbf{y} = [y_1, y_2, \ldots, y_m]^\mathrm{T}$ is controlled by a decoupling and linearisation network ensuring that the map between the new system input v_i and system output y_i is linear with dynamics $G_i(s)$ specified in the linearisation process for $i = 1, 2, \ldots, m$ and that this system output y_i is independent of all inputs v_j for $i \neq j$, see Figure 5.6b. This problem statement implies that the number of controlled variables equals the number of manipulated variables, but this is no limiting restriction for power train test bed control. The decoupling and linearisation is realised based on the new m-dimensional input vector

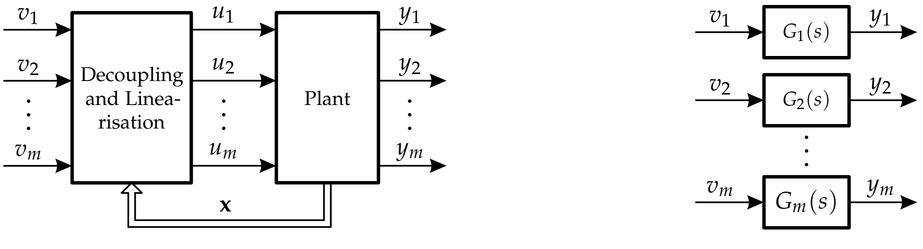

(a) Control structure.

(b) Control objective.

Figure 5.6: Input–output decoupling and feedback linearisation principle.

$\mathbf{v} = [v_1, v_2, \ldots, v_m]^{\mathrm{T}}$ and a static feedback of the state vector $\mathbf{x} = [x_1, x_2, \ldots, x_N]^{\mathrm{T}}$, where N is the system order. The plant considered is the affine input system given by equations of the form

$$\frac{\mathrm{d}\mathbf{x}}{\mathrm{d}t} = \mathbf{a}(\mathbf{x}) + \sum_{k=1}^{m} \mathbf{b}_k(\mathbf{x}) u_k \tag{5.23a}$$

$$y_i = c_i(\mathbf{x}) \quad \text{for} \quad i = 1, 2, \ldots, m. \tag{5.23b}$$

The relative degree δ_i is determined for every system output y_i with $i = 1, 2, \ldots, m$ as for SISO plants by differentiation of the corresponding output with respect to time

$$\begin{aligned}
y_i &= c_i(\mathbf{x}) \\
\frac{\mathrm{d}y_i}{\mathrm{d}t} &= L_{\mathbf{a}} c_i(\mathbf{x}) + \sum_{k=1}^{m} \underbrace{L_{\mathbf{b}_k} c_i(\mathbf{x})}_{0} u_k \\
y_i^{(2)} &= L_{\mathbf{a}}^2 c_i(\mathbf{x}) + \sum_{k=1}^{m} \underbrace{L_{\mathbf{b}_k} L_{\mathbf{a}} c_i(\mathbf{x})}_{0} u_k \\
&\vdots \\
y_i^{(\delta_i - 1)} &= L_{\mathbf{a}}^{\delta_i - 1} c_i(\mathbf{x}) + \sum_{k=1}^{m} \underbrace{L_{\mathbf{b}_k} L_{\mathbf{a}}^{\delta_i - 2} c_i(\mathbf{x})}_{0} u_k \\
y_i^{(\delta_i)} &= L_{\mathbf{a}}^{\delta_i} c_i(\mathbf{x}) + \sum_{k=1}^{m} \underbrace{L_{\mathbf{b}_k} L_{\mathbf{a}}^{\delta_i - 1} c_i(\mathbf{x})}_{\substack{\neq 0 \text{ for at least} \\ \text{one } k \in \{1,2,\ldots,m\}}} u_k,
\end{aligned} \tag{5.24}$$

where

$$L_{\mathbf{a}} c_i(\mathbf{x}) := \frac{\partial c_i(\mathbf{x})}{\partial \mathbf{x}} \mathbf{a}(\mathbf{x}) \tag{5.25}$$

is called the Lie derivative of c_i with respect to the vector $\mathbf{a}$ or along $\mathbf{a}$ [130]. In all time derivatives $y_i^{(l)}$ for $l = 1, 2, .., \delta_i - 1$ the Lie derivatives along $\mathbf{b}_k$ are zero for $k = 1, 2, \ldots, m$ while in $y_i^{(\delta_i)}$ the Lie derivative along $\mathbf{b}_k$ is non-zero for at least one $k \in \{1, 2, \ldots, m\}$.

When the relative degree δ_i is determined for every system output y_i, the relations

$$\begin{aligned}
y_1^{(\delta_1)} &= L_{\mathbf{a}}^{\delta_1} c_1(\mathbf{x}) + \sum_{k=1}^{m} L_{\mathbf{b}_k} L_{\mathbf{a}}^{\delta_1 - 1} c_1(\mathbf{x}) u_k \\
y_2^{(\delta_2)} &= L_{\mathbf{a}}^{\delta_2} c_2(\mathbf{x}) + \sum_{k=1}^{m} L_{\mathbf{b}_k} L_{\mathbf{a}}^{\delta_2 - 1} c_2(\mathbf{x}) u_k \\
&\vdots \\
y_m^{(\delta_m)} &= L_{\mathbf{a}}^{\delta_m} c_m(\mathbf{x}) + \sum_{k=1}^{m} L_{\mathbf{b}_k} L_{\mathbf{a}}^{\delta_m - 1} c_m(\mathbf{x}) u_k
\end{aligned} \tag{5.26}$$

can be formulated. These equations can be summarised in vector-matrix notation

$$\widetilde{\mathbf{y}} = \widetilde{\mathbf{c}}(\mathbf{x}) + \overline{\mathbf{D}}(\mathbf{x}) \mathbf{u}, \tag{5.27}$$

where the m-dimensional vectors $\widetilde{\mathbf{y}}$ and $\widetilde{\mathbf{c}}(\mathbf{x})$ are defined as

$$\widetilde{\mathbf{y}} := \begin{bmatrix} y_1^{(\delta_1)} \\ y_2^{(\delta_2)} \\ \vdots \\ y_m^{(\delta_m)} \end{bmatrix}, \quad \widetilde{\mathbf{c}}(\mathbf{x}) := \begin{bmatrix} L_{\mathbf{a}}^{\delta_1} c_1(\mathbf{x}) \\ L_{\mathbf{a}}^{\delta_2} c_2(\mathbf{x}) \\ \vdots \\ L_{\mathbf{a}}^{\delta_m} c_m(\mathbf{x}) \end{bmatrix} \tag{5.28}$$

while the matrix $\overline{\mathbf{D}}(\mathbf{x}) \in \mathbb{R}^{m \times m}$ is given as

$$\overline{\mathbf{D}}(\mathbf{x}) := \begin{pmatrix} L_{\mathbf{b}_1} L_{\mathbf{a}}^{\delta_1 - 1} c_1(\mathbf{x}) & L_{\mathbf{b}_2} L_{\mathbf{a}}^{\delta_1 - 1} c_1(\mathbf{x}) & \cdots & L_{\mathbf{b}_m} L_{\mathbf{a}}^{\delta_1 - 1} c_1(\mathbf{x}) \\ L_{\mathbf{b}_1} L_{\mathbf{a}}^{\delta_2 - 1} c_2(\mathbf{x}) & L_{\mathbf{b}_2} L_{\mathbf{a}}^{\delta_2 - 1} c_2(\mathbf{x}) & \cdots & L_{\mathbf{b}_m} L_{\mathbf{a}}^{\delta_2 - 1} c_2(\mathbf{x}) \\ \vdots & \vdots & \ddots & \vdots \\ L_{\mathbf{b}_1} L_{\mathbf{a}}^{\delta_m - 1} c_m(\mathbf{x}) & L_{\mathbf{b}_2} L_{\mathbf{a}}^{\delta_m - 1} c_m(\mathbf{x}) & \cdots & L_{\mathbf{b}_m} L_{\mathbf{a}}^{\delta_m - 1} c_m(\mathbf{x}) \end{pmatrix}. \tag{5.29}$$

If a new m-dimensional system input $\mathbf{w}$ is introduced in a way that

$$\mathbf{w} = \widetilde{\mathbf{y}} \tag{5.30}$$

holds, decoupling and linearity is ensured [133]. Based on this relationship and according to Equation (5.27), the system input $\mathbf{u}$ can be determined if the matrix $\overline{\mathbf{D}}(\mathbf{x})$ is regular:

$$\mathbf{u} = -\overline{\mathbf{D}}^{-1}(\mathbf{x}) \left(\widetilde{\mathbf{c}}(\mathbf{x}) - \mathbf{w} \right) \tag{5.31}$$

If the new manipulated variable w_i is chosen as

$$w_i = -a_{i,\delta_i - 1} y_i^{(\delta_i - 1)} - a_{i,\delta_i - 2} y_i^{(\delta_i - 2)} - \cdots - a_{i,0} y_i + V_i v_i \quad \text{for} \quad i = 1, 2, \ldots, m, \tag{5.32}$$

the dynamics of the controlled SISO plant is defined by the choice of the controller coefficients $a_{i,j}$:

$$y_i^{(\delta_i)} + a_{i,\delta_i-1} y_i^{(\delta_i-1)} + a_{i,\delta_i-2} y_i^{(\delta_i-2)} + \cdots + a_{i,0} y_i = V_i v_i \quad \text{for} \quad i = 1, 2, \ldots, m \tag{5.33}$$

By the use of Equation (5.24), the final control law can be formulated

$$\mathbf{u} = -\overline{\mathbf{D}}^{-1}(\mathbf{x}) \begin{bmatrix} L_{\mathbf{a}}^{\delta_1} c_1(\mathbf{x}) + \cdots + a_{1,1} L_{\mathbf{a}} c_1(\mathbf{x}) + a_{1,0} c_1(\mathbf{x}) - V_1 v_1 \\ L_{\mathbf{a}}^{\delta_2} c_2(\mathbf{x}) + \cdots + a_{2,1} L_{\mathbf{a}} c_2(\mathbf{x}) + a_{2,0} c_2(\mathbf{x}) - V_2 v_2 \\ \vdots \\ L_{\mathbf{a}}^{\delta_m} c_m(\mathbf{x}) + \cdots + a_{m,1} L_{\mathbf{a}} c_m(\mathbf{x}) + a_{m,0} c_m(\mathbf{x}) - V_m v_m \end{bmatrix}. \tag{5.34}$$

As mentioned, the matrix $\overline{\mathbf{D}}(\mathbf{x})$ must be regular to be able to completely decouple the system. However, if the plant contains some *internal dynamics*, ensuring asymptotic stability may still be problematic. For analysing the internal dynamics the vector relative degree $\boldsymbol{\delta}$ and total relative degree δ of the system are of importance. System (5.23) has a vector relative degree

$$\boldsymbol{\delta} = \begin{bmatrix} \delta_1 & \delta_2 & \cdots & \delta_m \end{bmatrix}^{\mathrm{T}} \tag{5.35}$$

if

1. $L_{\mathbf{b}_k} L_{\mathbf{a}}^{l-1} c_i(\mathbf{x}) = 0$ for $i = 1, \ldots, m$, $k = 1, \ldots, m$, $l = 1, \ldots, \delta_i - 1$ and
2. the decoupling matrix $\overline{\mathbf{D}}(\mathbf{x})$ is regular.

The sum of all δ_i

$$\delta = \delta_1 + \delta_2 + \cdots + \delta_m \tag{5.36}$$

is the total relative degree of System (5.23).

To prove asymptotic stability, the transformation $\mathbf{z} = \mathbf{t}(\mathbf{x})$ into *Byrnes-Isidori normal form* is applied:

$$\mathbf{z} = \begin{bmatrix} z_1 \\ \vdots \\ z_N \end{bmatrix} = \begin{bmatrix} \boldsymbol{\xi} \\ \boldsymbol{\eta} \end{bmatrix} = \mathbf{t}(\mathbf{x}) = \begin{bmatrix} c_1(\mathbf{x}) \\ L_{\mathbf{a}} c_1(\mathbf{x}) \\ \vdots \\ L_{\mathbf{a}}^{\delta_1 - 1} c_1(\mathbf{x}) \\ \vdots \\ c_m(\mathbf{x}) \\ L_{\mathbf{a}} c_m(\mathbf{x}) \\ \vdots \\ L_{\mathbf{a}}^{\delta_m - 1} c_m(\mathbf{x}) \\ t_{\delta+1}(\mathbf{x}) \\ \vdots \\ t_N(\mathbf{x}) \end{bmatrix} \tag{5.37}$$

The first δ_1 elements of $\mathbf{z}$ and $\boldsymbol{\xi}$ are given by the system output y_1 and its $\delta_1 - 1$ time derivatives. The remaining elements of $\boldsymbol{\xi}$ are the other system outputs y_i and their $\delta_i - 1$ time derivatives for $i = 2, 3, \ldots, m$. The $N - \delta$ missing elements of $\mathbf{z}$ are summarised in $\boldsymbol{\eta}$ and given by functions $t_j(\mathbf{x})$. The choice of these functions is not unique, but restricted by the requirement that $\mathrm{d}\mathbf{t}/\mathrm{d}\mathbf{x}$ must be regular. Then the inverse transformation

$$\mathbf{x} = \mathbf{t}^{-1}(\mathbf{z}) \tag{5.38}$$

exists as well. If Transformation (5.37) is applied to System (5.23), the plant in Byrnes-Isidori normal form

$$\frac{\mathrm{d}\mathbf{z}}{\mathrm{d}t} = \frac{\mathrm{d}}{\mathrm{d}t}\begin{bmatrix} \xi_1 \\ \xi_2 \\ \vdots \\ \xi_{\delta_1} \\ \vdots \\ \xi_{\delta-\delta_m+1} \\ \vdots \\ \xi_\delta \\ \eta_1 \\ \vdots \\ \eta_{N-\delta} \end{bmatrix} = \begin{bmatrix} \xi_2 \\ \xi_3 \\ \vdots \\ \varphi_1(\boldsymbol{\xi}, \boldsymbol{\eta}, \mathbf{u}) \\ \vdots \\ \xi_{\delta-\delta_m+2} \\ \vdots \\ \varphi_m(\boldsymbol{\xi}, \boldsymbol{\eta}, \mathbf{u}) \\ q_1(\boldsymbol{\xi}, \boldsymbol{\eta}, \mathbf{u}) \\ \vdots \\ q_{N-\delta}(\boldsymbol{\xi}, \boldsymbol{\eta}, \mathbf{u}) \end{bmatrix} \tag{5.39}$$

results. The functions $\varphi_i(\boldsymbol{\xi}, \boldsymbol{\eta}, \mathbf{u})$ for $i = 1, 2, \ldots, m$ describe the δ_i^{th} time derivative of system output y_i as given in Equation (5.26). If the Control law (5.34) is applied, the closed-loop control system in Byrnes-Isidori normal form is

$$\frac{\mathrm{d}}{\mathrm{d}t}\begin{bmatrix} \xi_1 \\ \xi_2 \\ \vdots \\ \xi_{\delta_1} \\ \vdots \\ \xi_{\delta-\delta_m+1} \\ \vdots \\ \xi_\delta \\ \eta_1 \\ \vdots \\ \eta_{N-\delta} \end{bmatrix} = \begin{bmatrix} \xi_2 \\ \xi_3 \\ \vdots \\ -a_{1,0}\xi_1 - a_{1,1}\xi_2 - \cdots - a_{1,\delta_1-1}\xi_{\delta_1} + V_1 v_1 \\ \vdots \\ \xi_{\delta-\delta_m+2} \\ \vdots \\ -a_{m,0}\xi_{\delta-\delta_m+1} - a_{m,1}\xi_{\delta-\delta_m+2} - \cdots - a_{m,\delta_m-1}\xi_\delta + V_m v_m \\ q_1(\boldsymbol{\xi}, \boldsymbol{\eta}, \mathbf{u}) = \tilde{q}_1(\boldsymbol{\xi}, \boldsymbol{\eta}, \mathbf{v}) \\ \vdots \\ q_{N-\delta}(\boldsymbol{\xi}, \boldsymbol{\eta}, \mathbf{u}) = \tilde{q}_{N-\delta}(\boldsymbol{\xi}, \boldsymbol{\eta}, \mathbf{v}) \end{bmatrix} . \tag{5.40}$$

This representation clearly shows that the input–output behaviour (external dynamics) is given by the dynamics of $\boldsymbol{\xi}$ while the internal dynamics is given by the dynamics of $\boldsymbol{\eta}$. If δ is equal to N, the system has maximum relative degree and consequently no internal dynamics. Asymptotic stability can then be guaranteed by selecting the coefficients $a_{i,j}$ such that the denominator polynomial of the transfer function related to Equation (5.33) is a Hurwitz stable polynomial for $i = 1, 2, \ldots, m$. If however $\delta < N$ holds, System (5.23) with Control law (5.34) contains a non-observable subsystem of order $N - \delta$. The dynamics of this subsystem is given by

$$\frac{\mathrm{d}\boldsymbol{\eta}}{\mathrm{d}t} = \begin{bmatrix} \widetilde{q}_1(\boldsymbol{\xi}, \boldsymbol{\eta}, \mathbf{v}) \\ \vdots \\ \widetilde{q}_{N-\delta}(\boldsymbol{\xi}, \boldsymbol{\eta}, \mathbf{v}) \end{bmatrix}. \tag{5.41}$$

To be able to guarantee asymptotic stability of the overall control system, in addition to the external dynamics also these internal dynamics must be asymptotically stable.

In [47] a control strategy based on these ideas was proposed to control a test bed for differential gears as presented in Figure 3.1. In the following sections, the results for this three machine testing configuration shall be given once again; additionally, a modification for the use for two machine configurations is presented. The decoupling networks are designed to minimise loop interactions and to ensure that the dynamics of the resulting SISO plants are suitable for the design of additional feedback controllers for rotational speed and torque. This approach based on solving the control problem in two steps is chosen because then, the decoupling problem is separated from the tracking problem and the feedback tracking controllers could be realised as PI controllers making the control concept easy to handle for test bed operators.

5.4.1 Two Machine Configuration

The decoupling and linearisation procedure is applied to the reduced mathematical model of the test bed for transmissions derived in Section 5.3.3. Here the first controlled variable y_1 is the torque measured at the input drive

$$y_1 = T_{f1} = \widetilde{c}_s \Delta\varphi \tag{5.42}$$

while the second system output is the angular velocity of the load drive

$$y_2 = \omega_2. \tag{5.43}$$

The dynamics of the plant are

$$\frac{\mathrm{d}\omega_1}{\mathrm{d}t} = -\frac{\widetilde{c}_s \Delta\varphi}{I_{m1}} + \frac{T_{ag1,ref.}}{I_{m1}} \tag{5.44a}$$

$$\frac{\mathrm{d}\omega_2}{\mathrm{d}t} = \frac{i_{gb}\widetilde{c}_s\Delta\varphi}{I_{m2}} + \frac{T_{ag2,ref.}}{I_{m2}} \tag{5.44b}$$

$$\frac{\mathrm{d}\Delta\varphi}{\mathrm{d}t} = \omega_1 - i_{gb}\omega_2. \tag{5.44c}$$

To determine the relative degrees, the first time derivative of y_1 is calculated

$$\frac{\mathrm{d}y_1}{\mathrm{d}t} = \widetilde{c}_s\omega_1 - \widetilde{c}_s i_{gb}\omega_2. \tag{5.45}$$

Since $\mathrm{d}y_1/\mathrm{d}t$ does not depend on either $T_{ag1,ref.}$ or $T_{ag2,ref.}$, the second time derivative is determined; for completeness a potentially time dependent transmission ratio is assumed

$$\frac{\mathrm{d}^2y_1}{\mathrm{d}t^2} = -\widetilde{c}_s^2\left(\frac{1}{I_{m1}} + \frac{i_{gb}^2}{I_{m2}}\right)\Delta\varphi + \frac{\widetilde{c}_s T_{ag1,ref.}}{I_{m1}} - \frac{i_{gb}\widetilde{c}_s T_{ag2,ref.}}{I_{m2}} - \widetilde{c}_s\omega_2\frac{\mathrm{d}i_{gb}}{\mathrm{d}t}. \tag{5.46}$$

Consequently, the relative degree belonging to the controlled variable y_1 is $\delta_1 = 2$. The first time derivative of y_2 is

$$\frac{\mathrm{d}y_2}{\mathrm{d}t} = \frac{i_{gb}\widetilde{c}_s\Delta\varphi}{I_{m2}} + \frac{T_{ag2,ref.}}{I_{m2}}; \tag{5.47}$$

therefore, the relative degree of system output y_2 is $\delta_2 = 1$.

Remark 1 *The sum of relative degrees is three, which is equal to the number of state variables in System* (5.44). *For this reason, the dynamic system described by Equation* (5.44) *with outputs defined in Equation* (5.42) *and Equation* (5.43) *has no internal dynamics.*

For the given plant the decoupling matrix $\overline{\mathbf{D}}(\mathbf{x})$ is independent of the state vector $\mathbf{x}$:

$$\overline{\mathbf{D}} = \begin{pmatrix} \frac{\widetilde{c}_s}{I_{m1}} & -\frac{i_{gb}\widetilde{c}_s}{I_{m2}} \\ 0 & \frac{1}{I_{m2}} \end{pmatrix} \tag{5.48}$$

As $\overline{\mathbf{D}}$ is clearly regular, the decoupling network can be determined; due to the upper triangular form of $\overline{\mathbf{D}}$, computing the inverse of $\overline{\mathbf{D}}$ is unnecessary and a step-by-step calculation of the manipulated variables $u_1 = T_{ag1,ref.}$ and $u_2 = T_{ag2,ref.}$ is possible. In the input–output decoupling process the dynamics of the resulting decoupled SISO plants can be assigned. According to the relative degree $\delta_2 = 1$, the desired dynamics of the system output y_2 is chosen as the first-order dynamic system[2]

$$G_2(s) := \frac{y_2(s)}{v_2(s)} = \frac{1}{I_{m2}s}, \tag{5.49}$$

---

[2] This plant dynamics is not bounded input – bounded output (BIBO) stable; stability is ensured by the additional feedback speed controller.

so that the system output y_2 is controlled by the virtual control input v_2, which will be the output of a speed controller, but independent of the virtual control input v_1 [130]. The dynamics are defined as a simple (scaled) integrator because many suitable speed controllers are available for this system class. Writing down the corresponding differential equation

$$\frac{\mathrm{d}y_2}{\mathrm{d}t} = \frac{\mathrm{d}\omega_2}{\mathrm{d}t} = \frac{v_2}{I_{m2}} \tag{5.50}$$

and using Equation (5.44b) results in the desired air-gap torque for the electric drive *M2*:

$$T_{ag2,ref.} = v_2 - i_{gb}\widetilde{c}_s\Delta\varphi \tag{5.51}$$

This desired air-gap torque $T_{ag2,ref.}$ is composed of two parts; the first component is the virtual control input v_2, which will be the output of the feedback speed controller. Additionally, the output torque of the transmission has to be compensated. According to Equation (5.18b), this is exactly the measured shaft torque T_{f2}; therefore, no load torque estimation is necessary and the calculation formula for the manipulated variable $T_{ag2,ref.}$ can be simplified:

$$T_{ag2,ref.} = v_2 - T_{f2} \tag{5.52}$$

If the air-gap torque $T_{ag2,ref.}$ is calculated according to Equation (5.51) or Equation (5.52), changes in testing torque do not affect the angular velocity ω_2. As the shaft torque measurement is used directly, also phenomena that were not modelled (e.g. disturbances resulting from gear shifts) are compensated. This feedforward *load torque compensation* is sporadically used to improve disturbance rejection in speed control applications, see e.g. [135]. In many industrial applications a torque sensor is not available. In these cases the load torque must be estimated. Thus, using the measured load torque simplifies the control structure by removing the observer. Implementing this strategy in practice however is not trivial. Directly considering the measured shaft torque T_f in the desired air-gap torque $T_{ag,ref.}$ is critical concerning dead times in the inverter system. Dead times above a certain level in the inverter's torque control loop can cause instability of the speed control loop, especially if higher resonance frequencies in the multi-mass mechanical system have to be considered. To avoid this problem, the measured shaft torque is often low-pass filtered. This however degrades disturbance rejection properties as well. But if a hardware set-up optimised for small dead times and fast torque dynamics is available, the measured load torque can be added directly without filtering. However, using speed control with feedforward load torque compensation might degrade the vibration damping properties [36]. Therefore, the input drive *M1* must be used to actively damp resonant torque oscillations.

Also for the remaining system output y_1 the desired dynamics have to be specified according to the relative degree $\delta_1 = 2$. In general,

$$G_1(s) := \frac{y_1(s)}{v_1(s)} = \frac{V}{s^2 + a_1 s + a_0} \tag{5.53}$$

with $a_0 > 0$ and $a_1 > 0$ is a suitable approach for the dynamics of y_1. The differential equation corresponding to Equation (5.53)

$$\frac{\mathrm{d}^2 y_1}{\mathrm{d}t^2} + a_1 \frac{\mathrm{d}y_1}{\mathrm{d}t} + a_0 y_1 = V v_1 \tag{5.54}$$

in combination with the definition of the system output y_1 in Equation (5.42), its time derivatives according to (5.45) and (5.46), and the dynamics of the output y_2 as specified in (5.49) or (5.50) results in

$$T_{ag1,ref.} = \left(\widetilde{c}_s - a_0 I_{m1}\right)\Delta\varphi - a_1 I_{m1}\left(\omega_1 - i_{gb}\omega_2\right) + I_{m1} i_{gb}\frac{v_2}{I_{m2}} + I_{m1}\omega_2 \frac{\mathrm{d}i_{gb}}{\mathrm{d}t} + \frac{V I_{m1}}{\widetilde{c}_s} v_1. \tag{5.55}$$

To reduce this formula, the coefficient a_0 can be chosen as $a_0 = \widetilde{c}_s / I_{m1}$; then the dependency on $\Delta\varphi$ is removed. Additionally, $V = a_0$ must hold for unity gain. This gives

$$T_{ag1,ref.} = v_1 + I_{m1}\left(i_{gb}\frac{v_2}{I_{m2}} + \omega_2 \frac{\mathrm{d}i_{gb}}{\mathrm{d}t}\right) - a_1 I_{m1}\left(\omega_1 - i_{gb}\omega_2\right). \tag{5.56}$$

Consequently, the resulting torque transfer function is

$$G_1(s) = \frac{\widetilde{c}_s}{I_{m1}s^2 + a_1 I_{m1} s + \widetilde{c}_s}. \tag{5.57}$$

If the transfer function is rewritten as

$$G_1(s) = \frac{\widetilde{c}_s}{I_{m1}s^2 + \widetilde{d}_{s,des.} s + \widetilde{c}_s}, \tag{5.58}$$

a physical interpretation is possible. This transfer function is close to the dynamics of the mechanical system, which can be regarded as an undamped two-mass oscillator with the moment of inertia of the speed controlled machine tending to infinity because of load torque compensation. I_{m1} is the moment of inertia of the input drive while $\widetilde{c}_s$ is the torsional stiffness parameter of the elastic shaft. The new parameter $\widetilde{d}_{s,des.}$ is the shaft's desired damping coefficient. This means that the natural frequency of the decoupled system remains unmodified while the damping is increased by feedback control. The choice of (5.58) can be motivated by a differentiation of (5.44c) with respect to time. If additionally (5.44a) is used and the dynamics of the system output y_2 is fixed according to (5.50), one obtains

$$\frac{\mathrm{d}^2\Delta\varphi}{\mathrm{d}t^2} = -\frac{\widetilde{c}_s\Delta\varphi}{I_{m1}} + \frac{T_{ag1,ref.}}{I_{m1}} - i_{gb}\frac{v_2}{I_{m2}} - \omega_2\frac{\mathrm{d}i_{gb}}{\mathrm{d}t}. \tag{5.59}$$

Pure decoupling would require the desired electromagnetic torque $T_{ag1,ref.}$ to be chosen as

$$T_{ag1,ref.} = \widetilde{T}_{ag1} + I_{m1}i_{gb}\frac{v_2}{I_{m2}} + I_{m1}\omega_2\frac{\mathrm{d}i_{gb}}{\mathrm{d}t} \tag{5.60}$$

with $\widetilde{T}_{ag1}$ being the new virtual control. Replacing $T_{ag1,ref.}$ in (5.59) by (5.60) gives

$$\frac{\mathrm{d}^2\Delta\varphi}{\mathrm{d}t^2} = -\frac{\widetilde{c}_s\Delta\varphi}{I_{m1}} + \frac{\widetilde{T}_{ag1}}{I_{m1}}, \tag{5.61}$$

which is exactly the dynamics of the mentioned undamped two-mass oscillator with the moment of inertia of the speed controlled machine tending to infinity. The natural angular frequency resulting from Equation (5.61) is $\omega_0 = \sqrt{\widetilde{c}_s/I_{m1}}$, which is lower than the natural angular frequency of the coupled dynamic system given in Equation (5.22); this is due to feedforward disturbance torque compensation at the load drive.

Finally, also the reference air-gap torque for machine *M1* can be rewritten for clarity

$$T_{ag1,ref.} = v_1 + \underbrace{I_{m1}\frac{\mathrm{d}\left(i_{gb}\omega_2\right)}{\mathrm{d}t}}_{=:T_{accel.}} - \underbrace{\widetilde{d}_{s,des.}\left(\omega_1 - i_{gb}\omega_2\right)}_{=:T_{damp.}}. \tag{5.62}$$

This desired air-gap torque $T_{ag1,ref.}$ is composed of the virtual control input v_1, the damping torque $T_{damp.}$ to reduce torsional vibrations, and the decoupling torque $T_{accel.}$ for accelerating the moment of inertia I_{m1} when the angular velocity of the input drive must be changed. This is necessary when the angular velocity of the load drive is modified or when a gear shift occurs and therefore the transmission ratio changes. The only remaining tuning parameter is $\widetilde{d}_{s,des.}$.

The goals at the beginning of the decoupling and feedback linearisation process were to decouple the speed and torque control loops and to damp torsional vibrations. In spite of an integrated controller design process where both goals were handled at once, the results given by Equation (5.62) and Equation (5.52) can again be divided into these two measures. Equation (5.52) is exclusively responsible for decoupling; in Equation (5.62) $T_{accel.}$ is used for decoupling while $T_{damp.}$ provides for vibration damping. The functionality of these measures is even independent from each other; the decoupling components can be activated without active damping if no additional damping is required and the damping torque can be used without decoupling if desired. This property can simplify controller testing in practice as these two measures can be implemented and examined separately.

In Figure 5.7 the resulting control scheme is presented. The decoupling structure was designed in such a way that only measurable signals are required; therefore, no state observer is needed. Some of the calculations in the decoupling network are based on i_{gb}; for this reason, the transmission ratio must be known for control. Load torque compensation used to improve speed control is independent of the transmission ratio; however, for vibration damping and for decoupling the torque controlled input drive, the transmission ratio is essential. If the test bed automation system actuates the transmission, the current gear and therefore also the transmission ratio i_{gb} are known. This testing situation was discussed in Section 3.10. If the gear shifts are performed automatically, i_{gb} can be estimated based on gearbox input and output speed. During the gear shifts the transmission ratio must be changed. The precise timing of this process can be interpreted as a tuning parameter for control. The decoupling torque $T_{accel.}$ is non-zero if the term $i_{gb}\omega_2$ changes. This can easily be handled if a constant gear is assumed; ${}^{\mathrm{d}i_{gb}}/_{\mathrm{d}t}$ is then zero and the decoupling torque is only active when the angular velocity ω_2 of the load drive is changed. If a gear shift occurs, the transmission ratio changes; since the speed of the load drive is typically kept constant during the gear shift, the angular velocity of the input drive must change. In this situation, the term $I_{m1}\omega_2{}^{\mathrm{d}i_{gb}}/_{\mathrm{d}t}$ is exactly the torque required to accelerate the input drive with rotor inertia I_{m1} to the angular velocity suitable for the next gear. A combination of these two situations is feasible as well.

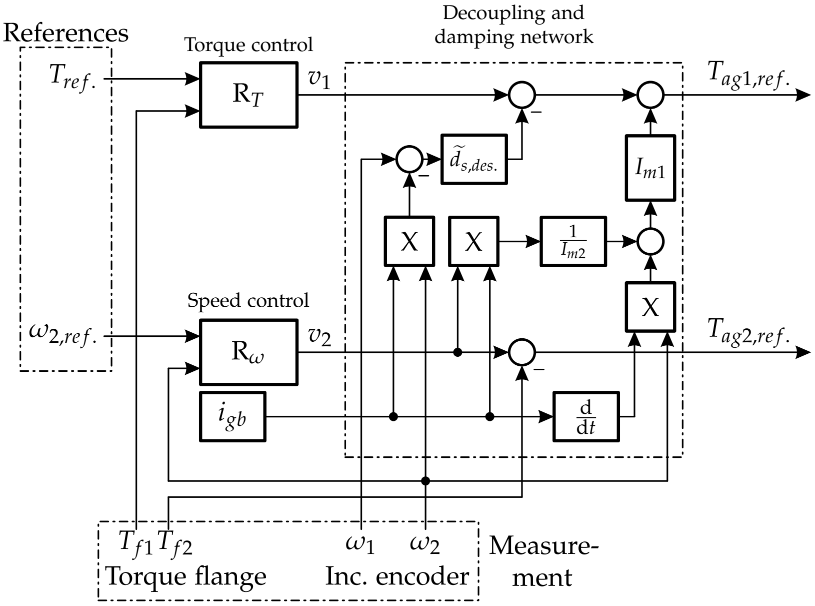
References
$T_{ref.}$
$\omega_{2,ref.}$
Torque control
R_T
v_1
Speed control
R_ω
v_2
i_{gb}
Decoupling and damping network
$\tilde{d}_{s,des.}$
X
X
X
$\frac{1}{I_{m2}}$
I_{m1}
$\frac{\mathrm{d}}{\mathrm{d}t}$
−
−
−
$T_{ag1,ref.}$
$T_{ag2,ref.}$
T_{f1} T_{f2}
Torque flange
ω_1 ω_2
Inc. encoder
Measurement

Figure 5.7: Proposed control structure for a test bed for transmissions.

5.4.2 Three Machine Configuration

Also for three machine testing configurations shown in Figure 3.1 and Figure 3.24 used to test differential gears a decoupling controller is designed following the approach used for the test system for transmissions. Here the most general situation including the adapter gearboxes is discussed; a controller for the reduced problem without those gearboxes can then be derived easily from this controller for the extended test set-up. Controller design is based on the reduced mathematical model discussed in Section 5.3.2 where the system dynamics were determined as

$$\frac{\mathrm{d}\omega_1}{\mathrm{d}t} = -\frac{\widetilde{c}_s \Delta\varphi}{I_1} + \frac{T_{ag1,ref.}}{I_1} \tag{5.63a}$$

$$\frac{\mathrm{d}\omega_2}{\mathrm{d}t} = \frac{i'_d \widetilde{c}_s \Delta\varphi}{2I_2} - \frac{T'_{dsl}}{2I_2} + \frac{T_{ag2,ref.}}{I_2} \tag{5.63b}$$

$$\frac{\mathrm{d}\omega_3}{\mathrm{d}t} = \frac{i'_d \widetilde{c}_s \Delta\varphi}{2I_3} + \frac{T'_{dsl}}{2I_3} + \frac{T_{ag3,ref.}}{I_3} \tag{5.63c}$$

$$\frac{\mathrm{d}\Delta\varphi}{\mathrm{d}t} = \omega_1 - \frac{i'_d \omega_2}{2} - \frac{i'_d \omega_3}{2}. \tag{5.63d}$$

For this testing situation the first system output y_1 is the total output torque of the differential gear

$$y_1 = T_{sum} = i_{gb2} i'_d \widetilde{c}_s \Delta\varphi; \tag{5.64}$$

the remaining outputs are the angular velocities of the load drives $M2$ and $M3$

$$y_2 = \omega_2 \tag{5.65a}$$

$$y_3 = \omega_3. \tag{5.65b}$$

In contrast to before, this dynamic system is non-linear because of the friction torque T'_{dsl}. Nevertheless, the relative degrees are determined starting with the differential gear's total output torque $T_{sum} = y_1$ as given by Equation (5.64). The first derivative with respect to time is

$$\frac{\mathrm{d}y_1}{\mathrm{d}t} = i_{gb2} i'_d \widetilde{c}_s \left(\omega_1 - i'_d \frac{\omega_2 + \omega_3}{2} \right). \tag{5.66}$$

Since $\mathrm{d}y_1/\mathrm{d}t$ does not depend on a control input, the second time derivative

$$\frac{\mathrm{d}^2 y_1}{\mathrm{d}t^2} = i_{gb2} i'_d \widetilde{c}_s \left(\frac{\mathrm{d}\omega_1}{\mathrm{d}t} - i'_d \frac{\frac{\mathrm{d}\omega_2}{\mathrm{d}t} + \frac{\mathrm{d}\omega_3}{\mathrm{d}t}}{2} \right) \tag{5.67}$$

is determined. According to Equation (5.63), $\mathrm{d}^2 y_1/\mathrm{d}t^2$ definitely depends on the control inputs meaning that the relative degree of the output variable y_1 is $\delta_1 = 2$.

The second system output is the angular velocity of the electric motor *M2*, i.e. $y_2 = \omega_2$. According to Equation (5.63b), the first derivative with respect to time is

$$\frac{\mathrm{d}y_2}{\mathrm{d}t} = \frac{1}{I_2}\left(T_{ag2,ref.} + \frac{i'_d}{2}\widetilde{c}_s\Delta\varphi - \frac{T'_{dsl}}{2}\right). \tag{5.68}$$

Since $\mathrm{d}y_2/\mathrm{d}t$ already depends on the system input $T_{ag2,ref.}$, the relative degree of y_2 is $\delta_2 = 1$. As the third plant output is the angular velocity of *M3* and according to (5.63b) and (5.63c) the dynamics are similar to y_2, the corresponding relative degree is also $\delta_3 = 1$.

Remark 2 *The sum of relative degrees is four, which is equal to the number of state variables in System* (5.63). *For this reason, the dynamic system described by Equation* (5.63) *with outputs as defined in Equation* (5.64) *and Equation* (5.65) *has no internal dynamics.*

The decoupling matrix $\overline{\mathbf{D}}(\mathbf{x})$ is again independent of the state vector $\mathbf{x}$:

$$\overline{\mathbf{D}} = \begin{pmatrix} \frac{i_{gb2}i'_d\widetilde{c}_s}{I_1} & -\frac{i_{gb2}i'^2_d\widetilde{c}_s}{2I_2} & -\frac{i_{gb2}i'^2_d\widetilde{c}_s}{2I_3} \\ 0 & \frac{1}{I_2} & 0 \\ 0 & 0 & \frac{1}{I_3} \end{pmatrix} \tag{5.69}$$

Since as before $\overline{\mathbf{D}}$ is clearly regular, the decoupling network can be determined; due to the special form of $\overline{\mathbf{D}}$, computing the inverse is unnecessary and a step-by-step calculation of the manipulated variables is possible. If the dynamics for the controlled variables y_2 and y_3 are chosen as

$$G_2(s) := \frac{y_2(s)}{v_2(s)} = \frac{1}{I_{m2}s} \tag{5.70}$$

$$G_3(s) := \frac{y_3(s)}{v_3(s)} = \frac{1}{I_{m3}s}, \tag{5.71}$$

the desired air-gap torques for machines *M2* and *M3* are

$$T_{ag2,ref.} = v_2 + \underbrace{\frac{I_{gb2}}{I_{m2}}v_2}_{T_{accel.,gb2}} - \underbrace{\left(\frac{i'_d}{2}\widetilde{c}_s\Delta\varphi - \frac{T'_{dsl}}{2}\right)}_{T'_{do1}} \tag{5.72}$$

$$T_{ag3,ref.} = v_3 + \underbrace{\frac{I_{gb3}}{I_{m3}}v_3}_{T_{accel.,gb3}} - \underbrace{\left(\frac{i'_d}{2}\widetilde{c}_s\Delta\varphi + \frac{T'_{dsl}}{2}\right)}_{T'_{do2}}. \tag{5.73}$$

These desired air-gap torques $T_{ag2,ref.}$ and $T_{ag3,ref.}$ are composed of three parts; the first component is the virtual control input, which will be the output of the speed controller. Additionally, the output torque of the differential gear scaled by the inverse of the transmission ratio i_{gb2} and the torque required to accelerate the moment of inertia of the adapter gearboxes have to be compensated. Since according to Equation (5.13b) and Equation (5.13c) this is exactly the measured shaft torque, no load torque estimation is necessary and the calculation formula for the manipulated variables $T_{ag2,ref.}$ and $T_{ag3,ref.}$ can be simplified:

$$T_{ag2,ref.} = v_2 - T_{f2} \tag{5.74}$$

$$T_{ag3,ref.} = v_3 - T_{f3} \tag{5.75}$$

This is the same result as in Section 5.4.1 although the testing situation is completely different. Consequently, the feedforward load torque compensation scheme based on the shaft torque measurement can universally be applied when in spite of strong disturbances excellent speed control performance is desired. An important requirement for using this strategy however is a high-performance inverter system.

If the dynamics of the remaining system output y_1 is chosen as

$$G_1(s) := \frac{y_1(s)}{v_1(s)} = \frac{\tilde{c}_s}{I_1 s^2 + \tilde{d}_{s,des.} s + \tilde{c}_s}, \tag{5.76}$$

the desired air-gap torque of the electric machine *M1* is

$$T_{ag1,ref.} = \frac{v_1}{i_{gb2} i'_d} - \tilde{d}_{s,des.} \left(\omega_1 - i'_d \frac{\omega_2 + \omega_3}{2} \right) + \frac{I_1 i'_d}{2} \left(\frac{\mathrm{d}\omega_2}{\mathrm{d}t} + \frac{\mathrm{d}\omega_3}{\mathrm{d}t} \right). \tag{5.77}$$

Finally, using the dynamics for the outputs y_2 and y_3 as specified in Equation (5.70) and Equation (5.71) avoids the determination of the angular acceleration of the drives *M2* and *M3* to be needed and we get

$$T_{ag1,ref.} = \frac{v_1}{i_{gb2} i'_d} - \underbrace{\tilde{d}_{s,des.} \left(\omega_1 - i'_d \frac{\omega_2 + \omega_3}{2} \right)}_{=: T_{damp.}} + \underbrace{I_1 \frac{i'_d}{2} \left(\frac{v_2}{I_{m2}} + \frac{v_3}{I_{m3}} \right)}_{=: T_{accel.}}. \tag{5.78}$$

Thus, the desired air-gap torque $T_{ag1,ref.}$ is composed of the virtual control input v_1, which is scaled to obtain unity gain, the decoupling torque $T_{accel.}$ for accelerating the moment of inertia I_1 when the angular velocities are changed, and the damping torque $T_{damp.}$ to reduce torsional vibrations. The friction torque T'_{dsl} is only changing the torque distribution to the two outputs of the differential gear and consequently does not affect the total testing torque. Also this result is very close to the findings of Section 5.4.1 for the two machine testing configuration.

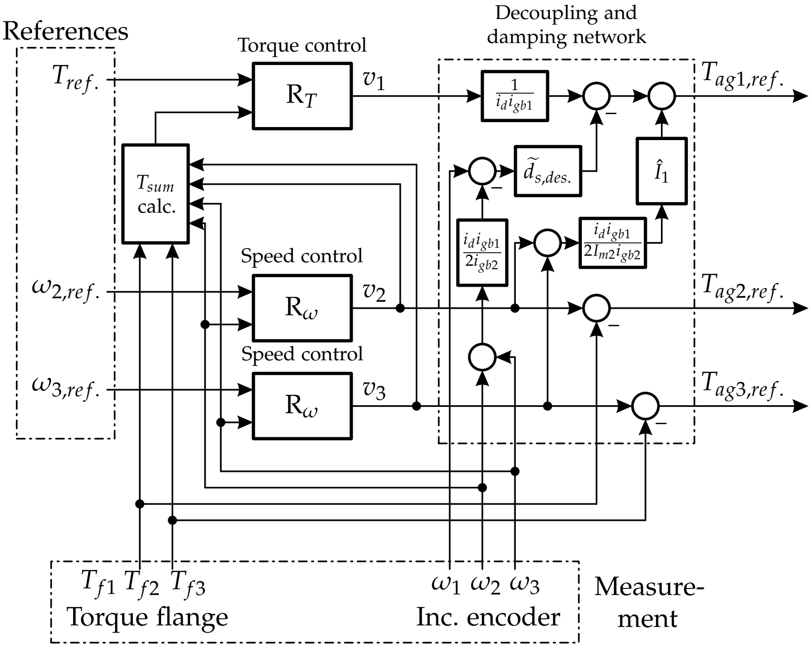
References
$T_{ref.}$
$\omega_{2,ref.}$
$\omega_{3,ref.}$
Torque control
R_T
v_1
T_{sum} calc.
Speed control
R_ω
v_2
Speed control
R_ω
v_3
Decoupling and damping network
$\frac{1}{i_d i_{gb1}}$
$\widetilde{d}_{s,des.}$
$\hat{I}_1$
$\frac{i_d i_{gb1}}{2 i_{gb2}}$
$\frac{i_d i_{gb1}}{2 I_{m2} i_{gb2}}$
$T_{ag1,ref.}$
$T_{ag2,ref.}$
$T_{ag3,ref.}$
T_{f1} T_{f2} T_{f3}
Torque flange
ω_1 ω_2 ω_3
Inc. encoder
Measurement

Figure 5.8: Proposed control structure for a test bed for differential gears with adapter gearboxes and symmetric mechanical structure implying $I_{m2} = I_{m3}$, $c_{s2} = c_{s3}$, and $i_{gb2} = i_{gb3}$.

In Figure 5.8 the resulting control scheme is presented for identical rotor inertias of machines *M2* and *M3* ($I_{m2} = I_{m3}$). The decoupling structure was designed in such a way that only measurable signals are used; then no state observer is needed. In commercial testing situations the moments of inertia of the three adapter gearboxes are potentially unknown, but all three desired air-gap torques initially depend on at least one of these inertias. This does not cause problems for machines *M2* and *M3* because the load torque is measured at the shafts connecting induction machine and gearbox and Equation (5.74) and Equation (5.75) can be used instead of Equations (5.72) and (5.73). However, the acceleration torque $T_{accel.}$ in Equation (5.78) depends on I_1, which is the sum of the moments of inertia of gearbox 1 and electric machine *M1*. Therefore, Equation (5.78) cannot be used directly. The easiest alternative is to replace the total moment of inertia I_1 by the induction machine's moment of inertia I_{m1}. Of course, this will result in imperfect decoupling when there is a change in rotational speed. Another possibility is to replace the system parameter I_1 in Equation (5.78) by the new controller parameter $\hat{I}_1$ and to manually tune it in experiments until a change in rotational speed no longer affects the total testing torque. In Figure 5.8 the approach with the new controller parameter $\hat{I}_1$ is shown.

If a testing configuration without adapter gearboxes is considered, only minor modifications are required: the transmission ratios i_{gb1} and i_{gb2} must be set to one and $\hat{I}_1$ can be replaced by the input drive's rotor inertia I_{m1}.

5.4.3 Selecting the Active Damping Parameter

An important tuning parameter in Equation (5.62) and Equation (5.78) is the desired damping coefficient $\widetilde{d}_{s,des.}$ in the torque transfer function. To analyse the effect of this controller parameter, the poles of the torque transfer function $G_1(s)$ defined in Equation (5.76) for the three machine configuration are determined[3]

$$s_{1,2} = -\frac{\widetilde{d}_{s,des.}}{2I_1} \pm j\sqrt{\frac{\widetilde{c}_s}{I_1} - \left(\frac{\widetilde{d}_{s,des.}}{2I_1}\right)^2}. \tag{5.79}$$

Due to the decoupling network, the pole locations are not affected by the moments of inertia and the speed control parameters of the load drives. If the denominator polynomial $p(s)$ of the torque transfer function is written as

$$p(s) = s^2 + 2\zeta\omega_0 s + \omega_0^2, \tag{5.80}$$

with ζ being the damping ratio and ω_0 being the undamped natural angular frequency, the dependency of ζ on the controller parameter $\widetilde{d}_{s,des.}$

$$\zeta = \frac{\widetilde{d}_{s,des.}}{2\sqrt{\widetilde{c}_s I_1}} \tag{5.81}$$

can easily be specified.

With $\widetilde{d}_{s,des.}$ equal to zero the two poles will be imaginary; ζ is then equal to zero resulting in undamped torque oscillations. If $\widetilde{d}_{s,des.}$ is increased, the damping ratio ζ rises, which leads to under-damped system behaviour. When $\widetilde{d}_{s,des.}$ is equal to $2\sqrt{\widetilde{c}_s I_1}$, the two previously conjugate-complex poles become a double real pole and ζ is then equal to one meaning that the system is critically damped and that resonance oscillations vanish. If $\widetilde{d}_{s,des.}$ is increased further, the system becomes over-damped leading to slower torque dynamics than with critical damping. These effects are shown in Figure 5.9 and will be further investigated in simulation later.

5.5 Speed Control

In addition to the decoupling network including active vibration damping, feedback speed controllers R_ω for the load drives have to be added to the control scheme.

---

[3] The torque transfer function for the two machine configuration is similar: only the definition of the equivalent torsional stiffness parameter is different and I_1 must be replaced by the rotor inertia of the input drive I_{m1}.

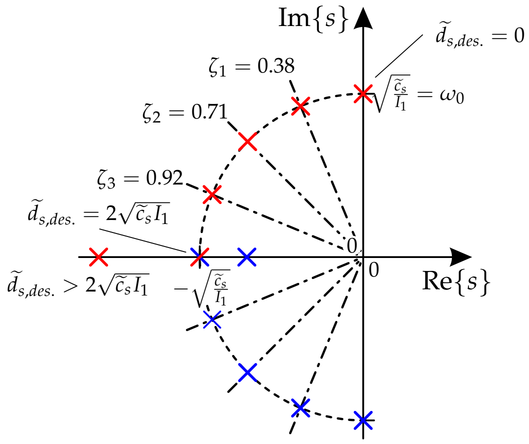
Im{s}
$\tilde{d}_{s,des.} = 0$
$\zeta_1 = 0.38$
$\sqrt{\frac{\tilde{c}_s}{I_1}} = \omega_0$
$\zeta_2 = 0.71$
$\zeta_3 = 0.92$
$\tilde{d}_{s,des.} = 2\sqrt{\tilde{c}_s I_1}$
0
0
Re{s}
$\tilde{d}_{s,des.} > 2\sqrt{\tilde{c}_s I_1}$
$-\sqrt{\frac{\tilde{c}_s}{I_1}}$

Figure 5.9: Poles and damping ratio of the torque transfer function depending on the controller parameter $\tilde{d}_{s,des.}$.

The nominal plant to control is given by the transfer function

$$G_2(s) = \frac{\omega_2(s)}{v_2(s)} = \frac{1}{I_{m2}s} \tag{5.82}$$

that was specified in the design of the decoupling network. This nominal transfer function originates from a significantly reduced system model. In practice, torque disturbances $T_{dist.}(s)$ due to imperfect decoupling, friction losses, and air-gap torque deviations such as torque harmonics [54] or stationary torque estimation errors [51] have to be expected:

$$\omega_2(s) = \frac{1}{I_{m2}s}\left[v_2\left(s\right) - T_{dist.}\left(s\right)\right] \tag{5.83}$$

Many different controller types are capable of controlling this plant. In the following sections, two approaches are further discussed; these proved to provide the desired control performance and can easily be applied in practice since parameter tuning is rather simple. Other controllers based on *sliding mode control*, see e.g. [136], such as the super twisting controller were analysed in simulation. If chosen appropriately, these can guarantee finite time convergence, but for this speed control application no improvement regarding performance could be achieved. Because of the decoupling scheme, disturbances for this control loop are significantly reduced and therefore the great robustness properties of the sliding mode controllers are not that relevant.

5.5.1 PI Control

To be able to eliminate steady-state tracking errors caused by torque disturbances, a PI controller can be used:

$$v_2(s) = k_{p2}\left[\omega_{2,ref.}\left(s\right) - \omega_2\left(s\right)\right] + \frac{k_{i2}}{s}\left[\omega_{2,ref.}\left(s\right) - \omega_2\left(s\right)\right] \tag{5.84}$$

This speed control approach is typically available on every commercial inverter system and therefore widely used in industrial applications [12, 137]. Since feedforward load torque compensation is applied, controller design can be performed easily e.g. by using loop shaping [138] without knowing any system parameters except for the electric machine's rotor inertia. Due to limited air-gap torque, usually additional *anti-windup (AW)* measures are necessary; in industrial practice often the conditioning technique proposed by Hanus is applied [139].

5.5.2 P Control with Disturbance Observer

An alternative speed control concept is based on using a P controller with an additional *disturbance observer* [51]. For observer design the plant is given in a state-space representation

$$I_{m2}\frac{\mathrm{d}\omega_2}{\mathrm{d}t} = v_2 - T_{dist.}; \tag{5.85}$$

the disturbance torque $T_{dist.}$ is unknown, but assumed to be constant ($\mathrm{d}T_{dist.}/\mathrm{d}t = 0$). Then the differential equations for the observer are

$$I_{m2}\frac{\mathrm{d}\hat{\omega}_2}{\mathrm{d}t} = v_2 - \hat{T}_{dist.} \tag{5.86a}$$

$$\frac{\mathrm{d}\hat{T}_{dist.}}{\mathrm{d}t} = 0, \tag{5.86b}$$

where $\hat{\omega}_2$ and $\hat{T}_{dist.}$ are estimates for angular velocity respectively disturbance torque. If the dynamics of the disturbance estimate $\hat{T}_{dist.}$ are chosen as

$$\frac{\mathrm{d}\hat{T}_{dist.}}{\mathrm{d}t} = I_{m2}\hat{b}\left(\frac{\mathrm{d}\hat{\omega}_2}{\mathrm{d}t} - \frac{\mathrm{d}\omega_2}{\mathrm{d}t}\right), \tag{5.87}$$

the disturbance observer results:

$$\frac{\mathrm{d}\hat{T}_{dist.}}{\mathrm{d}t} = \hat{b}\left(v_2 - I_{m2}\frac{\mathrm{d}\omega_2}{\mathrm{d}t} - \hat{T}_{dist.}\right) \tag{5.88}$$

By the use of the parameter $\hat{b} > 0$, the dynamics of this differential equation and of the estimation error $e_{T_{dist.}} := \hat{T}_{dist.} - T_{dist.}$ can be specified. To avoid the need of determining $\mathrm{d}\omega_2/\mathrm{d}t$, an auxiliary variable z is introduced

$$z := \hat{b}I_{m2}\omega_2 + \hat{T}_{dist.}. \tag{5.89}$$

The dynamics of this variable now do not explicitly depend on the angular acceleration $\mathrm{d}\omega_2/\mathrm{d}t$

$$\frac{\mathrm{d}z}{\mathrm{d}t} = -\hat{b}z + \hat{b}\left(v_2 + \hat{b}I_{m2}\omega_2\right) \tag{5.90}$$

and can thus be implemented easily. The disturbance torque estimate can be calculated based on z and ω_2

$$\hat{T}_{dist.} = z - \hat{b} I_{m2} \omega_2. \tag{5.91}$$

If the controller is chosen as

$$v_2 = k_{p2} \left(\omega_{2,ref.} - \omega_2 \right) + \hat{T}_{dist.} \tag{5.92}$$

and the disturbance observer converged ($\hat{T}_{dist.} = T_{dist.}$), the rotational speed dynamics are

$$I_{m2} \frac{\mathrm{d}\omega_2}{\mathrm{d}t} = k_{p2} \left(\omega_{2,ref.} - \omega_2 \right). \tag{5.93}$$

As for the classic PI controller, also with this approach two controller parameters must be tuned. By selecting the proportional gain $k_{p2} > 0$, the dynamics of the speed control loop can be specified while the dynamics of the disturbance observer are given by the choice of $\hat{b}$.

5.6 Torque Control

To make sure that the testing torque is equal to its reference value $T_{ref.}$ in steady-state, a torque controller R_T must be added. The nominal plant is given by the transfer function

$$G_1(s) = \frac{\widetilde{c}_s}{I_1 s^2 + \widetilde{d}_{s,des.} s + \widetilde{c}_s} \tag{5.94}$$

that was specified in the design of the decoupling network. The DC gain of the Torque transfer function (5.94) was chosen to be one. Furthermore, for $\widetilde{d}_{s,des.} > 0$ this system is BIBO stable; thus, the reference torque might be reached even without feedback torque controller. But as for the speed control plant, here the real plant will deviate from this nominal plant description as well. Because of losses and possibly uncertain induction machine parameters [52], a feedback torque controller is usually necessary to be able to guarantee a vanishing steady-state torque error. The torque controller's main objective is to fulfil the steady-state requirements; the dynamic behaviour of the torque control loop can also be adjusted by the controller parameter $\widetilde{d}_{s,des.}$. Basically, many control approaches are applicable for this control problem. In practice, PI controllers with additional feedforward control, as will be briefly discussed in Section 5.6.1, are widely used. However, in simulation modern sliding mode control was analysed too. These experiments showed that their high controller gain for small tracking errors is problematic. The torque transfer function does not describe the oscillatory behaviour of the plant exactly. In reality, also higher eigenfrequencies are relevant. With high controller gains these torsional vibration modes can easily be excited.

A problem sometimes related to torque control is the choice of the measurement signals used for feedback control. For test systems without any additional gearboxes the flange torques measured at the electric drives are typically used directly as feedback signals because the torques at the UUT are close to these measured torques. However, according to Figure 3.1, on a test bed with adapter gearboxes there are no torque sensors located directly at the UUT. If such a test system for differential gears is considered and the objective is to control the differential's total output torque, this quantity is unknown and must be estimated. An easy way to overcome this problem is to use again the data from the torque measuring flanges at the electric drives $M2$ and $M3$ and to scale them by the transmission ratio of the output gearboxes $i_{gb2} = i_{gb3}$:

$$T_{sum} = i_{gb2}\left(T_{f2} + T_{f3}\right) \tag{5.95}$$

Because of possible losses in the gearboxes, this is not a perfect solution, but these loss torques could be measured before the test-run and then compensated by adding the loss torque for gearbox 2 $T_{l,gb2}$ and gearbox 3 $T_{l,gb3}$; these are often modelled as functions of angular velocity:

$$T_{sum} = i_{gb2}\left(T_{f2} + T_{l,gb2}(\omega_2) + T_{f3} + T_{l,gb3}(\omega_3)\right) \tag{5.96}$$

Additionally, when there is a change in rotational speed, the moments of inertia of the gearboxes at the differential gear's outputs are causing a torque error on account of the torque needed to accelerate or decelerate. But these torques for gearbox 2 $T_{accel.,gb2}$ and gearbox 3 $T_{accel.,gb3}$ could also be compensated:

$$T_{sum} = i_{gb2}\left(T_{f2} + T_{l,gb2}(\omega_2) + T_{accel.,gb2} + T_{f3} + T_{l,gb3}(\omega_3) + T_{accel.,gb3}\right) \tag{5.97}$$

If the acceleration torques are replaced according to Equation (5.72) and Equation (5.73),

$$T_{sum} = i_{gb2}\left(T_{f2} + T_{l,gb2}(\omega_2) + \frac{I_{gb2}}{I_{m2}}v_2 + T_{f3} + T_{l,gb3}(\omega_3) + \frac{I_{gb3}}{I_{m3}}v_3\right) \tag{5.98}$$

results. Both compensations could also be considered by modifying the reference torque $T_{ref.}$ appropriately.

5.6.1 PI Control

To make sure that torque control is simple and easy to tune for test bed operators, a PI controller with additional feedforward control action is often used in practice:

$$v_1(s) = k_{ff1}T_{ref.}(s) + k_{p1}\left[T_{ref.}(s) - T_{sum}(s)\right] + \frac{k_{i1}}{s}\left[T_{ref.}(s) - T_{sum}(s)\right] \tag{5.99}$$

Since the main objective is to guarantee vanishing steady-state tracking error, for some applications an integrating controller including feedforward control has proven to be sufficient; k_{p1} is then set to zero. As for the speed controller, controller windup can be avoided by applying the conditioning technique [139] or by limiting the integrator if an integrating controller without proportional action is applied.

5.7 Closed-loop System Analysis

In this section some considerations regarding the stability of the closed-loop system are conducted. By the use of the state vector

$$\mathbf{x} := \begin{bmatrix} \omega_1 & \omega_2 & \Delta\varphi \end{bmatrix}^{\mathrm{T}}, \tag{5.100}$$

a state-space representation of the test system for transmissions can be given:[4]

$$\frac{\mathrm{d}\mathbf{x}}{\mathrm{d}t} = \begin{pmatrix} 0 & 0 & -\frac{\widetilde{c}_s}{I_{m1}} \\ 0 & 0 & \frac{i_{gb}\widetilde{c}_s}{I_{m2}} \\ 1 & -i_{gb} & 0 \end{pmatrix} \mathbf{x} + \begin{pmatrix} \frac{1}{I_{m1}} & 0 \\ 0 & \frac{1}{I_{m2}} \\ 0 & 0 \end{pmatrix} \begin{bmatrix} T_{ag1,ref.} \\ T_{ag2,ref.} \end{bmatrix} \tag{5.101}$$

As shown in Section 5.3.3, due to the lack of internal damping, this system is not asymptotically stable. In a first step, the speed control loop is closed by applying a PI controller

$$T_{ag2,ref.}(s) = \left(k_{p2} + \frac{k_{i2}}{s}\right) \left[\omega_{2,ref.}(s) - \omega_2(s)\right] - \gamma_\omega i_{gb} \widetilde{c}_s \Delta\varphi(s), \tag{5.102}$$

where with γ_ω feedforward load torque compensation is adjusted. Setting γ_ω to zero disables the decoupling measure; for $\gamma_\omega = 1$ decoupling is effective. With the extended state vector

$$\mathbf{x}_1 := \begin{bmatrix} \omega_1 & \omega_2 & \Delta\varphi & \lambda_{\omega_2} \end{bmatrix}^{\mathrm{T}}, \tag{5.103}$$

where λ_{ω_2} is an internal controller state, the LTI state-space model of this closed-loop system is

$$\frac{\mathrm{d}\mathbf{x}_1}{\mathrm{d}t} = \underbrace{\begin{pmatrix} 0 & 0 & -\frac{\widetilde{c}_s}{I_{m1}} & 0 \\ 0 & -\frac{k_{p2}}{I_{m2}} & \frac{(1-\gamma_\omega) i_{gb}\widetilde{c}_s}{I_{m2}} & \frac{1}{I_{m2}} \\ 1 & -i_{gb} & 0 & 0 \\ 0 & -k_{i2} & 0 & 0 \end{pmatrix}}_{=:\mathbf{A}_1} \mathbf{x}_1 + \begin{pmatrix} \frac{1}{I_{m1}} & 0 \\ 0 & \frac{k_{p2}}{I_{m2}} \\ 0 & 0 \\ 0 & k_{i2} \end{pmatrix} \begin{bmatrix} T_{ag1,ref.} \\ \omega_{2,ref.} \end{bmatrix}. \tag{5.104}$$

---

[4] For clarity only the test system for transmissions is discussed in this section; test beds for differential gears can be treated similarly.

For stability analysis the characteristic polynomial of $\mathbf{A}_1$ is determined:

$$\Delta_1(s) = s^4 + \frac{k_{p2}}{I_{m2}} s^3 + \left(\frac{k_{i2}}{I_{m2}} + \frac{\widetilde{c}_s}{I_{m1}} + \frac{(1-\gamma_\omega)\, i_{gb}^2 \widetilde{c}_s}{I_{m2}} \right) s^2 + \frac{\widetilde{c}_s k_{p2}}{I_{m1} I_{m2}} s + \frac{\widetilde{c}_s k_{i2}}{I_{m1} I_{m2}} \quad (5.105)$$

If the conventional control is used ($\gamma_\omega = 0$), it can be proven by the Liénard-Chipart criterion that $\Delta_1(s)$ is a *Hurwitz stable* polynomial for $k_{i2} > 0$[5] and $k_{p2} > 0$ and that System (5.104) is asymptotically stable [138].[6] For this situation the speed control parameters could be used to maximise vibration damping. However, if decoupling is effective ($\gamma_\omega = 1$), the characteristic polynomial can be written as

$$\Delta_1(s) = \left(s^2 + \frac{\widetilde{c}_s}{I_{m1}} \right) \left(s^2 + \frac{k_{p2}}{I_{m2}} s + \frac{k_{i2}}{I_{m2}} \right). \quad (5.106)$$

For this case $\Delta_1(s)$ is not Hurwitz stable as two zeros are on the imaginary axis. These are not affected by the speed control parameters; therefore, the speed controller cannot improve vibration damping properties. For this reason, the active damping measure is essential to be able to guarantee stability. Since a constant gear is assumed, the reference air-gap torque for *M1* is

$$T_{ag1,ref.} = v_1 - \widetilde{d}_{s,des.} \left(\omega_1 - i_{gb} \omega_2 \right) + \gamma_T i_{gb} I_{m1} \frac{v_2}{I_{m2}}. \quad (5.107)$$

With γ_T the decoupling torque can be enabled ($\gamma_T = 1$) respectively disabled ($\gamma_T = 0$). The state-space model for the closed-loop system is

$$\frac{\mathrm{d}\mathbf{x}_1}{\mathrm{d}t} = \underbrace{\begin{pmatrix} -\frac{\widetilde{d}_{s,des.}}{I_{m1}} & \frac{i_{gb}\widetilde{d}_{s,des.}}{I_{m1}} - \frac{\gamma_T i_{gb} k_{p2}}{I_{m2}} & \frac{\gamma_T (1-\gamma_\omega) i_{gb}^2 \widetilde{c}_s}{I_{m2}} - \frac{\widetilde{c}_s}{I_{m1}} & \frac{\gamma_T i_{gb}}{I_{m2}} \\ 0 & -\frac{k_{p2}}{I_{m2}} & \frac{(1-\gamma_\omega) i_{gb} \widetilde{c}_s}{I_{m2}} & \frac{1}{I_{m2}} \\ 1 & -i_{gb} & 0 & 0 \\ 0 & -k_{i2} & 0 & 0 \end{pmatrix}}_{=:\widetilde{\mathbf{A}}_1} \mathbf{x}_1 + \begin{pmatrix} \frac{1}{I_{m1}} & \frac{\gamma_T i_{gb} k_{p2}}{I_{m2}} \\ 0 & \frac{k_{p2}}{I_{m2}} \\ 0 & 0 \\ 0 & k_{i2} \end{pmatrix} \begin{bmatrix} v_1 \\ \omega_{2,ref.} \end{bmatrix}. \quad (5.108)$$

---

[5] Selecting k_{i2} strictly positive is required to stabilise the internal controller state λ_{ω_2}; if k_{i2} was zero, this system state would not be needed and the system order could be reduced by one. As a PI controller was selected to control rotational speed, zero integral gain is only theoretically relevant.

[6] Positive system parameters I_{m1}, I_{m2}, and $\widetilde{c}_s$ are presumed here and henceforth; furthermore, the transmission ratio i_{gb} is assumed to be constant and non-zero.

If decoupling is active either for the speed controlled drive ($\gamma_\omega = 1$) or for the torque controlled drive ($\gamma_T = 1$),[7] the characteristic polynomial of $\widetilde{\mathbf{A}}_1$ is

$$\widetilde{\Delta}_1(s) = \left(s^2 + \frac{\widetilde{d}_{s,des.}}{I_{m1}}s + \frac{\widetilde{c}_s}{I_{m1}}\right)\underbrace{\left(s^2 + \frac{k_{p2}}{I_{m2}}s + \frac{k_{i2}}{I_{m2}}\right)}_{=:\Delta_{\omega_2}(s)}. \tag{5.109}$$

This representation shows the big advantage of decoupling the control loops: the parameter $\widetilde{d}_{s,des.} > 0$ can now be used to stabilise the torque control loop, while with the speed control parameters $k_{p2} > 0$ and $k_{i2} > 0$ the dynamics of the speed control loop are adjusted. As proven by Equation (5.109), then asymptotic stability of the overall control system can be guaranteed as well. This representation can additionally be used to tune the speed control parameters by demanding the zeros of $\Delta_{\omega_2}(s)$ to be real:

$$0 < k_{i2} \leq \frac{k_{p2}^2}{4I_{m2}} \tag{5.110}$$

To stabilise the system is also possible by only using the active damping measure while decoupling is ineffective; however, proving stability analytically is more difficult as separating the characteristic polynomial into two parts, where only one part depends on the speed controller parameters, is not possible in general.

If furthermore the torque control loop is closed by a PI controller with additional feedforward control

$$v_1(s) = k_{ff1}T_{ref.}(s) + \left(k_{p1} + \frac{k_{i1}}{s}\right)\left[T_{ref.}(s) - T_{f1}(s)\right], \tag{5.111}$$

where $T_{f1} = \widetilde{c}_s\Delta\varphi$ is the torque at the input drive, the state vector must be extended by the internal controller state λ_T

$$\mathbf{x}_2 := \begin{bmatrix}\omega_1 & \omega_2 & \Delta\varphi & \lambda_{\omega_2} & \lambda_T\end{bmatrix}^\mathrm{T}. \tag{5.112}$$

---

[7] Only if decoupling is effective for both electric drives, the two control loops are completely decoupled. But one decoupling measure is sufficient to be able to factorise the characteristic polynomial according to Equation (5.109).

The state-space model for the closed-loop system is then given by

$$\frac{\mathrm{d}\mathbf{x}_2}{\mathrm{d}t} = \underbrace{\begin{pmatrix} -\frac{\widetilde{d}_{s,des.}}{I_{m1}} & \frac{i_{gb}\widetilde{d}_{s,des.}}{I_{m1}} - \frac{\gamma_T i_{gb} k_{p2}}{I_{m2}} & \frac{\gamma_T(1-\gamma_\omega) i_{gb}^2 \widetilde{c}_s}{I_{m2}} - \frac{\widetilde{c}_s}{I_{m1}} - \frac{k_{p1}\widetilde{c}_s}{I_{m1}} & \frac{\gamma_T i_{gb}}{I_{m2}} & \frac{1}{I_{m1}} \\ 0 & -\frac{k_{p2}}{I_{m2}} & \frac{(1-\gamma_\omega) i_{gb}\widetilde{c}_s}{I_{m2}} & \frac{1}{I_{m2}} & 0 \\ 1 & -i_{gb} & 0 & 0 & 0 \\ 0 & -k_{i2} & 0 & 0 & 0 \\ 0 & 0 & -k_{i1}\widetilde{c}_s & 0 & 0 \end{pmatrix}}_{=:\mathbf{A}_2} \mathbf{x}_2$$

$$+ \begin{pmatrix} \frac{k_{ff1}+k_{p1}}{I_{m1}} & \frac{\gamma_T i_{gb} k_{p2}}{I_{m2}} \\ 0 & \frac{k_{p2}}{I_{m2}} \\ 0 & 0 \\ 0 & k_{i2} \\ k_{i1} & 0 \end{pmatrix} \begin{bmatrix} T_{ref.} \\ \omega_{2,ref.} \end{bmatrix}. \tag{5.113}$$

If decoupling is active for at least one of the two electric drives, the characteristic polynomial of $\mathbf{A}_2$ is

$$\Delta_2(s) = \left[s^3 + \frac{\widetilde{d}_{s,des.}}{I_{m1}} s^2 + \left(\frac{\widetilde{c}_s}{I_{m1}} + \frac{k_{p1}\widetilde{c}_s}{I_{m1}} \right) s + \frac{k_{i1}\widetilde{c}_s}{I_{m1}} \right] \left(s^2 + \frac{k_{p2}}{I_{m2}} s + \frac{k_{i2}}{I_{m2}} \right). \tag{5.114}$$

It can easily be shown that this is a Hurwitz stable polynomial for positive speed controller parameters $k_{p2} > 0$ and $k_{i2} > 0$, a positive active damping parameter $\widetilde{d}_{s,des.} > 0$, and torque controller parameters subjected to

$$-1 < k_{p1} \tag{5.115a}$$

$$0 < k_{i1} < \frac{\widetilde{d}_{s,des.}}{I_{m1}} \left(1 + k_{p1}\right). \tag{5.115b}$$

These final results prove that because of the active damping measure ($\widetilde{d}_{s,des.} > 0$), the admissible range for the torque control parameters can be significantly increased. Theoretically, with $\widetilde{d}_{s,des.} = 0$ no stabilising PI torque controller with $k_{i2} > 0$ would exist. However, zero shaft damping and losses were assumed for modelling; in reality, the system would contain some internal damping. This allows to nevertheless find some stabilising torque control parameters. But as system damping is typically weak, it is usually challenging to identify suitable controller parameters without active damping.

5.8 Closed-loop Simulation Results

In this section the control concept based on feedback input–output decoupling, active vibration damping, and feedback controllers for rotational speed and torque presented before is tested in simulation. These simulations are performed by the use of the simulation models discussed in Chapter 3 and Chapter 4. Additionally, simulation studies with the conventional control structure typically used on these test beds as shown in Figure 5.10 for a test system for differential gears are carried out. These standard controllers are based on independently designed feedback controllers without any decoupling and active oscillation damping. Due to its simplicity, this control concept is widely used in practice, see e.g. [21]. Since the following simulation studies deal with two particular testing situations that were already discussed in Chapter 4, the parameters for the conventional control scheme could be taken directly from the test bed. As will be seen in the following figures, with this simple control strategy the attainable control performance is rather limited.

5.8.1 Control of a Test System for Differential Gears with Adapter Gearboxes

In this section results of numerical simulations of the test system for differentials with adapter gearboxes as shown in Figure 3.1 are presented. This testing configuration was chosen for these simulation studies since due to the additional gearboxes it is mechanically rather complex and thus challenging for control. Simulation results for a testing situation without adapter gearboxes are presented in Chapter 7 in the context of handling constraints. At first, the proposed control concept as

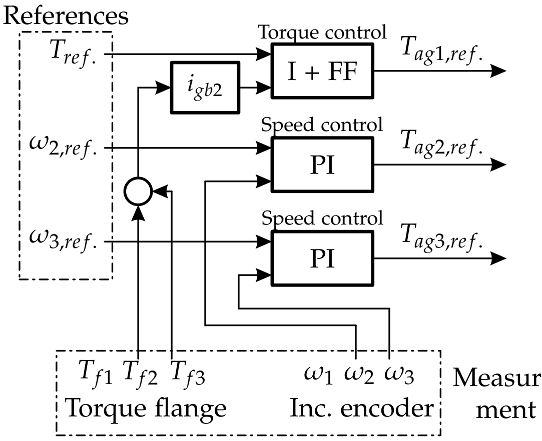

Figure 5.10: Conventional control structure for a test bed for differential gears with adapter gearboxes with symmetric mechanical structure implying $i_{gb2} = i_{gb3}$.

depicted in Figure 5.8 is compared to the conventional control structure as given in Figure 5.10. Then some aspects regarding decoupling and reference tracking for the multivariable control strategy are discussed in detail.

Figure 5.11 presents the reference profiles for the differential gear's total output torque and the rotational speeds of the drives *M2* and *M3* that will be used to test various controller settings. Please note that there are two different reference speed profiles: the dashed profile will be used to demonstrate the problems related to the conventional control concept while the more challenging solid profile is used to prove the advantages of the proposed control structure.

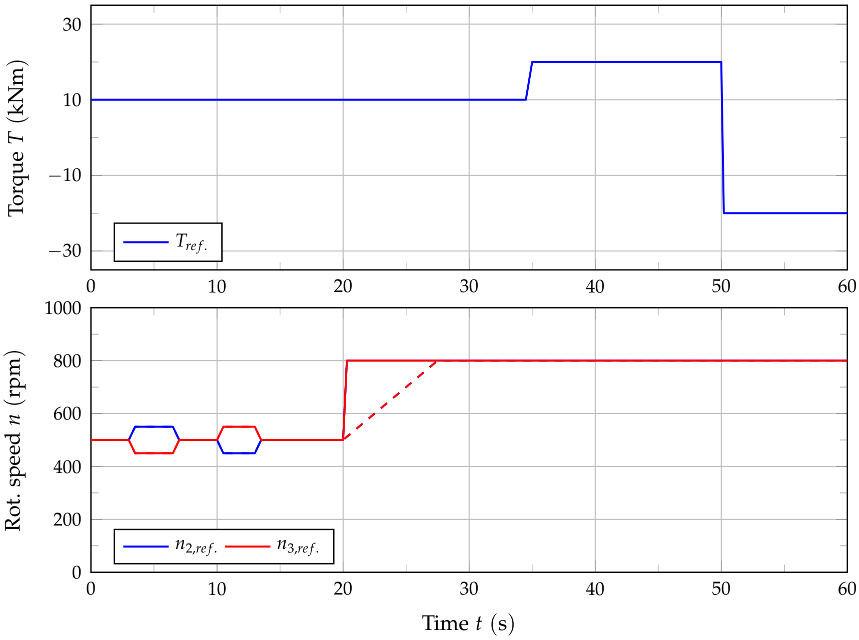

Figure 5.11: Control of a test bed for differential gears with adapter gearboxes, references for the differential's total output torque and for the rotational speeds of *M2* and *M3*.

Figure 5.12 shows the total output torque of the differential gear and the rotational speeds of the drives *M2* and *M3* when the conventional control strategy without decoupling and active damping is used. This results in unacceptable torsional vibrations at approximately 1.3 Hz, which is the first resonance frequency of the mechanical structure. In this situation the input drive oscillates against the two load drives. The oscillations start when the rotational speed of the input drive *M1* changes. Without a decoupling network, the torque required to accelerate the input drive leads to a change in shaft torque. This load variation excites resonance oscillations although the rotational speeds are changed very slowly. At the beginning of the test-run, when the rotational speed of one output drive is reduced while the other is accelerated to test the differential gear's slip-limiting functionality, no problems arise because the rotational speed of *M1* remains constant. The changes in reference torque at $t \approx 35\,\mathrm{s}$ and $t \approx 50\,\mathrm{s}$ are again causing a change in shaft torque and are therefore also exciting resonance oscillations. These torsional vibrations occur although the air-gap torque of *M1* is changed quite slowly because a conservative torque controller with only minor feedforward control is applied. According to Equation (5.79), undamped resonance oscillations are to be expected without active damping. Fortunately, on account of losses and some internal damping of the cardan shafts, the torsional vibrations should be weakly damped. Figure 5.12 though shows unstable system behaviour; this is caused by the feedback torque controller with integral action. However, even without feedback control the system's damping properties would be problematic.

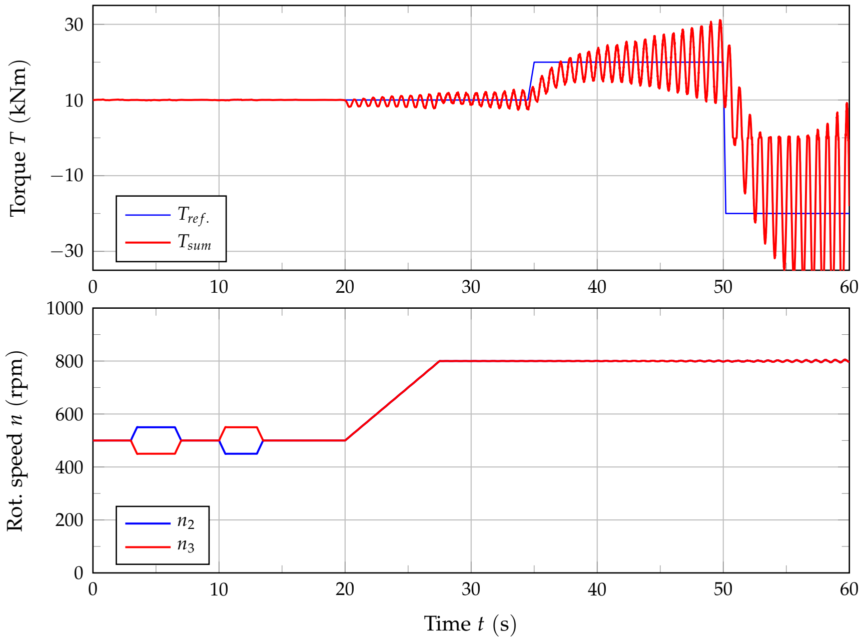

Figure 5.12: Control of a test bed for differential gears with adapter gearboxes, simulation results with the conventional control strategy for the controlled variables T_{sum}, n_2, and n_3.

Figure 5.13 presents the realisable improvement by the use of the proposed control strategy including decoupling and active damping. Additionally, the system behaviour for a disabled decoupling network is presented. As before, PI controllers were used for speed control while for torque control an integrating controller with additional feedforward control was used. Independently of the decoupling, with active damping the system is now sufficiently damped, meaning that resonant oscillations are no longer critical. This allows the use of a much faster torque controller with substantial feedforward control resulting in significantly improved tracking of the reference torque profile. With enabled decoupling network the coupling of torque and rotational speeds is reduced, so that even with the more challenging speed reference profile the total output torque of the differential gear is hardly affected by the change in rotational speeds.

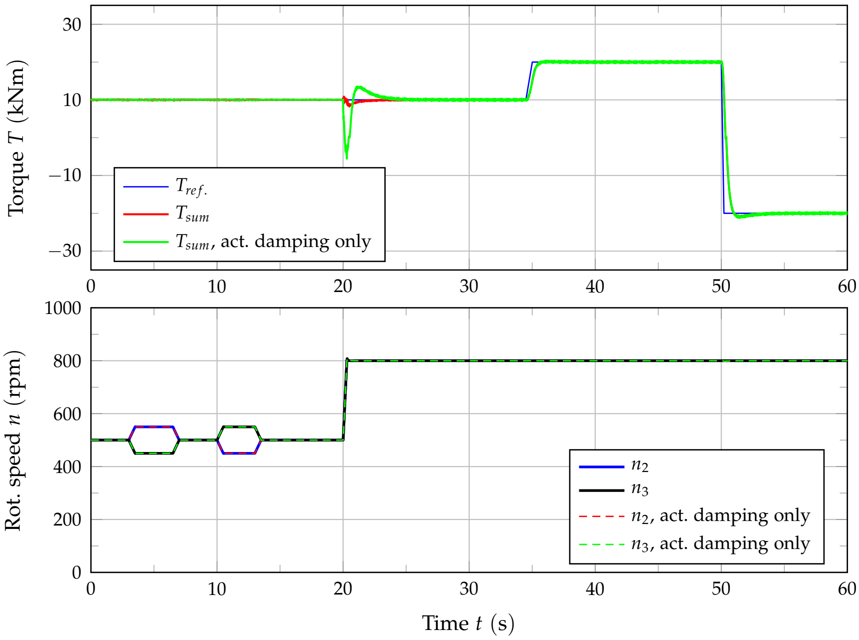

Figure 5.13: Multivariable control of a test bed for differential gears with adapter gearboxes, simulation results with the proposed control strategy and active damping only for the controlled variables T_{sum}, n_2, and n_3.

Figure 5.14, Figure 5.15, and Figure 5.16 focus on the positive effects of the decoupling network with enabled active damping. In Figure 5.14 and Figure 5.15 the influence of a change in rotational speed on the differential gear's total output torque is presented for various settings for the decoupling parameter $\hat{I}_1$. In simulation the total torque at the outputs of the UUT is known, these curves are label 'real'; however, this information cannot be used for feedback torque control. Instead, the effective testing torque must be estimated based on the flange torques T_{f2} and T_{f3}, these curves are labelled 'est.'. Without decoupling ($\hat{I}_1 = 0$) a change in rotational speed leads to significant torque variations. If the decoupling network is activated, the torque error can be reduced substantially. As mentioned before, the acceleration torque $T_{accel.}$ cannot be determined exactly because the moment of inertia of gearbox 1 is unknown. If just the moment of inertia of the electric drive is compensated, the remaining torque variations might be unsatisfactory, especially if the estimated testing torque is evaluated. Therefore, the controller parameter $\hat{I}_1$ was increased to improve the decoupling. It is obvious that even with manually tuned $\hat{I}_1$ perfect decoupling cannot be achieved because of the complexity of the mechanical system and the many simplifications used in Section 5.3 to determine a system model suitable for controller design.

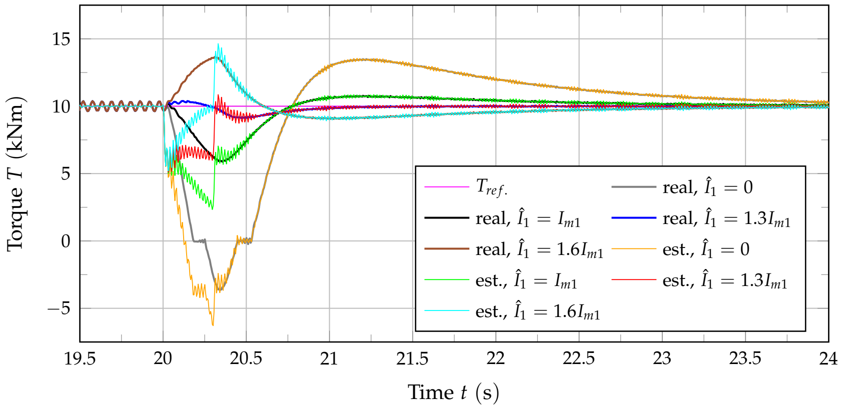

Figure 5.14: Simulation results for T_{sum} with act. damping, decoupling, and varying $\hat{I}_1$, real testing torque at the UUT and testing torque estimated by considering gearbox losses according to Equation (5.96).

In the experiments presented in Figure 5.14 the testing torque estimate did only include gearbox losses; the acceleration torque for the gearboxes was not considered. Therefore, a significant difference between real testing torque and estimated testing torque remains during the acceleration phase. For this reason, the testing torque estimate deviates from the testing torque reference. However, since the torque controller's action is primarily based on feedforward control, the error in the testing torque estimation is hardly affecting the real testing torque. In the results shown in Figure 5.15 also the acceleration torques of the gearboxes are considered in the estimated testing torque. Consequently, the difference between real testing torque and testing torque estimate is significantly reduced. Then in practice, when the real testing torque is unknown, the estimate can be used to characterise the testing conditions for the UUT.

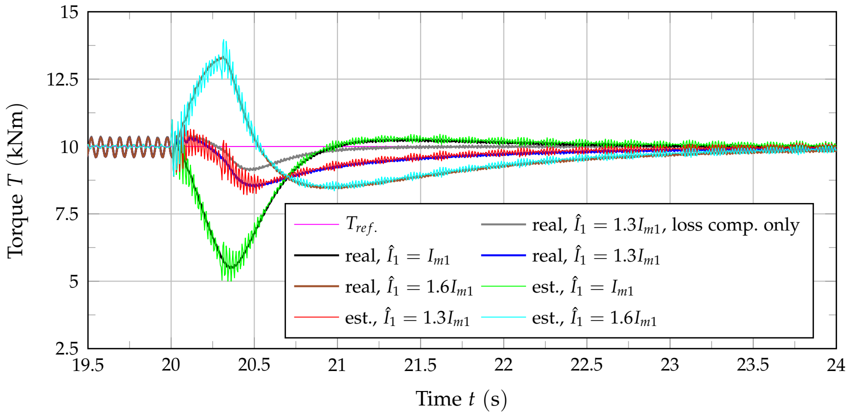

Figure 5.15: Simulation results for T_{sum} with act. damping, decoupling, and varying $\hat{I}_1$, real testing torque at the UUT and testing torque estimated by considering gearbox losses and acceleration torques according to Equation (5.98).

In Figure 5.16 the effect of a load torque change on the rotational speed of the electric drive *M2* is presented. If the decoupling network is deactivated, a change in load torque directly affects the rotational speed n_2. With the decoupling network this interaction can be almost entirely eliminated because of load torque compensation. This situation shows the realisable improvement by control measures; the minor remaining deviations are due to time delays, parasitic dynamics, and limitations in the torque measuring systems and in the inverter's torque control loop. In Figure 5.16 results obtained by the use of a PI controller and a P controller with disturbance observer are compared. Those were tuned for similar disturbance rejection properties; therefore, the results are nearly identical.

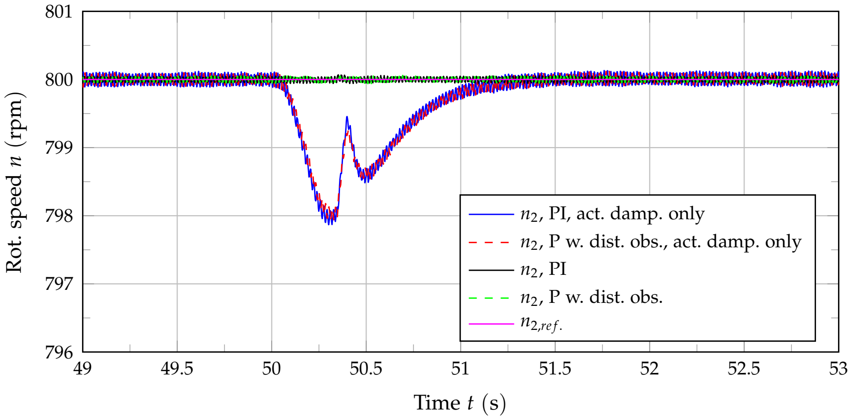

Figure 5.16: Simulation results for rotational speed n_2 with different speed controllers with and without decoupling.

In Figure 5.17 these speed controllers are compared regarding their reference tracking performance. This ramp response clearly shows that the two controllers

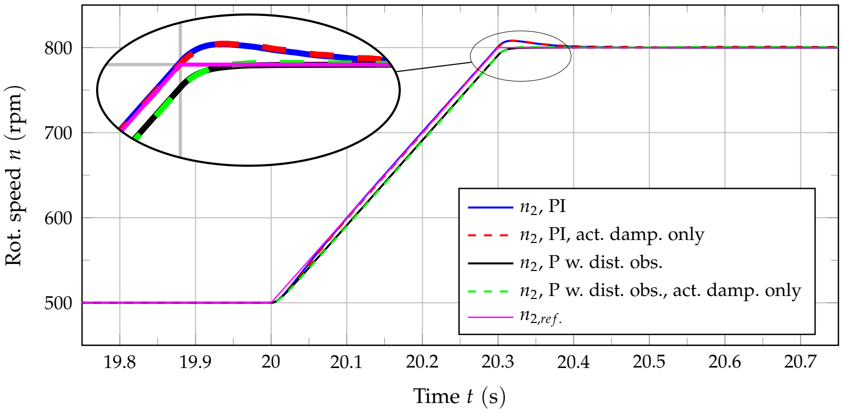

Figure 5.17: Simulation results for a ramp response of n_2 with different speed controllers for complete decoupling and active damping only.

differ in their reference tracking behaviour. If the PI controller is used, the ramp response experiment shows an overshoot; with the P controller with disturbance observer, this overshoot can be avoided. The drawback of this approach is that there is a remaining tracking error during the rotational speed ramp. Figure 5.17 also shows that the reference tracking performance of both speed controller types is hardly affected by the decoupling measures.

Figure 5.18 focuses on the adjustment of the active damping parameter $\widetilde{d}_{s,des.}$. In addition to damping resonant oscillations, the damping torque $T_{damp.}$ defined in Equation (5.78) affects the closed-loop torque dynamics as well. In Figure 5.18 a ramp response of the differential gear's total output torque is presented for various settings for $\widetilde{d}_{s,des.}$ and resulting damping ratios ζ. One can see that when the damping ratio is low, the torque response is fast, but torsional vibrations are still present. With a higher damping ratio the torque oscillations completely vanish, but the torque dynamics become slower. A good compromise between good oscillation damping and fast torque dynamics is to increase $\widetilde{d}_{s,des.}$ until critical damping is reached. This can either be done analytically according to Equation (5.81) if the equivalent torsional stiffness $\widetilde{c}_s$ and the moment of inertia I_1 are known, or directly in experiments on the test bed. This specific setting was also used for the previous simulations.

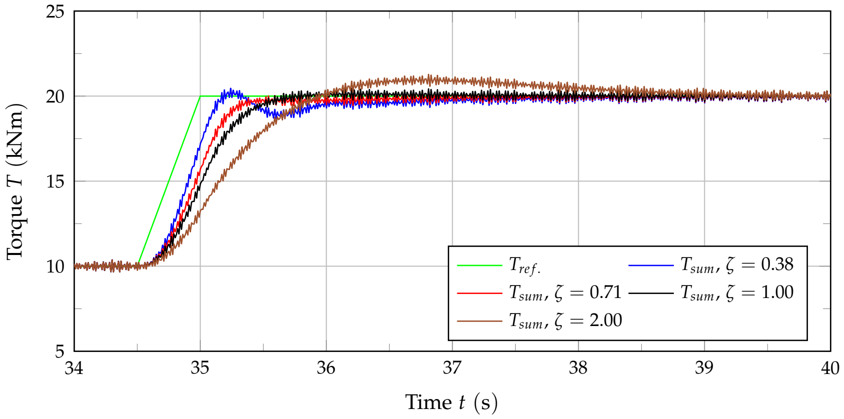

Figure 5.18: Simulation results for a ramp response of the differential gear's total output torque T_{sum} with decoupling, active damping, and varying damping parameter $\widetilde{d}_{s,des.}$.

In addition to these simulation studies, this specific control problem was also analysed in experiments on a commercial test bed; the measurement results are presented in Chapter 6.

5.8.2 Control of a Test System for Transmissions

In this section the control of a test bed for transmissions as shown in Figure 3.2 is discussed. The multivariable control strategy proposed in Section 5.4.1 is compared to the conventional SISO approach depicted in Figure 5.19. For simulation the model presented in Section 3.10, which was verified by a comparison with measurement data in Section 4.6, was used. These simulation results were already based on the conventional control concept and are reused at this point to show the improvements by the new control. The test-run is composed of speed and torque ramps in different gears. Gear shifts are performed without load, which is indicated in Figure 5.20 by the reference testing torque $T_{ref.}$ that is close to zero when gear shifts occur. These gear shifts are the main challenge for control. In Figure 5.20 the torques at input and load drive are shown for the conventional control concept (labelled 'conv.') and for the proposed multivariable control strategy (labelled 'prop.'). With the conventional control the testing torque was actively increased

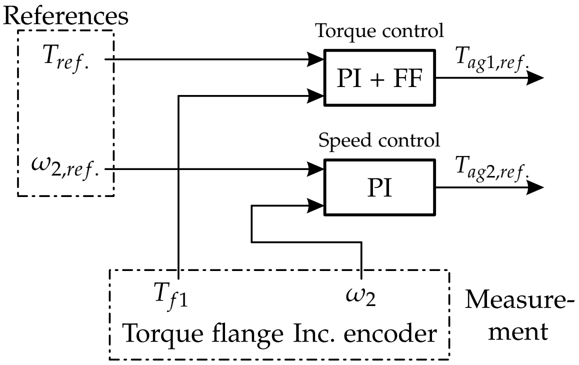

Figure 5.19: Conventional control structure for a test bed for transmissions.

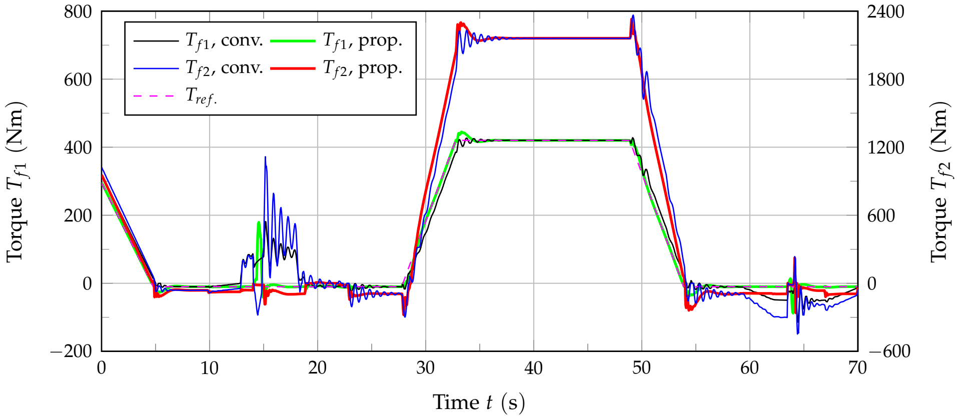

Figure 5.20: Control of a test system for transmissions, simulated flange torques T_{f1} and T_{f2} for the conventional controller and the proposed multivariable control.

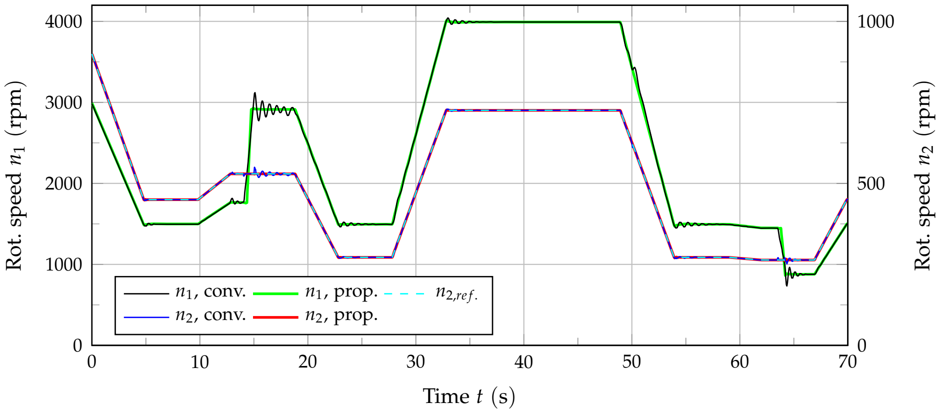

Figure 5.21: Control of a test system for transmissions, simulated rot. speeds n_1 and n_2 for the conventional controller and the proposed multivariable control.

when a down-shift was planned and reduced before an up-shift took place. For the down-shift this procedure was necessary to accelerate the input drive during the phase of interrupted power transfer to make sure that the ratio of gearbox input speed and gearbox output speed is brought near the transmission ratio of the next gear. The situation for the up-shift is similar, here the input drive must be decelerated. However, the rotational speed of the input drive is never exactly at the desired value when the clutch within the transmission is closed; therefore, some synchronisation takes place. This torque disturbance causes resonant torque oscillations, which are clearly visible in Figure 5.20 and also in Figure 5.21 where the rotational speeds of the electric drives are shown. These torque peaks can potentially damage UUT and test bed. This specific problem can be overcome by the use of the proposed control strategy. If during the phase of power interruption the transmission ratio i_{gb} is linearly changed within the control structure, the term $I_{m1}\omega_2 \mathrm{d}i_{gb}/\mathrm{d}t$ in the decoupling torque represents the torque needed to change the rotational speed of the input drive to the value suitable for the next gear. Furthermore, the damping torque $\widetilde{d}_{s,des.}\left(\omega_1 - i_{gb}\omega_2\right)$ acts as a speed controller to bring ω_1 close to its desired value $i_{gb}\omega_2$. Then, when the clutch within the transmission is closed, less synchronisation is required and torsional vibrations can be significantly reduced. The remaining resonant oscillations decay fast because of active damping. Also in other situations than gear shifts such as at the beginning and the end of torque ramps the active damping measure prevents most torsional vibrations.

As for the test system for differential gears, the speed control performance was primarily improved by load torque compensation. Additionally, the measures implemented to improve the synchronisation at the end of the gear shifts also reduce the disturbance torque for the speed control loop and therefore decrease the speed tracking error for these special situations. The decoupling torque applied to the input drive when the rotational speed of the load drive is changed slightly improves the system behaviour for situations where testing torque and rotational speed are changed simultaneously. However, because of rather slow changes of rotational speed, the effects are minor compared to the other improvements.

Chapter 6

Experimental Results

In this chapter some experimental results are presented to show the performance of the proposed modifications regarding test bed control. To provide most realistic results, these experiments were conducted on *full–scale test systems*. The use of small–scale laboratory plants is problematic since often some aspects of their behaviour are different and as a consequence, controllers giving satisfying results with the laboratory plants might fail on the full-scale test system. However, because of the limited availability of commercial test beds for controller testing, not every control aspect that was discussed in simulation could be tested in practice. For this reason, only some selected results are given in this chapter.

6.1 Multivariable Control of a Test Bed for Differential Gears with Adapter Gearboxes

The proposed control strategy for the testing of differential gears as depicted in Figure 5.8 has been tested on a commercial test bed for differential gears equipped with three 700 kW induction machines and adapter gearboxes as shown in Figure 3.1 in Section 3.1. Some further characteristic technical parameters of the test bed are summarised in Table D.1 in Appendix D. Control for exactly this test system was already discussed in simulation in the previous chapter. The multivariable control scheme presented in Figure 5.8 was implemented on real-time processing hardware and a typical test-run for rear axle truck differentials was performed. To keep torque control simple and easy to tune, an integrating controller with additional feedforward control action as discussed in Section 5.6.1 was used. The speed controllers R_ω were chosen as PI controllers (see Section 5.5.1). Due to mechanical restrictions concerning the UUT, a quite conservative test-run with slow speed and torque changes had to be performed. To see the progress made by the new control strategy, in the first test-run the old control concept, as shown in

Figure 5.10, based on individually designed controllers for rotational speed and torque without decoupling and active damping, was used. Figure 6.1 shows the measured rotational speeds of the three electric drives and Figure 6.2 presents the differential gear's total output torque and the torques measured by the torque sensors at machines *M*2 and *M*3. The total testing torque T_{sum} was estimated based on the torque flange measurements T_{f2} and T_{f3}. According to Section 5.6, gearbox losses were compensated, but the torque required to accelerate the gearboxes was not considered as rotational speeds were changed rather slowly. To once more prove the accuracy of the simulation model used in the previous chapter and to highlight the significance of the results regarding control performance presented there, also some simulation results are included in Figures 6.1 – 6.4.

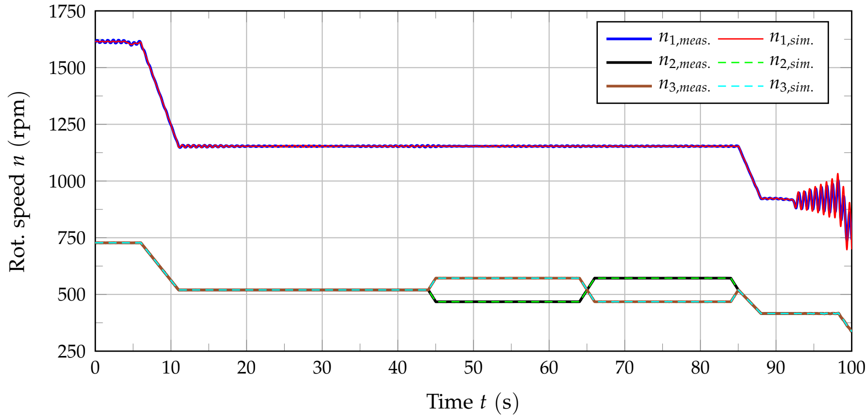

Figure 6.1: Measured and simulated rotational speeds on a test bed for axle differentials with adapter gearboxes with the conventional control.

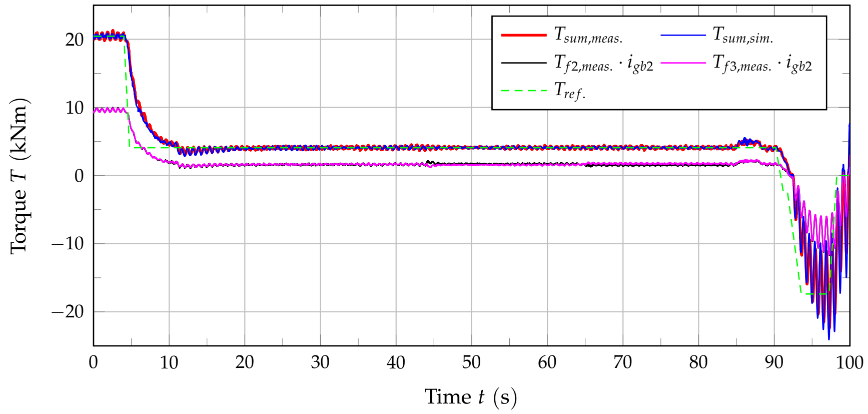

Figure 6.2: Measured and simulated torques on a test bed for axle differentials with adapter gearboxes with the conventional control.

Both figures show that torsional vibrations are a serious problem through the entire test-run, but especially at $t \approx 90\,\mathrm{s}$ when the sign of the testing torque is changing.

Due to gear play, there is a strong excitation of resonant oscillations; in combination with low internal damping of the cardan shafts large torque oscillations arise leading to an emergency shut-down of the test bed. Figure 6.2 furthermore shows that, because no decoupling network is used, a change in rotational speed directly affects the differential gear's total output torque and additionally excites resonance oscillations. Therefore, the same test-run has been performed using the new control concept including input–output decoupling and active oscillation damping. The rotational speeds of the electric drives are shown in Figure 6.3 while the torques are presented in Figure 6.4.

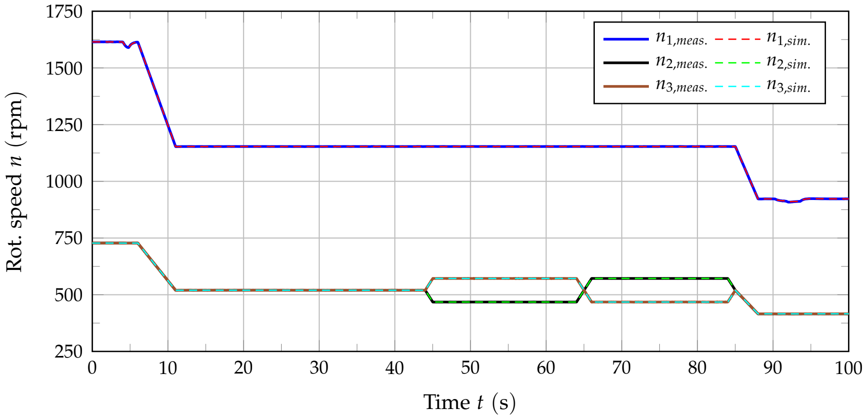

Figure 6.3: Measured and simulated rotational speeds on a test bed for axle differentials with adapter gearboxes with input–output decoupling and active damping.

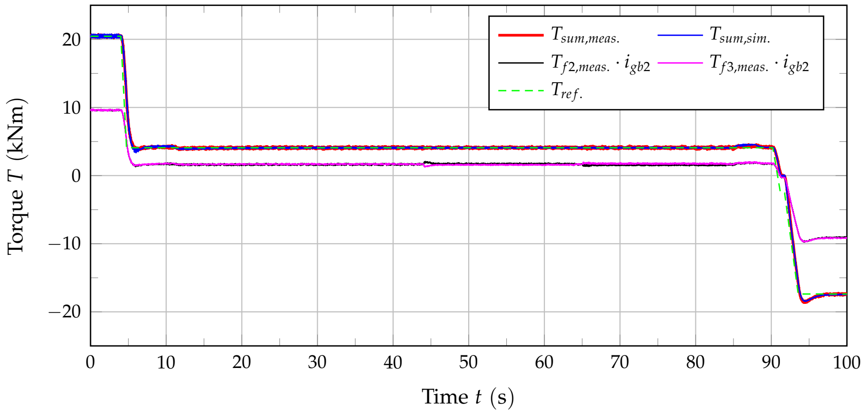

Figure 6.4: Measured and simulated torques on a test bed for axle differentials with adapter gearboxes with input–output decoupling and active damping.

The superiority of the new control concept becomes obvious during the entire test-run. Torsional vibrations are now sufficiently damped, meaning that resonance phenomena are no longer critical, even if the excitation is strong e.g. because of gear play. Additionally, this improved oscillation damping allows the use of a faster torque controller with significant feedforward control action to improve the tracking of the torque reference. The decoupling network also made it possible to reduce the interaction of rotational speeds and torque. Figure 6.4 especially shows that now a change in rotational speeds causes less testing torque variations. On account of the quite conservative test-run with slow speed and torque changes, the benefits of the decoupling network are not as significant as before in Chapter 5; however, the positive effect of the damping strategy is obvious.

6.2 Multivariable Control of a Back-to-Back Configuration

With the test system for differential gears discussed before no experiments including high dynamic changes of testing torque could be performed. Because of the complex mechanical system consisting of the UUT, adapter gearboxes, and many cardan shafts, testing torque dynamics were limited. As a consequence, another mechanical test set-up was used to conduct further experiments. The 575 kW induction machines *M1* and *M2* were directly connected by a rather short shaft; this setting is called 'back-to-back' configuration and is shown in Figure 6.5. To control the electric drives, the control concept initially developed for testing a transmission as shown in Figure 5.7 was applied. The only modification is that the transmission ratio i_{gb} was chosen permanently one. The input drive *M1* was torque controlled, the load drive *M2* was operated in speed control mode. For the first experiment the decoupling terms were deactivated and only the active damping measure was tested. In the experiment the speed reference $\omega_{2,ref.}$ was kept constant while the testing torque reference $T_{ref.}$ was changed. The recorded data are presented in Figure 6.6. T_{f1} and T_{f2} are torques measured by the torque measuring flanges at

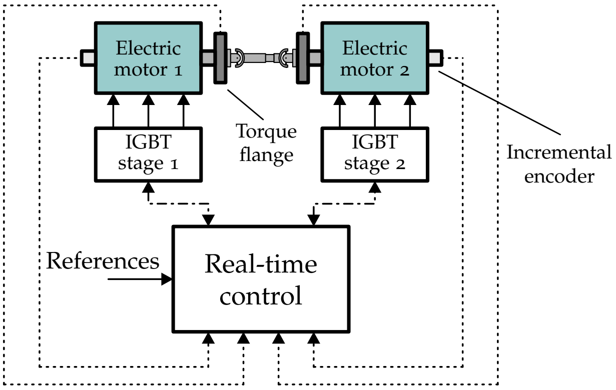

Figure 6.5: Back-to-back testing configuration with KS R2R frequency converters.

machines *M1* and *M2*; n_1 and n_2 are the rotational speeds of these electric drives. Results presented in blue and green were recorded with active damping, results shown in red and black were obtained with disabled active damping. Clearly, in this situation even without active damping torsional vibrations are not as strong as before in Section 6.1. This is due to the different mechanical setting that is significantly simpler and does not include any transmission ratios. For this mechanical set-up the first resonant frequency is at approximately 17 Hz and therefore higher than before. However, also for this setting active damping is beneficial as torsional vibrations can be eliminated.

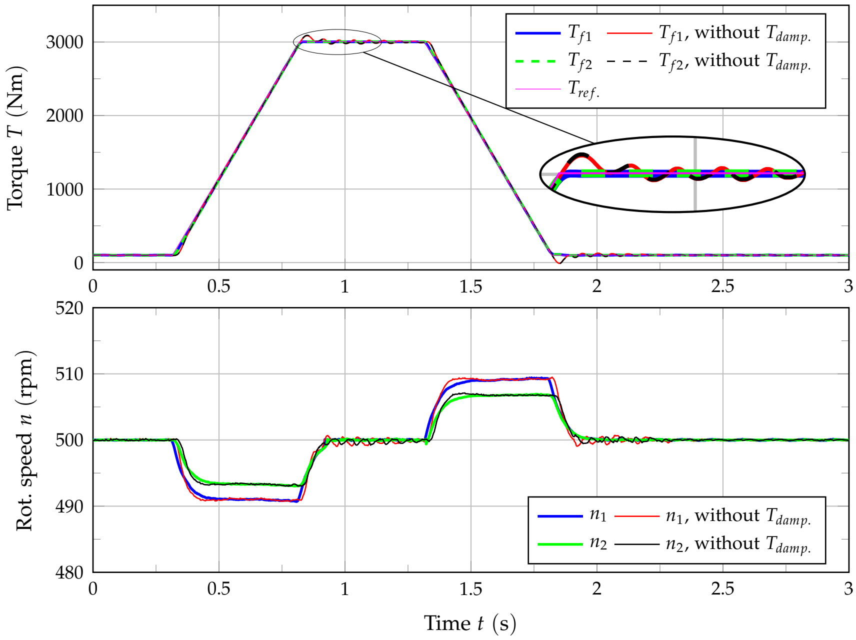

Figure 6.6: Back-to-back testing configuration, changes of testing torque with and without active damping applied to electric drive *M1*.

For the next experiment the active damping measure was enabled and the coupling of rotational speed and testing torque was analysed. As before, the speed reference $\omega_{2,ref.}$ was kept constant while the testing torque reference $T_{ref.}$ was changed. Since the decoupling torque for the input drive $T_{accel.}$ is not needed with constant rotational speed reference, in particular the decoupling scheme for the load drive is analysed in the following figures. The measurement results are presented in Figure 6.7: curves in blue and green were recorded with load torque compensation, in red and black results without decoupling are shown. Because the fast change of testing torque is a strong disturbance for the speed controller of *M2*, here the effect of the decoupling measure (load torque compensation) is clearly visible. Without decoupling a speed tracking error of approximately 10 rpm occurs during the change of testing torque. With decoupling the rotational speed n_2 shown in

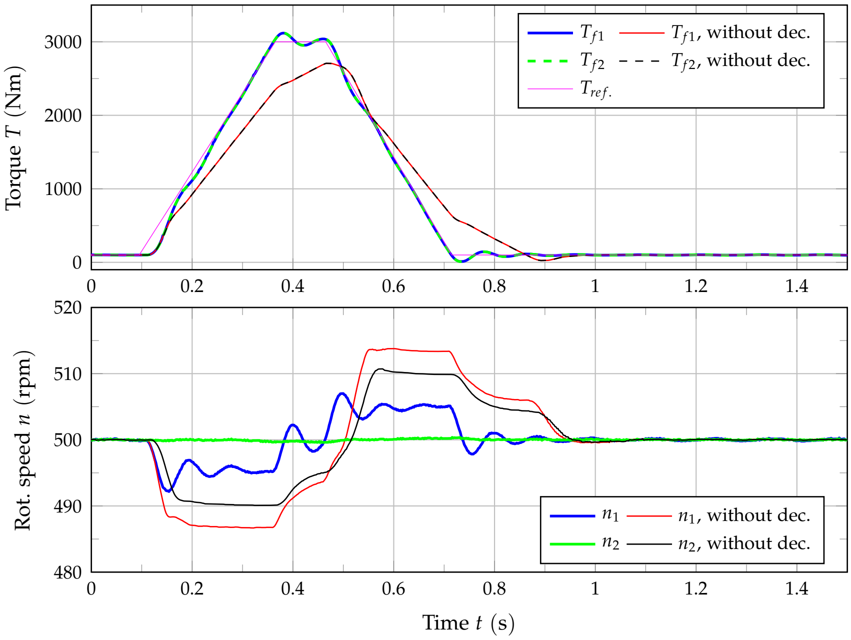

Figure 6.7: Back-to-back testing configuration, changes of testing torque with and without load torque compensation for the load drive $M2$.

green is hardly affected. The rotational speed of the input drive must vary for both situations because otherwise the torsion angle of the mechanical shaft cannot change. Since the torque transmitted by a flexible shaft is directly related to its torsion angle, a change of shaft torque always requires different rotational speeds at the two ends of the shaft. Also the testing torque is positively affected by the decoupling measure; as the angular velocity of the load drive remains constant, adjusting the angular position of the input drive to reach the desired shaft torque is easier.

6.3 Active Damping Control for a Test Bed for Centre Differentials

Finally, the active damping strategy was used to improve the performance of another test bed for differential gears. In contrast to Section 6.1, where an axle differential was tested, here tests for a centre differential were performed. Therefore, the situation regarding control was different: the input drive $M1$ was operated in speed control mode while the load drives $M2$ and $M3$ were torque controlled with references $T_{2,ref.}$ and $T_{3,ref.}$. The first experiment was performed with the conventional control strategy based on three individual PI controllers; in the second experiment the active damping measure for $M2$ and $M3$ was added to improve control performance. In Figure 6.8 the rotational speeds of the electric drives are presented. In Figure 6.9 the measured torques and the torque references for *M*2 and *M*3 are shown.

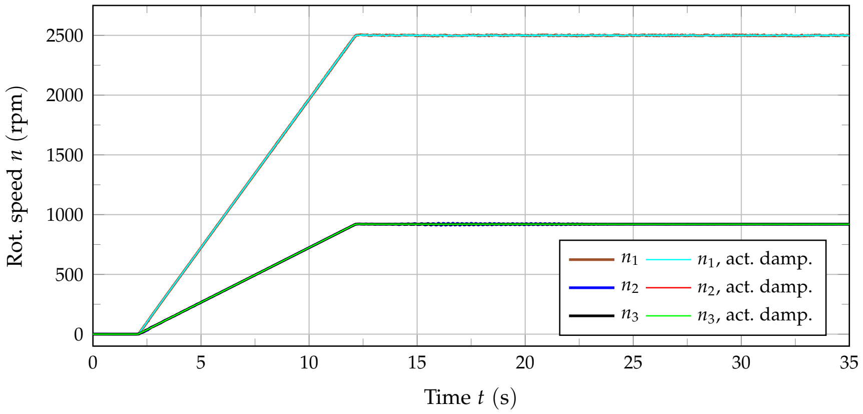

Figure 6.8: Measured rotational speeds on a test bed for centre differentials with and without active damping.

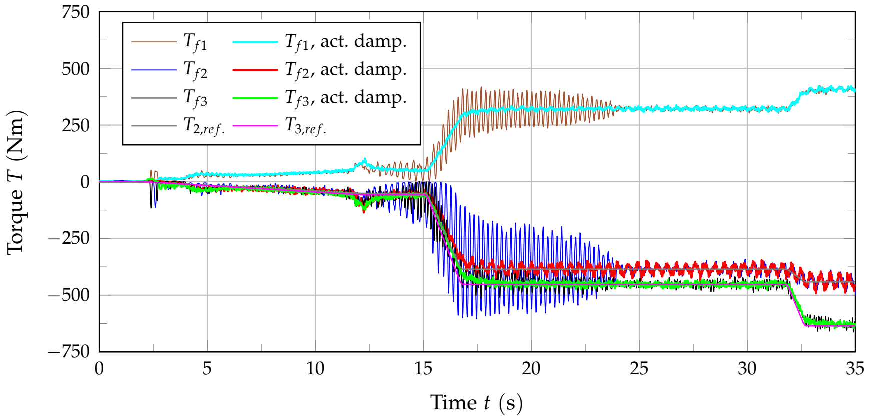

Figure 6.9: Measured torques on a test bed for centre differentials with and without active damping.

Figure 6.9 shows that without additional damping measures the control performance is limited. The reason for these torsional vibrations is a problematic mechanical test set-up including significant gear play and rather long cardan shafts. Furthermore, the test bed is equipped with an older inverter system with limited performance. However, when the active damping strategy is applied, torsional vibrations can be reduced significantly. These results indicate that the active damping scheme, which was initially part of the multivariable control concept, can also improve the system performance when applied separately with older, less powerful inverter systems.

Chapter 7

Handling Constraints

At this point various controllers for automotive test systems have been proposed and successfully tested in numerical simulations as well as in real-world experiments. In the simulations all actuator constraints and limitations were considered, but the references for testing torque and testing rotational speeds were chosen so that these limitations were not exceeded. In general, this assumption is not admissible as test bed operators might demand testing profiles that cannot be reached by the electric drives. While selecting the testing torque appropriately is quite simple, choosing the rotational speed profiles might be more complicated since here the angular accelerations and the testing torque are important.[1]

7.1 Introduction

On a power train test bed, the admissible operating range regarding testing torque and testing rotational speed is restricted by the *operational limits* of the electric drives. As shown in Figure 7.1, an electric motor's operating range regarding rotational speed is specified by a minimal angular velocity ω_{min} and a maximal angular velocity ω_{max}. Torque limits are given by a minimal respectively maximal electromagnetic torque $T_{ag,min}$ and $T_{ag,max}$, which are typically constant over a wide range of rotational speed. As mentioned in Appendix A, the feasible air-gap torque decreases at high rotational speed because of field weakening. The rated torque can normally be delivered until the rated angular velocity ω_r is reached. The operating range is usually symmetric regarding rotational speed ($-\omega_{min} = \omega_{max}$) and torque ($-T_{ag,min} = T_{ag,max}$). These restrictions for rotational speed and air-gap torque for

---

[1] In this chapter only constraints regarding the test system are considered; further eventually more restrictive limits required to protect the UUT are not discussed. Since the control loops for rotational speed and testing torque were designed for good reference tracking, this can be handled by adequately choosing the references.

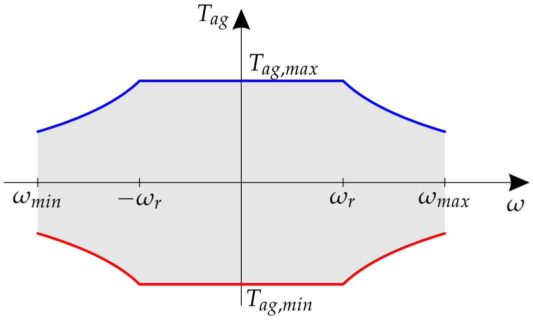

Figure 7.1: Operating range of an electric drive.

each individual electric drive and the transmission ratios in the mechanical system must be combined to be able to finally specify the operating range of the test system. As high performance inverter systems are assumed, no restrictions regarding torque dynamics must be considered.

With the conventional control as shown in Figure 5.10 for a test bed for differential gears, handling the actuator constraints is rather simple. Since couplings are not considered, the control loops for rotational speed and torque are treated as independent from each other and consequently, for each controller only the constraints related to one actuator are relevant. Therefore, constraints do not necessarily have to be considered in the controller design. Only for controllers containing integrating behaviour controller windup must be avoided. This can easily be realised by the use of the classic AW procedure proposed by Hanus [139] if a PI controller is used respectively by limiting the integrator if a purely integrating controller is applied. For the multivariable controllers proposed in this work to improve the system performance, handling the actuator constraints is more complex. As can be seen in Figure 7.2, now the air-gap torque reference is no longer given by the feedback controller's output only.[2] To be able to provide decoupling, the outputs of other feedback controllers and some system states must be considered as well. For instance, v_2, which is the output of the feedback speed controller, affects the (limited) manipulated variables $T_{ag1,ref.}$ and $T_{ag2,ref.}$. Therefore, the classic conditioning technique proposed by Hanus cannot be applied [139]. If electromagnetic torques that are not within the operating range of the electric drives are demanded by the controller, decoupling can no longer be guaranteed. This might be acceptable, but if the torque limit of the input drive is reached, active damping can no longer be provided. This might result in potentially dangerous torsional vibrations.

This problem is rarely discussed in literature on automotive testing. In the field of power train testing no publication that considers the operating range of the

---

[2] This control structure is similar to the controller shown in Figure 5.8 where a test bed for differentials with adapter gearboxes was discussed. This test set-up does not include adapter gearboxes; additionally, in this application the testing torque is given for the differential's input.

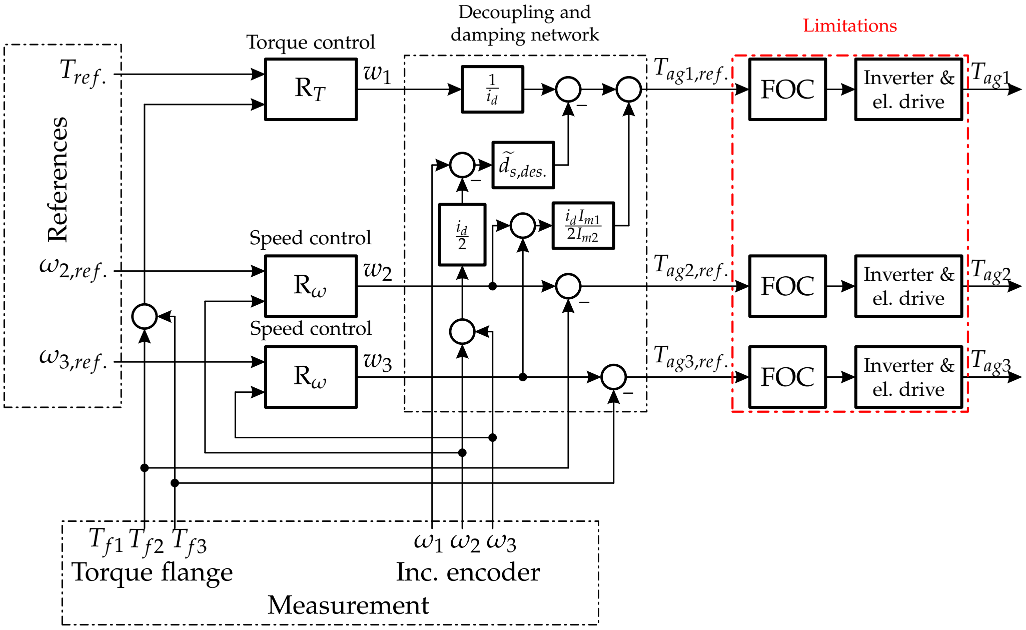
Decoupling and damping network
Limitations
Torque control
References
$T_{ref.}$
R_T
w_1
$\frac{1}{i_d}$
$\tilde{d}_{s,des.}$
$\frac{i_d}{2}$
$\frac{i_d I_{m1}}{2 I_{m2}}$
$T_{ag1,ref.}$
FOC
Inverter & el. drive
T_{ag1}
Speed control
$\omega_{2,ref.}$
R_ω
w_2
$T_{ag2,ref.}$
FOC
Inverter & el. drive
T_{ag2}
Speed control
$\omega_{3,ref.}$
R_ω
w_3
$T_{ag3,ref.}$
FOC
Inverter & el. drive
T_{ag3}
T_{f1} T_{f2} T_{f3}
Torque flange
ω_1 ω_2 ω_3
Inc. encoder
Measurement

Figure 7.2: Multivariable control of a test bed for differential gears, torque control w.r.t. the differential's input torque.

electric drives for controller design is known to the author. However, as for the general control problem, also for this aspect literature in the field of engine testing is available.

Many control strategies for engine test beds recently published rely on optimisation based techniques such as MPC where constraints and limitations can be directly considered in the optimisation problem to be solved [26, 140]. Also in the related field of controlling elastic drive systems MPC is a popular method to be able to consider constraints directly [37, 109, 112–115]. However, due to the computational effort required to solve a constrained optimisation problem, real-time implementation is typically problematic. In particular for control problems where a short sampling time is necessary it is often infeasible to solve the optimisation problem online. Therefore, in [29] a different approach for ICE test bed control is proposed. Here an inverse plant model is used to calculate the needed actuator torques; a Kalman filter based algorithm then shapes the trajectories for testing rotational speed and torque to minimise constraint violations. But since controller tuning is not intuitive, both mentioned approaches are not suitable for use in industrial practice. For the MPC controller the desired system behaviour must be specified by a cost function based on weighting matrices, also for the Kalman filtering approach many tuning parameters are to be selected. This is problematic as test bed operators would not know how to adjust controller parameters for a given testing configuration. These issues discussed here in the context of test bed control are relevant for many other applications as well.

Therefore, instead of considering the constraints directly in the control algorithms often the references for the feedback controllers are shaped so that constraints can be met [141]. The fundamental idea of this approach is presented in Figure 7.3. The basic feedback controller that is already available remains unmodified and forms together with the plant the closed-loop system; additionally, a pre-filter is added to shape the references. These add-on control schemes are called *command governors* or *reference governors* and have been introduced for both linear and non-linear systems. This approach is often attractive for practitioners because the feedback controller can be designed without considering constraints; therefore, existing controllers and tuning rules can be preserved. For more details on reference governors and their application see [141–145].

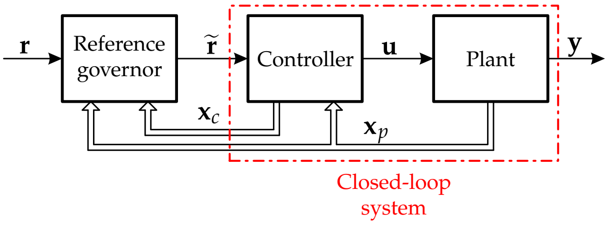

Figure 7.3: Reference governor structure.

7.2 Reference Governor

The basic idea of the reference governor was given in Figure 7.3. The common intent of the reference governor is to preserve the dynamics of the closed-loop system whenever possible. Therefore, they typically determine the shaped reference command $\tilde{\mathbf{r}}$ as close to the original reference $\mathbf{r}$ as possible while nevertheless the constraints are maintained. Usually, the reference governor is active only for short time intervals. Thus, $\tilde{\mathbf{r}}$ and $\mathbf{r}$ are identical most of the time. The conventional reference governor uses the current state vector of the plant $\mathbf{x}_p$, the controller states $\mathbf{x}_c$, and the original references $\mathbf{r}$ to compute the shaped references $\tilde{\mathbf{r}}$ for the feedback controller. Since this control structure is usually implemented on a digital system, in this work only the discrete time approach is discussed. To design the reference governor, a mathematical model of the closed-loop system is required; therefore, the state vectors of plant $\mathbf{x}_p$ and controller $\mathbf{x}_c$ are combined:

$$\mathbf{x} := \begin{bmatrix} \mathbf{x}_p \\ \mathbf{x}_c \end{bmatrix} \tag{7.1}$$

The discrete time state-space model of the nominal closed-loop system shown in Figure 7.3 is given as a LTI system

$$\mathbf{x}_{k+1} = \mathbf{A}\mathbf{x}_k + \mathbf{B}\tilde{\mathbf{r}}_k \tag{7.2a}$$

$$\widetilde{\mathbf{y}}_k = \mathbf{C}\mathbf{x}_k + \mathbf{D}\widetilde{\mathbf{r}}_k, \tag{7.2b}$$

where $\mathbf{x}$ is the N-dimensional state vector, $\widetilde{\mathbf{r}}$ is the m-dimensional reference vector for the closed-loop system and in $\widetilde{\mathbf{y}}$ the p quantities that are subjected to constraints according to

$$\mathbf{S}\widetilde{\mathbf{y}}_k \leq \mathbf{s} \quad \forall\, k \geq 0 \tag{7.3}$$

are summarised.[3] These could be the manipulated variables as well as certain system states. System (7.2) is a mathematical model for the closed-loop system and thus represents the combination of plant and controller. Since the closed-loop system is typically designed to be asymptotically stable, the matrix $\mathbf{A}$ is assumed to be a Schur matrix.[4] Furthermore, the pair $(\mathbf{A}, \mathbf{C})$ is assumed to be observable. Key objective at time instant k_x is to choose $\widetilde{\mathbf{r}}_{k_x}$ in a way that

$$\|\mathbf{r}_{k_x} - \widetilde{\mathbf{r}}_{k_x}\| \tag{7.4}$$

is minimised and that the Constraints (7.3) are maintained for all $k \geq k_x$. This calculation procedure is repeated in every sampling interval. To avoid confusion caused by different indices for the current time instant and for predictions into the future, $k_x = 0$ is assumed henceforth.[5] The basic idea of the reference governor is to choose the shaped reference $\widetilde{\mathbf{r}}_0$ in a way that, when *constantly applied* to the system, the constraints are maintained for all $k \geq 0$

$$\mathbf{S}\hat{\widetilde{\mathbf{y}}}_k \leq \mathbf{s} \quad \forall\, k \geq 0, \tag{7.5}$$

where $\hat{\widetilde{\mathbf{y}}}_k$ is an estimate for the system outputs subjected to constraints at time instant k, which is calculated according to

$$\hat{\widetilde{\mathbf{y}}}_k = \mathbf{C}\mathbf{A}^k\mathbf{x}_0 + \mathbf{C}\left(\mathbf{I}_N - \mathbf{A}\right)^{-1}\left(\mathbf{I}_N - \mathbf{A}^k\right)\mathbf{B}\widetilde{\mathbf{r}}_0 + \mathbf{D}\widetilde{\mathbf{r}}_0 \quad \text{for } k = 0, 1, \ldots \tag{7.6}$$

with $\mathbf{I}_N$ being the $N \times N$ identity matrix. Calculating an optimal $\widetilde{\mathbf{r}}_0$ seems to be simple at first glance as the Inequality constraints (7.5) are linear, but there is an infinite number of constraints. As the Inequality constraints (7.5) are forming a convex set, for every $\epsilon_\infty \in (0, 1)$ a $k^* \in \mathbb{N}$ exists so that when

$$\mathbf{S}\hat{\widetilde{\mathbf{y}}}_\infty \leq (1 - \epsilon_\infty)\,\mathbf{s} \tag{7.7a}$$

$$\mathbf{S}\hat{\widetilde{\mathbf{y}}}_k \leq \mathbf{s} \quad \forall\, k = 0, 1, \ldots, k^* \tag{7.7b}$$

holds, the Inequality constraints (7.5) are also fulfilled for $k > k^*$ [141]. Consequently, because of these tightened steady-state limits, only a finite number of constraints must be considered when the optimisation problem is solved.

---

[3] Selecting the constraints as a polyhedral set simplifies the following considerations; in general, also $\widetilde{\mathbf{y}}_k \in \widetilde{\mathbf{Y}}\ \forall\, k \geq 0$ where $\widetilde{\mathbf{Y}} \subset \mathbb{R}^p$ is a prescribed set could be assumed.

[4] A Schur matrix is a square matrix with real entries and with eigenvalues of absolute value less than one [146, 147].

[5] Since System (7.2) is a time-invariant system, this time shift is admissible.

The set of pairs $(\widetilde{\mathbf{r}}_0, \mathbf{x}_0)$ satisfying Equation (7.7) is called 'safe set' $\widetilde{\mathbf{O}}_\infty$ and can be computed offline. If the set of admissible outputs is defined as

$$\widetilde{\mathbf{Y}} = \{\widetilde{\mathbf{y}} : \mathbf{S}\widetilde{\mathbf{y}} \le \mathbf{s}\}\,, \tag{7.8}$$

the safe set can be written as

$$\begin{aligned}\widetilde{\mathbf{O}}_\infty = \Big\{ (\widetilde{\mathbf{r}}_0, \mathbf{x}_0) : \mathbf{C}\left(\mathbf{I}_N - \mathbf{A}\right)^{-1} \mathbf{B}\widetilde{\mathbf{r}}_0 + \mathbf{D}\widetilde{\mathbf{r}}_0 \in \left(1 - \epsilon_\infty\right) \widetilde{\mathbf{Y}}, \\ \mathbf{C}\mathbf{A}^k \mathbf{x}_0 + \mathbf{C}\left(\mathbf{I}_N - \mathbf{A}\right)^{-1} \left(\mathbf{I}_N - \mathbf{A}^k\right) \mathbf{B}\widetilde{\mathbf{r}}_0 + \mathbf{D}\widetilde{\mathbf{r}}_0 \in \widetilde{\mathbf{Y}}\ \forall\ 0 \le k \le k^* \Big\}.\end{aligned} \tag{7.9}$$

If Equation (7.9) is evaluated for $k = 0, 1, \ldots, k^*$,

$$\widetilde{\mathbf{O}}_\infty = \left\{ (\widetilde{\mathbf{r}}_0, \mathbf{x}_0) : \underbrace{\begin{pmatrix} \mathbf{SC}\left(\mathbf{I}_N - \mathbf{A}\right)^{-1} \mathbf{B} + \mathbf{SD} & \mathbf{0} \\ \mathbf{SD} & \mathbf{SC} \\ \mathbf{SCB} + \mathbf{SD} & \mathbf{SCA} \\ \vdots & \vdots \\ \mathbf{SCA}^{k^*-1}\mathbf{B} + \mathbf{SCA}^{k^*-2}\mathbf{B} + \cdots + \mathbf{SCB} + \mathbf{SD} & \mathbf{SCA}^{k^*} \end{pmatrix}}_{=:\mathbf{A}_\infty} \begin{bmatrix} \widetilde{\mathbf{r}}_0 \\ \mathbf{x}_0 \end{bmatrix} \le \underbrace{\begin{bmatrix} \left(1 - \epsilon_\infty\right) \mathbf{s} \\ \mathbf{s} \\ \mathbf{s} \\ \vdots \\ \mathbf{s} \end{bmatrix}}_{=:\mathbf{b}_\infty} \right\} \tag{7.10}$$

results and by the use of matrix $\mathbf{A}_\infty$ and vector $\mathbf{b}_\infty$ the safe set $\widetilde{\mathbf{O}}_\infty$ is given by

$$\widetilde{\mathbf{O}}_\infty = \left\{ (\widetilde{\mathbf{r}}_0, \mathbf{x}_0) : \mathbf{A}_\infty \begin{bmatrix} \widetilde{\mathbf{r}}_0 \\ \mathbf{x}_0 \end{bmatrix} \le \mathbf{b}_\infty \right\}. \tag{7.11}$$

The key idea of the reference governor is to find a vector $\widetilde{\mathbf{r}}_0$ that is together with the given state vector $\mathbf{x}_0$ in the safe set $\widetilde{\mathbf{O}}_\infty$ and that furhtermore minimises $\|\mathbf{r}_0 - \widetilde{\mathbf{r}}_0\|$. The number of inequalities forming the safe set $\widetilde{\mathbf{O}}_\infty$ can be computationally problematic; therefore, often 'almost' redundant inequalities are removed before the optimisation problem is solved [141].

Since at this point all predicted system outputs $\hat{\hat{\mathbf{y}}}_k$ for $k = 0, 1, \ldots, k^*$ are included in $\widetilde{\mathbf{O}}_\infty$, the current time instant can be labelled k again without losing lucidity. Then a rather simple optimisation problem (*scalar reference governor*)

$$\begin{gathered} \max h_k \text{ subject to} \\ (\widetilde{\mathbf{r}}_k, \mathbf{x}_k) \in \widetilde{\mathbf{O}}_\infty \text{ and} \\ h_k \in [0, 1] \end{gathered} \tag{7.12}$$

with

$$\widetilde{\mathbf{r}}_k = \widetilde{\mathbf{r}}_{k-1} + h_k \left(\mathbf{r}_k - \widetilde{\mathbf{r}}_{k-1} \right) \tag{7.13}$$

can be formulated. If no constraints are violated, h_k is one and $\widetilde{\mathbf{r}}_k = \mathbf{r}_k$ holds, meaning that the reference governor does not affect the control system. If the original reference is potentially causing a constraint violation, h_k is reduced. $h_k = 0$ is the extreme case; here the shaped reference remains constant ($\widetilde{\mathbf{r}}_k = \widetilde{\mathbf{r}}_{k-1}$). This approach is intuitive for SISO systems, but can be restrictive for MIMO systems because a single weighting parameter h_k is applied for shaping every reference. Therefore, for MIMO control systems the more general optimisation problem

$$\begin{gathered} \min \| \mathbf{r}_k - \widetilde{\mathbf{r}}_k \| \text{ subject to} \\ (\widetilde{\mathbf{r}}_k, \mathbf{x}_k) \in \widetilde{\mathbf{O}}_\infty \end{gathered} \tag{7.14}$$

can be formulated. Often the *vector reference governor* with reference update

$$\widetilde{\mathbf{r}}_k = \widetilde{\mathbf{r}}_{k-1} + \mathbf{H}_k \left(\mathbf{r}_k - \widetilde{\mathbf{r}}_{k-1} \right) \tag{7.15}$$

with $\mathbf{H}_k = \operatorname{diag}(h_{i,k})$ is chosen. The quantities $h_{i,k}$ are subjected to $0 \leq h_{i,k} \leq 1$ for $i = 1, 2, \ldots, m$ and selected to minimise the cost function $\left(\mathbf{r}_k - \widetilde{\mathbf{r}}_k \right)^\mathrm{T} \mathbf{Q} \left(\mathbf{r}_k - \widetilde{\mathbf{r}}_k \right)$ with positive definite $\mathbf{Q} = \mathbf{Q}^\mathrm{T}$ subjected to $(\widetilde{\mathbf{r}}_k, \mathbf{x}_k) \in \widetilde{\mathbf{O}}_\infty$.

If for above problems a solution for the optimisation problems exists at $k = 0$, the constraints are maintained for all k (feasibility). Furthermore, for a constant set-point $\mathbf{r}$ the command $\widetilde{\mathbf{r}}$ converges to the best approximation of $\mathbf{r}$ that satisfies the constraints in finite time [141].

7.3 Reference Governor for a Test Bed for Differential Gears

In this section a reference governor for the test bed for differentials as shown in Figure 3.24 controlled by the multivariable controller presented in Figure 7.2 is developed. In Section 5.3.1 the plant dynamics were given as

$$\frac{\mathrm{d}\omega_1}{\mathrm{d}t} = -\frac{\widetilde{c}_s \Delta\varphi}{I_{m1}} + \frac{T_{ag1,ref.}}{I_{m1}} \tag{7.16a}$$

$$\frac{d\omega_2}{dt} = \frac{i_d\widetilde{c}_s\Delta\varphi}{2I_{m2}} - \frac{T_{dsl}}{2I_{m2}} + \frac{T_{ag2,ref.}}{I_{m2}} \tag{7.16b}$$

$$\frac{d\omega_3}{dt} = \frac{i_d\widetilde{c}_s\Delta\varphi}{2I_{m3}} + \frac{T_{dsl}}{2I_{m3}} + \frac{T_{ag3,ref.}}{I_{m3}} \tag{7.16c}$$

$$\frac{d\Delta\varphi}{dt} = \omega_1 - \frac{i_d\omega_2}{2} - \frac{i_d\omega_3}{2}. \tag{7.16d}$$

In the decoupling controller the reference air-gap torques are calculated as

$$T_{ag1,ref.} = v_1 - \widetilde{d}_{s,des.}\left(\omega_1 - i_d\frac{\omega_2+\omega_3}{2}\right) + I_{m1}\frac{i_d}{2}\left(\frac{v_2}{I_{m2}} + \frac{v_3}{I_{m3}}\right) \tag{7.17a}$$

$$T_{ag2,ref.} = v_2 - \left(\frac{i_d}{2}\widetilde{c}_s\Delta\varphi - \frac{T_{dsl}}{2}\right) \tag{7.17b}$$

$$T_{ag3,ref.} = v_3 - \left(\frac{i_d}{2}\widetilde{c}_s\Delta\varphi + \frac{T_{dsl}}{2}\right); \tag{7.17c}$$

this is similar to Section 5.4.2 where a test system for differential gears with adapter gearboxes was discussed. Only the virtual control v_1 is scaled differently as in this application the reference torque is given for the differential's input and no moment of inertia or transmission ratio of an adapter gearbox must be considered.

To guarantee that actuator constraints do not affect the control performance, the reference air-gap torques must fulfil

$$-T_{ag1,max} \leq T_{ag1,ref.} \leq T_{ag1,max} \tag{7.18a}$$

$$-T_{ag2,max} \leq T_{ag2,ref.} \leq T_{ag2,max} \tag{7.18b}$$

$$-T_{ag3,max} \leq T_{ag3,ref.} \leq T_{ag3,max} \tag{7.18c}$$

at every point in time while angular velocities must satisfy

$$-\omega_{1,max} \leq \omega_1 \leq \omega_{1,max} \tag{7.19a}$$

$$-\omega_{2,max} \leq \omega_2 \leq \omega_{2,max} \tag{7.19b}$$

$$-\omega_{3,max} \leq \omega_3 \leq \omega_{3,max}. \tag{7.19c}$$

For the design of the reference governor a mathematical model for the closed-loop system is required. Combining Equation (7.16) and Equation (7.17) gives

$$\frac{d\omega_1}{dt} = \frac{v_1}{I_{m1}} - \frac{\widetilde{c}_s\Delta\varphi}{I_{m1}} - \frac{\widetilde{d}_{s,des.}}{I_{m1}}\left(\omega_1 - i_d\frac{\omega_2+\omega_3}{2}\right) + \frac{i_d}{2}\left(\frac{v_2}{I_{m2}} + \frac{v_3}{I_{m3}}\right) \tag{7.20a}$$

$$\frac{d\omega_2}{dt} = \frac{v_2}{I_{m2}} \tag{7.20b}$$

$$\frac{d\omega_3}{dt} = \frac{v_3}{I_{m3}} \tag{7.20c}$$

$$\frac{\mathrm{d}\Delta\varphi}{\mathrm{d}t} = \omega_1 - \frac{i_d\omega_2}{2} - \frac{i_d\omega_3}{2}; \tag{7.20d}$$

these are the dynamics that were specified in the decoupling process.[6] By the use of the state vector

$$\mathbf{x}_p := \begin{bmatrix}\omega_1 & \omega_2 & \omega_3 & \Delta\varphi\end{bmatrix}^{\mathrm{T}} \tag{7.21}$$

and the given sampling interval T_d, a linear discrete time system model can be determined

$$\mathbf{x}_{p,k+1} = \mathbf{A}_p\mathbf{x}_{p,k} + \mathbf{B}_p\mathbf{v}_k, \tag{7.22}$$

where the vector $\mathbf{v}$ is composed of the virtual controls v_1, v_2, and v_3.

To complete the closed-loop system model with $\tilde{\mathbf{r}}$ as system input and $\tilde{\mathbf{y}}$ as system output, the discrete time feedback controllers for the differential's input torque $T_{f1} = \tilde{c}_s\Delta\varphi$

$$v_{1,k} = k_{ff1}\tilde{r}_{1,k} + k_{p1}\left(\tilde{r}_{1,k} - \tilde{c}_s\Delta\varphi_k\right) + \lambda_{T,k} \tag{7.23a}$$

$$\lambda_{T,k+1} = \lambda_{T,k} + T_d k_{i1}\left(\tilde{r}_{1,k} - \tilde{c}_s\Delta\varphi_k\right) \tag{7.23b}$$

and the angular velocities of drives $M2$

$$v_{2,k} = k_{p2}\left(\tilde{r}_{2,k} - \omega_{2,k}\right) + \lambda_{\omega_2,k} \tag{7.24a}$$

$$\lambda_{\omega_2,k+1} = \lambda_{\omega 2,k} + T_d k_{i2}\left(\tilde{r}_{2,k} - \omega_{2,k}\right) \tag{7.24b}$$

and $M3$

$$v_{3,k} = k_{p3}\left(\tilde{r}_{3,k} - \omega_{3,k}\right) + \lambda_{\omega_3,k} \tag{7.25a}$$

$$\lambda_{\omega_3,k+1} = \lambda_{\omega 3,k} + T_d k_{i3}\left(\tilde{r}_{3,k} - \omega_{3,k}\right) \tag{7.25b}$$

are given. λ_T, λ_{ω_2}, and λ_{ω_3} are the internal state variables of the PI controllers. Based on the new extended state vector for plant and controller

$$\mathbf{x}_k := \begin{bmatrix}\omega_{1,k} & \omega_{2,k} & \omega_{3,k} & \Delta\varphi_k & \lambda_{T,k} & \lambda_{\omega_2,k} & \lambda_{\omega_3,k}\end{bmatrix}^{\mathrm{T}} \tag{7.26}$$

and the shaped reference vector $\tilde{\mathbf{r}} = [\tilde{r}_1,\ \tilde{r}_2,\ \tilde{r}_3]^{\mathrm{T}}$ the discrete time mathematical model for the closed-loop system consisting of plant and controller can be given:

$$\mathbf{x}_{k+1} = \mathbf{A}\mathbf{x}_k + \mathbf{B}\tilde{\mathbf{r}}_k \tag{7.27}$$

To be finally also able to define the closed-loop system's outputs, the manipulated variables (reference air-gap torques) that are subjected to constraints are determined

$$\tilde{y}_{1,k} = v_{1,k} - \tilde{d}_{s,des.}\left(\omega_{1,k} - i_d\frac{\omega_{2,k} + \omega_{3,k}}{2}\right) + I_{m1}\frac{i_d}{2}\left(\frac{v_{2,k}}{I_{m2}} + \frac{v_{3,k}}{I_{m3}}\right) \tag{7.28a}$$

---

[6] All controllers are implemented in discrete time; for this reason, the decoupling is realised in discrete time as well. However, as the sampling frequency is high, decoupling can be assumed to be in continuous time. Then some of the following steps are more clear.

$$\widetilde{y}_{2,k} = v_{2,k} - \left(\frac{i_d}{2}\widetilde{c}_s\Delta\varphi_k - \frac{T_{dsl,k}}{2}\right) \tag{7.28b}$$

$$\widetilde{y}_{3,k} = v_{3,k} - \left(\frac{i_d}{2}\widetilde{c}_s\Delta\varphi_k + \frac{T_{dsl,k}}{2}\right). \tag{7.28c}$$

By the use of the vector of constrained outputs $\widetilde{\mathbf{y}} = [\widetilde{y}_1,\ \widetilde{y}_2,\ \widetilde{y}_3]^{\mathrm{T}}$, these equations can be summarised to

$$\widetilde{\mathbf{y}}_k = \mathbf{C}\mathbf{x}_k + \mathbf{D}\widetilde{\mathbf{r}}_k + \mathbf{W}T_{dsl,k}. \tag{7.29}$$

The slip-limiting torque T_{dsl} only affects the constrained outputs, not the system dynamics. Therefore, considering T_{dsl} in the prediction model is not necessary. More precisely, T_{dsl} is even only relevant for the air-gap torques of *M2* and *M3*. Consequently, if the classic reference governor approach was applied, the constraints for *M2* and *M3* given by Equation (7.18) would have to be chosen more conservative such that the reference air-gap torques are within the limits for every T_{dsl} that is to be expected [141]. However, this torque margin would limit the achievable speed dynamics and the feasible testing torque significantly. Therefore, instead of the maximum slip-limiting torque only its actual value T_{dsl} is considered. For this reason, a changing slip-limiting torque can lead to constraint violations. The relevance of this aspect is investigated later in simulation.

To reduce the number of inequality constraints, the limitations regarding the angular velocities of the electric drives as given by Equation (7.19) are handled before the actual reference governor by appropriately limiting the rotational speed references. Since speed control loops are designed for good reference tracking with only little overshoot, limiting the references appropriately provides for angular velocities within the allowed range. Then at each point in time only constraints regarding the electromagnetic torques are relevant for the reference governor:

$$\underbrace{\begin{pmatrix} 1 & 0 & 0 \\ -1 & 0 & 0 \\ 0 & 1 & 0 \\ 0 & -1 & 0 \\ 0 & 0 & 1 \\ 0 & 0 & -1 \end{pmatrix}}_{=:\mathbf{S}} \widetilde{\mathbf{y}} \leq (1-\epsilon_1) \begin{pmatrix} 1 & 0 & 0 \\ -1 & 0 & 0 \\ 0 & 1 & 0 \\ 0 & -1 & 0 \\ 0 & 0 & 1 \\ 0 & 0 & -1 \end{pmatrix} \underbrace{\begin{bmatrix} T_{ag1,max} \\ T_{ag2,max} \\ T_{ag3,max} \end{bmatrix}}_{=:\mathbf{u}_{max}} \tag{7.30}$$

$\epsilon_1 \in [0, 1)$ is a small tuning parameter introduced to make the constraints slightly more restrictive so that some actuator torque reserve is available to compensate for phenomena that were not modelled. In the standard reference governor design constraints are expected to be constant; however, as shown in Figure 7.1, the available air-gap torque depends on the motor's rotational speed and is therefore slowly time-varying. Selecting $\epsilon_1 > 0$ can be beneficial to nevertheless obtain the desired behaviour of the reference governor. If the steady-state constraints are tightened by the use of the parameter $\epsilon_\infty \in (0,1)$, the number of inequalities that define the safe set $\widetilde{\mathbf{O}}_\infty$ is reduced to a finite number. By using the matrix $\mathbf{A}_\infty \in \mathbb{R}^{(6(k^*+2)\times 11)}$

$$\mathbf{A}_\infty := \begin{pmatrix} \mathbf{SC}\left(\mathbf{I}_N - \mathbf{A}\right)^{-1}\mathbf{B} + \mathbf{SD} & \mathbf{0} & \mathbf{SW} \\ \mathbf{SD} & \mathbf{SC} & \mathbf{SW} \\ \mathbf{SCB} + \mathbf{SD} & \mathbf{SCA} & \mathbf{SW} \\ \vdots & \vdots & \vdots \\ \mathbf{SCA}^{k^*-1}\mathbf{B} + \mathbf{SCA}^{k^*-2}\mathbf{B} + \cdots + \mathbf{SCB} + \mathbf{SD} & \mathbf{SCA}^{k^*} & \mathbf{SW} \end{pmatrix} \tag{7.31}$$

and matrix $\mathbf{B}_\infty \in \mathbb{R}^{(6(k^*+2)\times 3)}$

$$\mathbf{B}_\infty := (1-\epsilon_1) \begin{pmatrix} (1-\epsilon_\infty)\,\mathbf{S} \\ \mathbf{S} \\ \mathbf{S} \\ \vdots \\ \mathbf{S} \end{pmatrix}, \tag{7.32}$$

the safe set $\widetilde{\mathbf{O}}_\infty$ can be formulated similar to Equation (7.10) as

$$\widetilde{\mathbf{O}}_\infty = \left\{ \left(\widetilde{\mathbf{r}}_0, \mathbf{x}_0, T_{dsl,0}\right) : \mathbf{A}_\infty \begin{bmatrix} \widetilde{\mathbf{r}}_0 \\ \mathbf{x}_0 \\ T_{dsl,0} \end{bmatrix} \leq \mathbf{B}_\infty \mathbf{u}_{max} \right\}. \tag{7.33}$$

To reduce the number of inequality constraints in the optimisation problem, the steady-state inequalities are analysed; these are given by the first six rows of $\mathbf{A}_\infty$ and $\mathbf{B}_\infty$:

$$-\left(1-\epsilon_1\right)\left(1-\epsilon_\infty\right) T_{ag1,max} \leq \widetilde{r}_{1,k} \leq \left(1-\epsilon_1\right)\left(1-\epsilon_\infty\right) T_{ag1,max} \tag{7.34a}$$

$$-\left(1-\epsilon_1\right)\left(1-\epsilon_\infty\right) T_{ag2,max} \leq -\frac{i_d}{2}\widetilde{r}_{1,k} + \frac{1}{2}T_{dsl,k} \leq \left(1-\epsilon_1\right)\left(1-\epsilon_\infty\right) T_{ag2,max} \tag{7.34b}$$

$$-\left(1-\epsilon_1\right)\left(1-\epsilon_\infty\right) T_{ag3,max} \leq -\frac{i_d}{2}\widetilde{r}_{1,k} - \frac{1}{2}T_{dsl,k} \leq \left(1-\epsilon_1\right)\left(1-\epsilon_\infty\right) T_{ag3,max} \tag{7.34c}$$

These constraints obviously affect the reference testing torque $\widetilde{r}_1$ only. Since Conditions (7.34) are rather simple, excluding them from the actual optimisation problem can be computationally beneficial. Therefore, the reference governor is realised as a step-by-step calculation scheme as shown in Figure 7.4. In step ① the reference torque r_1 is limited to $\overline{r}_1$ according to (7.34) to meet the stationary torque limits of the three electric drives. In steps ② and ③ the rotational speed references r_2 and r_3 are limited to $\overline{r}_2$ respectively $\overline{r}_3$ according to the operating ranges of the electric drives. Then in step ④ the remaining reduced optimisation problem can be solved.

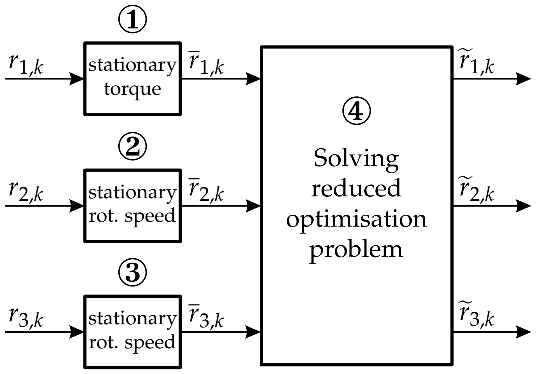

Figure 7.4: Reference governor implementation.

7.3.1 Optimisation Based Approach

As suggested in Section 7.2, the vector reference governor

$$\begin{bmatrix}\tilde{r}_{1,k}\\ \tilde{r}_{2,k}\\ \tilde{r}_{3,k}\end{bmatrix} = \begin{bmatrix}\tilde{r}_{1,k-1}\\ \tilde{r}_{2,k-1}\\ \tilde{r}_{3,k-1}\end{bmatrix} + \begin{pmatrix}h_{1,k} & 0 & 0\\ 0 & h_{2,k} & 0\\ 0 & 0 & h_{3,k}\end{pmatrix}\left(\begin{bmatrix}\bar{r}_{1,k}\\ \bar{r}_{2,k}\\ \bar{r}_{3,k}\end{bmatrix} - \begin{bmatrix}\tilde{r}_{1,k-1}\\ \tilde{r}_{2,k-1}\\ \tilde{r}_{3,k-1}\end{bmatrix}\right) \tag{7.35}$$

with $0 \leq h_{i,k} \leq 1$ for $i \in \{1,2,3\}$ is applied. Due to the fact that the inequality constraints are linear, the cost function is chosen to be a linear function too. Consequently, the optimisation problem to be solved is

$$\begin{aligned} &\min -\alpha_T h_{1,k} - \alpha_\omega h_{2,k} - \alpha_\omega h_{3,k} \text{ subject to}\\ &\tilde{\mathbf{A}}_\infty \begin{bmatrix}\tilde{\mathbf{r}}_k\\ \mathbf{x}_k\\ T_{dsl,k}\end{bmatrix} \leq \tilde{\mathbf{B}}_\infty \mathbf{u}_{max} \text{ and}\\ &0 \leq h_{i,k} \leq 1 \text{ for } i \in \{1,2,3\}, \end{aligned} \tag{7.36}$$

where by $\tilde{\mathbf{A}}_\infty$ and $\tilde{\mathbf{B}}_\infty$ the inequality constraints apart from the Steady-state criteria (7.34) are given. The constant parameters $\alpha_T > 0$ and $\alpha_\omega > 0$ are introduced to be able to modify the behaviour of the reference governor regarding the priority of either testing torque or testing rotational speed. This representation also allows the torque limit $\mathbf{u}_{max}$ to vary when the machine's rotational speed is in the field weakening region. For practical reasons, the optimisation problem must be modified for some situations. When a differential gear is tested, typically identical rotational speeds for the differential's outputs are demanded in some testing phases, while in other tests the rotational speeds of *M2* and *M3* are required to be different. This distinction should be maintained by the reference governor. Therefore, if $|\bar{r}_{2,k} - \bar{r}_{3,k}| < \mu$ and $|\tilde{r}_{2,k-1} - \tilde{r}_{3,k-1}| < \mu$, where μ is a small positive parameter, the dimension of the optimisation problem is reduced because $h_{2,k} = h_{3,k}$ is required.

Before the Optimisation problem (7.36) can be solved the state vector $\mathbf{x}$ and the slip-limiting torque T_{dsl} must be known. Within the state variables only the torsion angle $\Delta\varphi$ is unknown; the rotational speeds of the electric machines are measured and the internal controller states λ_T, λ_{ω_2}, and λ_{ω_3} are known as well. Since the torque at the input drive is measured, by $\widehat{\Delta\varphi}_k \approx {}^{T_{f1,k}}/_{\tilde{c}_s}$ an estimate for the torsion angle is available. Thus, the only remaining quantity is the friction torque T_{dsl}. This is the difference in the differential's output torques and can be estimated according to $\hat{T}_{dsl,k} \approx T_{f3,k} - T_{f2,k}$. These quantities can be low-pass filtered to increase the robustness against high frequency disturbances.

As the closed-loop system model is only an approximation of the test bed dynamics, the Optimisation problem (7.36) might be infeasible in practice. Then the inequality constraints are violated even with $\tilde{\mathbf{r}}_k = \tilde{\mathbf{r}}_{k-1}$. To avoid this situation, slack variables are introduced to soften the torque constraints if necessary. Also in situations with changing slip-limiting torque these slack variables might be required. The final optimisation problem is a linear program and can be solved e.g. by using the simplex algorithm. This optimisation might be problematic regarding real-time execution, but these restrictions are not relevant for simulation.

In Figure 7.5, Figure 7.6, and Figure 7.7 simulation results obtained by the use of the optimisation based reference governor are presented.[7] The simulation model for the test bed is identical to the system used in Section 4.4; for control the concept shown in Figure 7.2 is applied. The operating ranges of the electric drives are summarised in Table 7.1 while some other system parameters are given in Table C.1. The references for the feedback controllers are generated by the reference governor based on the original references $r_1 = T_{ref.}$, $r_2 = \omega_{2,ref.}$, and $r_3 = \omega_{3,ref.}$. These references were chosen, so that neither stationary torque limits nor rotational speed limits are violated. Furthermore, the rotational speed references were outside the

Parameter	Value	Unit
$T_{ag1,max}$	930	N m
n_{r1}	6684	rpm
$n_{1,max}$	9000	rpm
$T_{ag2,max}$, $T_{ag3,max}$	3700	N m
n_{r2}, n_{r3}	1800	rpm
$n_{2,max}$, $n_{3,max}$	6000	rpm

Table 7.1: Operating ranges of the electric drives *M1*, *M2*, and *M3* on a test bed for differential gears.

---

[7] In the following figures, as common, rotational speeds are shown instead of angular velocities.

field-weakening region. Simulation experiments including also these situations are discussed in Section 7.3.3.

In Figure 7.5 input and output signals of the reference governor are presented. In each of the three plots a single reference signal is discussed. In addition to the original references, the shaped references are shown for different reference governor settings. While the weighting parameter $\alpha_T = 1$ was kept constant, α_ω was 1 respectively 100 to demonstrate the effect of these parameters. Clearly, this setting is only relevant if in addition to $\tilde{r}_2 \neq \bar{r}_2$ or $\tilde{r}_3 \neq \bar{r}_3$ also $\tilde{r}_1 \neq \bar{r}_1$ holds. Otherwise, only torque or only rotational speed must be adjusted making the weighting parameters ineffective. In general, the higher α_ω is the faster the rotational speed references are adjusted causing the testing torque to have less priority. This is obvious at $t \approx 0.7\,\mathrm{s}$ and $t \approx 5\,\mathrm{s}$. Additionally, the influence of the prediction horizon k^* was analysed by choosing the extreme settings $k^* = 5000$ respectively $k^* = 0$. At a sampling frequency of 10 kHz the first setting implies a 0.5 s prediction while with the latter setting prediction is completely disabled. Interestingly, the

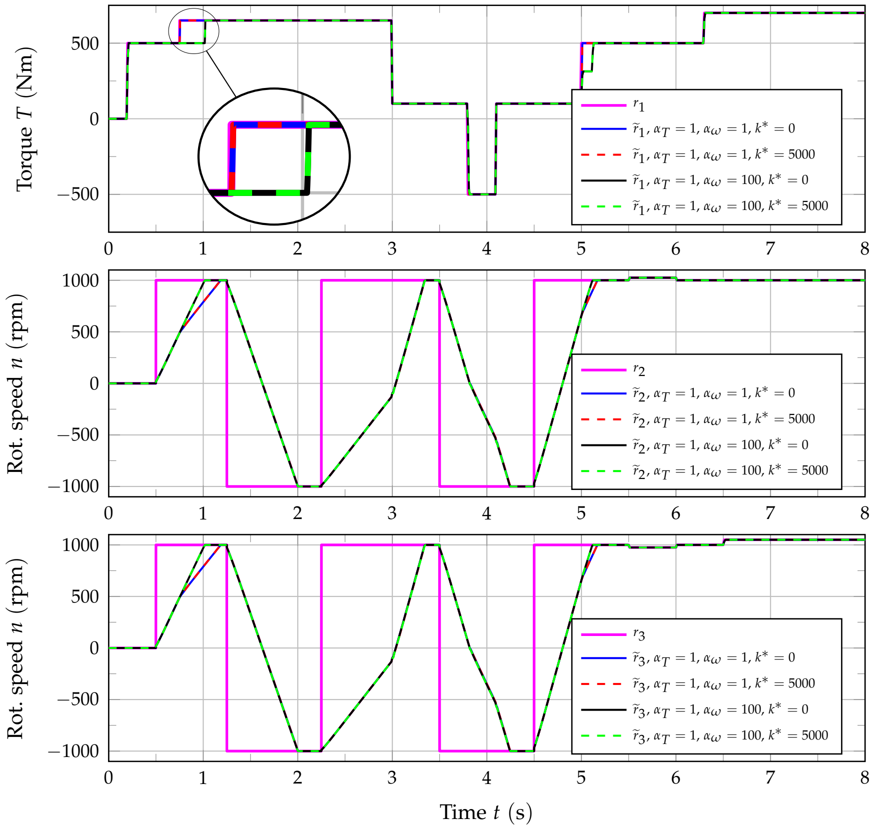

Figure 7.5: Multivariable control of a test bed for differential gears, simulation results obtained by the use of an optimisation based reference governor with varying prediction horizon k^*, constant α_T, and varying weighting parameter α_ω, shaped and original references.

effect of changing the prediction horizon is minor; in Figure 7.5 no difference in shaped references is visible. This does not hold for every conceivable control problem, but some characteristics of the test bed control scheme discussed here minimize the effect of prediction. An important factor is that the PI controllers for rotational speed are only demanding torque when a change in rotational speed is required. As soon as the set-point is reached, only some losses must be covered since the testing torque is compensated by load torque compensation. Furthermore, control loops were designed for only little overshoot, which makes it easier to handle the constraints. Finally, because of the short sampling interval, the change of the manipulated variables within one sampling interval is mostly determined by the controllers' proportional gains. This makes the dynamics of the integrating controller state less significant.

In Figure 7.6 the three manipulated variables (electromagnetic torques) are presented, again with different settings for α_ω and k^* while α_T was constant. In this figure

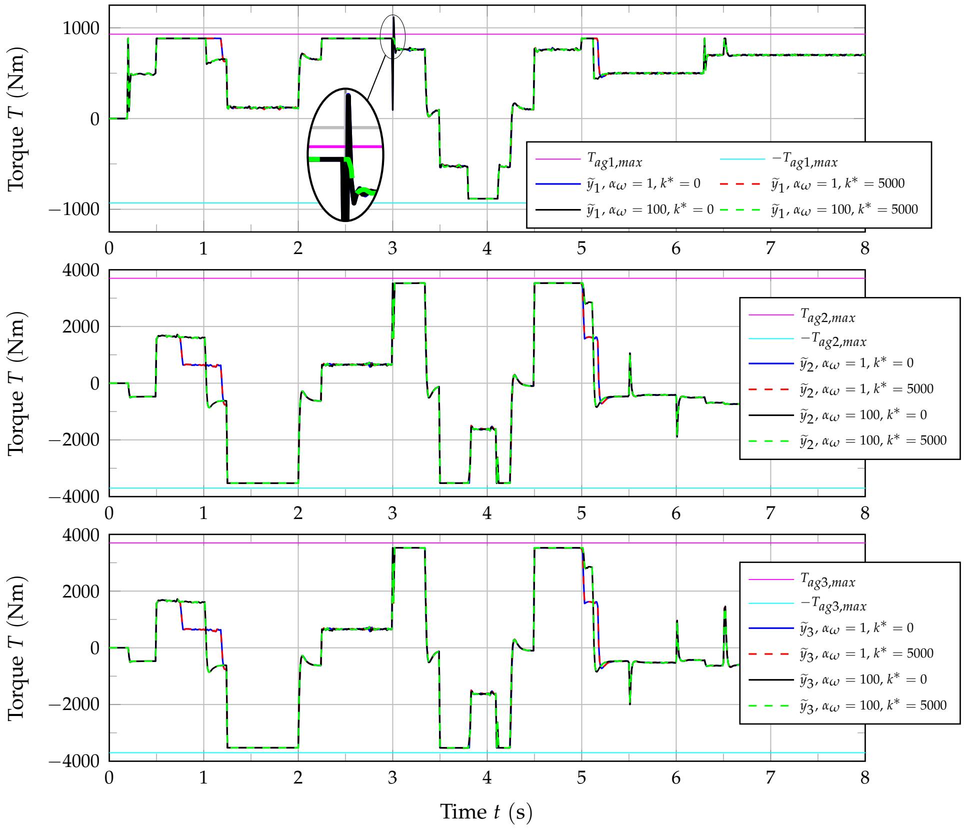

Figure 7.6: Multivariable control of a test bed for differential gears, simulation results obtained by the use of an optimisation based reference governor with varying prediction horizon k^*, constant $\alpha_T = 1$, and varying weighting parameter α_ω, manipulated variables.

the outputs of the control structure depicted in Figure 7.2 are shown without any additional limitations that would be made in the inverter control algorithm if limits were exceeded. Additionally, the plots include maximum and minimum air-gap torques. It can be seen that the constraints can be maintained in almost the entire experiment. Since the parameter for tightening the torque limits was selected as $\epsilon_1 = 0.05$, in most situations some torque reserve is left. Only with $k^* = 0$ the limits are violated at $t \approx 3\,\mathrm{s}$ for a rather short time interval.

In Figure 7.7 the controlled variables y_1, which is the testing torque at the differential's input, and $y_2 = n_2$ and $y_3 = n_3$, which are the rotational speeds of the load drives, are presented for different settings for α_ω while α_T was constant. Additionally, the shaped references $\tilde{r}_1$, $\tilde{r}_2$, and $\tilde{r}_3$ are depicted. As, according to Figure 7.5, the influence of the prediction horizon k^* on the shaped references is minor, here only results for $k^* = 0$ are shown. Figure 7.7 shows excellent reference tracking without any problematic torsional vibrations. This once more proves that the multivariable control concept proposed in this work is suitable for such applications. These simulation results show the full potential of the combination of the fast

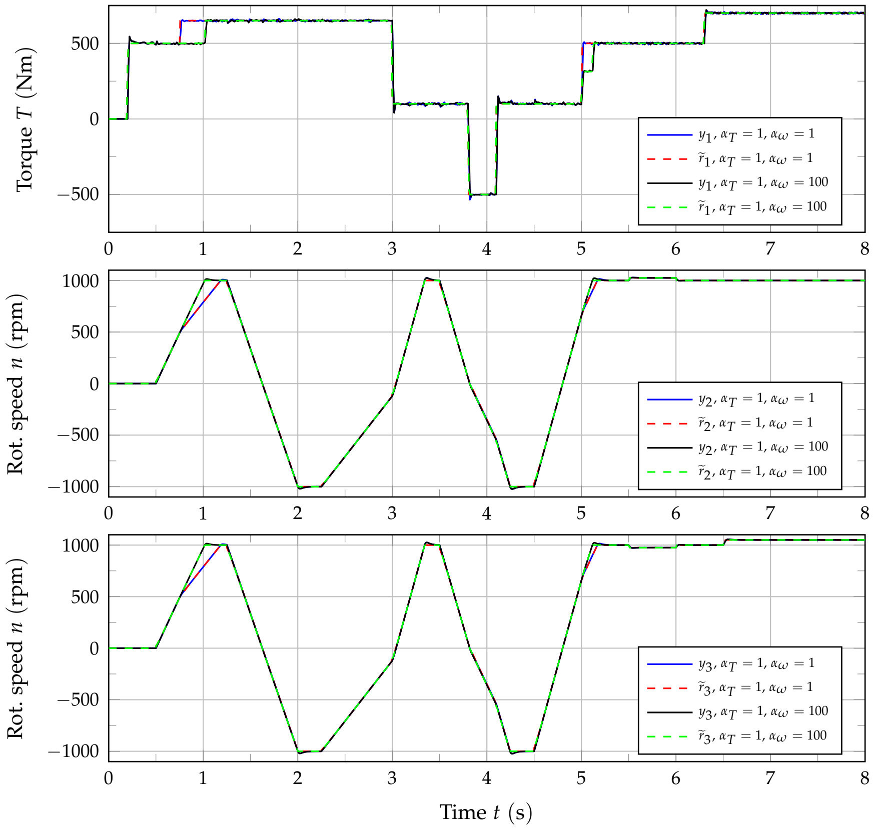

Figure 7.7: Multivariable control of a test bed for differential gears, simulation results obtained by the use of an optimisation based reference governor with prediction horizon $k^* = 0$, constant α_T, and varying weighting parameter α_ω, shaped references and controlled variables.

inverter system and the proposed control strategy. Since here no adapter gearboxes are complicating the mechanical system, the tracking performance could be further increased compared to the results discussed in Section 5.8.1. In particular the torque control performance is improved as due to the simpler mechanical system, the decoupling torque $T_{accel.}$ is more accurate and consequently decoupling is more effective.

7.3.2 Simplified Sequential Approach

Solving the Optimisation problem (7.36) with a high number of inequality constraints is computationally rather expensive. Since this calculation must be performed online, using the optimisation based reference governor in practice is unrealistic. To potentially reduce complexity, the optimisation problem is further analysed at the beginning this section. The previous simulations showed that the influence of the prediction horizon on the reference governor behaviour is minor. With $k^* = 0$ the limits of the electric drive *M1* were slightly exceeded at $t \approx 3\,\mathrm{s}$, but only for a short time instant. With $k^* = 5000$ this constraint violation can be avoided, but this comes at the cost that the number of inequality constraints is significantly higher. Therefore, in industrial practice reducing k^* is beneficial regarding implementation and execution on real-time processing hardware. Isolated constraint violations resulting from this approach can often be accepted.

If the extreme case is chosen and no prediction is performed ($k^* = 0$), the number of inequality constraints that must be taken into account at every sampling interval is significantly reduced as besides the stationary limits given by Equation (7.34), only

$$-T_{ag1,max} \leq \widetilde{y}_{1,k} \leq T_{ag1,max} \tag{7.37a}$$

$$-T_{ag2,max} \leq \widetilde{y}_{2,k} \leq T_{ag2,max} \tag{7.37b}$$

$$-T_{ag3,max} \leq \widetilde{y}_{3,k} \leq T_{ag3,max} \tag{7.37c}$$

must be maintained. Then the matrix $\widetilde{\mathbf{A}}_\infty$ defining these inequality constraints

$$\widetilde{\mathbf{A}}_\infty \begin{bmatrix} \widetilde{\mathbf{r}}_k \\ \mathbf{x}_k \\ T_{dsl,k} \end{bmatrix} \leq \widetilde{\mathbf{B}}_\infty \begin{bmatrix} T_{ag1,max} \\ T_{ag2,max} \\ T_{ag3,max} \end{bmatrix} \tag{7.38}$$

is

$$\widetilde{\mathbf{A}}_\infty = \begin{pmatrix} x & x & x & \cdots \\ x & x & x & \cdots \\ 0 & x & 0 & \cdots \\ 0 & x & 0 & \cdots \\ 0 & 0 & x & \cdots \\ 0 & 0 & x & \cdots \end{pmatrix} \begin{array}{l} \text{pos. torque limit } M1 \\ \text{neg. torque limit } M1 \\ \text{pos. torque limit } M2 \\ \text{neg. torque limit } M2 \\ \text{pos. torque limit } M3 \\ \text{neg. torque limit } M3 \end{array} \tag{7.39}$$

where x denotes an arbitrary entry. In the first two rows the constraints regarding the electric drive *M1* are given, the next two rows stand for the torque limits of *M2*, in rows five and six the constraints for the electric drive *M3* are set. The first column of $\widetilde{\mathbf{A}}_\infty$ defines the effect of the testing torque reference $\widetilde{r}_1$, the second column is responsible for $\widetilde{r}_2$ while the third column stands for $\widetilde{r}_3$. Consequently, the constraints regarding the electromagnetic torque for the input drive *M1* depend on all three references, while due to certain zeros in $\widetilde{\mathbf{A}}_\infty$ the situation for the load drives is different. The control output for *M2* does not depend on $\widetilde{r}_1$ and $\widetilde{r}_3$ and the control output for *M3* is independent of $\widetilde{r}_1$ and $\widetilde{r}_2$.

For this reason, instead of formulating a global optimisation problem the shaped references can be computed *sequentially*. This situation is presented in Figure 7.8. Under the assumption that stationary limits are already considered (steps ① – ③),

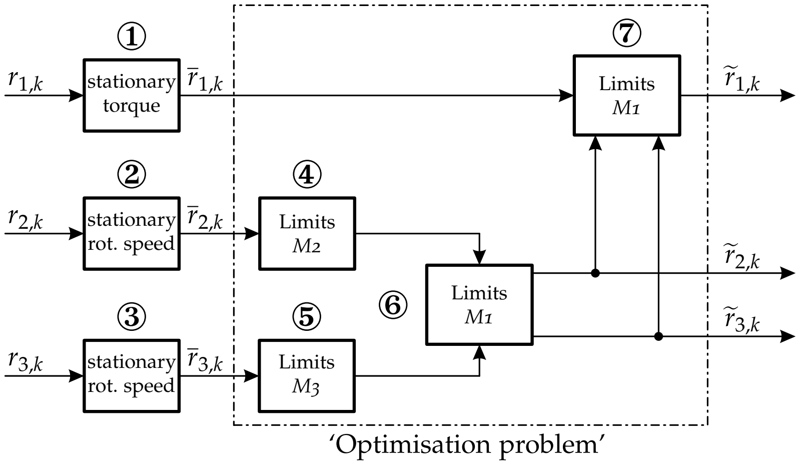

Figure 7.8: Simplified sequential reference governor approach.

in step ④ the quantity $\widetilde{r}_{2,k}$ can be chosen such that it is as close to $\bar{r}_{2,k}$ as possible while nevertheless the constraints regarding the electromagnetic torque of *M2* are met. Then in step ⑤ the same procedure can be repeated for $\widetilde{r}_{3,k}$ and the torque limits for *M3*. In step ⑥ these references may be further modified to make sure that the torque limits of *M1* are maintained; because $\widetilde{r}_{1,k}$ is not known yet, it could be assumed to remain constant ($\widetilde{r}_{1,k} = \widetilde{r}_{1,k-1}$). Finally, in step ⑦ $\widetilde{r}_{1,k}$ can be selected for already fixed $\widetilde{r}_{2,k}$ and $\widetilde{r}_{3,k}$ such that the torque limits of *M1* are met.

As the manipulated variables are directly affected by changes in the references, the reference governor can be written in an incremental form

$$\widetilde{r}_{1,k} = \widetilde{r}_{1,k-1} + \Delta\widetilde{r}_{1,k} \tag{7.40a}$$
$$\widetilde{r}_{2,k} = \widetilde{r}_{2,k-1} + \Delta\widetilde{r}_{2,k} \tag{7.40b}$$
$$\widetilde{r}_{3,k} = \widetilde{r}_{3,k-1} + \Delta\widetilde{r}_{3,k} \tag{7.40c}$$

with

$$
\begin{aligned}
0 &\leq \operatorname{sgn}\left(\bar{r}_{1,k} - \tilde{r}_{1,k-1}\right) \Delta\tilde{r}_{1,k} \leq \operatorname{sgn}\left(\bar{r}_{1,k} - \tilde{r}_{1,k-1}\right) \left(\bar{r}_{1,k} - \tilde{r}_{1,k-1}\right) && \text{(7.41a)} \\
0 &\leq \operatorname{sgn}\left(\bar{r}_{2,k} - \tilde{r}_{2,k-1}\right) \Delta\tilde{r}_{2,k} \leq \operatorname{sgn}\left(\bar{r}_{2,k} - \tilde{r}_{2,k-1}\right) \left(\bar{r}_{2,k} - \tilde{r}_{2,k-1}\right) && \text{(7.41b)} \\
0 &\leq \operatorname{sgn}\left(\bar{r}_{3,k} - \tilde{r}_{3,k-1}\right) \Delta\tilde{r}_{3,k} \leq \operatorname{sgn}\left(\bar{r}_{3,k} - \tilde{r}_{3,k-1}\right) \left(\bar{r}_{3,k} - \tilde{r}_{3,k-1}\right). && \text{(7.41c)}
\end{aligned}
$$

The underlying idea is simple; if $\Delta\tilde{r}_{i,k} = \bar{r}_{i,k} - \tilde{r}_{i,k-1}$ for $i \in \{1,2,3\}$, the references remain unmodified. However, if this would violate any constraints, these new incremental references $\Delta\tilde{r}_{i,k}$ must be appropriately restricted. Equation (7.41) guarantees that the distance between shaped and original reference cannot be increased by $\Delta\tilde{r}_{i,k}$.[8] Based on the incremental references the manipulated variables that must fulfil (7.37) are:

$$
\begin{aligned}
\tilde{y}_{1,k} = {} & \left(k_{ff1} + k_{p1}\right)\left(\tilde{r}_{1,k-1} + \Delta\tilde{r}_{1,k}\right) + \frac{i_d I_{m1}}{2I_{m2}} k_{p2}\left(\tilde{r}_{2,k-1} + \Delta\tilde{r}_{2,k}\right) + \frac{i_d I_{m1}}{2I_{m2}} \lambda_{\omega_2,k} \\
& - \frac{i_d}{2}\left(\frac{I_{m1}}{I_{m2}} k_{p2} - \tilde{d}_{s,des.}\right)\omega_{2,k} + \frac{i_d I_{m1}}{2I_{m3}} k_{p3}\left(\tilde{r}_{3,k-1} + \Delta\tilde{r}_{3,k}\right) + \frac{i_d I_{m1}}{2I_{m3}} \lambda_{\omega_3,k} \\
& - \frac{i_d}{2}\left(\frac{I_{m1}}{I_{m3}} k_{p3} - \tilde{d}_{s,des.}\right)\omega_{3,k} - \tilde{d}_{s,des.}\omega_{1,k} - k_{p1}\underbrace{\tilde{c}_s \hat{\Delta\varphi}_k}_{\approx T_{f1,k}} + \lambda_{T,k}
\end{aligned}
\tag{7.42a}
$$

$$
\tilde{y}_{2,k} = k_{p2}\left(\tilde{r}_{2,k-1} + \Delta\tilde{r}_{2,k}\right) + \lambda_{\omega_2,k} - k_{p2}\omega_{2,k} - \underbrace{\left(\frac{i_d}{2}\tilde{c}_s \hat{\Delta\varphi}_k - \frac{\hat{T}_{dsl,k}}{2}\right)}_{\approx T_{f2,k}}
\tag{7.42b}
$$

$$
\tilde{y}_{3,k} = k_{p3}\left(\tilde{r}_{3,k-1} + \Delta\tilde{r}_{3,k}\right) + \lambda_{\omega_3,k} - k_{p3}\omega_{3,k} - \underbrace{\left(\frac{i_d}{2}\tilde{c}_s \hat{\Delta\varphi}_k + \frac{\hat{T}_{dsl,k}}{2}\right)}_{\approx T_{f3,k}}
\tag{7.42c}
$$

The slip-limiting torque T_{dsl} and the torsion angle $\Delta\varphi$ must no longer be estimated because the measured shaft torques can be used directly; then also the torsional stiffness parameter $\tilde{c}_s$ is not required to be known.

As demonstrated by Equation (7.42b), $\tilde{y}_{2,k}$ only depends on $\Delta\tilde{r}_{2,k}$ and is independent of the other incremental references. Therefore, by Equation (7.37b) an upper and lower bound for $\Delta\tilde{r}_{2,k}$, which make sure that the air-gap torque limits for *M2* are met, is given. If the initial $\Delta\tilde{r}_{2,k} = \bar{r}_{2,k} - \tilde{r}_{2,k-1}$ is outside this admissible range, it is limited, see step ④ in Figure 7.9. Additionally, as $\bar{r}_{2,k} - \tilde{r}_{2,k-1} \leq 0$ in Figure 7.9, according to Equation (7.41b) also $\Delta\tilde{r}_{2,k} \leq 0$ must be ensured. The same method can be applied to select $\Delta\tilde{r}_{3,k}$ so that the limits of *M3* are maintained (step ⑤). Then, in step ⑥ the torque limits of *M1* must be checked. To do so, at first $\Delta\tilde{r}_{1,k} = 0$ is

---

[8] This situation should not occur as $\Delta\tilde{r}_{2,k} = 0$ should always be feasible; however, since by $k^* = 0$ no predictions are considered, minor constraint violations are to be expected in practice.

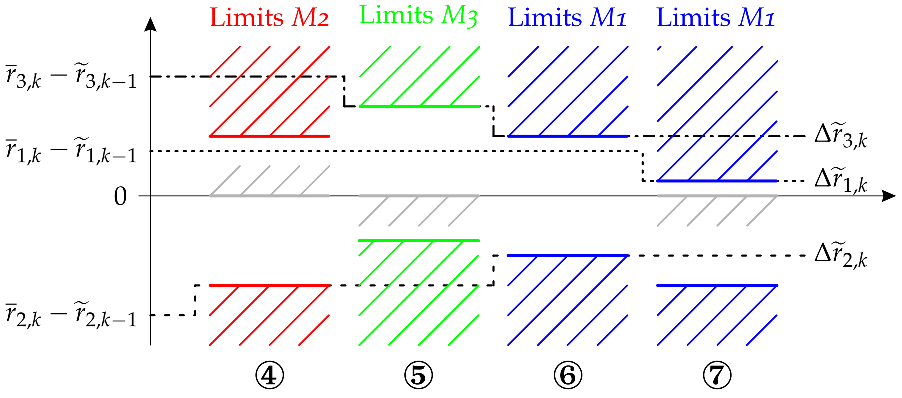
Limits *M2*
Limits *M3*
Limits *M1*
Limits *M1*
$\bar{r}_{3,k} - \tilde{r}_{3,k-1}$
$\bar{r}_{1,k} - \tilde{r}_{1,k-1}$
0
$\bar{r}_{2,k} - \tilde{r}_{2,k-1}$
$\Delta\tilde{r}_{3,k}$
$\Delta\tilde{r}_{1,k}$
$\Delta\tilde{r}_{2,k}$
④
⑤
⑥
⑦

Figure 7.9: Simplified sequential reference governor approach, detail.

assumed and $\Delta\tilde{r}_{2,k}$ and $\Delta\tilde{r}_{3,k}$ are further limited if necessary. With this strategy the available electromagnetic torque of *M1* is completely used for accelerating the electric drives for some conditions and therefore no change in testing torque is possible. For this reason, if necessary some actuator torque can be specified as a reserve to ensure a certain rate of change for the testing torque. Since $\tilde{y}_{1,k}$ depends on $\Delta\tilde{r}_{2,k}$ and $\Delta\tilde{r}_{3,k}$, maintaining the limits of *M1* is more complicated and only specifying individual bounds for these variables is not sufficient. In Figure 7.10 this situation is shown in detail. According to Equation (7.42a), selecting both

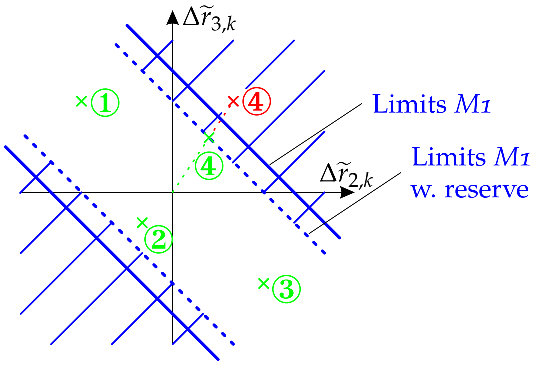
$\Delta\tilde{r}_{3,k}$
×①
×④
Limits *M1*
×
④
$\Delta\tilde{r}_{2,k}$
Limits *M1*
w. reserve
×②
×③

Figure 7.10: Reference governor simplified approach, step ⑥.

$\Delta\tilde{r}_{2,k}$ and $\Delta\tilde{r}_{3,k}$ positive increases $\tilde{y}_{1,k}$, while with different signs these effects can mutually compensate. This comes from the properties of the UUT; if one output of the differential gear is decelerated at a certain rate while the other is accelerated at the same rate, the angular velocity of the differential's input does not change. For this reason, no air-gap torque must be generated by the input drive to put decoupling into effect. This situation is shown at $t = 5.5\,\mathrm{s}$ in Figure 7.5 respectively Figure 7.6. On the contrary, at $t = 6.5\,\mathrm{s}$ the rotational speed of only one load drive is changed and as a consequence $\tilde{y}_1$ is affected too. These aspects are depicted in Figure 7.10. Three desired settings for $\Delta\tilde{r}_{2,k}$ and $\Delta\tilde{r}_{3,k}$ are feasible; these are drawn in green. Situation ④ is initially outside the limits and therefore shown in red. In the reference governor algorithm this configuration must be mapped into the admissible range. Finally, with given $\Delta\widetilde{r}_{2,k}$ and $\Delta\widetilde{r}_{3,k}$ in step ⑦ also $\Delta\widetilde{r}_{1,k}$ must be limited so that Equation (7.42a) holds.

However, due to the modified calculation scheme, different results compared to the optimisation based approach are to be expected. To analyse these differences, numerical simulations were performed. The results are presented in Figure 7.11 and Figure 7.12 and are labelled 'sequ.'. In Figure 7.11 original and shaped references are shown for the sequential calculation with prediction horizon $k^* = 0$. To be able

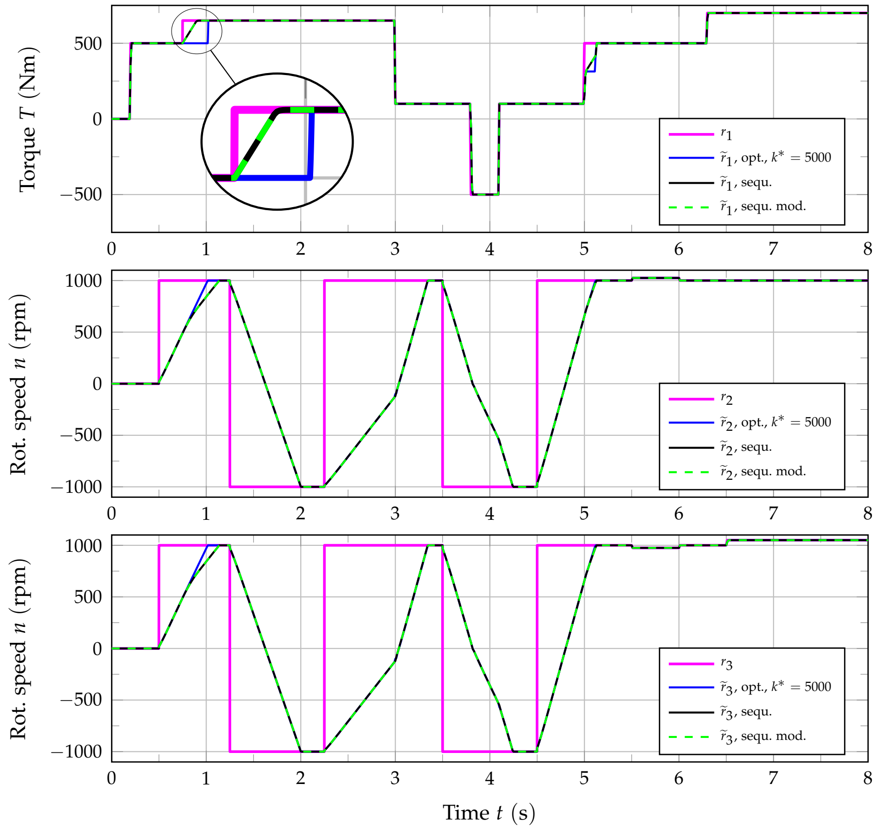

Figure 7.11: Multivariable control of a test bed for differential gears, comparative simulation results obtained by the use of a reference governor without prediction with sequential reference shaping and an optimisation based reference governor with constant parameters $\alpha_T = 1$ and $\alpha_\omega = 100$, shaped and original references.

to assess the performance, also results generated by the use of the optimisation based reference governor are depicted. These are labelled 'opt.'.As discussed in Section 7.3.1, the selection of the prediction horizon is uncritical for the optimisation based algorithm; therefore, only the results for $k^* = 5000$ are included here. In general, the results of both reference governors are very similar for most situations. Differences only occur when testing torque and rotational speeds are changed simultaneously; this is obvious at $t \approx 0.7\,\mathrm{s}$ and at $t \approx 5\,\mathrm{s}$. Since α_ω was chosen significantly higher than α_T for the optimisation based algorithm, the priority was on changing the rotational speed first. In the sequential calculation scheme according to Figure 7.8 the situation would be similar because $\Delta\widetilde{r}_{1,k}$ is determined last when $\Delta\widetilde{r}_{2,k}$ and $\Delta\widetilde{r}_{3,k}$ were already fixed. However, in the calculation algorithm a minimal rate of change for the testing torque can be selected; this parameter was chosen as $1000\,\mathrm{N\,m/s}$. For this reason, the testing torque reference is also adjusted although the priority is actually on changing testing rotational speeds.

In Figure 7.12 the three manipulated variables (electromagnetic torques) are presented, again in comparison to simulation results generated with the optimisation based approach. This figure shows a violation of the torque limits of *M1* at $t \approx 3\,\mathrm{s}$; this results from the lack of prediction. However, if the simplified reference governor calculation scheme is slightly modified so that instead of Equation (7.41) only

$$\operatorname{sgn}(\bar{r}_{1,k} - \widetilde{r}_{1,k-1})\,\Delta\widetilde{r}_{1,k} \leq \operatorname{sgn}(\bar{r}_{1,k} - \widetilde{r}_{1,k-1})\,(\bar{r}_{1,k} - \widetilde{r}_{1,k-1}) \tag{7.43a}$$

$$\operatorname{sgn}(\bar{r}_{2,k} - \widetilde{r}_{2,k-1})\,\Delta\widetilde{r}_{2,k} \leq \operatorname{sgn}(\bar{r}_{2,k} - \widetilde{r}_{2,k-1})\,(\bar{r}_{2,k} - \widetilde{r}_{2,k-1}) \tag{7.43b}$$

$$\operatorname{sgn}(\bar{r}_{3,k} - \widetilde{r}_{3,k-1})\,\Delta\widetilde{r}_{3,k} \leq \operatorname{sgn}(\bar{r}_{3,k} - \widetilde{r}_{3,k-1})\,(\bar{r}_{3,k} - \widetilde{r}_{3,k-1}) \tag{7.43c}$$

must hold, this constraint violation can be avoided. This implies that incremental references that increase the distance to the original references are allowed as well. Curves related to this approach are labelled ‘sequ. mod.’.

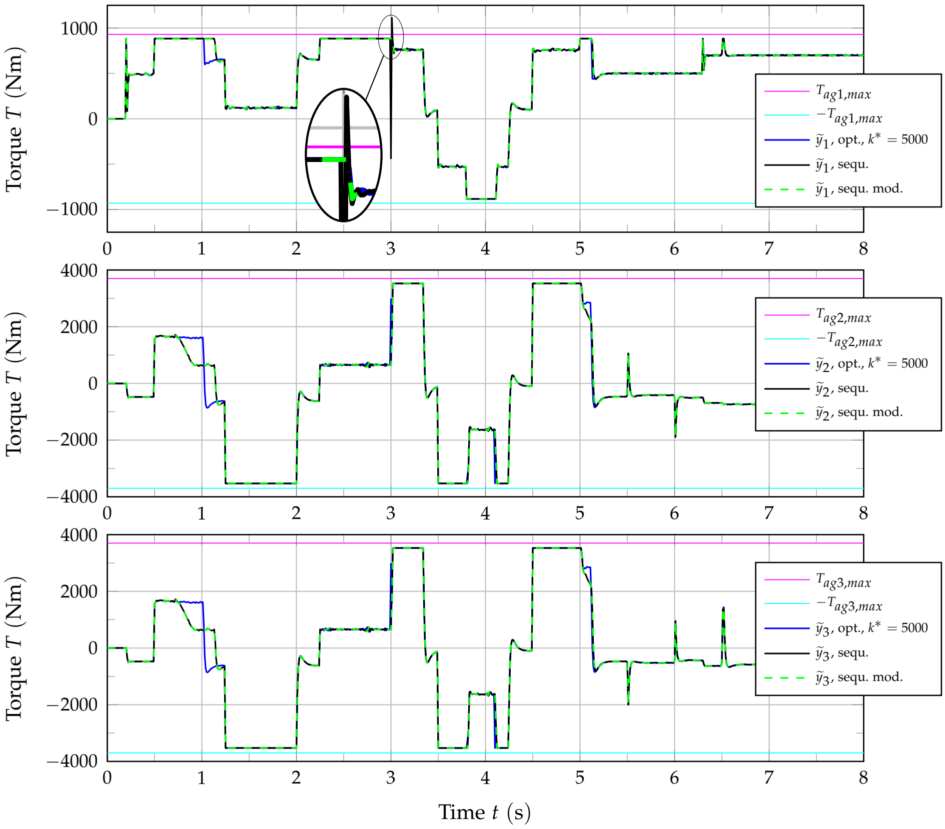

Figure 7.12: Multivariable control of a test bed for differential gears, comparative simulation results obtained by the use of a reference governor without prediction with sequential reference shaping and an optimisation based reference governor with constant parameters $\alpha_T = 1$ and $\alpha_\omega = 100$, manipulated variables.

7.3.3 Comparative Numerical Simulations with Field Weakening

In the previous sections two reference governor approaches were analysed by the use of numerical simulations. These experiments did neither include situations where the stationary torque limits are reached nor rotational speeds in the field weakening region. Here these special situations are further discussed. In Figure 7.13 shaped and original references are shown while in Figure 7.14 the manipulated variables are presented. In this figure also upper and lower limits for the electromagnetic torques are depicted; in the field-weakening range these depend on the rotational speeds of the electric drives. As all reference governor settings yield similar results, the torque limits are shown for only one experiment. In each plot the simplified reference governor discussed in Section 7.3.2 is compared to the optimisation based strategy from Section 7.3.1. In general, the results are very similar.

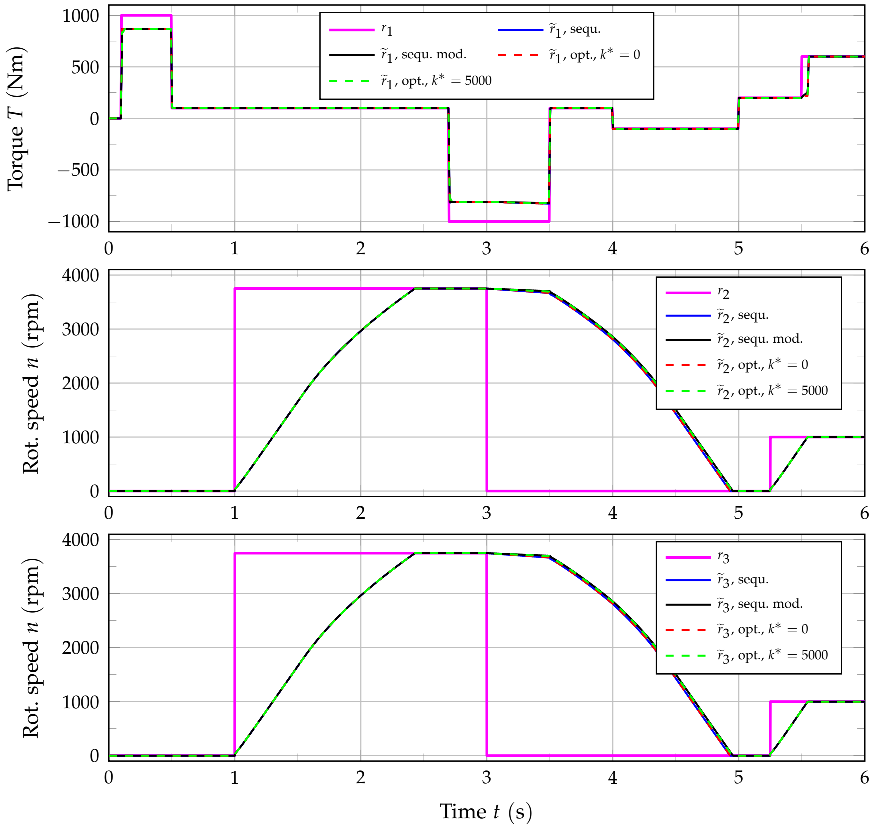

Figure 7.13: Multivariable control of a test bed for differential gears, comparative simulation results obtained by the use of the simple sequential reference shaping and an optimisation based reference governor with constant parameters $\alpha_T = 1$ and $\alpha_\omega = 100$, original and shaped references with field-weakening.

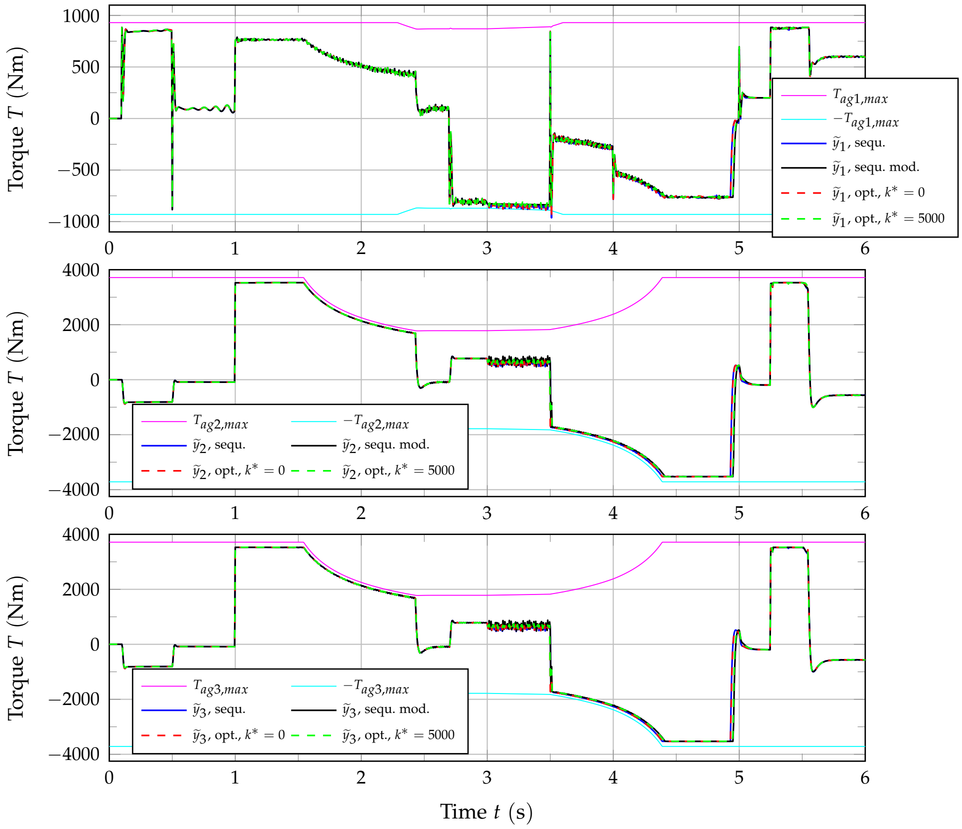

Figure 7.14: Multivariable control of a test bed for differential gears, comparative simulation results obtained by the use of the simple sequential reference shaping and an optimisation based reference governor with constant parameters $\alpha_T = 1$ and $\alpha_\omega = 100$, manipulated variables with field-weakening.

At $t \approx 0.1\,\mathrm{s}$ the reference torque is set to $1000\,\mathrm{N\,m}$, which exceeds the torque limits of *M1*. Therefore, the stationary limits are active at this point and $\tilde{r}_1$ is limited to $T_{ag1,max}\,(1-\epsilon_\infty)\,(1-\epsilon_1)$. Within the simulations these parameters for tightening the torque limits were set to $\epsilon_\infty = 0.02$ respectively $\epsilon_1 = 0.05$. After the testing torque was reduced again the rotational speed set-points are increased and the electric machines begin to accelerate. At $t \approx 1.5\,\mathrm{s}$ the rated speed of the load drives is exceeded; consequently, the available air-gap torque begins to decrease. This directly results in reduced acceleration of the load drives. At $t \approx 2.7\,\mathrm{s}$ the testing torque reference is set to $-1000\,\mathrm{N\,m}$; therefore, the stationary limits are effective again and the required testing torque cannot be reached. Beginning at $t \approx 3.0\,\mathrm{s}$ the rotational speed of the load drives should be reduced again. Since the input drive's torque capacity is already mostly used to provide the demanded testing torque, rotational speeds can only be reduced slowly. Not until the testing torque is adapted at $t \approx 3.5\,\mathrm{s}$ rotational speeds can be changed significantly.

According to Figure 7.14, also in this experiment torque limits are respected; only some insignificant violations regarding the limits of *M1* occur. These can be reduced by applying a reference shaping algorithm including prediction or by using the modification of the simplified sequential calculation scheme.

As the reference governor approach without prediction is very simple but nevertheless provides satisfying reference shaping, it is the preferable concept for practical usage. The idea of using incremental references that must be limited in certain situations is intuitive and can easily be implemented on real-time processing hardware.

Chapter 8

Conclusions and Outlook

In this work power train test systems are analysed and improved by applying a new control concept. To be able to develop new controllers, mathematical models describing the test beds are needed, for controller design as well as for assessing new strategies regarding control in numerical simulation. The term *power train test bed* is used to refer to a wide range of different testing solutions; their mechanical structure usually strongly depends on the power train configuration to be tested. As these systems are mechanically that diverse, a modular modelling approach is applied. In a first step, mathematical models are developed for the individual components typically required for testing such as electric drives, mechanical shafts, and adapter gearboxes and for the power train components to be tested such as differential gears, transmissions, or clutches. Then these individually rather simple models can be combined to finally obtain a mathematical description of the test bed behaviour that can be used for simulation. The big advantage of this approach is that these sub-models can be reused when the testing configuration is modified or when another test system should be modelled.

Performing numerical simulations with these mathematical models is complicated by the physical nature of many power train components. Their working principle is often based on using Coulomb and static friction torques to synchronise and finally lock together rotating bodies. Systems containing these types of friction are often called a variable dynamic dimension system (VDDS) as in situations when some bodies are locked, the system order is reduced. Handling this system behaviour correctly in simulation is important; therefore, one main contribution of this thesis is a suitable simulation strategy for such systems. Based on an existing concept applicable for systems with a maximum order reduction of one a friction calculation method for systems with a potential order reduction of two such as the lossy limited-slip differential gear is explicitly presented. Additionally, an extension for more complex systems with even more friction elements is outlined. This simulation strategy is implemented in the Matlab®/Simulink® software environment. Thereby, a numerically efficient simulation of the power train test beds to control is possible. This is successfully demonstrated on the basis of three different test systems. A comparison of these simulation results and measurement data from the test beds shows a good match and therefore proves that the selected modelling approach and the proposed friction simulation strategy are capable of delivering realistic results. This is important as controller testing is typically done simulation based.

Additionally, the conventional control concept for power train test systems based on independently designed speed and torque controllers is analysed in this work. It is illustrated that the interactions of speed and torque control loops can lead to poor control performance, especially if the test-run contains fast speed or torque changes. Furthermore, the presence of strong excitation means that resonant torque oscillations can be critical if the internal damping of the mechanical system is low. To overcome these problems, simplified mathematical models for two and three machine testing configurations are presented and a new multivariable control approach is developed. Simulation studies and experimental results indicate that the presented new control concept based on input–output decoupling and active oscillation damping tackles both discussed problems. The main benefits of the new controllers are the decoupling elements to reduce the interactions of speed and torque control loops and an active damping strategy capable of reducing resonant torque oscillations. This new controller is easy to implement, does not require much computing power, and is based on just a few known system parameters. A drawback of the multivariable control approach is that handling actuator constrains is more complicated. For this reason, a reference shaping pre-filter based on the reference governor approach is added to the control scheme. As the classic reference governor requires to solve an optimisation problem, a reduced representation that is executable in real-time is presented. The behaviour of different reference governor concepts is shown on the basis of closed-loop simulations of a test bed for differential gears. It turns out that for the given testing configuration a computationally significantly reduced reference governor is sufficient since its results are close to the classic optimisation based approach.

Since the field of power train testing is rather wide, this thesis had to focus on some specific testing situations and problem settings; therefore, it cannot be guaranteed that all control measures that were successfully tested in this work are applicable for other test systems as well. But the ideas presented in this thesis should be a solid foundation for handling also other testing situations. Consequently, expanding the multivariable control concept for the use on other test systems and performing more experiments on commercial test beds is an important goal for the future. Another potential research topic could be investigating other feedback controllers than the standard PI solutions. Additionally, the reference shaping pre-filters were analysed only in simulation in this thesis; therefore, a validation by experiments on some commercial test systems is planned.

Appendix

Appendix A

Fundamentals of Field-oriented Control

In the following sections the basic ideas regarding *field-oriented control (FOC)* and implicitly *induction machine (IM) modelling* are given. FOC is a variable-frequency drive control method that can be applied to control three-phase electric motors, IMs as well as permanent magnet synchronous machines (PMSMs). Here just the IM is considered, controlling and modelling a PMSM is similar. For more details and further explanations see e.g. [22, 23, 50].

A.1 Fundamental Wave Model

Instead of considering each winding and its associated physical quantities such as voltage, current, and flux linkage separately often *space vectors* are used. Those are obtained from the three-phase system by projections (*Clarke transformation*) of the form

$$\vec{i}_S^S = \begin{bmatrix} i_{S\alpha} \\ i_{S\beta} \end{bmatrix} = \frac{2}{3} \begin{pmatrix} 1 & -\frac{1}{2} & -\frac{1}{2} \\ 0 & \frac{\sqrt{3}}{2} & -\frac{\sqrt{3}}{2} \end{pmatrix} \begin{bmatrix} i_a \\ i_b \\ i_c \end{bmatrix} \tag{A.1}$$

into a stationary two-axis orthogonal reference frame.[1] The subscript 'S' denotes that this current is a stator quantity, the superscript 'S' denotes that this vector belongs to a stator fixed coordinate system. The currents i_a, i_b, and i_c are the stator phase currents, $i_{S\alpha}$ and $i_{S\beta}$ are the two components of the stator current space vector $\vec{i}_S^S$. These variables are in general time dependent; for notational convenience this time dependence is not explicitly shown. This transformation can obviously also be carried out for every other three-phase quantity. The reverse procedure (inverse Clarke transformation) is of the form

---

[1] Typically ungrounded motors with balanced three-phase currents are assumed and the transformation into only two coordinates without considering the zero component is sufficient [23].

$$\begin{bmatrix} i_a \\ i_b \\ i_c \end{bmatrix} = \begin{pmatrix} 1 & 0 \\ -\frac{1}{2} & \frac{\sqrt{3}}{2} \\ -\frac{1}{2} & -\frac{\sqrt{3}}{2} \end{pmatrix} \begin{bmatrix} i_{S\alpha} \\ i_{S\beta} \end{bmatrix}. \tag{A.2}$$

Those space vectors are often interpreted as complex numbers

$$\underline{i}_S^S = i_{S\alpha} + j i_{S\beta}. \tag{A.3}$$

Typically, three different coordinate systems or reference frames are used for modelling and control of IMs; these are shown in Figure A.1. Each space vector is defined by its two orthogonal components and the corresponding coordinate system; Figure A.1 exemplarily shows the stator current space vector $\underline{i}_S$. The stator reference frame is stationary, while the rotor reference frame is fixed to the rotor and therefore rotates at rotor speed ω when the motor has a single pole pair. If the number of pole pairs p is arbitrary, the rotor reference frame rotates at

$$\omega_e = p\omega. \tag{A.4}$$

The same relation holds for the angular alignment of the rotor reference frame

$$\varphi_e = p\varphi, \tag{A.5}$$

where φ is the angular rotor position. Henceforth, the superscript 'R' denotes the rotor reference frame. The third coordinate system is aligned with the rotor flux and rotates at synchronous speed, i.e. at the sum of ω_e and slip frequency

$$\omega_s = \frac{\mathrm{d}\rho}{\mathrm{d}t}, \tag{A.6}$$

where ρ is the slip angle. Here the superscript 'Ψ' indicates the rotating rotor flux oriented reference frame. Quantities can be transformed from one coordinate system into another via rotational operators. For transforming from (α,β) coordinates in the stator reference frame to (d,q) coordinates in the rotor flux reference frame and vice versa the so-called *Park transform*

$$\underline{i}_S^\Psi = \mathrm{e}^{-j(\rho+\varphi_e)} \underline{i}_S^S \tag{A.7}$$

and inverse Park transform

$$\underline{i}_S^S = \mathrm{e}^{j(\rho+\varphi_e)} \underline{i}_S^\Psi \tag{A.8}$$

are used. Transformations involving the rotor coordinate system are similar, see e.g. [23].

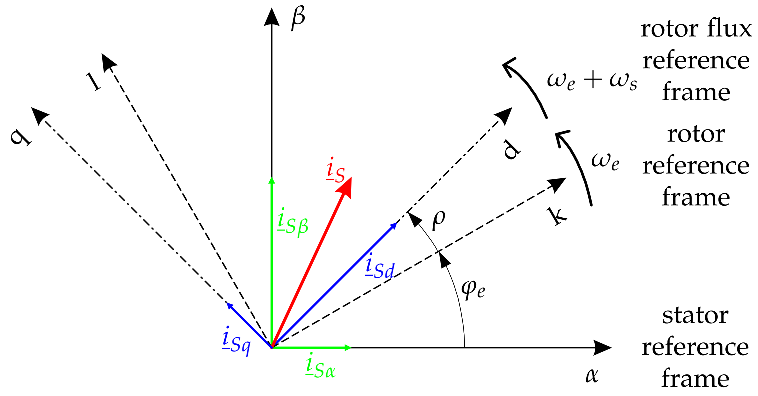

Figure A.1: Reference frames relevant for FOC of IMs.

Based on this concept consisting of a space vector representation and different coordinate systems a mathematical model of the IM can be derived. According to Kirchhoff's voltage law, the stator windings can be described in the stator fixed coordinate system by

$$\underline{u}_S^S = R_S \underline{i}_S^S + \frac{\mathrm{d}\underline{\Psi}_S^S}{\mathrm{d}t}, \tag{A.9}$$

where $\underline{u}_S^S$ is the stator voltage space vector, $\underline{\Psi}_S^S$ is the stator flux linkage space vector, and R_S is the stator resistance.[2] The rotor is typically modelled in the rotor fixed coordinate system, here a squirrel cage rotor is assumed

$$0 = R_R^{'} \underline{i}_R^R + \frac{\mathrm{d}\underline{\Psi}_R^R}{\mathrm{d}t}. \tag{A.10}$$

$\underline{i}_R^R$ is the rotor current space vector, $\underline{\Psi}_R^R$ is the rotor flux linkage space vector, and $R_R^{'}$ is the rotor resistance.[3] Transformation into the stationary stator fixed coordinate system gives

$$0 = R_R^{'} \underline{i}_R^S + \frac{\mathrm{d}\underline{\Psi}_R^S}{\mathrm{d}t} - j\omega_e \underline{\Psi}_R^S. \tag{A.11}$$

To link currents and magnetic fluxes, the flux linkage space vector for stator

$$\underline{\Psi}_S^S = L_S \underline{i}_S^S + L_m \underline{i}_R^S \tag{A.12}$$

and rotor

$$\underline{\Psi}_R^S = L_m \underline{i}_S^S + L_R \underline{i}_R^S \tag{A.13}$$

can be defined. The quantities stator inductance L_S

$$L_S := L_{\sigma S} + L_m \tag{A.14}$$

---

[2] Symmetric phase windings with identical parameters such as resistance and inductance are assumed.

[3] The apostrophe marks equivalent circuit parameters that were transformed from the rotor to the stator [23].

and rotor inductance L_R

$$L_R := L'_{\sigma R} + L_m \tag{A.15}$$

can be calculated base on the mutual inductance L_m and the leakage inductances $L_{\sigma S}$ and $L'_{\sigma R}$ for stator respectively rotor. Combining above equations gives a system of equations describing the behaviour of the electrical subsystem of the IM in the stationary stator fixed coordinate system.

$$\boxed{\begin{aligned} \frac{\mathrm{d}\underline{\Psi}_S^S}{\mathrm{d}t} &= -R_S \underline{i}_S^S + \underline{u}_S^S \\ \frac{\mathrm{d}\underline{\Psi}_R^S}{\mathrm{d}t} &= -R'_R \underline{i}_R^S + j\omega_e \underline{\Psi}_R^S \\ \underline{i}_S^S &= \frac{1}{L_S L_R - L_m^2} \left(L_R \underline{\Psi}_S^S - L_m \underline{\Psi}_R^S \right) \\ \underline{i}_R^S &= \frac{1}{L_S L_R - L_m^2} \left(-L_m \underline{\Psi}_S^S + L_S \underline{\Psi}_R^S \right) \end{aligned}} \tag{A.16}$$

The system inputs are the stator voltage space vector $\underline{u}_S$ and the rotor's angular velocity ω while the most important system output is the electromagnetic air-gap torque

$$T_{ag} = \frac{3}{2} p \,\mathrm{Im}\left\{ \underline{\Psi}_S^{S*} \underline{i}_S^S \right\}, \tag{A.17}$$

where $\underline{\Psi}_S^{S*}$ is the conjugate complex stator flux linkage space vector. The mechanical subsystem can be described by Newton's differential equation of motion.

A.2 Rotor Flux Oriented Reference Frame

Above equations are often used within numerical simulations of IMs; FOC however is traditionally directly related to a *rotor flux oriented reference frame*, see Figure A.1. All the space vectors for voltage, current, and magnetic flux can be transformed from the stationary stator reference frame into a rotating rotor flux oriented reference frame. This transformation is often called *dq-transformation* as it leads to a (d,q) coordinate system with orthogonal components along d (direct) and q (quadrature) axis. A typical electrical quantity in this reference frame is consequently composed of a d- and q-component

$$\underline{i}_S^\Psi = i_{Sd} + j i_{Sq}. \tag{A.18}$$

Only the rotor flux space vector has due to the special choice of the reference frame just a d-component

$$\underline{\Psi}_R^\Psi = \Psi_{Rd} + j0. \tag{A.19}$$

Transforming Equation (A.11) into (d,q) coordinates results in the following differential equation describing the rotor circuit:

$$0 = \frac{R_R'}{L_R}\left(\underline{\Psi}_R^\Psi - L_m \underline{i}_S^\Psi\right) + \frac{\mathrm{d}\underline{\Psi}_R^\Psi}{\mathrm{d}t} + j\omega_s \underline{\Psi}_R^\Psi \tag{A.20}$$

Typically d- and q-component or when working with complex numbers real and imaginary part of Equation (A.20) are treated separately:

$$\text{Re}: \quad \frac{\mathrm{d}\Psi_{Rd}}{\mathrm{d}t} = \frac{R_R'}{L_R}\left(L_m i_{Sd} - \Psi_{Rd}\right) \tag{A.21a}$$

$$\text{Im}: \quad \frac{\mathrm{d}\rho}{\mathrm{d}t} = \omega_s = \frac{R_R' L_m i_{Sq}}{L_R \Psi_{Rd}} \tag{A.21b}$$

It becomes obvious that the rotor flux $\underline{\Psi}_R$ can be controlled by the d-component i_{Sd} of the stator current while it is independent of i_{Sq}. The electromagnetic air-gap torque T_{ag} is given by

$$T_{ag} = \frac{3}{2} p \frac{L_m}{L_R} \Psi_{Rd} i_{Sq} \tag{A.22}$$

and can obviously be controlled by the q-component i_{Sq} of the stator current. This represents the basic idea of FOC: one stator current component is used to define the magnetic flux while the other can be used to set the torque. Also Equation (A.9) describing the stator circuit can be transformed from the stationary stator reference frame into rotor flux oriented coordinates

$$\underline{u}_S^\Psi = R_S \underline{i}_S^\Psi + j\left(\omega_s + \omega_e\right)\left(L_\sigma \underline{i}_S^\Psi + \frac{L_m}{L_R}\underline{\Psi}_R^\Psi\right) + L_\sigma \frac{\mathrm{d}\underline{i}_S^\Psi}{\mathrm{d}t} + \frac{L_m}{L_R}\frac{\mathrm{d}\underline{\Psi}_R^\Psi}{\mathrm{d}t}. \tag{A.23}$$

L_σ is the leakage inductance and can be calculated according to

$$L_\sigma := \frac{L_S L_R - L_m^2}{L_R}. \tag{A.24}$$

When Equation (A.23) is separated into d- and q-component or real and imaginary part,

$$\text{Re}: \quad u_{Sd} = R_S i_{Sd} + L_\sigma \frac{\mathrm{d}i_{Sd}}{\mathrm{d}t} - \left(\omega_s + \omega_e\right) L_\sigma i_{Sq} + \left(\frac{L_m}{L_R}\right)^2 R_R' \left(i_{Sd} - \frac{\Psi_{Rd}}{L_m}\right) \tag{A.25a}$$

$$\text{Im}: \quad u_{Sq} = R_S i_{Sq} + L_\sigma \frac{\mathrm{d}i_{Sq}}{\mathrm{d}t} + \left(\omega_s + \omega_e\right)\left(L_\sigma i_{Sd} + \frac{L_m}{L_R}\Psi_{Rd}\right) \tag{A.25b}$$

results. If the slip frequency ω_s is substituted according to Equation (A.21b) and ω_e is replaced according to Equation (A.4), the two differential equations

$$u_{Sd} = R_S i_{Sd} + L_\sigma \frac{\mathrm{d}i_{Sd}}{\mathrm{d}t} - \left(\frac{R_R' L_m i_{Sq}}{L_R \Psi_{Rd}} + p\omega\right) L_\sigma i_{Sq} + \left(\frac{L_m}{L_R}\right)^2 R_R' \left(i_{Sd} - \frac{\Psi_{Rd}}{L_m}\right) \tag{A.26a}$$

$$u_{Sq} = R_S i_{Sq} + L_\sigma \frac{\mathrm{d}i_{Sq}}{\mathrm{d}t} + \left(\frac{R_R' L_m i_{Sq}}{L_R \Psi_{Rd}} + p\omega \right) \left(L_\sigma i_{Sd} + \frac{L_m}{L_R} \Psi_{Rd} \right) \tag{A.26b}$$

relevant for current control can be obtained. The stator voltage $\underline{u}_S$ is the control input. Typically, before feedback current controllers are designed cross coupling terms and non-linearities are compensated. Therefore, both components of the stator voltage space vector are composed of one part for compensation ($u_{Sd,comp.}$ and $u_{Sq,comp.}$) and another part for control ($u_{Sd,cont.}$ and $u_{Sq,cont.}$):

$$u_{Sd} = u_{Sd,comp.} + u_{Sd,cont.} \tag{A.27a}$$

$$u_{Sq} = u_{Sq,comp.} + u_{Sq,cont.} \tag{A.27b}$$

If those compensation terms are chosen as

$$u_{Sd,comp.} = -\left(\frac{R_R' L_m i_{Sq}}{L_R \Psi_{Rd}} + p\omega \right) L_\sigma i_{Sq} + \left(\frac{L_m}{L_R} \right)^2 R_R' \left(i_{Sd} - \frac{\Psi_{Rd}}{L_m} \right) \tag{A.28a}$$

$$u_{Sq,comp.} = \left(\frac{R_R' L_m i_{Sq}}{L_R \Psi_{Rd}} + p\omega \right) \left(L_\sigma i_{Sd} + \frac{L_m}{L_R} \Psi_{Rd} \right), \tag{A.28b}$$

the control task is reduced to controlling two identical linear first-order dynamic systems:

$$u_{Sd,cont.} = R_S i_{Sd} + L_\sigma \frac{\mathrm{d}i_{Sd}}{\mathrm{d}t} \tag{A.29a}$$

$$u_{Sq,cont.} = R_S i_{Sq} + L_\sigma \frac{\mathrm{d}i_{Sq}}{\mathrm{d}t} \tag{A.29b}$$

Concluding this section, in System (A.30) the equations relevant for control are summarised:

$$\boxed{\begin{aligned} \frac{\mathrm{d}i_{Sd}}{\mathrm{d}t} &= \frac{1}{L_\sigma} \left(u_{Sd,cont.} - R_S i_{Sd} \right) \\ \frac{\mathrm{d}i_{Sq}}{\mathrm{d}t} &= \frac{1}{L_\sigma} \left(u_{Sq,cont.} - R_S i_{Sq} \right) \\ \frac{\mathrm{d}\Psi_{Rd}}{\mathrm{d}t} &= \frac{R_R'}{L_R} \left(L_m i_{Sd} - \Psi_{Rd} \right) \\ \frac{\mathrm{d}\rho}{\mathrm{d}t} &= \frac{R_R' L_m i_{Sq}}{L_R \Psi_{Rd}} \\ T_{ag} &= \frac{3}{2} p \frac{L_m}{L_R} \Psi_{Rd} i_{Sq} \end{aligned}} \tag{A.30}$$

A.3 Field-oriented Control

In Figure A.2 a block diagram of the cascaded control concept used within FOC for IMs is presented. The IM and the output stage of the inverter represent the plant while the remaining blocks belong to the control scheme. Usually, control is realised on a digital signal processor system; as a consequence, the control implementation is in discrete time. All the controllers act in the rotating rotor flux oriented reference frame and are designed for the plant given by (A.30). Control is based on measurements of the stator phase currents and the machine's rotational speed. The phase currents are transformed into (d,q) coordinates by the subsequent use of Transformation (A.1) and an additional rotation according to Equation (A.7) based on the angle φ_e (angular rotor position multiplied by the number of pole pairs) and the slip angle ρ estimated in the previous sampling interval. Then the rotor flux Ψ_{Rd} and slip angle ρ are obtained by the use of an observer utilising Equation (A.21a) and Equation (A.21b). There are many strategies for estimating these quantities available, see e.g. [50]; direct measurement is rarely applied for practical reasons. Based on the estimated rotor flux and the given rotor flux reference the rotor flux controller, frequently a PI controller, can be calculated resulting in the desired d-component of the stator current. The rotor flux reference is usually not altered from outside the inverter system but chosen internally, typically as a constant for lower rotational speeds and as a decreasing function of rotational speed for higher rotational speeds (field weakening). Additionally, the needed q-component of the stator current can be determined by the use of Equation (A.22) for the given torque reference.[4] Due to limitations regarding the inverter, not every

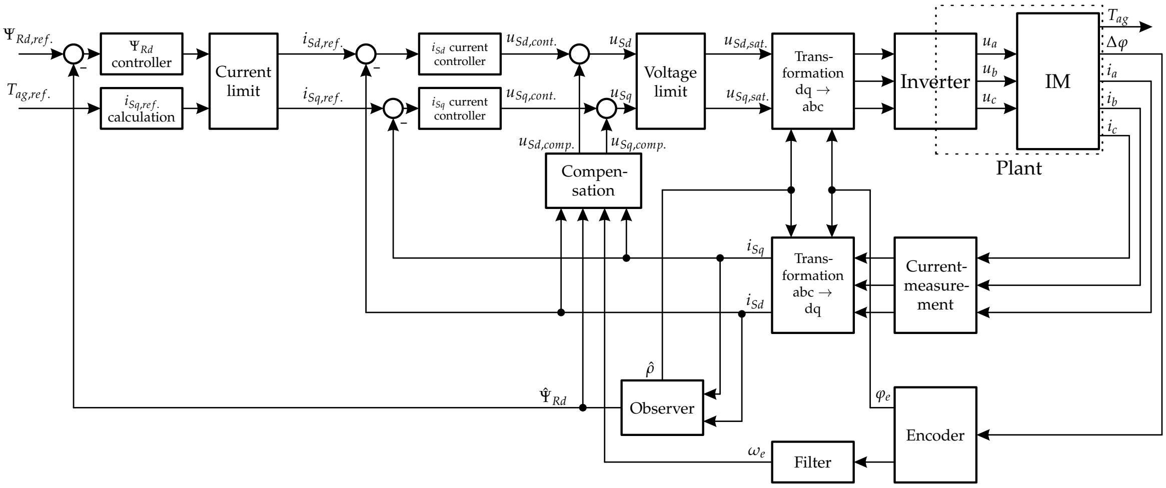
$\Psi_{Rd,ref.}$
$T_{ag,ref.}$
Ψ_{Rd} controller
$i_{Sq,ref.}$ calculation
Current limit
$i_{Sd,ref.}$
$i_{Sq,ref.}$
i_{Sd} current controller
i_{Sq} current controller
$u_{Sd,cont.}$
$u_{Sq,cont.}$
u_{Sd}
u_{Sq}
Voltage limit
$u_{Sd,sat.}$
$u_{Sq,sat.}$
Trans-formation dq → abc
Inverter
u_a
u_b
u_c
IM
T_{ag}
$\Delta\varphi$
i_a
i_b
i_c
Plant
$u_{Sd,comp.}$
$u_{Sq,comp.}$
Compen-sation
i_{Sq}
i_{Sd}
Trans-formation abc → dq
Current-measure-ment
$\hat{\rho}$
$\hat{\Psi}_{Rd}$
Observer
φ_e
Encoder
ω_e
Filter
−

Figure A.2: FOC of IMs, control concept.

---

[4] For FOC the desired air-gap torque is the relevant reference quantity; if speed control is demanded, an additional control loop is added to determine this quantity based on the rotational speed reference and the measured motor speed.

desired stator current space vector can be realised. As the length of the current space vector has to be restricted to $I_{S,max}$,

$$\sqrt{i^2_{Sd,ref.} + i^2_{Sq,ref.}} \leq I_{S,max} \tag{A.31}$$

must hold. Therefore, in the 'Current limit' block the references for d- and q-component both have to be considered simultaneously.

Then the current controllers (typically PI) for d- and q-component of the stator current can be calculated. To finally obtain the desired stator voltage space vector, the terms for compensating cross couplings and non-linearities (Equation (A.28a) and Equation (A.28b)) have to be added. Depending on the given DC-link voltage the length of the stator voltage space vector is limited inherently to $U_{S,max}$. For this reason, the calculated stator voltage vector should be truncated within the control algorithm so that

$$\sqrt{u^2_{Sd} + u^2_{Sq}} \leq U_{S,max} \tag{A.32}$$

holds; as again the vector length is relevant, d- and q-component both have to be considered simultaneously. The resulting voltage space vector is then transformed into (a,b,c) coordinates. Finally, the semiconductors in the inverter are actuated based on a pulse-width modulation strategy.

Appendix B

Combination of Mechanical Shafts

When complex mechanical systems such as the driveline test rigs discussed in this work must be modelled, often the necessity of *reducing the complexity* of the mathematical models describing the system dynamics arises. Typically, systems with distributed parameters are reduced to lumped systems consisting of concentrated elements such as moments of inertias and inertia-free torsionally flexible shafts. If, for instance for model based controller design, further simplifications are desired, certain initially separate discrete elements have to be combined. This process is demonstrated for the three-mass oscillator shown in Figure B.1. This three-mass oscillator might represent the mechanics of a test bed for transmissions as shown in Figure 3.2. Then I_1 and I_2 are the moments of inertia of input drive and load drive while I_3 is the moment of inertia of the UUT. c_{s1} and d_{s1} are the parameters of the input shaft; c_{s2} and d_{s2} are torsional stiffness respectively damping coefficient of shaft 2 at the transmission's output. The moment of inertia of the electric drives is often significantly bigger than the moment of inertia of the UUT. Therefore, $I_3 \rightarrow 0$ can be assumed and the mechanical system is reduced to the structure shown in Figure B.2. Here a two-mass oscillator where the two masses are connected by

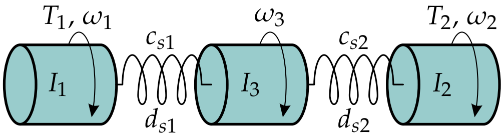

Figure B.1: Three-mass oscillator.

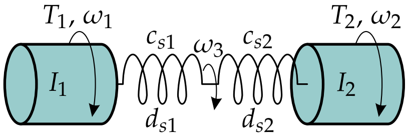

Figure B.2: Three-mass oscillator with $I_3 \rightarrow 0$.

two elastic shafts is shown. To simplify even further, these two torsionally flexible shafts with parameters c_{s1}, d_{s1}, c_{s2}, and d_{s2} should be replaced by one shaft element with equivalent parameters for torsional stiffness $\widetilde{c}_s$ and damping $\widetilde{d}_s$. This minimal mechanical system structure is presented in Figure B.3. The two equivalent shaft parameters shall be determined in this section. However, as will be shown, this system reduction from Figure B.2 to Figure B.3 can only be performed without any change of system dynamics for special parameter settings.

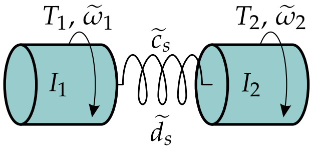

Figure B.3: Two-mass oscillator.

For the mechanical structure presented in Figure B.1 the rotational dynamics of the inertias I_1, I_2, and I_3 are given by

$$I_1 \frac{\mathrm{d}\omega_1}{\mathrm{d}t} = T_1 - T_{s1} \tag{B.1a}$$

$$I_2 \frac{\mathrm{d}\omega_2}{\mathrm{d}t} = T_2 + T_{s2} \tag{B.1b}$$

$$I_3 \frac{\mathrm{d}\omega_3}{\mathrm{d}t} = T_{s1} - T_{s2} \tag{B.1c}$$

$$\frac{\mathrm{d}\varphi_i}{\mathrm{d}t} = \omega_i \text{ for } i \in \{1,2,3\} \tag{B.1d}$$

with shaft torques

$$T_{s1} = d_{s1}(\omega_1 - \omega_3) + c_{s1}(\varphi_1 - \varphi_3) \tag{B.2a}$$

$$T_{s2} = d_{s2}(\omega_3 - \omega_2) + c_{s2}(\varphi_3 - \varphi_2)\,. \tag{B.2b}$$

If $I_3 \to 0$ is assumed, the torque transmitted along both shafts must be identical:

$$d_{s1}(\omega_1 - \omega_3) + c_{s1}(\varphi_1 - \varphi_3) = d_{s2}(\omega_3 - \omega_2) + c_{s2}(\varphi_3 - \varphi_2) \tag{B.3}$$

Equation (B.3) can be used to describe the rotational behaviour of the point where in Figure B.2 the two shafts meet. This balance of torques must also hold in a differential form

$$\frac{\mathrm{d}}{\mathrm{d}t}\left[d_{s1}(\omega_1 - \omega_3) + c_{s1}(\varphi_1 - \varphi_3)\right] = \frac{\mathrm{d}}{\mathrm{d}t}\left[d_{s2}(\omega_3 - \omega_2) + c_{s2}(\varphi_3 - \varphi_2)\right]. \tag{B.4}$$

Since system parameters are assumed to be constant,

$$d_{s1}\left(\frac{\mathrm{d}\omega_1}{\mathrm{d}t} - \frac{\mathrm{d}\omega_3}{\mathrm{d}t}\right) + c_{s1}(\omega_1 - \omega_3) = d_{s2}\left(\frac{\mathrm{d}\omega_3}{\mathrm{d}t} - \frac{\mathrm{d}\omega_2}{\mathrm{d}t}\right) + c_{s2}(\omega_3 - \omega_2) \tag{B.5}$$

is equivalent to Equation (B.4). From these equations a differential equation for ω_3 results:

$$(d_{s1}+d_{s2})\frac{\mathrm{d}\omega_3}{\mathrm{d}t} = \left(c_{s1}-\frac{d_{s1}^2}{I_1}\right)\omega_1 + \left(c_{s2}-\frac{d_{s2}^2}{I_2}\right)\omega_2 + \left(\frac{d_{s1}^2}{I_1}+\frac{d_{s2}^2}{I_2}-c_{s1}-c_{s2}\right)\omega_3 - \frac{c_{s1}d_{s1}}{I_1}\varphi_1 - \frac{c_{s2}d_{s2}}{I_2}\varphi_2 + \left(\frac{c_{s1}d_{s1}}{I_1}+\frac{c_{s2}d_{s2}}{I_2}\right)\varphi_3 + \frac{d_{s1}}{I_1}T_1 + \frac{d_{s2}}{I_2}T_2 \tag{B.6}$$

As Equation (B.6) is a differential equation, the mechanical system shown in Figure B.2 can not always be replaced by the simple two-mass oscillator. However, there are parameter settings where the two elastic shafts can be combined without any affect on system dynamics. This is the case when the angular velocity ω_3 is a linear combination of the angular velocities ω_1 and ω_2. If for instance the damping parameters of both shafts are zero ($d_{s1} = d_{s2} = 0$), Equation (B.3) gives

$$c_{s1}\left(\varphi_1-\varphi_3\right) = c_{s2}\left(\varphi_3-\varphi_2\right) \tag{B.7}$$

while Equation (B.5) results in

$$c_{s1}\left(\omega_1-\omega_3\right) = c_{s2}\left(\omega_3-\omega_2\right). \tag{B.8}$$

Consequently, the quantities φ_3 and ω_3 are

$$\varphi_3 = \frac{c_{s1}\varphi_1 + c_{s2}\varphi_2}{c_{s1}+c_{s2}} \tag{B.9a}$$

$$\omega_3 = \frac{c_{s1}\omega_1 + c_{s2}\omega_2}{c_{s1}+c_{s2}} \tag{B.9b}$$

with ${}^{\mathrm{d}\varphi_i}/_{\mathrm{d}t} = \omega_i$ for $i \in \{1,2,3\}$ being fulfilled as well. Then the shaft torque is

$$T_{s1} = T_{s2} = c_{s1}\left(\varphi_1 - \frac{c_{s1}\varphi_1 + c_{s2}\varphi_2}{c_{s1}+c_{s2}}\right) = \frac{c_{s1}c_{s2}}{c_{s1}+c_{s2}}\left(\varphi_1-\varphi_2\right) \tag{B.10}$$

and the equivalent shaft parameters for the two-mass oscillator are

$$\widetilde{d}_s = 0 \qquad \widetilde{c}_s = \frac{c_{s1}c_{s2}}{c_{s1}+c_{s2}}. \tag{B.11}$$

If the shaft's damping parameters are non-zero, only the parameter setting

$$\frac{c_{s1}}{c_{s2}} = \frac{d_{s1}}{d_{s2}} \tag{B.12}$$

results in

$$\varphi_3 = \frac{c_{s1}\varphi_1 + c_{s2}\varphi_2}{c_{s1}+c_{s2}} \tag{B.13a}$$

$$\omega_3 = \frac{d_{s1}\omega_1 + d_{s2}\omega_2}{d_{s1} + d_{s2}} \tag{B.13b}$$

where ${}^{\mathrm{d}\varphi_i}/_{\mathrm{d}t} = \omega_i$ for $i \in \{1, 2, 3\}$ is also fulfilled. Consequently, the shaft torque is

$$\begin{aligned} T_{s1} = T_{s2} &= d_{s1}\left(\omega_1 - \frac{d_{s1}\omega_1 + d_{s2}\omega_2}{d_{s1} + d_{s2}}\right) + c_{s1}\left(\varphi_1 - \frac{c_{s1}\varphi_1 + c_{s2}\varphi_2}{c_{s1} + c_{s2}}\right) \\ T_{s1} = T_{s2} &= \frac{d_{s1}d_{s2}}{d_{s1} + d_{s2}}\left(\omega_1 - \omega_2\right) + \frac{c_{s1}c_{s2}}{c_{s1} + c_{s2}}\left(\varphi_1 - \varphi_2\right) \end{aligned} \tag{B.14}$$

and the equivalent shaft parameters for the two-mass oscillator are

$$\widetilde{d}_s = \frac{d_{s1}d_{s2}}{d_{s1} + d_{s2}} \qquad \widetilde{c}_s = \frac{c_{s1}c_{s2}}{c_{s1} + c_{s2}}. \tag{B.15}$$

With these two special parameter settings the dynamics of the angular velocity ω_3 as given by Equation (B.6) does not depend on ω_3 and φ_3 and therefore these state variables are not required to describe the system dynamics. Consequently, the simple two-mass oscillator can be used instead without changing the system dynamics. If at least one of the damping parameters d_{s1} respectively d_{s2} is non-zero[1] and Equation (B.12) does not hold, this simplification of using a two-mass oscillator containing only one elastic shaft is not exact for any parameters $\widetilde{d}_s$ and $\widetilde{c}_s$. To nevertheless determine equivalent shaft parameters so that at least a good approximation can be achieved, a state-space representation of the mechanical system shown in Figure B.2 is desired. With the state vector

$$\mathbf{x} := \begin{bmatrix}\omega_1 & \omega_2 & \omega_3 & \varphi_1 & \varphi_2 & \varphi_3\end{bmatrix}^{\mathrm{T}} \tag{B.16}$$

---

[1] Non-zero shaft damping coefficients are convenient for some of the following calculations and are therefore presumed.

the system dynamics can be described by the LTI system

$$\frac{\mathrm{d}\mathbf{x}}{\mathrm{d}t} = \underbrace{\begin{pmatrix} -\frac{d_{s1}}{I_1} & 0 & \frac{d_{s1}}{I_1} & -\frac{c_{s1}}{I_1} & 0 & \frac{c_{s1}}{I_1} \\ 0 & -\frac{d_{s2}}{I_2} & \frac{d_{s2}}{I_2} & 0 & -\frac{c_{s2}}{I_2} & \frac{c_{s2}}{I_2} \\ \frac{c_{s1}-\frac{d_{s1}^2}{I_1}}{d_{s1}+d_{s2}} & \frac{c_{s2}-\frac{d_{s2}^2}{I_2}}{d_{s1}+d_{s2}} & \frac{\frac{d_{s1}^2}{I_1}+\frac{d_{s2}^2}{I_2}-c_{s1}-c_{s2}}{d_{s1}+d_{s2}} & \frac{-\frac{c_{s1}d_{s1}}{I_1}}{d_{s1}+d_{s2}} & \frac{-\frac{c_{s2}d_{s2}}{I_2}}{d_{s1}+d_{s2}} & \frac{\frac{c_{s1}d_{s1}}{I_1}+\frac{c_{s2}d_{s2}}{I_2}}{d_{s1}+d_{s2}} \\ 1 & 0 & 0 & 0 & 0 & 0 \\ 0 & 1 & 0 & 0 & 0 & 0 \\ 0 & 0 & 1 & 0 & 0 & 0 \end{pmatrix}}_{=:\mathbf{A}} \mathbf{x} \\ + \begin{pmatrix} \frac{1}{I_1} & 0 \\ 0 & \frac{1}{I_2} \\ \frac{d_{s1}}{I_1(d_{s1}+d_{s2})} & \frac{d_{s2}}{I_2(d_{s1}+d_{s2})} \\ 0 & 0 \\ 0 & 0 \\ 0 & 0 \end{pmatrix} \begin{bmatrix} T_1 \\ T_2 \end{bmatrix}. \tag{B.17}$$

In general, the dynamic dimension of this system is higher than that of the simple two-mass oscillator as shown in Figure B.3. When the state vector is

$$\widetilde{\mathbf{x}} := \begin{bmatrix} \widetilde{\omega}_1 & \widetilde{\omega}_2 & \widetilde{\varphi}_1 & \widetilde{\varphi}_2 \end{bmatrix}^{\mathrm{T}}, \tag{B.18}$$

the dynamics of this system are given by

$$\frac{\mathrm{d}\widetilde{\mathbf{x}}}{\mathrm{d}t} = \underbrace{\begin{pmatrix} -\frac{\widetilde{d}_s}{I_1} & \frac{\widetilde{d}_s}{I_1} & -\frac{\widetilde{c}_s}{I_1} & \frac{\widetilde{c}_s}{I_1} \\ \frac{\widetilde{d}_s}{I_2} & -\frac{\widetilde{d}_s}{I_2} & \frac{\widetilde{c}_s}{I_2} & -\frac{\widetilde{c}_s}{I_2} \\ 1 & 0 & 0 & 0 \\ 0 & 1 & 0 & 0 \end{pmatrix}}_{=:\widetilde{\mathbf{A}}} \widetilde{\mathbf{x}} + \begin{pmatrix} \frac{1}{I_1} & 0 \\ 0 & \frac{1}{I_2} \\ 0 & 0 \\ 0 & 0 \end{pmatrix} \begin{bmatrix} T_1 \\ T_2 \end{bmatrix}. \tag{B.19}$$

Obviously, the dynamics of System (B.17) and System (B.19) are different in general. To determine suitable equivalent shaft parameters $\widetilde{c}_s$ and $\widetilde{d}_s$ for the two-mass oscillator so that its behaviour is similar to System (B.17), the characteristic polynomials of the dynamic matrices $\mathbf{A}$ and $\widetilde{\mathbf{A}}$ are compared. The characteristic polynomial corresponding to System (B.17) is

$$\begin{aligned}\Delta(s) = s^6 + &\left[\frac{c_{s1}+c_{s2}}{d_{s1}+d_{s2}} + \frac{d_{s1}d_{s2}}{d_{s1}+d_{s2}}\left(\frac{1}{I_1}+\frac{1}{I_2}\right)\right] s^5 \\ &+ \frac{c_{s1}d_{s2}+c_{s2}d_{s1}}{d_{s1}+d_{s2}}\left(\frac{1}{I_1}+\frac{1}{I_2}\right) s^4 + \frac{c_{s1}c_{s2}}{d_{s1}+d_{s2}}\left(\frac{1}{I_1}+\frac{1}{I_2}\right) s^3.\end{aligned} \tag{B.20}$$

The dynamics of the LTI system are determined by the zeros of the characteristic polynomial, where the conjugate complex zeros are most important as they define the system's oscillatory behaviour.[2] The zeros located at $s = 0$ indicate integrating system behaviour and are not considered in the following. Two of the three remaining zeros are assumed to be conjugate complex of the form $s_{1,2} = -\zeta \pm j\omega_0$; consequently, the remaining zero $s_3 = -\gamma$ must be real. Then the characteristic polynomial can be written as

$$\begin{aligned}\Delta(s) &= (s-s_1)(s-s_2)(s-s_3) \\ \Delta(s) &= s^3 + (2\zeta+\gamma)s^2 + \left(\omega_0^2+\zeta^2+2\zeta\gamma\right)s + \gamma\omega_0^2 + \gamma\zeta^2.\end{aligned} \tag{B.21}$$

By equating the coefficients of Equation (B.20) and Equation (B.21), the system of equations

$$2\zeta+\gamma = \frac{c_{s1}+c_{s2}}{d_{s1}+d_{s2}} + \frac{d_{s1}d_{s2}}{d_{s1}+d_{s2}}\left(\frac{1}{I_1}+\frac{1}{I_2}\right) \tag{B.22a}$$

$$\omega_0^2+\zeta^2+2\zeta\gamma = \frac{c_{s1}d_{s2}+c_{s2}d_{s1}}{d_{s1}+d_{s2}}\left(\frac{1}{I_1}+\frac{1}{I_2}\right) \tag{B.22b}$$

$$\omega_0^2\gamma+\zeta^2\gamma = \frac{c_{s1}c_{s2}}{d_{s1}+d_{s2}}\left(\frac{1}{I_1}+\frac{1}{I_2}\right) \tag{B.22c}$$

results.

For the simple two-mass oscillator with only one torsionally flexible shaft mathematically described by System (B.19) the conjugate complex pair of zeros of the characteristic polynomial is

$$\widetilde{s}_{1,2} = -\widetilde{\zeta} \pm j\widetilde{\omega}_0 = -\left(\frac{\widetilde{d}_s}{2I_1}+\frac{\widetilde{d}_s}{2I_2}\right) \pm j\sqrt{\left(\frac{\widetilde{c}_s}{I_1}+\frac{\widetilde{c}_s}{I_2}\right) - \left(\frac{\widetilde{d}_s}{2I_1}+\frac{\widetilde{d}_s}{2I_2}\right)^2}. \tag{B.23}$$

If these two mechanical systems have identical damping ratios ($\zeta = \widetilde{\zeta}$) and natural angular frequencies ($\omega_0 = \widetilde{\omega}_0$), their oscillatory behaviour is similar. By using these relationships and Equation (B.23), Equation (B.22) can be written as

---

[2] For relevant problem settings the assumption that the characteristic polynomial of the dynamic matrix contains a conjugate complex pair of zeros is admissible as the mechanical systems are usually poorly damped.

$$\gamma + \widetilde{d}_s \left(\frac{1}{I_1} + \frac{1}{I_2} \right) = \frac{c_{s1} + c_{s2}}{d_{s1} + d_{s2}} + \frac{d_{s1} d_{s2}}{d_{s1} + d_{s2}} \left(\frac{1}{I_1} + \frac{1}{I_2} \right) \tag{B.24a}$$

$$\widetilde{c}_s + \gamma \widetilde{d}_s = \frac{c_{s1} d_{s2} + c_{s2} d_{s1}}{d_{s1} + d_{s2}} \tag{B.24b}$$

$$\gamma \widetilde{c}_s = \frac{c_{s1} c_{s2}}{d_{s1} + d_{s2}}. \tag{B.24c}$$

Solving this non-linear system of equations for the unknown quantities γ, $\widetilde{c}_s$, and $\widetilde{d}_s$ is still extensive. If the equivalent torsional stiffness parameter is chosen as

$$\widetilde{c}_s = \frac{c_{s1} c_{s2}}{c_{s1} + c_{s2}} \tag{B.25}$$

to guarantee that the torsional twist is correctly modelled for stationary situations, the quantity γ directly results from Equation (B.24c)

$$\gamma = \frac{c_{s1} + c_{s2}}{d_{s1} + d_{s2}}. \tag{B.26}$$

Since γ is rather big for typical problem settings, the dynamics of System (B.17) are primarily determined by the conjugate complex pair of zeros of the characteristic polynomial. $\widetilde{d}_s$ can then be determined from Equation (B.24b):

$$\widetilde{d}_s = \frac{c_{s1}^2 d_{s2} + c_{s2}^2 d_{s1}}{(c_{s1} + c_{s2})^2} \tag{B.27}$$

However, following this approach Equation (B.24a) is not exactly fulfilled. If γ from Equation (B.26) and $\widetilde{d}_s$ from Equation (B.27) is used,

$$\frac{c_{s1} + c_{s2}}{d_{s1} + d_{s2}} + \frac{c_{s1}^2 d_{s2} + c_{s2}^2 d_{s1}}{(c_{s1} + c_{s2})^2} \left(\frac{1}{I_1} + \frac{1}{I_2} \right) \approx \frac{c_{s1} + c_{s2}}{d_{s1} + d_{s2}} + \frac{d_{s1} d_{s2}}{d_{s1} + d_{s2}} \left(\frac{1}{I_1} + \frac{1}{I_2} \right) \tag{B.28}$$

remains. For relevant problem settings the torsional stiffness parameters are typically rather big while the shafts' damping coefficients are small. Therefore, Equation (B.28) is at least approximately fulfilled for most problem settings. Consequently, $\widetilde{c}_s$ calculated according to Equation (B.25) and $\widetilde{d}_s$ determined according to Equation (B.27) are good approximations that shall be used whenever some shafts must be combined. These equations also include the two special parameter settings already discussed before.

Finally, the obtained results are presented in a graphical form by the zeros of the characteristic polynomials for the system parameters given in Table B.1. Two

Table B.1: System parameters for the comparative analysis of the three-mass oscillator with $I_3 \to 0$ and the simplified two-mass oscillator.

Parameter	Value			Unit
	setting 1	setting 2	time domain	
I_1	5	5	5	$\mathrm{kg\,m^2}$
I_2	10	10	10	$\mathrm{kg\,m^2}$
c_{s1}	3	3	3	kN m/rad
c_{s2}	6	12	6	kN m/rad
d_{s1}	5	5	5	N m s/rad
d_{s2}	$0\ldots20$	$0\ldots20$	1	N m s/rad

different system configurations entitled 'setting 1' and 'setting 2' are analysed, those differ in the torsional elasticity c_{s2} of shaft 2. For both configurations the damping coefficient d_{s2} of shaft 2 was varied and the zeros of the characteristic polynomials were determined numerically. In Figure B.4 one of the conjugate complex pair of zeros is presented. Labelled 'exact' are the zeros of the Characteristic polynomial (B.20) of the three-mass oscillator with $I_3 \to 0$; the quantities related to the two-mass oscillator with only one elastic shaft are labelled 'prop. approx.' when the equivalent shaft parameters were determined according to Equation (B.25) and Equation (B.27) and 'conv. approx.' when these parameters were chosen according to Equation (B.15). As these latter equivalent shaft parameters are only valid for special parameter settings of the original system, deviations are to be expected. With the modified parameter selection however a good match with the original system behaviour is achieved; consequently, the zeros belonging to the original system are covered by the data belonging to the reduced system in Figure B.4.

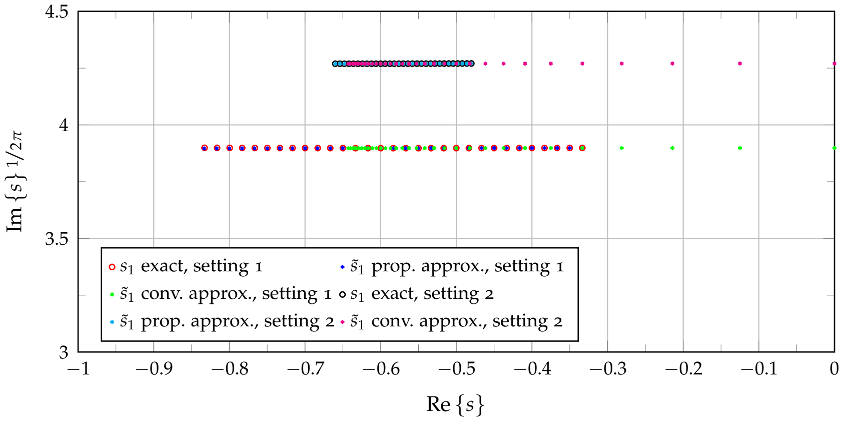

Figure B.4: Conjugate complex zero of the characteristic polynomial of the exact dynamic model including two elastic shafts and of the simplified two-mass oscillator with only one shaft for two parameter settings and varying d_{s2}.

To further underline these results, also time domain simulations were performed. The system parameters used for this numerical simulation are given in Table B.1 too. The system was excited by a one second pulse of the input torque T_1 while T_2 was zero. The results are presented in Figure B.5 and Figure B.6. In the first plot the rotational speed of the rotating body I_1 is shown and in the second plot the rotational speed of the second moving body I_2 is displayed. The results obtained with the dynamic model of the mechanical system containing two shafts are labelled n_1 and n_2 while the results based on the classical two-mass oscillator are labelled $\widetilde{n}_1$ and $\widetilde{n}_2$. The behaviour of the two-mass oscillator with the equivalent shaft parameters chosen according to Equation (B.25) and Equation (B.27) presented in blue is obviously very close to the behaviour of the original system shown in green.

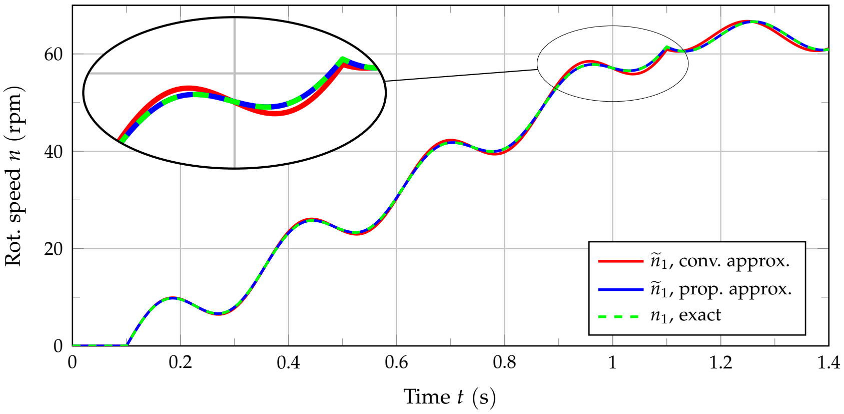

Figure B.5: Simulated rotational speed n_1 for the exact dynamic model including two elastic shafts and for the simplified two-mass oscillator with only one shaft.

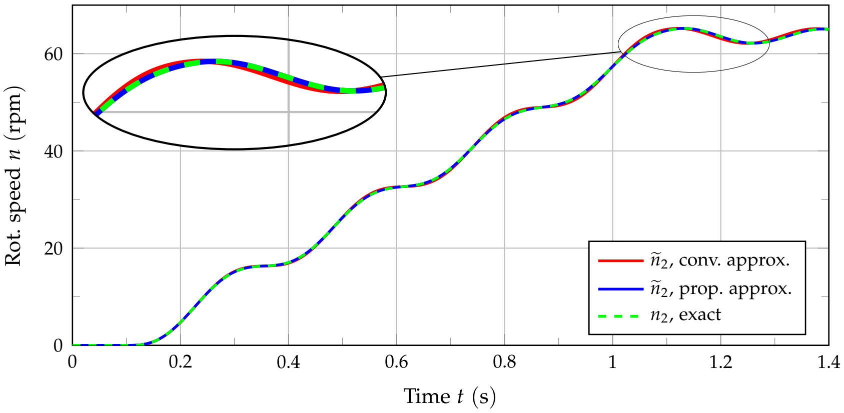

Figure B.6: Simulated rotational speed n_2 for the exact dynamic model including two elastic shafts and for the simplified two-mass oscillator with only one shaft.

Finally, the idea previously presented is applied to more complex mechanical systems. If for instance three torsionally flexible shafts are to be combined, this calculation of equivalent shaft parameters can be done twice. At first, two shafts are combined and the equivalent shaft parameters are

$$\widetilde{c}_{s12} = \frac{c_{s1}c_{s2}}{c_{s1}+c_{s2}} \tag{B.29a}$$

$$\widetilde{d}_{s12} = \frac{c_{s1}^2 d_{s2} + c_{s2}^2 d_{s1}}{\left(c_{s1}+c_{s2}\right)^2} = \frac{\widetilde{c}_{s12}^2}{c_{s1}^2} d_{s1} + \frac{\widetilde{c}_{s12}^2}{c_{s2}^2} d_{s2}. \tag{B.29b}$$

Then the parameters of the remaining third shaft can be considered resulting in the equivalent torsional stiffness

$$\widetilde{c}_s = \frac{\widetilde{c}_{s12}c_{s3}}{\widetilde{c}_{s12}+c_{s3}} = \frac{1}{\frac{1}{\widetilde{c}_{s12}}+\frac{1}{c_{s3}}} = \frac{1}{\frac{1}{c_{s1}}+\frac{1}{c_{s2}}+\frac{1}{c_{s3}}} = \frac{c_{s1}c_{s2}c_{s3}}{c_{s1}c_{s2}+c_{s1}c_{s3}+c_{s2}c_{s3}} \tag{B.30}$$

and in the equivalent shaft damping coefficient

$$\begin{aligned}\widetilde{d}_s &= \frac{\widetilde{c}_{s12}^2 d_{s3} + c_{s3}^2 \widetilde{d}_{s12}}{\left(\widetilde{c}_{s12}+c_{s3}\right)^2} = \frac{\widetilde{c}_s^2}{\widetilde{c}_{s12}^2}\widetilde{d}_{s12} + \frac{\widetilde{c}_s^2}{c_{s3}^2} d_{s3} = \frac{\widetilde{c}_s^2}{\widetilde{c}_{s12}^2}\left(\frac{\widetilde{c}_{s12}^2}{c_{s1}^2} d_{s1} + \frac{\widetilde{c}_{s12}^2}{c_{s2}^2} d_{s2}\right) + \frac{\widetilde{c}_s^2}{c_{s3}^2} d_{s3} \\ \widetilde{d}_s &= \frac{\widetilde{c}_s^2}{c_{s1}^2} d_{s1} + \frac{\widetilde{c}_s^2}{c_{s2}^2} d_{s2} + \frac{\widetilde{c}_s^2}{c_{s3}^2} d_{s3}.\end{aligned} \tag{B.31}$$

Consequently, if k torsionally flexible shafts with individual parameters c_{si} and d_{si} for $i = 1, 2, \ldots, k$ shall be replaced by one shaft, its parameters can be calculated according to

$$\widetilde{c}_s = \frac{1}{\frac{1}{c_{s1}}+\frac{1}{c_{s2}}+\cdots+\frac{1}{c_{sk}}} \tag{B.32}$$

and

$$\widetilde{d}_s = \frac{\widetilde{c}_s^2}{c_{s1}^2} d_{s1} + \frac{\widetilde{c}_s^2}{c_{s2}^2} d_{s2} + \cdots + \frac{\widetilde{c}_s^2}{c_{sk}^2} d_{sk}. \tag{B.33}$$

Appendix C

Mathematical Model for Exemplary Mechanical System

In this section a mathematical model for the test bed for differential gears presented in Figure 3.24 is given. A graphical representation of the resulting system model was shown in Figure 3.25; here the corresponding differential equations describing the dynamics of the mechanical system are given.[1] Relevant physical quantities and system parameters were defined and explained in Section 3.8. For the angular velocities of the three IMs

$$I_{m1}\frac{\mathrm{d}\omega_1}{\mathrm{d}t} = T_{ag1} - T_{f1} \tag{C.1a}$$

$$I_{m2}\frac{\mathrm{d}\omega_2}{\mathrm{d}t} = T_{ag2} + T_{f2} \tag{C.1b}$$

$$I_{m3}\frac{\mathrm{d}\omega_3}{\mathrm{d}t} = T_{ag3} + T_{f3} \tag{C.1c}$$

$$\frac{\mathrm{d}\varphi_k}{\mathrm{d}t} = \omega_k \text{ for } k \in \{1,2,3\} \tag{C.1d}$$

holds. The quantities T_{f1}, T_{f2}, and T_{f3} are the torques transmitted by the elasticities within the torque measuring flanges

$$T_{f1} = d_{f1}\left(\omega_1 - \omega_{f1}\right) + c_{f1}\left(\varphi_1 - \varphi_{f1}\right) \tag{C.2a}$$

$$T_{f2} = d_{f2}\left(\omega_{f2} - \omega_2\right) + c_{f2}\left(\varphi_{f2} - \varphi_2\right) \tag{C.2b}$$

$$T_{f3} = d_{f3}\left(\omega_{f3} - \omega_3\right) + c_{f3}\left(\varphi_{f3} - \varphi_3\right). \tag{C.2c}$$

The dynamics of the state variables associated with the torque measuring flanges' inertias are

$$I_{f1}\frac{\mathrm{d}\omega_{f1}}{\mathrm{d}t} = T_{f1} - T_{s1} \tag{C.3a}$$

---

[1] For clarity gear play typically related to cardan shafts is not considered here.

$$I_{f2}\frac{\mathrm{d}\omega_{f2}}{\mathrm{d}t} = T_{s2} - T_{f2} \tag{C.3b}$$

$$I_{f3}\frac{\mathrm{d}\omega_{f3}}{\mathrm{d}t} = T_{s3} - T_{f3} \tag{C.3c}$$

$$\frac{\mathrm{d}\varphi_{fk}}{\mathrm{d}t} = \omega_{fk} \text{ for } k \in \{1,2,3\}\,. \tag{C.3d}$$

These depend on the torques transmitted by the cardan shafts connecting electric drives and torque transducers to the UUT

$$T_{s1} = d_{s1}\left(\omega_{f1} - \omega_{di}\right) + c_{s1}\left(\varphi_{f1} - \varphi_{di}\right) \tag{C.4a}$$

$$T_{s2} = d_{s2}\Bigg[\underbrace{\left(\frac{\omega_{di}}{i_d} + \frac{r_3}{r_1}\omega_{3b}\right)}_{\omega_{do1}} - \omega_{f2}\Bigg] + c_{s2}\Bigg[\left(\frac{\varphi_{di}}{i_d} + \frac{r_3}{r_1}\varphi_{3b}\right) - \varphi_{f2}\Bigg] \tag{C.4b}$$

$$T_{s3} = d_{s3}\Bigg[\underbrace{\left(\frac{\omega_{di}}{i_d} - \frac{r_3}{r_2}\omega_{3b}\right)}_{\omega_{do2}} - \omega_{f3}\Bigg] + c_{s3}\Bigg[\left(\frac{\varphi_{di}}{i_d} - \frac{r_3}{r_2}\varphi_{3b}\right) - \varphi_{f3}\Bigg]. \tag{C.4c}$$

The quantities ω_{di}, ω_{do1}, and ω_{do2} and the corresponding angular positions were not specified in Figure 3.25; these are the state variables describing the dynamics of the differential's input and outputs. Since the state variables used to model the differential gear do not include the angular velocities of the differential's output shafts ω_{do1} and ω_{do2}, these quantities are represented as a linear combination of the system states ω_{di} and ω_{3b}. The shaft torques given above also directly represent the input torque $T_{di} = T_{s1}$ and the output torques $T_{do1} = T_{s2}$ and $T_{do2} = T_{s3}$ of the differential gear. Finally, the differential equations describing the dynamics of the bevel gear differential are given

$$\begin{aligned} D_c\frac{\mathrm{d}\omega_{di}}{\mathrm{d}t} &= i_d^2\left(T_{s1} - T_{dl}\right)\left(I_1\frac{r_3^2}{r_1^2} + I_2\frac{r_3^2}{r_2^2} + I_3\right) - i_d T_{dsl}\left(I_2\frac{r_3}{r_2} - I_1\frac{r_3}{r_1}\right) \\ &\quad - i_d T_{s2}\left(I_2\frac{r_3^2}{r_2^2} + I_2\frac{r_3^2}{r_1 r_2} + I_3\right) - i_d T_{s3}\left(I_1\frac{r_3^2}{r_1^2} + I_1\frac{r_3^2}{r_1 r_2} + I_3\right) \end{aligned} \tag{C.5}$$

$$\begin{aligned} D_c\frac{\mathrm{d}\omega_{3b}}{\mathrm{d}t} &= i_d\left(T_{s1} - T_{dl}\right)\left(I_2\frac{r_3}{r_2} - I_1\frac{r_3}{r_1}\right) - T_{dsl}\left(I_d + I_1 + I_2\right) \\ &\quad - T_{s2}\left(I_d\frac{r_3}{r_1} + I_2\frac{r_3}{r_1} + I_2\frac{r_3}{r_2}\right) + T_{s3}\left(I_d\frac{r_3}{r_2} + I_1\frac{r_3}{r_1} + I_1\frac{r_3}{r_2}\right) \end{aligned} \tag{C.6}$$

$$\frac{\mathrm{d}\varphi_{di}}{\mathrm{d}t} = \omega_{di} \tag{C.7}$$

$$\frac{\mathrm{d}\varphi_{3b}}{\mathrm{d}t} = \omega_{3b}, \tag{C.8}$$

where

$$D_c = I_d \left(I_1 \frac{r_3^2}{r_1^2} + I_2 \frac{r_3^2}{r_2^2} + I_3 \right) + I_1 I_2 \left(\frac{r_3}{r_1} + \frac{r_3}{r_2} \right)^2 + I_1 I_3 + I_2 I_3. \tag{C.9}$$

This set of differential equations forms a dynamic system; the outputs of this system are the angular velocities of the electric drives ω_1, ω_2, and ω_3 and the torques measured by the measuring flanges as given by Equation (C.2). Above equations can be used to perform numerical simulations, but due to their complexity, it is difficult to gain insight in the system behaviour. Therefore, simplifications are demanded, especially regarding the differential gear. If the UUT is an axle differential, $I_1 = I_2$ and $r_1 = r_2$ can be assumed as these are typically symmetric. Then

$$D_c \frac{\mathrm{d}\omega_{di}}{\mathrm{d}t} = i_d^2 \left(2I_1 \frac{r_3^2}{r_1^2} + I_3 \right) \left(T_{s1} - T_{dl} - \frac{1}{i_d} T_{s2} - \frac{1}{i_d} T_{s3} \right) \tag{C.10}$$

$$D_c \frac{\mathrm{d}\omega_{3b}}{\mathrm{d}t} = \frac{r_3}{r_1} \left(I_d + 2I_1 \right) \left(-T_{s2} + T_{s3} - \frac{r_1}{r_3} T_{dsl} \right) \tag{C.11}$$

can be used instead of Equation (C.5) and Equation (C.6). With

$$I_{di} = \frac{I_d \left(2I_1 \frac{r_3^2}{r_1^2} + I_3 \right) + 4I_1^2 \frac{r_3^2}{r_1^2} + 2I_1 I_3}{i_d^2 \left(2I_1 \frac{r_3^2}{r_1^2} + I_3 \right)} \tag{C.12a}$$

$$I_{3b} = \frac{I_d \left(2I_1 \frac{r_3^2}{r_1^2} + I_3 \right) + 4I_1^2 \frac{r_3^2}{r_1^2} + 2I_1 I_3}{I_d \frac{r_3}{r_1} + 2I_1 \frac{r_3}{r_1}} \tag{C.12b}$$

these equations can be written even more compact

$$I_{di} \frac{\mathrm{d}\omega_{di}}{\mathrm{d}t} = T_{s1} - T_{dl} - \frac{1}{i_d} T_{s2} - \frac{1}{i_d} T_{s3} \tag{C.13}$$

$$I_{3b} \frac{\mathrm{d}\omega_{3b}}{\mathrm{d}t} = -T_{s2} + T_{s3} - \frac{r_1}{r_3} T_{dsl}. \tag{C.14}$$

In spite of these simplifications, the dynamic system given by Equations (C.1)–(C.4), (C.7), (C.8), (C.13), and (C.14) is still non-linear. Since linear models are demanded for many system analysis methods (e.g. modal analysis), the non-linearities shall be removed. To do so, the assumption that losses do not have to be considered ($T_{dl} = 0$) is used. To additionally eliminate the slip-limiting torque T_{dsl}, a differential gear with only weak slip-limiting functionality can be assumed and T_{dsl} can be set to zero as well. Then the differential gear can be described by

$$I_{di}\frac{\mathrm{d}\omega_{di}}{\mathrm{d}t} = T_{s1} - \frac{1}{i_d}T_{s2} - \frac{1}{i_d}T_{s3} \tag{C.15}$$

$$I_{3b}\frac{\mathrm{d}\omega_{3b}}{\mathrm{d}t} = -T_{s2} + T_{s3} \tag{C.16}$$

with the constants I_{di} and I_{3b} given above. Equation (C.16) directly shows that the differential's output torques must be identical for stationary situations. The differential equations for the remaining mechanical system do not need to be changed; consequently, a LTI system describing the system dynamics is given by Equations (C.1)–(C.4), (C.7), (C.8), (C.15), and (C.16).

If the differential gear's slip-limiting capacity cannot be neglected, operating points with different angular velocities of the differential's output axles can be excluded; then $\omega_{do} = \omega_{do1} = \omega_{do2} = \omega_{di}/i_d$ holds. This also implies a reduction of the dynamic dimension of the mathematical model for the differential gear from two to one as ω_{3b} is permanently zero. The dynamics of the differential gear can then be described by only one differential equation:

$$I_{di}\frac{\mathrm{d}\omega_{di}}{\mathrm{d}t} = T_{s1} - \frac{1}{i_d}T_{s2} - \frac{1}{i_d}T_{s3} \tag{C.17}$$

Since the system state ω_{3b} is no longer required, also the shaft torques T_{s2} and T_{s3} must be modified

$$T_{s2} = d_{s2}\left(\frac{\omega_{di}}{i_d} - \omega_{f2}\right) + c_{s2}\left(\frac{\varphi_{di}}{i_d} - \varphi_{f2}\right) \tag{C.18a}$$

$$T_{s3} = d_{s3}\left(\frac{\omega_{di}}{i_d} - \omega_{f3}\right) + c_{s3}\left(\frac{\varphi_{di}}{i_d} - \varphi_{f3}\right). \tag{C.18b}$$

This reduced mathematical model given by Equations (C.1)–(C.4a), (C.7), (C.17), and (C.18) is again a LTI system. Therefore, for both system models given above eigenvalues and eigenvectors of the dynamic matrix characterising torsional vibrations can be calculated. A realistic parameter setting is given in Table C.1.

Table C.1: Mechanical system parameters for an exemplary test system for differential gears.

Parameter	Value	Unit
I_{m1}	1.0	$\mathrm{kg\,m^2}$
I_{m2}	10.3	$\mathrm{kg\,m^2}$
I_{m3}	10.3	$\mathrm{kg\,m^2}$
I_{f1}	0.032	$\mathrm{kg\,m^2}$
I_{f2}	0.032	$\mathrm{kg\,m^2}$
I_{f3}	0.029	$\mathrm{kg\,m^2}$
I_{di}	0.022	$\mathrm{kg\,m^2}$
I_{3b}	0.04	$\mathrm{kg\,m^2}$
i_d	1.91	–
c_{f1}	380	kN m/rad
c_{f2}	220	kN m/rad
c_{f3}	220	kN m/rad
c_{s1}	57	kN m/rad
c_{s2}	57	kN m/rad
c_{s3}	57	kN m/rad
d_{f1}	0.5	N m s/rad
d_{f2}	0.5	N m s/rad
d_{f3}	0.5	N m s/rad
d_{s1}	2	N m s/rad
d_{s2}	2	N m s/rad
d_{s3}	2	N m s/rad

Appendix D

Parameters for Reduced Mechanical System

In Table D.1 the parameters of the simplified mechanical system of the test bed for differential gears with adapter gearboxes shown in Figure 5.4 are summarised. The torsional stiffness parameters in Table D.1 are the parameters of the cardan shafts connecting gearboxes and differential gear without any transformation because of different levels of rotational speeds. As stated in Chapter 3, the dynamic model used for simulation is much more complex and thus requires many additional parameters; for lucidity these are not included in Table D.1.

Parameter	Value	Unit
I_{m1}	3.25	$\mathrm{kg\,m^2}$
I_{m2}, I_{m3}	10.3	$\mathrm{kg\,m^2}$
I_{gb1}	1.05	$\mathrm{kg\,m^2}$
I_{gb2}, I_{gb3}	1.65	$\mathrm{kg\,m^2}$
c_{s1}	33	kN m/rad
c_{s2}, c_{s3}	240	kN m/rad
i_d	2.85	–
T_{dsl0}	0.50	N m
k_{dslT}	0.06	–
$k_{dsl\omega}$	0.06	N m s/rad
i_{gb1}	8.1	–
i_{gb2}, i_{gb3}	10.4	–

Table D.1: Parameters for the reduced mechanical system of a test bed for differential gears with adapter gearboxes.

Bibliography

[1] G. Kokalj, J. Lewis and C. Zach, 'Significant Reduction of Powertrain Calibration Effort in Production Programs — Automated Calibration of Drivability on Chassis Dyno and Powertrain Testbed', in *TM Symposium China*, Beijing, China, 2012.

[2] M. Werner, T. Kreutzer, C. Wagner and R. Bauer, 'End-of-line Testing of Combustion Engines on Highly Dynamic Test Beds', *ATZextra Worldwide*, vol. 20, pp. 40–43, November 2015. DOI: `10.1007/s40111-015-0505-4`.

[3] J. Pillas, F. Kirschbaum, R. Jakobi, A. Gebhardt and F. Uphaus, 'Model-Based Load Change Reaction Optimization using Vehicle Drivetrain Test Beds', in *14. Internationales Stuttgarter Symposium*, Stuttgart, Germany, 2014. DOI: `10.1007/978-3-658-05130-3_115`.

[4] J.-C. Goos, 'Evaluation of the Suitability of Test Stands for the Road Correspondent Investigation of Load Change Maneuvers', Master's thesis, Institute for Mechatronic Systems in Mechanical Engineering, Technische Universität Darmstadt, 2013.

[5] R. Bauer, 'New Methodology for Dynamic Drive Train Testing', in *ARAI SIAT Proceedings: Symposium on International Automotive Technology*, Pune, India, 2011. DOI: `10.4271/2011-26-0045`.

[6] J. Yoo, K. Pfeiffer and K. Kang, 'Front Loading NVH Test on the Highly Dynamic Powertrain Test Bed', in *SAE 2011 Noise and Vibration Conference and Exhibition*, Grand Rapids, MI, USA, 2011. DOI: `10.4271/2011-01-1512`.

[7] J. Happian-Smith, Ed., *An Introduction to Modern Vehicle Design*, Oxford: Butterworth-Heinemann, 2002, ISBN: 978-0-7506-5044-1.

[8] A. J. Martyr and M. A. Plint, *Engine Testing*, Theory and Practice, 3rd ed. Oxford: Butterworth-Heinemann, 2007, ISBN: 978-0-7506-8439-2. DOI: `10.1016/B978-075068439-2/50000-1`.

[9] D. Karnopp, 'Computer Simulation of Stick-Slip Friction in Mechanical Dynamic Systems', *ASME Journal of Dynamic Systems, Measurement, and Control*, vol. 107, pp. 100–103, 1 1985. DOI: `10.1115/1.3140698`.

[10] R. Morselli, R. Zanasi and G. Sandoni, 'Detailed and reduced dynamic models of passive and active limited-slip car differentials', *Mathematical and Computer Modelling of Dynamical Systems: Methods, Tools and Application in Engineering and Related Sciences*, vol. 12, pp. 347–362, 4 2006. DOI: `10.1080/13873950500066959`.

[11] I. Ibendorf, 'Hardware-in-the-Loop-Prüfstand für Schwingungsuntersuchungen an Fahrzeugantriebskomponenten', PhD thesis, Faculty of Mechanical Engineering and Marine Technology, University of Rostock, 2008.

[12] C. Schwärzler, 'Entwurf und Realisierung einer Mehrgrößenregelung für Antriebsstrang Prüfstände', Master's thesis, Institute for Automation and Control, Graz University of Technology, 2010.

[13] M. Paulweber and K. Lebert, *Mess- und Prüfstandstechnik*, Antriebsstrangentwicklung, Hybridisierung, Elektrifizierung. Wiesbaden: Springer Vieweg, 2014, ISBN: 978-3-658-04452-7. DOI: `10.1007/978-3-658-04453-4`.

[14] R. Vögl, E. Bogner, T. Ebner, T. D. D. Terra and G. Vitale, 'Innovative Anwendung des Rollenprüfstands für die Fahrbarkeitsabstimmung', *ATZ – Automobiltechnische Zeitschrift*, vol. 111, pp. 853–860, 11 2009. DOI: `10.1007/BF03224484`.

[15] R. Bauer, 'Neues Regelkonzept für die dynamische Antriebsstrangprüfung', in *17. Steirisches Seminar über Regelungstechnik und Prozessautomatisierung*, Leibnitz, Austria, 2011.

[16] R. Fietzek, 'Modellbildung, Regelung und Realisierung eines neuartigen Konzeptes für einen Gesamtfahrzeugprüfstand', PhD thesis, Department of Mechanical Engineering, Technische Universität Darmstadt, 2014.

[17] A. Albers, C. Schyr, A. Krueger and M. Pfeiffer, 'Fahrsimulation am Antriebsstrang-Prüfstand', in *Simulation und Simulatoren — Mobilität virtuell gestalten, Tagung der VDI-Gesellschaft Fahrzeug- und Verkehrstechnik in Hamburg*, Hamburg, Germany, 2003.

[18] M. Crampen, E. Danner, D. Naundorf and S. Osbahr, 'Dynamischer Antriebsstrangprüfstand als universelles Entwicklungswerkzeug', *ATZ – Automobiltechnische Zeitschrift*, vol. 105, pp. 1170–1177, 12 2003. DOI: `10.1007/BF03221598`.

[19] H.-P. Dohmen, K. Pfeiffer and C. Schyr, *Antriebsstrangprüftechnik: vom stationären Komponententest zum fahrmanöverbasierten Testen*. Landsberg: Verlag Moderne Industrie, 2009, ISBN: 978-3-937889-89-4.

[20] T. Haidinger, 'Modellierung und Regelung eines elektrischen Rotationsaktuators', PhD thesis, Faculty of Electrical and Information Engineering, Graz University of Technology, 2010.

[21] B. J. Bunker, M. A. Franchek and B. E. Thomason, 'Robust Multivariable Control of an Engine-Dynamometer System', *IEEE Transactions on Control Systems Technology*, vol. 5, pp. 189–199, 2 1997. DOI: `10.1109/87.556024`.

[22] S. N. Vukosavic, *Electrical Machines*. New York: Springer Science + Business Media, 2013, ISBN: 978-1-4614-0400-2. DOI: `10.1007/978-1-4614-0400-2`.

[23] D. Schröder, *Elektrische Antriebe — Grundlagen*, 4th ed. Berlin Heidelberg: Springer, 2009, ISBN: 978-3-642-02990-5. DOI: `10.1007/978-3-642-02990-5`.

[24] HBM, *T12 torque flange manual*, 2015. [Online]. Available: `www.hbm.com`.

[25] Heidenhain, *Brochure rotary encoders*, 2016. [Online]. Available: `http://www.heidenhain.com/fileadmin/pdb/media/img/349529-2G_Rotary_Encoders_en.pdf`.

[26] R. Priesner, 'Impedance Control of Internal Combustion Engine Test Beds', PhD thesis, Faculty of Mechanical and Industrial Engineering, Vienna University of Technology, 2013.

[27] J. Blumenschein, P. Schrangl, T. E. Passenbrunner and L. del Re, 'Easily Adaptable Model of Test Benches for Internal Combustion Engines', in *European Control Conference*, Zürich, Switzerland, 2013.

[28] M. Nomura, M. Suzuki, M. Hori and M. Terashima, 'Decoupling torque control system for automotive engine tester', *IEEE Transactions on Industry Applications*, vol. 36, pp. 467–474, 2 2000. DOI: `10.1109/28.833763`.

[29] E. Grünbacher, L. del Re, H. Kokal, M. Schmidt and M. Paulweber, 'Online Trajectory Shaping Strategy for Dynamical Engine Test Benches', in *IEEE International Conference on Control Applications*, Munich, Germany, 2006. DOI: `10.1109/CACSD-CCA-ISIC.2006.4777134`.

[30] M. Schmidt and J.-A. Kessel, 'Model-Based Torque Controller for Dynamical Engine Test Stands', in *American Control Confererce*, San Diego, CA, USA, 1999. DOI: `10.1109/ACC.1999.782364`.

[31] T. E. Passenbrunner, M. Sassano and L. del Re, 'Approximate Optimal Control of Internal Combustion Engine Test Beds', in *IEEE Conference on Decision and Control*, Orlando, FL, USA, 2011. DOI: `10.1109/CDC.2011.6161120`.

[32] M. Wipfler, R. Bauer, N. Dourdoumas and W. Rossegger, 'Regelungstechnische Methoden zur Drehschwingungsdämpfung eines Wellenstrangs am Beispiel eines Motorprüfstands', *e&i — Elektrotechnik und Informationstechnik*, vol. 133, pp. 142–152, 2 2016. DOI: `10.1007/s00502-016-0388-8`.

[33] M. Tallfors, 'Paramter Estimation and Model Based Control Design of Drive Train Systems', Licentiate Thesis, Department of Automatic Control, KTH Stockholm, 2005.

[34] J. G. O'Donovan, R. C. Kavanagh, J. M. D. Murphy and M. G. Egan, 'Modular Approach to Parameter Estimation in Geared and Linear Resonant Systems', *Control Engineering Practice*, vol. 12, pp. 75–86, 1 2004. DOI: `10.1016/S0967-0661(02)00318-0`.

[35] V. P. Makkapati, 'Performance improvement of servo drive systems involving elastic coupling', PhD thesis, Faculty of Electrical and Information Engineering, Graz University of Technology, 2016.

[36] K. Szabat and T. Orlowska-Kowalska, 'Vibration Suppression in a Two-Mass Drive System Using PI Speed Controller and Additional Feedbacks — Comperative Study', *IEEE Transactions on Industrial Electronics*, vol. 54, pp. 1193–1206, 2 2007. DOI: `10.1109/TIE.2007.892608`.

[37] M. Cychowski, R. Jaskiewicz and K. Szabat, 'Model Predictive Control of an Elastic Three-Mass Drive System with Torque Constraints', in *IEEE International Conference on Industrial Technology*, Viña del Mar, Chile, 2010. DOI: `10.1109/ICIT.2010.5472710`.

[38] F. Matthies, 'Beitrag zur Modellbildung von Antriebssträngen für Fahrbarkeitsuntersuchungen', PhD thesis, Faculty IV — Electrical Engineering and Computer Science, Technische Universität Berlin, 2013.

[39] M. Bachinger, M. Stolz and M. Horn, 'Fixed Step Clutch Modeling and Simulation for Automotive Real-Time Applications', in *American Control Conference*, Portland, OR, USA, 2014. DOI: `10.1109/ACC.2014.6858933`.

[40] ——, 'A novel drivetrain modelling approach for real-time simulation', *Mechatronics*, vol. 32, pp. 67–78, 2015. DOI: `10.1016/j.mechatronics.2015.10.006`.

[41] D. Tscharnuter, 'Optimale Auslegung des Antriebsstrangs von Kraftfahrzeugen', PhD thesis, Faculty of Mathematics, Technical University of Munich, 2000.

[42] R. Zanasi, G. Sandoni and R. Morselli, 'Simulation of a variable dynamic dimension systems: The clutch example', in *European Control Conference*, Porto, Protugal, 2001.

[43] P. Samanuhut, 'Modelling and Control of Automatic Transmission with Planetary Gears for Shift Quality', PhD thesis, Faculty of the Graduate School, University of Texas at Arlington, 2011.

[44] R. Morselli, R. Zanasi and P. Ferracin, 'Modelling and simulation of static and Coulomb friction in a class of automotive systems', *International Journal of Control*, vol. 79, pp. 508–520, 5 2006. DOI: `10.1080/00207170600586970`.

[45] M. Bătăuş, A. Maciac, M. Oprean and N. Vasiliu, 'Automotive Clutch Models for Real Time Simulation', *Proceedings of the Romanian Academy*, vol. 12, no. 2, pp. 109–116, 2011.

[46] L. Ljung, *System Identification: Theory for the User*. New Jersey: Prentice Hall PTR, 1987, ISBN: 978-0-13-881640-7.

[47] M. Forstinger, R. Bauer, A. Hofer and W. Rossegger, 'Multivariable control of a test bed for differential gears', *Control Engineering Practice*, vol. 57, pp. 18–28, December 2016. DOI: `10.1016/j.conengprac.2016.08.010`.

[48] K. Hasse, 'Zur Dynamik drehzahlgeregelter Antriebe mit stromrichtergespeisten Asynchron–Kurzschlussläufermaschinen', PhD thesis, Faculty of Electrical Energy, Technische Hochschule Darmstadt, 1969.

[49] F. Blaschke, 'Das Verfahren der Feldorientierung zur Regelung der Drehfeldmaschine', PhD thesis, Technische Universität Braunschweig, 1974.

[50] D. Schröder, *Elektrische Antriebe — Regelung von Antriebssystemen*, 3rd ed. Berlin Heidelberg: Springer, 2009, ISBN: 978-3-540-89612-8. DOI: `10.1007/978-3-540-89613-5`.

[51] D. Muschick, 'Online-Parameteridentifikation bei Asynchronmaschinen', PhD thesis, Faculty of Electrical and Information Engineering, Graz University of Technology, 2014.

[52] R. D. Lorenz, 'Tuning of Field-Oriented Induction Motor Controllers for High-Performance Applications', *IEEE Transactions on Industry Applications*, vol. 22, pp. 293–297, 2 1986. DOI: `10.1109/TIA.1986.4504717`.

[53] M. Forstinger, 'Comparison of Current Control Concepts for Field-Oriented Control of Three-Phase Machines', Master's thesis, Institute for Automation and Control, Graz University of Technology, 2013.

[54] Y. Plotkin, M. Stiebler and D. Hofmeyer, 'Sixth Torque Harmonic in PWM Inverter-Fed Induction Drives and its Compensation', *IEEE Transactions on Industry Applications*, vol. 41, pp. 1067–1074, 4 2005. DOI: `10.1109/TIA.2005.850999`.

[55] S. Vöth, *Dynamik schwingungsfähiger Systeme*. Wiesbaden: Friedr. Vieweg & Sohn Verlag, 2006, ISBN: 978-3-8348-0111-1.

[56] H. Kokal, 'Feed forward disturbance rejection by a multiple FIFO approach for varying system delay compensation', in *Advances in Mechatronics*, Linz: Trauner Verlag, 2014, ISBN: 978-3-99033-433-1.

[57] M. Nordin, J. Galic' and P.-O. Gutman, 'New Models for Backlash and Gear Play', *International Journal of Adaptive Control and Signal Processing*, vol. 11, pp. 49–63, 1 1997. DOI: `10.1002/(SICI)1099-1115(199702)11:1<49::AID-ACS394>3.0.CO;2-X`.

[58] M. Nordin and P.-O. Gutman, 'Controlling mechanical systems with backlash — a survey', *Automatica*, vol. 38, pp. 1633–1649, 10 2002. DOI: `10.1016/S0005-1098(02)00047-X`.

[59] J. Vörös, 'Modeling and identification of systems with backlash', *Automatica*, vol. 46, pp. 369–374, 2 2010. DOI: `10.1016/j.automatica.2009.11.005`.

[60] A. Lagerberg, 'Control and Estimation of Automotive Powertrains with Backlash', PhD thesis, Department of Signals and Systems, Chalmers University of Technology Göteborg, 2004.

[61] A. Mills, 'Robert Hooke's 'Universal Joint' and its Application to Sundials and the Sundial-Clock', *The Royal Society Journal of the History of Science*, vol. 61, pp. 219–236, 2 2007. DOI: `10.1098/rsnr.2006.0172`.

[62] M. Trzesniowski, *Rennwagentechnik*, 2nd ed. Wiesbaden: Vieweg + Teubner, 2010, ISBN: 978-3-8348-0857-8.

[63] D. B. Welbourn, 'Fundamental Knowledge of Gear Noise — A Survey', in *Conference on Noise and Vibrations of Engines and Transmissions*, Cranfield, England, 1979.

[64] M. Åkerblom, 'Gearbox Noise — Correlation with Transmission Error and Influence of Bearing Preload', PhD thesis, Department of Machine Design, KTH Stockholm, 2008.

[65] A. Myklebust, 'Modeling and Estimation for Dry Clutch Control', Licentiate Thesis, Department of Electrical Engineering, Linköping University, 2013.

[66] J. Deur, M. Hancock and F. Assadin, 'Modeling of Active Differential Dynamics', in *ASME International Mechanical Engineering Congress & Exposition*, Boston, MA, USA, 2008. DOI: `10.1115/IMECE2008-69248`.

[67] S. Andersson, A. Söderberg and S. Björklund, 'Friction models for sliding dry, boundary and mixed lubricated contacts', *Tribology International*, vol. 40, pp. 580–587, 4 2007. DOI: `10.1016/j.triboint.2005.11.014`.

[68] J. Loomann, *Zahnradgetriebe*. Berlin Heidelberg: Springer, 1988, ISBN: 978-3-662-10989-2. DOI: `10.1007/978-3-662-10989-2`.

[69] G. Lechner and H. Naunheimer, *Automotive Transmissions*, Fundamentals, Selection, Design and Application. Berlin Heidelberg: Springer, 1999, ISBN: 978-3-540-65903-7.

[70] M. K. Salaani and G. J. Heydinger, 'Powertrain and Brake Modeling of the 1994 Ford Taurus for the National Advanced Driving Simulator', *SAE Technical Paper*, 1998. DOI: `10.4271/981190`.

[71] M. Forstinger, R. Bauer and A. Hofer, 'Modelling and Simulation of Passive Limited-Slip Differentials', in *Vienna International Conference on Mathematical Modelling*, Vienna, Austria, 2015. DOI: `10.1016/j.ifacol.2015.05.057`.

[72] G. Genta, L. Morello, F. Cavallino and L. Filtri, *The Motor Car*, Past, Present and Future. Dordrecht: Springer Science + Business Media, 2014, ISBN: 978-94-007-8552-6. DOI: `10.1007/978-94-007-8552-6`.

[73] R. Isermann, Ed., *Elektronisches Management motorischer Fahrzeugantriebe*, Elektronik, Modellbildung, Regelung und Diagnose für Verbrennungsmotoren, Getriebe und Elektroantriebe, Wiesbaden: Vieweg + Teubner, 2010, ISBN: 978-3-8348-0855-4. DOI: `10.1007/978-3-8348-9389-5`.

[74] K. Reif, Ed., *Konventioneller Antriebsstrang und Hybridantriebe*, mit Brennstoffzellen und alternativen Kraftstoffen, Wiesbaden: Vieweg + Teubner, 2010, ISBN: 978-3-8348-1303-9. DOI: `10.1007/978-3-8348-9711-4`.

[75] G. Lucente, M. Montanari and C. Rossi, 'Modelling of an automated manual transmission system', *Mechatronics*, vol. 17, pp. 73–91, 2–3 2007. DOI: `10.1016/j.mechatronics.2006.11.002`.

[76] C. Dörr, H. Kalczynski, A. Rink and M. Sommer, 'Nine-Speed Automatic Transmission 9G-Tronic by Mercdes Benz', *ATZ worldwide*, vol. 116, pp. 20–25, 1 2014. DOI: `10.1007/s38311-014-0006-5`.

[77] J. Greiner, G. Indlekofer, H. Nauerz, J. Dorfschmid, T. Gödecke and C. Dörr, 'Siebengang-Automatikgetriebe von Mercedes-Benz', *ATZ – Automobiltechnische Zeitschrift*, vol. 105, pp. 920–930, 10 2003. DOI: `10.1007/BF03221588`.

[78] C. Breitfeld, A. Müller, A. Burger, M. Mischnick, E. Bauchrowitz and J. Schröder, 'Die weiterentwickelten Sechsgang-Automatikgetriebe von BMW', *ATZ – Automobiltechnische Zeitschrift*, vol. 108, pp. 820–830, 10 2006. DOI: `10.1007/BF03221822`.

[79] G. Wagner, H. Naunheimer, H. Scherer and A. Dick, 'Achtgang-Automatikgetriebe zur Reduzierung des Kraftstoffverbrauchs', *ATZ – Automobiltechnische Zeitschrift*, vol. 109, pp. 512–519, 6 2007. DOI: `10.1007/BF03221894`.

[80] H. A. Asl, N. L. Azad and J. McPhee, 'Modeling Torque Converter Characteristics in Automatic Drivelines: Lock-up Clutch and Engine Braking Simulation', in *ASME International Conference on Advanced Vehicle Technologies*, Chicago, IL, USA, 2012. DOI: `10.1115/DETC2012-70222`.

[81] G. Rill, 'Simulation von Kraftfahrzeugen', in *Fundamentals and Advances in the Engineering Sciences*, Wiesbaden: Vieweg + Teubner, 2007.

[82] S. Kahlbau, 'Mehrkriterielle Optimierung des Schaltablaufs von Automatikgetrieben', PhD thesis, Faculty of Mechanical Engineering, Electrical and Energy Systems, Brandenburgische Technische Universität, 2013.

[83] I.-G. Park, I.-K. Kim and M.-G. Kim, 'Vibrational Characteristics of Developed Harmonic Reduction Gear and Fault Diagnosis by Campbell Diagram', in *15th International Conference on Control, Automation and Systems*, Busan, Korea, 2015. DOI: `10.1109/ICCAS.2015.7364708`.

[84] M. Mauri, M. Rossi and M. Bruha, 'Generation of Torsional Excitation in a Variable-Speed-Drive System', in *International Symposium on Power Electronics, Electrical Drives, Automation and Motion*, Anacapri, Italy, 2016. DOI: `10.1109/SPEEDAM.2016.7525862`.

[85] L. Ineichen, 'Konzeptvergleich zur Bekämpfung der Torsionsschwingungen im Antriebsstrang eines Kraftfahrzeugs', PhD thesis, Department of Mechanical Engineering, Karlsruhe Institute of Technology, 2012.

[86] M. R. Hatch, *Vibration Simulation Using MATLAB and ANSYS*. Boca Raton: Chapman & Hall/CRC, 2000, ISBN: 978-1-58488-205-3.

[87] B. Armstrong-Hélouvry, P. Dupont and C. C. de Wit, 'A Survey of Models, Analysis Tools and Compensation Methods for the Control of Machines with Friction, Happi', *Automatica*, vol. 30, pp. 1083–1138, 7 1994. DOI: `10.1016/0005-1098(94)90209-7`.

[88] D. A. Haessig and B. Friedland, 'On the Modelling and Simulation of Friction', *ASME Journal of Dynamic Systems, Measurement, and Control*, vol. 113, pp. 354–362, 3 1991. DOI: `10.1115/1.2896418`.

[89] R. H. A. Hensen, 'Controlled Mechanical Systems with Friction', PhD thesis, Department of Mechanical Engineering, Eindhoven University of Technology, 2002. DOI: `10.6100/IR551394`.

[90] A. van der Schaft and H. Schumacher, 'An Introduction to Hybrid Dynamical Systems', in *Lecture Notes in Control and Information Sciences*, London: Springer, 2000, ISBN: 978-1-84628-542-4. DOI: `10.1007/BFb0109998`.

[91] F. Garofalo, L. Glielmo, L. Iannelli and F. Vasca, 'Smooth Engagement for Automotive Dry Clutch', in *IEEE Conference on Decision and Control*, Orlando, FL, USA, 2001. DOI: `10.1109/CDC.2001.980156`.

[92] J. H. Taylor, 'Rigorous Handling of State Events in MATLAB', in *IEEE Conference on Control Applications*, Albany, NY, USA, 1995. DOI: `10.1109/CCA.1995.555660`.

[93] M. Herchenhan, 'Methods for Modelling Propulsion Systems with Variable Order and Structure', *Automatisierungstechnik*, vol. 62, pp. 651–664, 9 2014. DOI: `10.1515/auto-2014-1110`.

[94] F. A. Tariku and R. J. Rogers, 'Improved Dynamic Friction Models for Simulation of One-Dimensional and Two-Dimensional Stick–Slip Motion', *ASME Journal of Tribology*, vol. 123, pp. 661–669, 4 2000. DOI: `10.1115/1.1331057`.

[95] S. Lunzman, D. Kennedy and S. Miller, 'Physical Modeling of Mechanical Friction in Simulink', *MATLAB Digest*, 2008.

[96] J. D. López, J. J. Espinosa and J. Agudelo, 'Decoupled Control for Internal Combustion Engines Research Test Beds', *Revista Facultad de Ingeniería Universidad de Antioquia*, vol. 59, pp. 23–31, 2011.

[97] D. Yanakiev, 'Adaptive Control of Diesel Engine-Dynamometer Systems', in *IEEE Conference on Decision and Control*, Tampa, FL, USA, 1998. DOI: `10.1109/CDC.1998.758506`.

[98] R. Priesner, C. Westermayer, S. Jakubek and R. Bauer, 'Predictive Control with Active Disturbance Rejection for Elastic Drive Systems', in *IEEE Conference on Industrial Electronics and Applications*, Singapore, 2012. DOI: `10.1109/ICIEA.2012.6360722`.

[99] E. Grünbacher and L. del Re, 'Robust Inverse Control for Combustion Engine Test Benches', in *American Control Conference*, Seattle, WA, USA, 2008. DOI: `10.1109/ACC.2008.4586926`.

[100] S. Qiang and L. Lin, 'Mechanical decoupling algorithm applied to electric drive test bed', *Mathematical Problems in Engineering*, vol. 2014, pp. 1–6, 2014. DOI: `10.1155/2014/710865`.

[101] K. Szabat and T. Orlowska-Kowalska, 'Application of the Kalman Filters to the High-Performance Drive System With Elastic Coupling', *IEEE Transactions on Industrial Electronics*, vol. 59, pp. 4226–4235, 11 2012. DOI: `10.1109/TIE.2012.2183836`.

[102] P. B. Schmidt and R. D. Lorenz, 'Design Principles and Implementation of Acceleration Feedback to Improve Performance of DC Drives', *IEEE Transactions on Industry Applications*, vol. 28, pp. 594–599, 3 1992. DOI: `10.1109/28.137444`.

[103] K. Yuki, T. Murakami and K. Ohnishi, 'Vibration Control of 2 Mass Resonant System by Resonance Ratio Control', in *IEEE International Conference on Industrial Electronics, Control and Instrumentation*, Maui, HI, USA, 1993. DOI: `10.1109/IECON.1993.339383`.

[104] Y. Hori, H. Iseki and K. Sugiura, 'Basic Consideration of Vibration Suppression and Disturbance Rejection Control of Multi-inertia System using SFLAC (State Feedback and Load Acceleration Control)', *IEEE Transactions on Industry Applications*, vol. 30, pp. 889–896, 4 1994. DOI: `10.1109/28.297904`.

[105] Y. Hori, H. Sawada and Y. Chun, 'Slow Resonance Ratio Control for Vibration Suppression and Disturbance Rejection in Torsional System', *IEEE Transactions on Industrial Electronics*, vol. 46, pp. 162–168, 1 1999. DOI: `10.1109/41.744407`.

[106] R. Muszynski and J. Deskur, 'Damping of Torsional Vibrations in High-Dynamic Industrial Drives', *IEEE Transactions on Industrial Electronics*, vol. 57, pp. 544–552, 2 2010. DOI: `10.1109/TIE.2009.2036034`.

[107] K. Sugiura and Y. Hori, 'Vibration Suppression in 2- and 3-Mass System Based on the Feedback of Imperfect Derivative of the Estimated Torsional Torque', *IEEE Transactions on Industrial Electronics*, vol. 43, pp. 56–64, 1 1996. DOI: `10.1109/41.481408`.

[108] S. Thomsen and F. W. Fuchs, 'Speed Control of Torsional Drive Systems with Backlash', in *European Conference on Power Electronics and Applications*, Barcelona, Spain, 2009.

[109] S. Thomsen, N. Hoffmann and F. W. Fuchs, 'PI control, PI-Based State Space Control, and Model-Based Predictive Control for Drive Systems With Elastically Coupled Loads — A Comparative Study', *IEEE Transactions on Industrial Electronics*, vol. 58, pp. 3647–3657, 8 2011. DOI: `10.1109/TIE.2010.2089950`.

[110] K. Szabat, T. Orlowska-Kowalska and M. Dybkowski, 'Indirect adaptive control of induction motor drive system with an elastic coupling', *IEEE Transactions on Industrial Electronics*, vol. 56, pp. 4038–4042, 10 2009. DOI: `10.1109/TIE.2009.2022514`.

[111] X. Jinbang, W. Wenyu, S. Anwen and Z. Yu, 'Detection and reduction of middle frequency resonance for an industrial servo', *Control Engineering Practice*, vol. 21, pp. 899–907, 7 2013. DOI: `10.1016/j.conengprac.2013.02.001`.

[112] M. Cychowski, K. Szabat and T. Orlowska–Kowalska, 'Constrained Model Predictive Control of the Drive System With Mechanical Elasticity', *IEEE Transactions on Industrial Electronics*, vol. 56, pp. 1963–1973, 6 2009. DOI: `10.1109/TIE.2009.2015753`.

[113] M. Cychowski and K. Szabat, 'Efficient real-time model predictive control of the drive system with elastic transmission', *IET Control Theory & Applications*, vol. 4, pp. 37–49, 1 2010. DOI: `10.1049/iet-cta.2008.0358`.

[114] M. Cychowski, P. Serkies, R. Nalepa and K. Szabat, 'Model Predictive Speed and Vibration Control of Dual-Inertia PMSM Drives', in *IEEE International Symposium on Industrial Electronics*, Gdańsk, Poland, 2011. DOI: `10.1109/ISIE.2011.5984451`.

[115] E. J. Fuentes, C. A. Silva and J. I. Yuz, 'Predictive Speed Control of a Two-Mass System Driven by a Permanent Magnet Synchronous Motor', *IEEE Transactions on Industrial Electronics*, vol. 59, pp. 2840–2848, 7 2012. DOI: `10.1109/TIE.2011.2158767`.

[116] S. Thomsen and F. W. Fuchs, 'Flatness Based Speed Control of Drive Systems with Resonant Loads', in *Annual Conference of the IEEE Industrial Electronics Society*, Glendale, AZ, USA, 2010. DOI: `10.1109/IECON.2010.5675188`.

[117] S. N. Vukosavić and M. R. Stojić, 'Suppression of Torsional Oscillations in a High-Performance Speed Servo Drive', *IEEE Transactions on Industrial Electronics*, vol. 45, pp. 108–117, 1 1998. DOI: `10.1109/41.661311`.

[118] P. Schmidt and T. Rehm, 'Notch Filter Tuning for Resonant Frequency Reduction in Dual Inertia Systems', in *IEEE Industry Applications Conference*, Phoenix, AZ, USA, 1999. DOI: `10.1109/IAS.1999.805973`.

[119] H. Wang, D.-H. Lee, Z.-G. Lee and J.-W. Ahn, 'Vibration Rejection Scheme of Servo Drive System with Adaptive Notch Filter', in *IEEE Power Electronics Specialists Conference*, Jeju, South Korea, 2006. DOI: `10.1109/PESC.2006.1712270`.

[120] S. H. Jeon, J.-M. Kim, K.-C. Jung, S.-K. Sul and J. Y. Choi, 'Decoupling Control of Bridle Rolls for Steel Mill Drive System', *IEEE Transactions on Industry Applications*, vol. 35, pp. 119–125, 1 1999. DOI: `10.1109/28.740855`.

[121] S.-H. Song and S.-K. Sul, 'A New Tension Controller for Continuous Strip Processing Line', *IEEE Transactions on Industry Applications*, vol. 36, pp. 633–639, 2 2000. DOI: `10.1109/28.833782`.

[122] M. A. Valenzuela, J. M. Bentley, P. C. Aguilera and R. D. Lorenz, 'Improved Coordinated Response and Disturbance Rejection in the Critical Sections of Paper Machines', *IEEE Transactions on Industry Applications*, vol. 43, pp. 857–869, 3 2007. DOI: `10.1109/TIA.2007.895816`.

[123] A. Angermann, 'Entkopplung von Mehrgrößensystemen durch Vorsteuerung am Beispiel von kontinuierlichen Fertigungsanlagen', PhD thesis, Department of Electrical and Computer Engineering, Technical University of Munich, 2004.

[124] S. Liu, X. Mei, F. Kong and K. He, 'A Decoupling Control Algorithm for Unwinding Tension System Based on Active Disturbance Rejection Control', *Mathematical Problems in Engineering*, vol. 2013, 2013. DOI: `10.1155/2013/439797`.

[125] J. Chen, Z. Yin, Y. Xiong and J. Quan, 'A Hybrid Control Method of Tension and Position for a Discontinuous Web Transport System', in *IEEE International Conference on Information and Automation*, Zhuhai, China, 2009. DOI: `10.1109/ICINFA.2009.5204933`.

[126] M. A. Valenzuela, J. M. Bentley and R. D. Lorenz, 'Evaluation of Torsional Oscillations in Paper Machine Sections', *IEEE Transactions on Industry Applications*, vol. 41, pp. 493–501, 2 2005. DOI: `10.1109/TIA.2005.844383`.

[127] P. Albertos and A. Sala, 'Multivariable Control Systems: An Engineering Approach', in *Advanced Textbooks in Control and Signal Processing*, London: Springer, 2004, ISBN: 1852337389.

[128] J. M. Maciejowski, *Multivariable Feedback Design*. Reading: Addison-Wesley, 1989, ISBN: 978-0-201-18243-9.

[129] S. Skogestad and I. Postlethwaite, *Multivariable Feedback Control*, Analysis and Design, 2nd ed. Chichester: Wiley, 1996, ISBN: 978-0-470-01167-6.

[130] A. Isidori, *Nonlinear Control Systems*, 3rd ed. London: Springer, 1995, ISBN: 978-3-540-19916-8. DOI: `10.1007/978-1-84628-615-5`.

[131] M. A. Henson and D. E. Seborg, Eds., *Nonlinear Process Control*, New Jersey: Prentice Hall PTR, 1996, ISBN: 978-0-13-625179-8.

[132] J. Adamy, *Nichtlineare Regelungen*. Berlin Heidelberg: Springer, 2009, ISBN: 978-3-642-00794-1. DOI: `10.1007/978-3-642-00794-1`.

[133] ——, *Nichtlineare Systeme und Regelungen*, 2nd ed. Berlin Heidelberg, 2014, ISBN: 978-3-642-45013-6. DOI: `10.1007/978-3-642-45013-6`.

[134] J. Lunze, *Regelungstechnik 2*, Mehrgrößensysteme, Digitale Regelung, 6th ed. Berlin Heidelberg: Springer, 2010, ISBN: 978-3-642-10198-4. DOI: `10.1007/978-3-642-10198-4`.

[135] M. Iwasaki and N. Matsui, 'Robust Speed Control of IM with Torque Feedforward Control', *IEEE Transactions on Industrial Electronics*, vol. 40, pp. 553–560, 6 1993. DOI: `10.1109/41.245892`.

[136] Y. Shtessel, C. Edwards, L. Fridman and A. Levant, *Sliding Mode Control and Observation*. New York: Springer Science + Business Media, 2014, ISBN: 978-0-8176-4893-0. DOI: `10.1007/978-0-8176-4893-0`.

[137] K. Kranawetter, 'Energieoptimale Positionsregelung einer Asynchronmaschine', Master's thesis, Institute for Automation and Control, Graz University of Technology, 2014.

[138] N. Dourdoumas and M. Horn, *Regelungstechnik*, Rechnerunterstützter Entwurf zeitkontinuierlicher und zeitdiskreter Regelkreise. München: Pearson Studium, 2004, ISBN: 978-3-8273-7059-4.

[139] R. Hanus, M. Kinnaert and J.-L. Henrotte, 'Conditioning Technique, a General Anti-windup and Bumpless Transfer Method', *Automatica*, vol. 23, pp. 729–739, 6 1987. DOI: `10.1016/0005-1098(87)90029-X`.

[140] E. Grünbacher, P. Langthaler, G. Steinmaurer, L. del Re and H. Kokal, 'Adaptive Inverse Torque Control of a Diesel Engine Using Adaptive Mapping Update', in *SEA World Congress*, Detroit, MI, USA, 2003. DOI: `10.4271/2003-01-0397`.

[141] I. Kolmanovsky, E. Garone and S. Di Cairano, 'Reference and Command Governors: A Tutorial on Their Theory and Automotive Applications', in *American Control Conference*, Portland, OR, USA, 2014. DOI: `10.1109/ACC.2014.6859176`.

[142] I. Kolmanovsky, U. Kalabić and E. G. Gilbert, 'Developments in Constrained Control Using Reference Governors', in *IFAC Conference on Nonlinear Model Predictive Control (NMPC)*, Noordwijkerhout, Netherlands, 2012. DOI: `10.3182/20120823-5-NL-3013.00042`.

[143] E. G. Gilbert, I. Kolmanovsky and K. T. Tan, 'Nonlinear control of discrete-time linear systems with state and control constraints: A reference governor with global convergence properties', in *IEEE Conference on Decision and Control*, Lake Buena Vista, FL, USA, 1994. DOI: `10.1109/CDC.1994.411031`.

[144] ——, 'Discrete-time reference governors and the nonlinear control of systems with state and control constraints', *International Journal of Robust and Nonlinear Control*, vol. 5, pp. 487–504, 5 1995. DOI: `10.1002/rnc.4590050508`.

[145] E. G. Gilbert and I. Kolmanovsky, 'Fast reference governors for systems with state and control constraints and disturbance inputs', *International Journal of Robust and Nonlinear Control*, vol. 9, pp. 1117–1142, 15 1999. DOI: `10.1002/(SICI)1099-1239(19991230)9:15<1117::AID-RNC447>3.0.CO;2-I`.

[146] M. Hazewinkel, Ed., *Encyclopaedia of Mathematics*, Supplement III, Dordrecht: Springer, 2002, ISBN: 978-0-306-48373-8. DOI: `10.1007/978-0-306-48373-8`.

[147] R. Bhatia, 'Matrix analysis', in *Graduate Texts in Mathematics*, New York: Springer, 1997, ISBN: 978-1-4612-0653-8. DOI: `10.1007/978-1-4612-0653-8`.